Aus dem Walther-Straub-Institut für Pharmakologie und Toxikologie der
Ludwig-Maximilians-Universität München
Vorstand: Prof. Dr. med. Thomas Gudermann

Characterization of cation channels and their role in mechanotransduction

Kumulative Dissertation
zum Erwerb des Doktorgrades der Naturwissenschaften
an der Medizinischen Fakultät
der Ludwig-Maximilians-Universität München

vorgelegt von
Anna-Lena Forst
aus Rheine
2015

Mit Genehmigung der Medizinischen Fakultät der Universität München

Betreuer: Prof. Dr. Michael Mederos y Schnitzler

Zweitgutachter: Prof. Dr. Alexander Faußner

Dekan: Prof. Dr. med. dent. Reinhard Hickel

Tag der mündlichen Prüfung: 28.01.2016

Eidesstattliche Versicherung

(Author's declaration)

Anna-Lena Forst

Ich erkläre hiermit an Eides statt, dass ich die vorliegende Dissertation mit dem Thema

Characterization of cation channels and their role in mechanotransduction

selbständig verfasst, mich außer der angegebenen keiner weiteren Hilfsmittel bedient und alle Erkenntnisse, die aus dem Schrifttum ganz oder annähernd übernommen sind, als solche kenntlich gemacht und nach ihrer Herkunft unter Bezeichnung der Fundstelle einzeln nachgewiesen habe.

Ich erkläre des Weiteren, dass die hier vorgelegte Dissertation nicht in gleicher oder in ähnlicher Form bei einer anderen Stelle zur Erlangung eines akademischen Grades eingereicht wurde.

_____ _____

Ort, Datum Unterschrift Doktorandin

For my parents

Table of contents

Abbreviations

20-HETE – 20-hydroxyeicosatetraenoic acid

5-BDBD – 5-(3-Bromophenyl)-1,3-dihydro-2*H*-benzofuro[3,2-*e*]-1,4-diazepin-2-one

α1 – adrenergic receptor type 1

AA – archidonic acid

AFM – atomic force microscopy

ARC – actin rich center

ASIC – acid sensing ion channels

AT_{1A} – angiotensin II receptor type 1A

AT_{1B} – angiotensin II receptor type 1B

AT_1R– angiotensin II receptor type 1

ATP – adenosine 5'-triphosphate

C- – carboxyl-

C. elegans – Caenorhabditis elegans

cAMP – adenosine 3-,5-cyclic monophosphate

Ca_V – voltage-gated calcium channel

CDH23 – cadherin 23

CHO – chinese hamster ovary

cm – centimeter

COS – CV-1 in Origin with SV40 genes

$CysLT_1R$ – cysteinyl leukotriene 1 receptor

DA5 – distal arthrogryposis Type 5

DAG – diacylglycerol

Deg/ENaC – Degenerin/Epithelial channel Na^+ channel

DNA – 2' deoxyribonucleic acid

DRG – dorsal root ganglia

EC – endothelial cell

ECM – extracellular matrix

EET – 5',6'-epoxyeicosatrienoic acid

ER – endoplasmic reticulum

ET_A – endothelin receptor type A

ET_B – endothelin receptor type B

F – force

FRET – Förster resonance energy transfer

GTP – guanosine 5'-triphosphate

GTPγS – guanosine 5'-O-[gamma-thio]triphosphate

GPCR – G protein-coupled receptor

Abbreviations

HEK293 – human embryonic kidney 293
HKC8 – human kidney cell 8
HT22 – a mouse hippocampal immortalized sub-line derived from parent HT4 cells
IP – inositolphosphate
IP_3 – inositol 1,4,5-trisphosphate
I_{SOC} – currents observed after store depletion
K_{2P} – K^+ two pore channel
L – length
LDL – low density lipoprotein
LRRC8 – leucine-rich repeat–containing 8
MEC – mechanosensory abnormalities
mmHg – millimeter mercury
mRNA – messenger RNA
MscL – mechanosensitive channel of large conductance
MscM – mechanosensitive channel of mini conductance
MscS – mechanosensitive channel of small conductance
N – Newton
N- – amino-
NFAT – nuclear factor of activated T-cells
NHE – Na^+/H^+ antiporter 3
NHERF – NHE regulating factor
NPT2a – Na^+/phosphate cotransporter type 2a
NompC – no mechanoreceptor potential channel
OAG – 1-oleoyl-2-acetyl-sn-glycerol
Orai1 – calcium channel calcium release-activated calcium channel protein 1
OVLT – organum vasculosum laminae terminalis
P – pressure
P_2X – purinergic channel
Pa – Pascal
PCDH15 – protocadherin 15
PDZ – post synaptic density protein, d*rosophila* disc large tumor suppressor, zonula occludens-1 protein
PKA – phosphokinase A
PKC – phoshokinase C
PLA_2 – phopholipase A_2
PLC – phopholipase C
PLD – phospholipase D

Abbreviations

PIP – phosphoinositol phosphate
PIP_2 – phosphatidylinositol 4,5- bisphosphate
PTH_1R – parathyroid hormone receptor 1
r – radius
RNA – ribonucleic acid
RNAi – RNA interference
SAI – slowly adapting type I
shRNA – small hairpin RNA
siRNA –small interfering RNA
SOC – store operated channel
SON – supraoptic nucleus
STIM1 – stromal interaction molecule 1
T – tension
TM – transmembrane
TMC – transmembrane channel-like
TMHS – tetraspan membrane protein of hair cells
TNP – 2,4,6-trinitrophenol
TNP-ATP – 2',3'-O-(2,4,6-Trinitrophenyl)adenosine-5'-triphosphate
TRAAK – TWIK-related arachidonic acid-stimulated K^+ channel
TREK – TWIK-related K^+ channel
TRP – Transient Receptor Potential
TRPA – ankyrin TRP
TRPC – canonical TRP
TRPM – melastatin TRP
TRPML – mucolipid TRP
TRPN –NompC-related TRP
TRPP – polycystin TRP
TRPV – vanilloid TRP
TRPY – yeast TRP
VACC – volume activated chloride channels
VRAC – volume-regulated anion channel
VSMC – vascular smooth muscle cell
VSOAC – volume sensitive organic anion channels

The use of abbreviations of common english words is done according to guidelines from the American Psychological Association (1994).

Publications

This dissertation contains results that are presented in the following publications:

Storch U, Forst AL, Philipp M, Gudermann T, Mederos y Schnitzler M. **Transient receptor potential channel 1 (TRPC1) reduces calcium permeability in heteromeric channel complexes**. J Biol Chem. 2012 Jan 27;287(5):3530-40.

Blodow S, Schneider H, Storch U, Wizemann R, Forst AL, Gudermann T, Mederos y Schnitzler M. **Novel role of mechanosensitive AT_{1B} receptors in myogenic vasoconstriction.** Pflugers Arch. 2014 Jul;466(7):1343-53.

Forst AL, Olteanu V, Mollet G, Wlodkowski T, Schaefer F, Dietrich A, Reiser J; Gudermann T, Mederos y Schnitzler M, Storch U. **Podocyte purinergic P_2X_4 channels are mechanotransducers that mediate cytoskeletal disorganization.** J Am Soc Nephrol. 2015 Jul 9. pii: ASN.2014111144. [published ahead of print]

Additionally, the results of another project were submitted to Nature Cell Biology:

Storch U*, Forst AL*, Pardatscher F, Philipp M, Ren H, Gregoritza M, Mederos y Schnitzler M, Gudermann T. (2015). **NHERF dissociation from TRPC4/5 proteins is required for channel gating by diacylglycerol.** *Submitted to Nature Cell Biology 29th July 2015.*
**shared first authorship*

Key findings of this project are reviewed in the section “Biophysical characterization of TRPC4 and TRPC5” that can be found on pages 116-128 of this thesis.

I Introduction

Mechanosensitivity refers to the ability of cells and tissues to convert specific mechanical stimuli into chemical and electrical signals inside the cell. Mechanosensitivity is inherent to a wide variety of cells in many different organisms ranging from bacteria to mammals. The primary target for mechanical stimulation is the cell surface with the plasma membrane, which can respond in variable physical stress. For example, mechanical stimulation can change the open probability of directly or indirectly mechanosensitive ion channels. Thus, mechanical stress can elicit a multitude of biochemical processes—both transient and long-lasting—inside a cell. Mechanosensitivity can be subdivided into the three different processes, namely mechanoperception, mechanotransduction and mechanoresponse. While mechanoperception describes the ability of proteins to perceive physical forces, mechanotransduction is the transmission of force to cellular elements. Mechanoresponse is the resulting conversion of mechanical stimuli into biologically adaptive electrical and chemical responses.

1. Role of mechanosensitivity in cells and organisms

An organism detects diverse sensory information with a variety of cells that respond to mechanical forces. Examples of mechanosensation in mammals are hearing which is perceived by hair cells in the inner ear, touch which is sensed by various cells inside the skin and pressure-induced vasoconstriction which is mediated by vascular smooth muscle cells and causes autoregulation of the blood flow. Although structurally different, the mechanoreceptors of these cells share several mechanistic features. The following section describes the recent understanding of the molecular basis of the sensations of touch, hearing and autoregulation of blood flow by arterial muscle cells.

1.1 Sensation of touch by cutaneous receptors

Touch is the detection of mechanical stimuli's impact on the skin, including innocuous and noxious mechanical stimuli. The impression of touch is formed by several modalities including pressure, skin stretch, vibration and temperature, and is detected by a diverse array of specialized cutaneous receptors that are localized in various layers of the skin. Somatosensory neurons reside within dorsal root ganglia (DRG) and cranial sensory ganglia and are divided into low- and high-threshold mechanoreceptors. The associated nerve fibers are broadly classified on the basis of degree of myelination and action potential conduction velocities into Aβ-, Aδ-, or C-fibers. In contrast to neurons that respond to innocuous touch and temperatures, sensory neurons known as nociceptors respond to painful sensations caused by intense mechanical, thermal or chemical stimulation (for review see Lumpkin and Caterina, 2007). Pain receptors are localized cutaneously, somatically or viscerally with varying frequency. The

underlying mechanisms that allow mechanoperception are ion channels that rapidly transform mechanical forces into electrical signals and depolarize the cell. This generates a receptor potential that results in action potential firing that propagates toward the central nervous system (Figure 1, left). Although depolarizing mechanosensitive ion currents in skin cells have been well characterized, the molecular identity of conducting ion channels has been obscure. Several channel families including transient receptor potential channel (TRP), degenerin/Epithelial Na^+ channel (Deg/ENaC), Piezo channel, as well as transmembrane channel-like (TMC) families have been proposed as mechanosensors in hair cells (summarized in Raudaut et al., 2012). However, additional research has questioned the requirement of most of these candidates in touch sensation. Although evidence from yeast has pointed to directly mechanogated TRP channels, experiments in mammals failed to confirm direct mechanosensitive properties of most TRP channels. Similar results were obtained for the Deg/ENaC channel family: Although the sensation of gentle touch in the *Caenorhabditis elegans* (*C. elegans*) is directly sensed by a Deg/ENaC channel complex that requires several accessory subunits for proper function, direct mechanosensitive characteristics of mammalian Deg/ENaC channels could not be validated (for review see Arnadottir and Chalfie, 2010). The presence of TMC1 and TMC2 proteins, which are both essential components of hair cell mechanotransduction, has not yet been confirmed in the somatosensory system. Studies with TMC1 mutant worms showed no apparent defects in touch avoidance, arguing against the relevance of TMC proteins in touch sensation (Chatzigeorgiou et al., 2013). Even Piezo channels, although likely directly responsive to mechanical stimuli, were not fully responsible for the sensation of touch in afferents. However, for the first time, it could be shown that Piezo2 channels function as mechanosensors in Merkel cells. Merkel cells are in close association with Aβ-afferent terminals and mediate a subset of slowly adapting responses to touch. For many years, it has been unclear whether Merkel cells are required for touch sensitivity and there was no evidence demonstrating that Merkel cells are directly activated by touch. In fact, Merkel cells have been believed to be merely supportive tissues for terminal afferent functions. However, independent researcher groups were able to show that Merkel cells, rather than Aβ-afferent nerve endings, are the primary sites of tactile transduction. Additionally, Piezo2 ion channels were identified as the Merkel cell mechanical transducers that convert tactile stimuli into calcium action potentials thereby actively tuning the firing rate of mechanosensory Aβ-afferents (Figure 1, right) (Ikeda and Gu, 2014; Maksimovic et al., 2014; Woo et al., 2014).

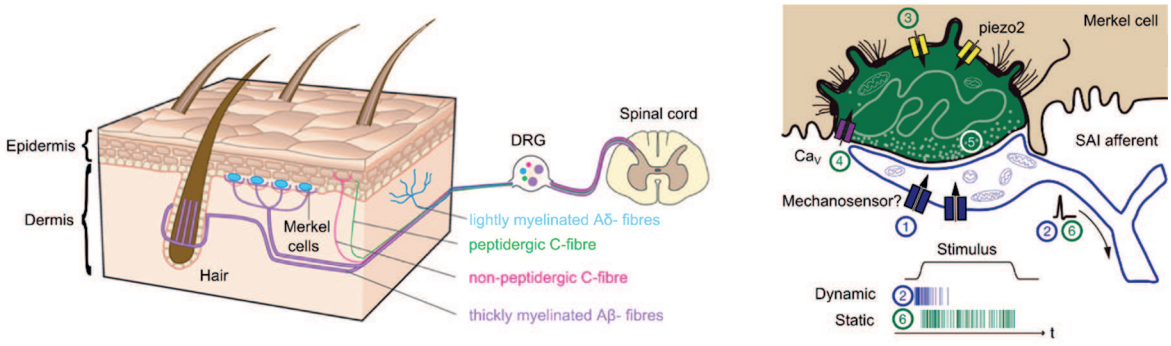

Figure 1: Sensation of touch by cutaneous receptors. Left: *Image adapted from Lumpkin and Caterina, 2007)*. The skin is innervated by somatosensory neurons that project via the dorsal root ganglia (DRG) to the spinal cord. Aβ-fibres, such as those that innervate Merkel cells and those around hair shafts, are thought to be touch receptors. Aδ-fibres and C-fibres include thermoreceptors and nociceptors. Right: *Image adapted from Maksimovic et al., 2014)*. Deformation of the skin opens mechanosensitive channels in slowly adapting type I (SAI) afferents (1) to initiate action potential firing at the onset of dynamic stimuli (2). The presence of Merkel cells boosts dynamic firing through Piezo2-independent mechanisms. Skin deformation simultaneously activates Piezo2 resulting in depolarized Merkel cells (3). Calcium entry through Piezo2 subsequently activates voltage-activated calcium channels (Ca_V) (4) and release of unidentified neurotransmitters (5) that trigger sustained firing of the SAI afferent (6).

1.2 Sensation of sound by hair cells in the inner ear

Hair cells reside in the inner ear and convert a mechanical stimulus into an electrical signal that is processed by the central nervous system. The mechanosensitive structure inside the hair cell is the hair bundle, which consists of actin-rich stereocilia. The stereocilia are laterally coupled to each other by intercilliary links. Additional tip links connect the tip of each stereocilium to the side of its tallest neighboring stereocilium. A mechanical stimulus will result in the deflection of the stereocilia towards the tallest stereocilium and the tip links are tensioned. This tension opens mechanosensitive cation channels of largely unknown identity located at the tip link (Figure 2). As a result, the cells will depolarize and release neurotransmitters at the base of the hair cells. In this way, the hair cell's excitation will be conveyed to the central nervous system (for review see Gillespie and Muller, 2009). Mutations in structures essential for the integrity of the mechanosensitive structures result in hearing deficiencies and have led to the identification of cadherin 23 and protocadherin 15 as tip linkers that form the upper and the lower part of the tip link respectively. However, the identity of the transducing channel remains elusive. It is known that mechanosensitive ion currents in hair cells are mediated by non-selective cation channels with high calcium permeability and adapt their response to sustained stimuli. Several proteins including ankyrin TRP 1 (TRPA1), melastanin TRP 1 (TRPM1), no mechanoreceptor potential C (NompC)-like TRP 1 (TRPN1), tetraspan membrane protein of hair cell stereocilia (TMHS), TMC1 and TMC2 have been raised

as putative mechanosensors, but so far, concluding evidence for either channel is missing (for review see Gillespie and Muller, 2009). TRPA1 and TRPM1 are expressed at the tips of hair cells, but mice lacking either channel have normal hearing and balance clearly arguing against TRPA1 or TRPM1 as hair cell conductance channels (Bautista et al., 2006; Gerka-Stuyt et al., 2013). TMHS channels, although clearly important for proper hearing in mice, regulate transducing conductance and adaptation and might be an accessory subunit of the hair cell's mechanosensitive apparatus (Xiong et al., 2012). On the contrary, evidence supports the hypothesis of TMC1 and TMC2 being transducing channels in hair cells. TMC1-deficient mice are deaf and so are humans carrying mutations in TMC1 (Kurima et al., 2002). The most convincing evidence is a point mutation in TMC1 that alters the permeation properties of transduction channels in native sensory cells, which can only be explained by the mutated protein either being part of the channel itself or being a pore regulatory subunit (Pan et al., 2013). However, in vitro data attributing the characteristics reminiscent to those found in sensory cells to TMC proteins are still missing. Of relevance are findings in *C. elegans* TMC1 mutant worms that show no apparent defects in touch avoidance, leaving the role of TMC1 ill-defined (Chatzigeorgiou et al., 2013).

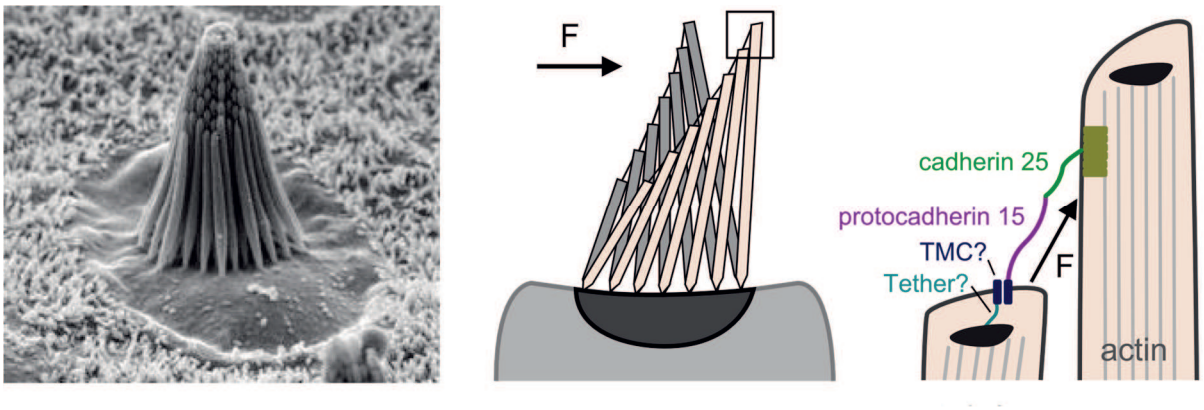

Figure 2: Sensation of sound by hair cells in the inner ear. Left: *Image adapted from Jiang, 2012*. Scanning electron micrograph of hair cell bundle in the inner ear. Middle: Force (F) in the form of mechanical waves or head movement results in deflection of the hair cells towards the largest cilia. Right: The tips of the hair cells are connected via tip linkers that are composed of protocadherin 15 and cadherin 23. Deflection of the hair cells causes the linker to tighten resulting in the opening of a mechanosensitive ion channel. The identity of the mechnotransducing channel is not yet clarified, but latest research suggests that transmembrane channel-like (TMC) proteins are at least part of the channel's pore.

1.3 Myogenic tone

Cells in the cardiovascular system are constantly subjected to mechanical forces due to the pulsatile nature of the blood flow caused by the beating heart. Endothelial cells as well as

vascular smooth muscle cells (VSMCs) of small resistance arteries harbor mechanosensitive structures in order to regulate blood flow independently of the nervous system. Disturbances of these mechanical loads contribute to cardiovascular diseases like hypertension, diabetes atherosclerosis and vascular restenosis (Cummins et al., 2007). In contrast to VSMCs of large arteries, VSMCs of small resistance arteries and arterioles constrict in response to elevated intraluminal pressure, an effect known as the Bayliss effect (Bayliss, 1902). Myogenic vasoconstriction is independent of the underlying endothelium (Bevan and Laher, 1991) and neuronal innervations and is therefore an intrinsic characteristic of VSMCs of small resistance arteries (Davis and Hill, 1999). Elevated intraluminal pressure causes a gradual depolarization in VSMCs that subsequently results in the opening of voltage-gated L-type calcium channels and increased intracellular calcium causing myogenic constriction (Figure 3) (Schubert and Brayden, 2005). The signaling cascades pertinent to myogenic vasoconstriction have been intensively investigated. Already 20 years ago, a mechanosensitive cation conductance mediated by mechanosensitive non-selective cation channels was recognized and it has been suggested that TRP channels could be the underlying mechanosensitive channels (for review see Sharif-Naeini et al., 2008). However, the hypothesis of inherent mechanosensitive TRP channels could not be substantiated although some TRP channels including vanilloid TRP 2 (TRPV2), canonical TRP 6 (TRPC6) and TRPM4 are known regulators of myogenic vasoconstriction (summarized in Vennekens and Nilius, 2007). Instead of direct mechanical TRP channel activation, TRPC activation was shown to be successive to mechanical activation of $G_{q/11}$ protein-coupled receptors ($G_{q/11}$PCRs) which subsequently signal to TRPC channels in a G protein- and phospholipase C-dependent manner (Mederos y Schnitzler et al., 2008). Importantly, the activation of $G_{q/11}$PCRs by mechanical cues is agonist-independent and results in increased intracellular calcium concentrations. Particularly angiotensin II type 1 receptors (AT_1Rs) are key elements for mechanosensation in VSMCs mediating up to 50% of myogenic vasoconstriction (Blodow et al., 2014). Additional blockage of cysteinyl leukotriene 1 receptors ($CysLT_1$Rs)—another $G_{q/11}$PCR—even added up to a blockage of roughly 60% of myogenic vasoconstriction (Storch et al., 2014). Similar results were found by inhibiting all $G_{q/11}$ protein signaling implying that 40% of myogenic tone is mediated by other mechanosensory elements of unknown identity.

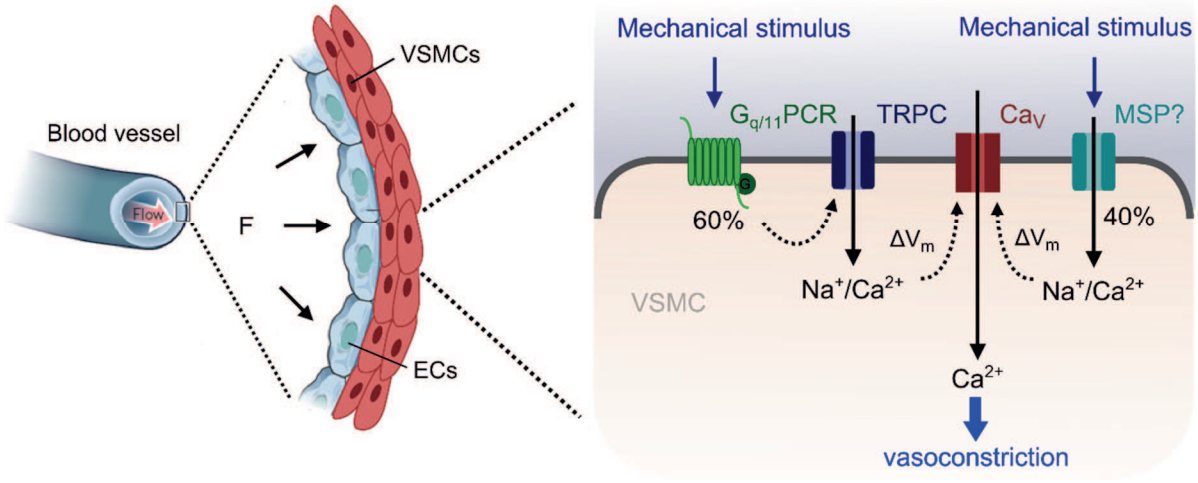

Figure 3: Mechanism of myogenic vasoconstriction. Left: *Image adapted from Hoffman et al., 2011*. Force (F) in the form of the pulsatile blood flow through the blood vessels causes stretching of blood vessel walls that are compromised of endothelial cells (ECs) and vascular smooth muscle cells (VSMCs). Right: In arterial VSMCs vasoconstriction occurs as a result of mechanical activation of $G_{q/11}$ protein-coupled receptors ($G_{q/11}$PCRs) (accounts for 60% of myogenic vasoconstriction) that subsequently activate canonical transient receptor potential channels (TRPCs). 40% of myogenic constriction is mediated by a mechanosensitive protein (MSP) of unknown identity. Activation of TRP channels and MSPs results in depolarizing of cells which in turn activates voltage-gated calcium channels (Ca_V) causing myogenic vasoconstriction.

2. Classifications of mechanical load

Mechanical load is described as a set of external forces acting on a structure. Force can be applied to objects in several ways and can mean normal stress, shear stress or stretch depending on the angle at which the force hits the surface of the object (Figure 4). A classification of different types of mechanical loads is described below.

Pressure or stress is defined as the ratio of applied force F to the surface of an object to the area A over which that force is distributed ($P = F \bullet A^{-1}$). Pressure is usually described in newtons per square meter ($N \bullet m^{-2}$) or pascal (Pa). In physiological context the units barye, equal to 1 dyne • cm^{-2} or 0.1 Pa are often used. Pressure can also be measured by its ability to displace a column of liquid like mercury in a manometer. Displacement of one millimeter of mercury is approximately equal to ≈133.322 Pa. In general, the threshold amount of force needed to evoke a mechanical response within a single cell is thought to be approximately 1 nN (equals appr. 1 Pa • 1000 cm^{-2}) while the critical force exerted on a single molecule is most likely within the few piconewtons range (Huang et al., 2004).

If the force is applied perpendicular to the area the resulting pressure is denoted as normal stress (σ) or direct stress (Figure 4, left). Normal stress can be further classified into tensile stress or compression stress. Tensile stress results when a body is subjected to tow equal

tensile forces resulting in an increase in the body's length. Compression occurs when a body is subjected to two equal and opposite pushes resulting in a decreased body length. The amount of compression and tension depends on the elasticity modulus of the material: Bones are not elastic and have a high elasticity modulus E ≈ 20 GPa while cells have an elasticity modulus of E ≈ 0.1–400 kPa (Kuznetsova et al., 2007; Rho et al., 1993). A physiological example of tension and compression stress applied to cells is the pressure exerted on cardiovascular vessel walls. Endothelial cells and VSMCs feel the pulsatile nature of the beating heart resulting in stretching of the cells. Typical values for pressures exerted on arteries are between <80 mmHg (<11 kPa) diastolic (pressure in the arteries between heartbeats) and 110 mmHg (≈15 kPa) systolic (pressure in the arteries when the heart beats) blood pressure.

If force is not applied normal but tangential or parallel to the surface of the body this stress is denoted as shear stress (Figure 4, right). Shear stress leads to a deformation of the body tilting those edges, which are vertical to the force and can be described as $\tau = F \bullet L^{-2}$ with L being the final length. Shear stress plays an important role in blood flow where the floating blood causes friction with the cell surface thereby resulting in the loss of velocity. Physiological shear stress values vary from 1 to 50 dyne cm^{-2} (0.1–5 Pa) depending on the vessel type (e.g., artery or vein) and the size of the organism (for review see Orr et al., 2006).

Forces applied to an object may result in the deformation of the body if the body is deformable. If the force is applied to a small area, the body will be deflected. Homogenous pressure will result in compression of the body. General terms to describe these deformations are stretch and strain. Stretch is defined as a dimensionless measure of compression (or elongation in case of traction force) of the body in the direction of the applied force and can be described as $\varepsilon = \Delta L \bullet L^{-1}$ with L being the initial length and ΔL being the change in length in direction of the stretch. Strain on the other hand represents a normalized displacement between particles in the body relative to a reference length: $\zeta = (L' - L) \bullet L^{-1}$ with L being the initial length which is stretched to final length L'. Comparing the levels of force with forces with imposed strain is challenging, since the elasticity of the cells and the underlying forces of interaction between the cells and the flexible substrate are usually unknown. However, by assuming the elasticity modulus to be 1 kPa, a stress of 100 Pa is sufficient to produce a 10% strain, a value usually used in stretch experiments (Huang et al., 2004).

Living organisms move. This causes interactions of moving particles with their surrounding. As a result of these interactions cells feel pressure, strain, stretch or stress or combinations thereof (Salameh and Dhein, 2013). Therefore, it might not be possible to experimentally discriminate between the forces living organisms percept. For example, a beating heart will result in pressure thereby stretching the vessel wall and in strain. Additionally, the resulting blood flow will cause a shear stress on the endothelial cells lining the vessels.

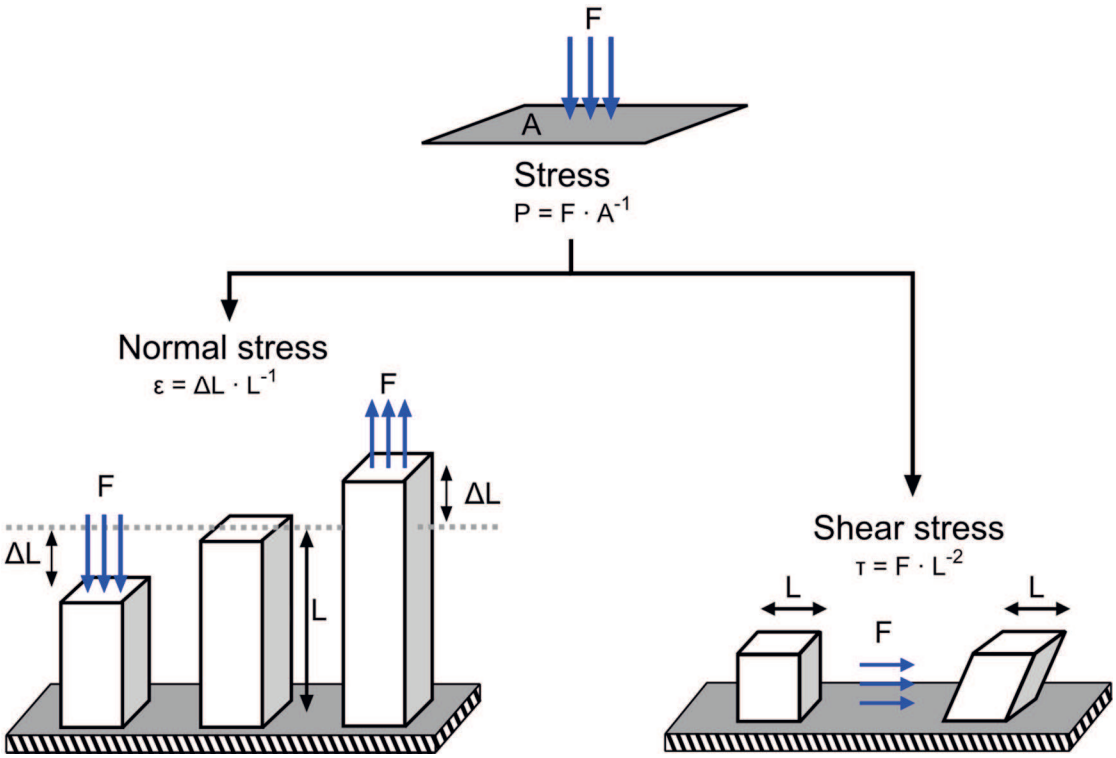

Figure 4: Classification of mechanical load. Mechanical load can be classified into categories according to the angle of the force (F) on the surface of the object. Normal stress describes forces that are perpendicular to the object resulting in pressure (P), while shear stress arises when force is applied tangential or parallel to the surface of the body. Normal stress can be further subdivided into compression stress resulting in a decrease of the body's length (L) (see left bar) and tension stress resulting in an increase of the body's length (see third bar from the left). Application of shear stress leads to tilting of the upper object's corners (see right cube).

3. Hypothetical modes of activation

Mechanical force acts on the plasma membrane thereby altering membrane tension. Since changes in membrane tension are the key driving force for mechanically activated proteins, most proteins that are commonly known as mechanosensitive are integral membrane proteins like ion channels, enzymes or receptors. The plasma membrane is made up by two layers of phospholipids whose hydrophobic tails line up against one another while the hydrophilic heads face the aqueous solution on both sides. As a result hereof, a lipid bilayer has different physical properties at different depths (see Figure 5, upper panel) (Cantor, 1999a). The membrane structure is disturbed by the presence of membrane proteins, which results in reorganization of the lipid bilayer which energetically stabilizes the membrane-bound protein (Figure 5). Hence, when the force profile of the bilayer is altered either by mechanical stretch or by protein displacement, the protein will adopt a new energetically favorable conformation. Two hypotheses describe how integral plasma membrane proteins directly perceive mechanical force: The “membrane model” and the “tethered model” (Figure 5). The “membrane model” or “force-from-lipids model” explains activation of these proteins as a result of an altered lateral pressure profile favoring an alternative conformational state of the mechanoreceptive protein (Figure 5, middle panel) (Cantor, 1999b). Examples for bilayer-gated proteins are the bacterial mechanosensitive channel subunits of large conductance (MscL) and the vertebrate background two pore potassium (K_{2P}) channels TREK-1 and TREK-2. Negative pressure subjected to reconstituted MscL channels in artificial membranes is sufficient to activate MscL, while TREK-1 and TREK-2 retain their mechanosensitivity in cytoskeleton-free membrane blebs, indicating a bilayer-gated mechanism of activation for these channels (Honore et al., 2006). The “tethered model” on the other hand favors the mediation of force through structural proteins. Linking proteins can be intracellular like binding to cytoskeleton, extracellular like binding to the extracellular matrix, or both (Figure 5, lower panel). The best studied example for this mode of activation is the Deg/ENaC complex, which is known to transduce gentle touch in *C. elegans* (for reviews see Brierley, 2010 and Kung, 2005). The Deg/ENaC complex comprises several proteins including the two ion channels MEC-4 and MEC-10, while other proteins like MEC-9 provide a link to the extracellular matrix. MEC-2, MEC-7 and MEC-10 on the internal side link the complex to the cytoskeleton.

Regardless of the mode of activation, the result of the mechanical stimulation is an altered force profile, making it energetically more favorable for the protein to assume a new conformation and hence exhibit a different function. In case of ion channels, this means adopting an ion-permeable conformation, while mechanosensitive GPCRs presumably shift to a conformation allowing for G protein activation. In any case, activation needs to result in downstream signaling events.

Besides directly mechanoperceptive structures, proteins can be indirectly mechanosensitive. Indirectly mechanosensitive structures are activated through a second messenger systems and transduce the mechanical stimuli sensed by upstream mechanosensors into the cell.

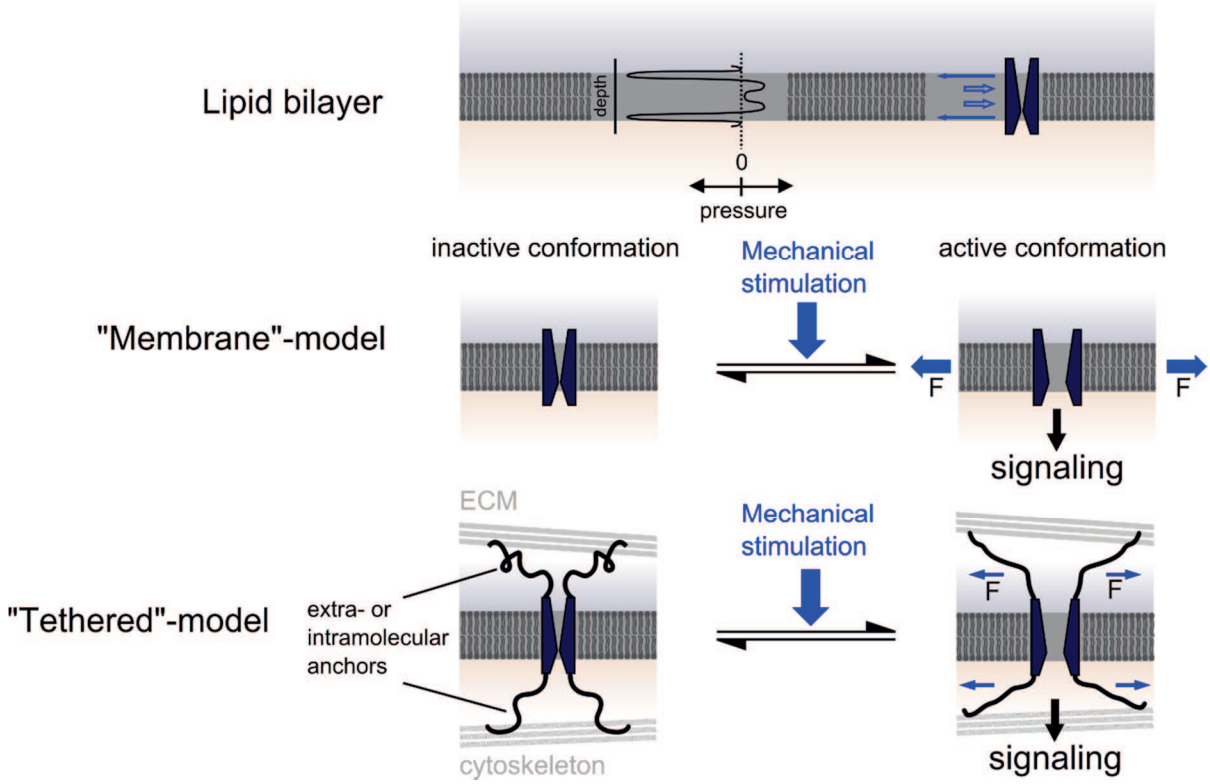

Figure 5: Description of intrinsic forces within the lipid bilayer and possible modes of activation for directly mechanoperceptive proteins. Upper panel: Lateral pressure profile plotted as its direction and magnitude along the depth of the bilayer (left), and a cartoon of a protein in section (right) (Cantor, 1997b). The narrow blue arrows represent the sharp tension near the lipid necks that is balanced by more diffused pressure inside the lipid bilayer (broad arrows). Lower panel: Upon mechanical stimulation the altered pressure profile allows the protein to adopt a more energetically favorable conformation that leads to downstream signaling (right) (For review see Brierley, 2010). The membrane model (second panel) proposes that stretch directly alters the membrane tension and therefore the lateral pressure profile at the protein-lipid interface. The tethered model (third panel) proposes that extra- and intracellular linkers confer direct mechanoperceptive properties to an integral membrane protein.

4. Techniques for mechanical probing of cells

Just like the diversity of agonists that mediate specific agonist-induced signaling, mechanotransducing stimuli, that induce specific downstream signaling cascades, are diverse. Mechanotransducing stimuli include changes in osmolarity, touch, texture, volume, proprioception, vibration and gravity. Understanding the molecular basis for mechanotransduction does not only require knowledge about the magnitude of the applied force but also information about the distribution of forces throughout the cell. Applied forces can be dynamic regarding their strength, duration and orientation and will result in distinct dynamic mechanoresponse. For example, cyclic stretch and static stretch of the same amplitude induce unique mechanoresponses in vascular endothelial cells (Zheng et al., 2008). Additionally, cells in a physiological setting might be subjected to more than one mechanical stimulus at the same time. Experimentally, the application of the right physiological stimulus is therefore a challenging subject. Although a wide variety of mechanical stimuli exist, it is generally accepted that the underlying perception mechanisms must be unified, regardless of the underlying mechanical stimulus. Therefore, the following techniques, though maybe not physiologically matched, have been successfully used to elicit a biological response after mechanical stimulation.

4.1 Patch clamp technique

Mechanosensitive ion channels are commonly analyzed using the patch clamp technique. This technique uses an electrode inside a glass micropipette to seal a lipid surface area or "patch" of a single cell or liposome (Sakmann and Neher, 1984). In this way, single channel recordings can be performed in either the cell-attached configuration, or the outside-out configuration or the inside-out configuration. A complication of the patch clamp technique is that sealing the cells already introduces a resting tension to the patch, which is approximately 3 mN • m^{-1} and equals approximately 30% of the strength needed to rupture a membrane (Sachs, 2010). Thus, all patch recordings are performed under stressed circumstances which can conceal a mechanosensitive ion channel activity due to inactivation of the channels over time.

Electrophysiological characterization of the channel of interest can be done by heterologous or endogenous expression of the channel in a cellular system or by reconstitution of the channel in an artificial lipid environment. A complication regarding measuring mechanosensitive ion channels arises from the fact that basically all cell types endogenously express mechanosensitive ion channels (for reviews see Sachs, 2010 and Haswell et al., 2011). This means that there is no null background when measuring the protein of interest in a cellular system. Therefore, reconstitution of the channel is the ultimate way to prove an inherent mechanosensitivity of ion channels. The mechanical stimulus can now be applied by several means: First, the patch pipette can excise either a negative or positive pressure. In

single-channel recordings, the application of pressure to the underlying patch results in membrane tension (T) thereby altering the lateral membrane pressure profile. An example of an intrinsic mechanosensitive channel successfully measured by application of pressure through the patch pipette is the bacterial MscL channel. It was demonstrated that MscL channels require a membrane tension of 18 mN • m^{-1} close to the force needed to rupture the bacterial membrane in order to open (Sukharev et al., 1997). In this way MscL channels provide a useful pressure relief valve for bacterial cells that are osmotically stressed.

An alternative to the application of pressure in single-cell recordings is the administration of a defined positive pressure through the patch pipette in the whole-cell configuration. In that case, cells will inflate resulting in membrane stretch, thereby possibly activating susceptible mechanosensitive structures. However, inflation of cells frequently causes a disruption of the seal making it a rather inconvenient way to administer mechanical load.

Besides administration of pressure through the patch pipette, the lateral membrane pressure profile can be altered by addition of amphiphilic substances that incorporate themselves into one side of the membrane thereby causing a bending of the lipids surrounding the channel. A commonly used amphiphilic substance is the GsMTx4 peptide isolated from the *Grammostola spatulata* spider. GsMTx4 supposedly suppresses mechanosensitive cation currents by incorporating itself into the lipid bilayer surrounding the channel thereby changing local curvature and mechanically stressing the channel toward the closed state (Suchyna et al., 2004). However, GsMTx4 is also heavily positively charged and could inhibit cation conductance by repelling incoming cations (for review see Bowmann et al., 2007). Unfortunately, GsMTx4 has no effect on mechanosensitive background K_{2P} channels and possibly other mechanosensitive channels leaving the function of GsMTx4 ill defined. Therefore, data obtained with GsMTx4 toxin have to be handled with great caution. Other amphiphilic substances include unsaturated fatty acids like arachidonic acid (AA), the acid aromatic compound 2,4,6-trinitrophenol (TNP) or general anesthetics like chlorpromazine, which have all been successfully used to open mechanosensitive channels (Cantor, 1997a; Martinac et al., 1990; Patel and Honore, 2001). Amphiphilic substances can be a useful tool to study and screen for mechanosensitive proteins, but they are not essential criteria to call a protein mechanosensitive.

A third way to introduce mechanical stress in patch clamping is the use of hypotonic or hypertonic bath solutions resulting in cell swelling or cell shrinkage, respectively. Both methods result in membrane stretch due to altered membrane tension. Cell swelling experiments are commonly used in electrophysiological whole-cell recordings, but can also be applied to cells in different experimental settings. Commonly used stimuli are in the order of Δ50 to Δ200 mOsmol • kg^{-1} (Hua et al., 2010; Mederos y Schnitzler et al., 2008; Spagnoli et al., 2008) which results in approximate osmotic pressure of 1.2 atm (122 kPa) and 4.9 atm (496 kPa)

using the Morse equation at room temperature and assuming that the solute is impermeable to the membrane. However, one should bear in mind that cell swelling means dilution of cytosolic factors like ions and macromolecules which might already be sufficient to affect ion channel function. Furthermore, osmotic stimuli do not generate uniform tension in the lipid bilayer since the curvature of adherent cells is not constant and depends on the cytoskeleton. Finally, a micromanipulator attached to a blunt object that gently touches the plasma membrane can be used in whole-cell recordings. However, data interpretation can be difficult since the compression-induced stress distribution is spatially limited and difficult to analyze on a molecular level and might not reach the locally-restricted mechanotransducing machinery.

4.2 Optical and magnetic tweezers

Other methods to induce mechanical stimuli are optical tweezers, which have been successfully used to overcome the problem of locally restricted mechanotransduction in primary cilium of epithelial cells (Resnick, 2010). Optical tweezers use radiation pressure from a focused laser beam to manipulate small particles. The advantage of optical tweezers is the precise amount of force that can be applied to the trapped particle: Ten to hundreds of piconewtons. In this way, optical tweezers can be used to control particle position, study membrane elasticity and force progression at the molecular scale. The disadvantage is that only one particle at a time can be controlled unless several optical tweezers are used in tandem (Leake et al., 2004).

Magnetic force application using paramagnetic beads is the magnetic counterpart to optical tweezers and allow the application of controlled linear or torque to a particle. Magnetic force application generates constant forces in the range of a few piconewtons and has been successfully used to demonstrate that integrins are more firmly attached to the cytoskeleton than acetylated low density lipoprotein (LDL) receptors (Wang and Ingber, 1995).

4.3 Atomic force microscopy

Atomic force microscopy (AFM) uses a probe consisting of a fine pyramidal tip attached to a cantilever that flexes as the tip pushes onto the surface. In contact mode, the deformation of substrate can be measured by measuring the flexure in the cantilever. AFM typically estimates cell stiffness in the range of hundreds of kilopascals making it a rather imprecise method. However, it is useful for mapping cell heterogeneity, for example, when mapping stiffer structures like focal adhesions (for review see Huang et al., 2014).

4.4 Hydrostatic pressure

The approaches addressed so far primarily apply to single cell experiments. Multiple cell analysis does not focus on mechanisms but rather on downstream effects resulting from

mechanical stimulation. Hydrostatic pressure can also easily subjected to a group of cells by using compressed air or a column filled with fluid above the cells being stimulated. Commonly used hydrostatic pressures are 5 to 30 cmH_20, which translates to approximate pressure values of 0.5 to 3 kPa (Mederos y Schnitzler et al., 2008; Olsen et al., 2011) although much higher pressures of 0.5 to 41 MPa have also been used successfully to show the effect of hydrostatic pressure on calcium influx (Horner and Wolfner, 2008; Mizuno, 2005).

4.5 Silicone-based membranes

Another method allowing application of normal stretch, in the form of tension and compression, to a group of cells can be achieved by growing cells on flexible silicone-based membranes that can be subjected to equibiaxial or uniaxial strain by using a regulated vacuum pressure to deform flexible-bottomed culture plates. Strain rates commonly vary from 0.1 to 10 Hz and the strain percentage ranges from <1% to >20% (Huang et al., 2004). The drawback of this method is its inability to distinguish between stretch and shear stress. Stretching the cells on the silicone membrane inevitable results in turbulences of the culture medium. This makes it impossible to distinguish between shear stress and normal stress.

4.6 Laminar shear stress

Shear stress can be relatively easily introduced to cells by gravity-induced perfusion. A more refined and measurable shear stress can be achieved by perfusion of cells in a fixed chamber. Fluctuations in flow rate can be administered by the use of pump systems. Typical shear stress levels range from 1 to 20 dyne • cm^{-2} (0.1–2 Pa), which has been shown to be the critical level of stress for a variety of biological responses (Huang et al., 2004).

5. Criteria for mechanoperceptive proteins

Criteria for calling a protein mechanoperceptive are not easily found. In contrast to the relatively well characterized mechanosensitive bacterial ion channels, the identification of mammalian ion channels has been more challenging. Eukaryotes may require protein complexes tethering the mechanosensitive protein to the intra- and extracellular matrix. Additionally, proteins may require a different mechanical stimulus than can be applied in experimental laboratory settings. However, the following criteria have been used to call a protein inherently mechanosensitive (Ernstrom and Chalfie, 2002; Mederos y Schnitzler et al., 2011; Morris, 1992):

1. The candidate shows an appropriate temporal and spatial expression.
2. Key components in the process of mechanotransduction are speed and sensitivity. The response time after mechanical stimulation should be fast and comply with physiological reaction times that are usually in the millisecond range (e.g. <5 ms for ion channels, <500 ms for GPCRs and <50 µs for membrane bound enzymes).
3. Intrinsic mechanosensitive proteins should convey the amplitude of the applied pressure as well as its strength resulting in a faster protein response if the stimulus is more intense (Gillespie and Walker, 2001; Storch et al., 2012b). However, the amplitude of the force exerted on the protein should always be in physiological meaningful ranges in order to guarantee adequate mechanosensing function of the candidate.
4. Mechanical stimulation should result in a distinct mechanical correlate of protein activation, for instance a detectable change in conformation.
5. Impairment of the protein function should eliminate or modify the mechanical response. Attenuation of the protein can be performed by mutating key amino acids within the protein, by using candidate-specific blockers, antagonists or inverse agonists or by down-regulation of the protein using molecular biology techniques. It is important to note, that the candidate mechanosensor should be pivotal for sensing the mechanical stimulus but not for subsequent downstream signaling. Hence, removal of the mechanoperceptive protein should eliminate the entire mechanoresponse.
6. Ultimately, to test for intrinsic mechanosensing properties, reconstruction of the candidate into an artificial lipid bilayer should be sufficient to create a mechanotransducing machinery. However, this method has only be applied to mechanoperceptive ion channels so far, since the application of the mechanical stimulus and the measurement of the channel's response can be directly conducted by using the patch clamp technique. However, it should be possible to measure GPCR activation in a lipid bilayer enriched with G proteins using a similar method as well. In

contrast, enzymes should be measured in cell-free enzymatic assay, in which a meaningful and measurable mechanical stimulus can be directly applied.

Recently, the establishment of a force coefficient similar to the Q_{10} value describing changes in the activation rate caused by a temperature increase of 10°C has been proposed (Mederos y Schnitzler et al., 2011). In analogy to the Q_{10} value, the present authors suggest the following to apply a meaningful correlate to the diverse mechanosensors: Ion channels can be monitored by their conductance rate, enzymes by their enzymatic reaction kinetics and GPCR by their G protein activation capability.
Besides directly mechanosensitive structures, proteins can be indirectly mechanosensitive through activation of second messengers, that signal the mechanical event to mechanotransducing proteins. This means that a structure upstream of the mechanotransducing protein is the actual mechanosensor, while the mechanotransducer converts the sensed force into a biological signaling process.

6. Mechanosensitivity influencing factors

A force must be transmitted to mechanosensitive elements before it can be sensed. In the simplest case—as is likely true for bacterial mechanosensitive channel subunits of large and small conductance (MscL and MscS)—application of force results in the deformation of the lipid bilayer altering the lipid membrane tension profile. Altered lipid tension favors a different conformation of the mechanosensitive channels that is accompanied by altered ion conductance properties. This means that modifications done to the composition and curvature of the lipid bilayer will automatically reflect on the function of lipid-bilayer gated proteins. Eukaryotes have developed a refined intra- and extracellular scaffold that supports the plasma membrane and proteins within. Therefore, a key feature of eukaryotic force sensing is that the transduction unit detects deflection of an external structure relative to an internal structure. This means that any modification done to the complex architecture of the mechanosensor including altering the extra- and intracellular matrix, as well as modifications of the lipid bilayer harboring the mechanosensor, will reflect on the function of the mechanosensitive protein. The integrative role of tethers in mechanical units is best studied in the Deg/ENaC ion channel complex. The Deg/ENaC channel pore is made up by the proteins MEC-4 and MEC-10. However, reconstitution of the channel subunits MEC-4 and MEC-10 in heterologous expression systems is not sufficient to obtain a mechanogating channel suggesting the requirement of tethers or other subunits for mechanical gating (Garcia-Anoveros et al., 1998). In fact, it has been convincingly demonstrated that MEC-4 and MEC-10 require auxiliary MEC subunits to form a mechanosensitive ion channel complex. Among the auxiliary MEC subunits are extra- and intracellular proteins including MEC-9, the β-tubulins MEC-7 and MEC-12, and the integral membrane protein MEC-2 (Bianchi, 2007; Bounoutas and Chalfie, 2007; O'Hagan et al., 2005; Wang et al., 2009).

6.1 Role of lipids

The lipid bilayer is a critical environment for membrane proteins and accounts for proteins conformation and function. Glycerophospholipids are the main structural component of biological membranes while minor parts being cholesterol and phosphatidylinositol. The formation of lipid bilayers is an energetically preferred process where the polar head of glycerophospholipids face the aqueous solution and the tail faces tails from inversed glycerophospholipids. As a result hereof, a lipid bilayer has different physical properties at different depths (Figure 5) (Cantor, 1999a). The free-energy reduction in ordering water and lipids at the interface is reflected in a large surface tension between the lipids polar head groups and the non-polar tails. However, pressure nearby serves to balance this tension, allowing the bilayer to self-assemble into a stable structure. This structure is disturbed by the presence of proteins in the proximity of lipids. Hence, altering the force profile by membrane

stretch or by lipid or protein displacement may make it more energetically favorable for the protein to adopt a different conformation. Besides external force, the composition of the membrane itself can alter the force profile. The prokaryotic MscL channel has been shown to be rather unselective regarding its lipid environment; MscL functions in bilayers made of ordinary lipids with charged or uncharged head groups, saturated or unsaturated tails and in various mixtures. However, application of cone-shaped amphiphilic substances such as AA results in the distortion of the membrane profile which modified the activity of MscL and MscS channels (Martinac et al., 1990). Other ways to alter the membrane force profile would include solubilization of the membrane, addition of lipid-soluble agents like the anesthetics procaine and tetracaine or heat-induced bilayer rearrangement (for review see Yoshimura and Sokabe, 2010).

Changing the lipid composition might also alter the electrical charge of the membrane. For example, depletion of phosphatidylinositol (3,4)-bisphosphate (PIP_2) into phosphoinositol phosphate (PIP) decreases the negative surface potential of the plasma membrane. This in turn can affect the proximate cation environment thereby affecting conformation and adaptation of mechanosensitive proteins (Hirono et al., 2004).

6.2 Role of the cytoskeleton

The cytoskeleton is composed of filaments, such as F-actin, intermediate filaments and microtubules. The cytoskeleton and proteins residing within the membrane are known to reciprocally influence each other (for review see Herve, 2014). Altering cytoskeletal properties will therefore ultimately affect mechanosensitive proteins in the plasma membrane as well. Cytoskeletal filaments are stable over minutes and hours thereby providing a mechanical continuity to the mechanosensing machinery. This continuity allows forces to propagate relatively long distances within the cells, although the general trend for forces is to decrease over distance. For instance, mechanical pulling at integrins has long-distance effects, which are transmitted by F-actin, microtubules and intermediate fibers (Hoffman et al., 2011; Matthews et al., 2006). On the one hand, tethering elements to the cytoskeleton is needed to provide structure to transduction units; on the other hand, stretching of actin stress fibers can also activate channels on the plasma membrane itself. By using optical tweezers, Hayakawa et al. (2008) could activate mechanosensitive channels near focal adhesions in cultured human umbilical vein endothelial cells. This study provides direct evidence that the cytoskeleton works as a force-transmitting device to activate channels in eukaryotic cells. To the contrary, cortical F-actin cytoskeleton can also exert a tonic inhibitory effect on mechanosensitive ion channels presumably by decreasing the radius of curvature of microdomains, leading to a decrease in membrane tension and stretch-activated channel activity (Hamill and McBride, 1997). Actin-mediated decrease in mechanosensitivity has been shown for the TWIK-related arachidonic

acid-stimulated potassium channel (TRAAK), that becomes more sensitive to mechanical stimulation once the actin cytoskeleton is disrupted (Maingret et al., 1999a).

6.3 Role of the extracellular matrix

Extracellular matrix proteins are primary molecules in vertebrate cells that provide structural and biochemical support to cells thereby regulating many cell processes like focal adhesion, cell-to-cell communication, differentiation or transition and absorption of mechanical load. Integrins are heterodimeric glycoproteins that span the membrane and link the extracellular matrix to the intracellular environment. Integrins have been implicated in multiple mechanotransduction processes including response to stretch, elevated hydrostatic pressure, fluid shear stress and osmotic forces (for review see Katsumi et al., 2004). Whether integrins act as direct mechanosensors or whether they function as transducer of the mechanical force is still under debate. Additional facets arise from numerous studies showing that increasing the force on integrin-containing adhesions results in the strengthening and enlargement of the adhesions (for review see Schwartz and DeSimone, 2008). This process involves conformational changes of the integrins themselves as well as recruitment of cytoskeletal proteins to the integrin-mediated connection, thus further increasing the difficulty to pinpoint the physiological role of integrins in mechanosensation.

Next to integrins, the one transmembrane spanning cadherins have also been implicated in mechanosensing. Cadherins appear to possess the features needed for force-dependent adhesion strengthening similar to integrins (for review see Schwartz and DeSimone, 2008).

7. Candidates for mechanosensitive proteins

The mechanism of mechanosensation has originated very early in evolution and is already present in bacteria and archaea. In these organisms, mechanosensitive channels are needed to protect the cells from osmotic shock. In higher organisms, highly specialized sensory cells are involved in the sensation of hearing, proprioception and touch. But every cell seems to be capable of mechanical stress sensation and integration of the stimulus into short-term and long-term effects. There is growing evidence that a wide array of membrane-bound proteins are involved in mechanosensation including GPCRs, integrins, membrane-bound enzymes and ion channels (Figure 6). The following section provides an overview over the latest literature of proteins involved in mechanosensation.

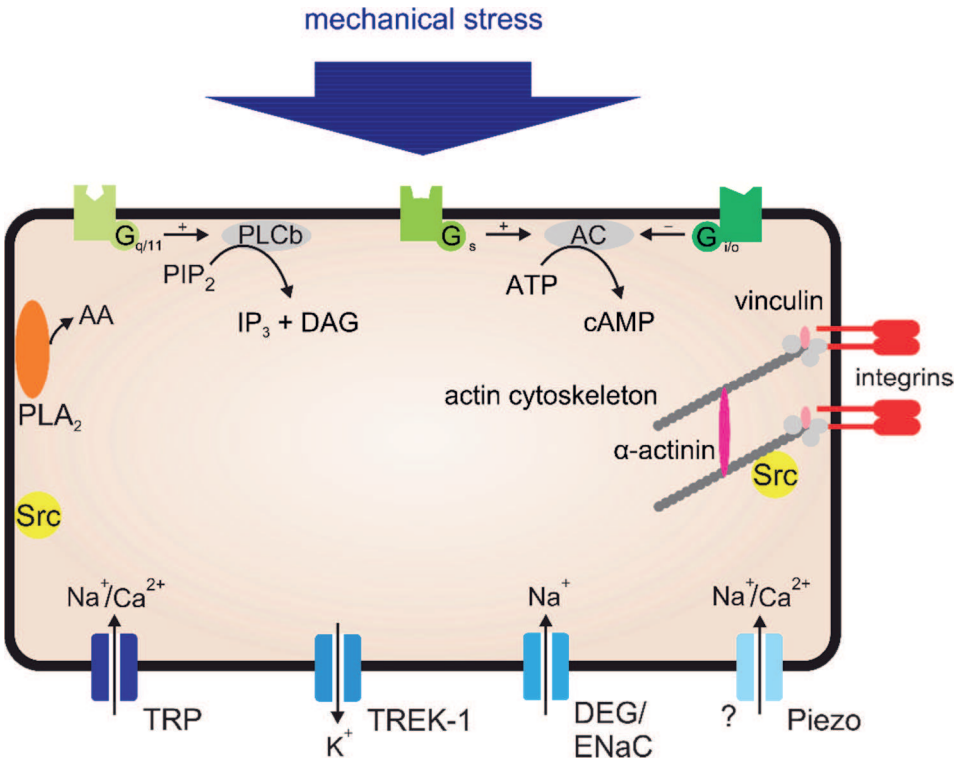

Figure 6: Potential mechanosensors in different cell types. *Adapted from Storch et al., (2012).* These proteins have been proposed to be activated by membrane stretch or by fluid shear stress. Possible mechanosensors are highlighted in color and non-mechanosensitive proteins in gray. Abbreviations: TRP = transient receptor potential; $G_{q/11}$PCRs = $G_{q/11}$ protein coupled receptors; PLC = phospholipase C; PLA_2 = phospholipase A_2; AA = arachidonic acid; AC = adenylyl cyclase; PIP_2 = phosphatidylinositol 4,5-bisphosphate; IP_3 = inositol trisphosphate; DAG = diacylgylcerol; Src = Src tyrosine kinase; cAMP = adenosine 3-,5-cyclic monophosphate; ATP = adenosine-5-triphosphate; Piezo = Piezo1 and Piezo 2, a newly discovered mechanosensitive cation channels; TREK-1 = TWIK-related potassium channel; Deg = degenerin; ENaC = epithelial sodium channel.

7.1 G protein-coupled receptors

GPCRs are a huge class of seven transmembrane spanning receptors that sense outside stimuli and convert them to intracellular signals. Mammalian genomes encode more than 1000 GPCRs. Most of them transduce sensory stimuli like olfactory and gustatory stimuli, while others can be activated by light, hormones, neurotransmitters, or paracrine factors. Activation of GPCRs causes conformational changes in the GPCR resulting in activation of the associated heterotrimeric G proteins. Depending on the coupled G_α protein (G_s, $G_{q/11}$, $G_{i/o}$, $G_{12/13}$), the activated guanosine-5'-triphosphate (GTP)-bound G_α-subunit subsequently dissociates from the βγ-subunit resulting in distinct intracellular signaling. GPCRs have various functions in many physiological processes like inflammation, cell growth and differentiation (for review see Wettschureck and Offermanns, 2005). Recently, GPCRs have been appreciated as mechanosensitive proteins. Best characterized is the $G_{q/11}$-coupled angiotensin II receptor (AT_1), which was shown to be activated by an agonist-independent pathway upon mechanical stimulation thereby mediating stretch-induced hypertrophy in cardiac myocytes (Zou et al., 2004). Additionally, AT_1 receptors were identified as mechanosensors mediating myogenic tone (Mederos y Schnitzler et al., 2011; Mederos y Schnitzler et al., 2008). Growing evidence points to GPCRs as intrinsically mechanoperceptive proteins, since studies using inter- and intramolecular Förster resonance energy transfer (FRET) showed that GPCRs adopt a different conformation upon mechanical stimulation (Candelario, 2012, Chachisvilis et al, 2012, for review see Mederos y Schnitzler et al., 2008). For instance, the $G_{q/11}$ protein-coupled bradykinin B_2 receptor expressed in bovine aortic endothelial cells was shown to change its conformation upon application of hypotonic solution or shear stress (Chachisvilis et al., 2006). Similar results have been found for many other GPCRs including the G_s- and $G_{q/11}$ protein-coupled parathyroid hormone type 1 receptor (PTH_1R) (Zhang et al., 2009). Activation of proteins by mechanical forces and agonists may or may not activate distinct protein conformations and thereby activation of different downstream signaling cascades. For the AT_1, the mechanically induced conformation was distinctly different from its agonist-induced conformation when modeled after the rhodopsin crystal structure (Yasuda et al., 2008). In another study, it was shown that G protein activation was not essential for mechanically induced activation enhancing the notion that GPCRs have distinct mechanically and agonist-induced receptor conformations (Rakesh et al., 2010).

7.2 Membrane-bound enzymes

Key components in the process of mechanotransduction are speed and sensitivity. Most enzyme reaction rates are several orders of magnitude faster than the time needed to activate receptors or ion channels. Therefore, it seems reasonable that enzymes are primary targets of mechanical forces since they can rapidly convert mechanical stimulus into an adaptive

response. Until now, several enzymes have been implicated in mechanoperception including the membrane-bound phospholipase A_2 (PLA_2), phospholipase C and D (PLC and PLD) and tyrosine kinases of the Src family.

PLA_2 catalytic activity was shown to be modulated by osmotic swelling of large unilamellar vesicles (Lehtonen and Kinnunen, 1995). Additionally, it was shown that PLA_2 was mechanically activated in human embryonic kidney (HEK293) cells and aortic myocytes leading to a TRPC6 activation in presence of the muscarinic type 5 receptor (Inoue et al., 2009). In skeletal muscles, direct mechanical activation did not only activate PLA_2, but also PLD while PLC could not get activated with direct mechanical stimulation (Vandenburgh et al., 1993). In contrast to the findings in skeletal cells, PLC could get activated in cerebral rat arteries using increased vascular pressure (Jarajapu and Knot, 2002) as well as in mesangial cells using helium gas to generate pressure in a sealed chamber (Kato et al., 1999). Pressure-induced activation in mesangial cells did not only modulate PLC but also tyrosine kinase activity. While PLC is probably indirectly activated by mechanical stimulation through activation of $G_{q/11}$PCRs, the mode of PLA_2.activation remains to be investigated.

The tyrosine kinase of the Src family has also been implicated in mechanoperception. Src is a known regulator of the integrin-cytoskeleton interaction and was mechanically activated in mesangial cells by pressure and human umbilical vein endothelial cells by using optical tweezers (Wang et al., 2005). Additionally, cell swelling-mediated contraction of tail arteries isolated from rats was shown to be Src-dependent. However, neither heterologous nor endogenous expression of Src was sufficient to cause a mechanotransducing effect in HEK293 cells (Mederos y Schnitzler et al., 2008). Therefore, it remains to be investigated whether tyrosine kinases play a role as direct or indirect mechanosensors.

7.3 Ion channels

Fast mechanosensitive responses are commonly thought to be directly mediated by mechanosensitive ion channels since the transduction time is too rapid to involve secondary messengers. Ion channels open with a latency of less than 5 ms and amplify the signal by conducting various ions (Arnadottir and Chalfie, 2010). Genetic screens and localization studies in bacteria and simple organisms like *C. elegans* and *Drosophila* have led to important progress in the identification and understanding of the molecular basis of mechanosensation. These studies have identified several ion channels including the MscL, Deg/ENaC and TRP channels as molecular components of mechanotransduction units, which directly perceive mechanical stimuli. However, the identification of mammalian mechanosensitive channels has been far more challenging, because mammalian channels might require a complex architecture of auxiliary subunits. Additionally, application of a physiologically matched stimulus in laboratory settings is difficult. Despite the difficulties, recent years have shed light

on the identity of mammalian mechanosensitive ion channels like Piezos and TMC proteins, although mechanical gating mechanisms of mechanosensitive ion channels are still largely elusive. An overview of all candidates presented here, their mode of mechanical activation including the relevant literature is given in Supplementary Table 1.

Bacterial channels

The first characterized channels directly gated by mechanical stimuli are the bacterial ion channels MscL (large conductance mechanosensitive channel with 3 nS), MscS (small conductance mechanosensitive channel with 1 nS) and MscM (mini conductance mechanosensitive channel with 0.3 nS). MscL and MscS begin to open at membrane tensions of 9.0 and 5.0 $mN \cdot m^{-1}$, respectively (Sukharev, 2002). This tension is close the tension needed to rupture the bacterial membrane. Therefore, these channels are likely needed to relieve turgor pressure upon osmotic shock. The best characterized channel MscL shares no sequence homology with known voltage-gated or ligand-gated ion channels although many bacteria and archaea express it. The crystal structure of MscL was resolved in the closed state by X-ray crystallography to 3.5 Å and showed that MscL has two transmembrane domains (TMs). Both N- and C-terminus face the cytoplasmatic side (Chang et al., 1998). MscL arrange itself into pentamers. The open state of MscL has a large water filled pore of 25 Å in diameter that is lined by all five TM1 subunits. Several studies showed that MscL undergoes a large conformational change and likely opens like the iris of the lens, such that TM1 helices tilt with respect to the membrane plane and causes the channel to flatten (Betanzos et al., 2002; Perozo et al., 2002a). The mechanism of mechanotransduction is still unknown but clearly depends on local and global asymmetries in the membrane tension profile at the lipid-protein interface. Studies that varied the thickness of the bilayer or added compounds that induce spontaneous membrane curvature directly impact the tension required to open MscL (Perozo et al., 2002b). Additionally, mutating amino acids that contribute to the protein-lipid interactions resulted in a loss-of-function phenotype (Yoshimura et al., 2004). These data support the hypothesis of a directly lipid-dependent mechanogated ion channel that does not depend on anchorage to extra- or intracellular components in order to sense mechanical stimuli. In contrast to MscL, the MscS channel is voltage-dependent (Martinac et al., 1987). The crystal structure of an open state MscS at a 3.9 Å resolution revealed that the channel is a heptamer, with each subunit containing three TMs. TM3 lines the pore of the channel, whereas TM1 and TM2 helices likely constitute the sensors for membrane tension and voltage (Bass et al., 2002). More specifically, membrane-embedded arginines in TM1 and TM2 are likely candidates for tension and voltage sensors. Although the structure and function of MscL and MscS are not yet fully understood, they provide useful information about mechanotransducing mechanisms, but unfortunately there is no eukaryotic counterpart.

Degenerin/Epithelial sodium channels

Another well-studied mechanosensitive ion channel comes from the Deg/ENaC family. In vertebrates, amiloride-sensitive ENaCs are hetero-oligomers of unknown stoichiometry. In most epithelia, it is composed of α-, β- and γ-subunits which share 30% sequence identity (Duc et al., 1994). The secondary structure and membrane topology contains two transmembrane domains TM1 and TM2 with intracellular N- and C-termini and is therefore similar to those of bacterial MscL and the adenosine 5'-triphosphate (ATP)-gated purinergic channels (Arnadottir and Chalfie, 2010). ENaC channels are expressed in many different organs and tissues, where they fulfill various functions including acid sensing (Kellenberger and Schild, 2002).

Deg/ENaC is a mechanosensitive ion channel complex, that was first discovered in *C. elegans* larvae, that were impaired in the sensation of gentle touch (Chalfie and Sulston, 1981). The conducting ion channels are composed of the proteins MEC-4 and MEC-10, which contribute to the pore of the channel complex. MEC-4 and MEC-10 cluster with their associated components, that are evenly spaced along the worm's microtubular processes. Among the MECs are extracellular proteins like MEC-9, which are thought to act as the gating spring, the β-tubulins MEC-7 and the α-tubulins MEC-12 and the integral membrane protein MEC-2. MEC-2 belongs to the stomatin family and contains several PDZ domains and is thought to connect the channel to microtubules (Bianchi, 2007; Bounoutas and Chalfie, 2007; O'Hagan et al., 2005; Wang et al., 2009). A sequence homology of the gating channels MEC-4 and MEC-10 with the bacterial MscL or MscS channels was not found, though a structural homology is likely. However, a crystal structure of the MEC complex is not yet available.

The identification of MEC-4 as a mechanotransduction molecule has led to the hypothesis of a general Deg/ENaC channel mechanosensitivity. Although several candidates have been proposed, evidence regarding the mechanoregulating role of ENaC is conflicting (Arnadottir and Chalfie, 2010). The *Drosophila* Deg/ENaC protein *pickpocket1* has also been proposed as a mechanosensory protein (Arnadottir and Chalfie, 2010). The protein is located in sensory dendrites of mechanoreceptors, but loss of *pickpocket1* did not result in a touch-insensitive phenotype (Ainsley et al., 2003). Instead, loss of *pickpocket1* caused an increase in crawling speed and an unusual straight path, suggesting a role of *pickpocket1* in proprioception (Ainsley et al., 2003; Arnadottir and Chalfie, 2010).

The data regarding mammalian ENaC channel is contradictory: while some groups reported mechanical activation of reconstituted ENaC in liposomes (Awayda et al., 1995), later studies could not verify these results (Awayda and Subramanyam, 1998). It is clear however, that mammalian ENaC activity can be modulated by mechanical stimulation in particular by fluid shear stress in the kidney (Althaus et al., 2007; Carattino et al., 2004; Satlin et al., 2001; Shi et al., 2011). However, the response time to shear stress was in the range of several seconds (Carattino et al., 2004) arguing against a direct mechanosensitivity of ENaC.

Other ENaC channel family members, that were suggested to have mechanosensitive properties, belong to the acid-sensing ion channels (ASICs) family. Several studies using various combinations of ASIC1, ASIC2 or ASCI3 gene-deficient mice showed that transgenic mice without any ASIC currents were more sensitive to mechanical and chemical pain, supporting only a regulatory role of ASIC channels in mechanotransduction (Mogil et al., 2005; Page et al., 2005; Price et al., 2001). Altogether, while the function of Deg/ENaC in *C. elegans* as mechanoperceptive ion channel complex has been convincingly shown, the function of mammalian ENaC channels is much less convincing. It is possible that mammalian ENaC channels have lost their mechanoperceptive properties during evolution or the studies provided so far have not yet matched the circumstances required for proper mechanoperception of mammalian ENaC channels.

Volume regulated anion channel

Volume regulated anion channels (VRAC), also known as volume sensitive organic anion channels (VSOACs) and volume activated chloride channels (VACCs) are activated by cell swelling thereby counteracting the osmotic imbalance between interior and exterior milieu. VRACs are ubiquitously expressed by mammalian cells and can be measured electrophysiologically as large conductance chloride channels that are dependent on intracellular ATP (Nilius et al., 1996). The molecular identity of VRAC has long been elusive and various proteins have been proposed as molecular candidates for VRACs including chloride channel protein 2 and 3 (ClC-2 and ClC3), membrane protein phospholmann, chloride conductance regulatory protein (I_{Cln}) and P-glycoprotein. All of which have been excluded as VRAC over time (summarized in Nilius and Droogmans, 2003, Nilius et al., 2000 and Nilius et al., 1996).

However, two independent recent studies provided convincing evidence of the new chloride channel family leucine-rich repeat–containing 8 (LRRC8) as an essential component of VRAC (Qiu et al., 2014; Voss et al., 2014). To identify VRAC, both studies used a ribonucleic acid interference (RNAi) fluorescence assay for hypotonicity-induced iodide influx. Only short hairpin RNA (shRNA) against LRRC8A could robustly suppress VRAC activity in both studies. LRRC8A has four closely related homologs (LRRC8B to LRRC8E), which all have four predicted transmembrane domains (N- and C-terminal reside inside). Interestingly, overexpression of LRRC8A rather decreased VRAC activity, prompting Voss and coworkers (2014) to investigate heteromeric channel assembly. Interestingly, only disruption of the LRRC8A gene or simultaneous disruption of multiple LRRC8 genes did abolish VRAC currents. In cells with no functional copy of either LRRC8 isoform, VRAC activity was completely abolished and could not be rescued by overexpression of LRRC8A. Reconstitution of currents with similar anion permeability as VRAC was only observed when LRRC8A was

co-expressed with either LRRC8C or LRRC8E. Like VRAC currents, LRRC8 proteins are found in vertebrates but not in other phyla such as arthropod, supporting the hypothesis of LRRC8 being an essential component of VRAC. Qiu et al. (2014) provided additional evidence of LRRC8A indeed being part of the VRAC channel pore and not an indirectly-regulating subunit: A threonine at position 44 within LRRC8A strongly suppressed VRAC currents when modified. Both studies provide strong evidence for LRRC8 being at least a regulatory subunit of VRAC: First, LRRC8A expression is essential for endogenous VRAC currents in various cell types. Second, LRRC8A is expressed in the plasma membrane and is broadly expressed in animal cells as would be expected from an ubiquitously expressed channel. Third, the point mutation T44 alters VRAC pore properties. However, additional research is needed to support the hypothesis of LRRC8A being part of the pore unit instead of being a regulatory subunit, and to investigate how LRRC8 proteins sense volume changes. So far, it is unclear whether LLRC8A responses to changes in macromolecular crowding, to changes in ionic strength over the membrane or to altered lateral pressure profiles.

Piezo channels

Recently, two new proteins named Piezo1 and Piezo2 (also known as Fam28a and Fam28b respectively) were suggested to be the first eukaryotic mechanically activated cation channels (Coste et al., 2010). Piezos are integral membrane proteins that span the membrane 24 to 36 times and are highly evolutionary conserved. Piezos are widely expressed in various tissues including bladder, colon, skin and lung (Coste et al., 2010). Piezo was found using an RNAi approach that screened cells patched in the whole-cell configuration and subjected to force applied via a piezo-driven probe. Knock-down of Piezo1 caused a pronounced decrease of the observed currents (Coste et al., 2010). Overexpression of Piezo1 and its homologue Piezo2 in HEK293 resulted in large mechanically activated currents very similar to the endogenous currents observed in earlier cell lines. In order to confirm that Piezo1 is indeed part of the channel pore and not an auxiliary subunit, the group of Patapoutian (2012) successfully blocked Piezo1-mediated currents with ruthenium red. Furthermore, they demonstrated that Piezo1 assembles into tetramers with no evidence of an additional protein being present in this complex (Coste et al., 2012). These data support the notion of Piezo1 indeed being a novel mechanosensitive cation channel. Furthermore, reconstitution of Piezo1 in artificial bilayers formed a ruthenium red-sensitive cation-permeable channel (Coste et al., 2012). *Drosophila melanogaster* flies deficient of their only Piezo copy dmPiezo were shown to be insensitive to noxious stimulation that ranged from 2 to 60 mN demonstrating a severe response deficit (Kim et al., 2012). However, knock-out of dmPiezo was not sufficient to completely abolish nociception, which could only be achieved by double knock-out of dmPiezo and the ENaC channel *pickpocket1* (Kim et al., 2012). Recently, it was shown that Piezo1 might be activated

by fluid shear stress as well. Ranade et al. (2014) showed that Piezo1 is essential for vascular remodeling, since loss of Piezo1 in mice is embryonic lethal due to defects in vascular development. Altogether, evidence points to Piezo1 being a direct mechanoperceptive ion channel for the following reasons: First, Piezo1 is expressed in sensory tissues like lung, bladder or skin and in sensory cells like Merkel cells and sensory neurons. Second, overexpression of Piezo1 results in mechanically activated channel activity with distinct biophysical and pore-related properties while knock-down of Piezo1 channels abrogates endogenous mechanosensitive ion channel activity. Third, isolated Piezo tetrameric complexes do not contain detectable amounts of other channel-like proteins and are pore-forming by themselves. Finally, purified Piezo1 reconstituted into artificial lipid bilayers gives rise to cation conductance.

While the above mentioned studies strongly support the notion of Piezo1 being an inherent mechanoperceptive ion channel, the mechanosensitive characteristics of Piezo2 are less understood. Several studies demonstrated the importance of Piezo2 in the sensation of touch and proprioception (Coste et al., 2013; Eijkelkamp et al., 2013; Ikeda and Gu, 2014; Schrenk-Siemens et al., 2014; Woo et al., 2014), but insight into the gating mechanisms is still lacking. Woo et al. (2014) reported that mice deficient of Piezo2 in the skin showed reduced firing rates upon mechanical stimulation and decreased behavioral response to gentle touch. Likewise, Ikeda and coworkers (2014) demonstrated that Merkel cells in rat whisker hair follicles are responsive to mechanical stimulation that were dependent on Piezo2. Next to Merkel cells, Piezo2 is expressed in both nociceptors and low threshold mechanoreceptors (LMTRs). Schrenk-Siemens et al. (2014) recapitulated sensory neuron development *in vitro* and generated LTMRs from human embryonic stem cells (hES) and inducible pluripotent cell-derived neurons (iPS). Rapid membrane indentation elicited robust rapidly adapting currents in hES cell-derived or iPS cell-derived neurons (Schrenk-Siemens et al., 2014). These currents could be blocked by ruthenium red and were absent in Piezo2$^{-/-}$ neurons. All above mentioned studies suggest that Piezo2 is essential for fast mechanotransduction in touch receptors. However, in contrast to Piezo1, Piezo2 seems to depend on the integrity of the cytoskeleton for proper mechanical gating. Eijkelkamp et al. (2013) showed that disruption of the actin- or microtubule cytoskeleton increased the threshold for Piezo2 activation. To the contrary, Piezo2 currents could be potentiated by activation of the cAMP-sensor Epac1, or by increased intracellular calcium concentrations (Eijkelkamp et al., 2013). *In vivo* data from this research group demonstrated that the Epac1-Piezo2 axis induces long-lasting allodynia that is prevented by the knockdown of Epac1 and attenuated by mouse Piezo2 knock-down. Piezo2 knock-down also enhanced thresholds for light touch, a phenotype inconsistent with the hypothesis of Piezo2 being a mechanosensor in touch neurons although it clearly indicates the importance of Piezo2 in touch and pain sensation. Recently, two gain-of-function mutations of

mutations in Piezo2 in patients with Distal Arthrogryposis Type 5 (DA5) were found by Coste et al. (2013). The authors suggest that DA5 is likely the result of altered behavior of stretch sensors like muscle spindles and Golgi tendon organs that are important for proprioception and muscle tone due to Piezo2 over-activation confirming a role of Piezo2 in sensory perception.

In summary, the data for a direct mechanoperceptive Piezo2 channel seems less convincing when compared to its homologue Piezo1: First, although Piezo2 expression results in mechanosensitive ion channel conduction and Piezo2 is expressed in sensory neurons like DRG and Merkel cells, knock-down of Piezo2 alters—but not abolishes—the sensation of touch and pain. Second, Piezo2 function is dependent on the integrity of the cytoskeleton suggesting that Piezo2 function requires auxiliary subunits. This argues against Piezo2 as an inherently mechanoperceptive ion channel. Future research will have to show if and how Piezo2 responses to pressure or whether additional regulatory subunits are required.

Transmembrane channel-like proteins

Tmc1 and *tmc2* genes encode integral membrane proteins containing six transmembrane domains and cytosolic N- and C-termini with a topology much like the K_v- and-TRP superfamily (Labay et al., 2010). TMC1 is expressed in mouse vestibular and cochlear hair cells and localizes to stereocilia tips while TMC2 is only expressed in vestibular systems in adult mice (Kawashima et al., 2011). Mutations of TMC1 are known to cause hearing loss in humans and mice, but there is no evidence of vestibular dysfunction associated with TMC1 (Kurima et al., 2002; Vreugde et al., 2002). This led to the hypothesis of TMC1 proteins being the transducing channels in inner ear hair cells. Recent findings in *C. elegans* TMC1 mutant worms support the notion of TMC1 proteins being non-selective cation channels when heterologously expressed in cells (Chatzigeorgiou et al., 2013). However, the *Beethoven* (*Bth*) and *deafness* (*dn*) mutations in TMC1 present normal mechanotransduction currents in mouse inner hair cells (Marcotti et al., 2006) while double TMC1- and TMC2-deficient mice are deaf and have a profound vestibular dysfunction (Kawashima et al., 2011). Interestingly, exogenous expression of either TMC1 or TMC2 rescued mechanotransduction of double-deficient mice indicating a functional redundancy of TMC1 and TMC2 proteins that may have accounted for normal mechanotransduction in *Bth*- and *dn*-mutations in TMC1. To investigate the hypothesis that TMC1 or TMC2 are indeed components of the cation conduction channel in hair cells, Pan et al. (2013) recorded currents from cochlear mouse hair cells with altered TMC expression. Single disruption of either *tmc1* or *tmc2* genes only suppressed current amplitudes while double disruption completely abolished mechanotransduction confirming a redundancy of TMC1 and TMC2. Interestingly, cells with a *Bth*-mutation (substituting methionine to lysine at residue 412) in TMC1 and no functional copy of TMC2 had higher current amplitudes. These

findings suggest that the *Bth*-mutation in TMC1 is a change-of-function mutation with altered core properties. Indeed, significant reductions in calcium permeability and adaptation time constants were observed in inner hair cells carrying the *Bth*-mutation. The higher current amplitudes found in whole-cell recordings are likely due to the higher expression of *Bth*-TMC1 channels. But how is TMC1 activated in hair cells? This question is still open, although a study from Chatzigeorgiou et al. (2013) showed in *C. elegans* that TMC1-deficient worms are impaired in salt-avoidance but had normal responses to touch, hypertonicity and chemical repellents, indicating a specific role in salt sensation rather than a role in mechanosensation.

In summary, the TMC-disruption and -mutation studies in mice support the notion that TMC1 proteins are regulatory components of the mechanosensitive hair channel. However, studies using reconstituted TMC1 channels subjected to mechanical stress are lacking, questioning whether TMC1 is indeed inherently mechanoperceptive. To the contrary, the findings in *C. elegans* argue against TMC1 as direct mechanosensor involved in the sensation of touch or osmolarity.

Potassium two pore channel family

The tandem K_{2P} has four predicted transmembrane domains with intracellular N- and C-termini. K_{2P} channels contain two putative pore forming regions and form hetero- and homodimers (Honore, 2007). Three family members are likely sensitive to membrane stretch: TREK-1 (TWIK-Related potassium channel 1), TREK-2 (TWIK-Related potassium channel 2) and TRAAK (TWIK-related arachidonic acid-stimulated potassium channel).

TREK-1 ($K_{2P2.1}$) is a background outward rectifier potassium channel widely distributed in multiple tissues with high levels in several brain regions including the olfactory bulb, the hippocampus and the cerebellum. Initial reports demonstrated that membrane stretch elicits TREK-1 activity in the cell-attached configuration as well as in inside-out patches with a half-maximal activation of -23 mmHg stretch (Patel et al., 1998). The latency of activation is a few milliseconds, suggesting that TREK-1 channels are likely directly gated by mechanical stimuli. Furthermore, insertion of the polyunsaturated fatty acid AA into one side of the membrane elicits channel opening in a PLA_2-independent manner. Next to membrane stretch, TREK-1 can also get activated using laminar shear stress and by changes in osmolarity (Patel et al., 1998). Interestingly, the TREK-1 pressure-activation curve can be shifted to the left by internal acidification leading to constitutive channel opening at atmospheric pressure under mild internal acidification (Maingret et al., 1999b). Two independent researcher groups reconstituted TREK-1 channels into liposomes (Berrier et al., 2013; Brohawn et al., 2014). While Berrier et al. (2013) found that TREK-1 was already fully activated when measured in inside-out patches and could be completely and reversibly closed by positive pressure, Brohawn and coworkers (2014) reported reversible activation of purified TREK-1 channels in

proteoliposomes by positive and negative pipette pressure regardless of the orientation of the channels inside the lipid bilayer with very low mechanical threshold (0.5–4 nN • m^{-1}). Physiologically, the mechanosensitivity of TREK-1 channels might be needed to balance the action of a yet unknown depolarizing mechanosensitive ion channel involved in touch sensation. This would explain why TREK-$1^{-/-}$ mice are more sensitive to low threshold mechanical stimuli and display an increased thermal and mechanical hyperalgesia (Alloui et al., 2006). The activity of both mechanosensors would determine the mechanical sensation and the sum of both mechanosensor responses would regulate the downstream effect (Alloui et al., 2006).

Like TREK-1, TREK-2 ($K_{2P10.1}$) is an outward rectifying background potassium channel that is expressed mainly in cerebellum, spleen, and testis. A number of cell types, including cerebellar granule neurons, dorsal root ganglionneurons and cortical astrocytes express TREK-2, where TREK-2 stabilizes the resting membrane potential. TREK-2 shares a 65% sequence homology with TREK-1. TREK-2 channels exhibit small and large conductance phenotypes, but both phenotypes are strongly stimulated by AA, intracellular acidification and membrane stretch with an half open probability of approximately -50 mmHg in inside-out and cell-attached patches (Bang et al., 2000). Like TREK-1, TREK-2 is more susceptible to negative pressure suggesting that a specific membrane deformation (convex curving) preferentially opens these channels (Patel et al., 2001).

TRAAK ($K_{2P4.1}$) is another two pore potassium channel that shows mechanotransducing properties (Lesage et al., 2000; Maingret et al., 1999a). Like TREK-1 and TREK-2, TRAAK is sensitive to AA, but TRAAK is exclusively expressed in neuronal tissues including brain, spinal cord, and retina. Additionally, TRAAK lacks sensitivity to cAMP and to internal pH modifications (Maingret et al., 1999a). TRAAK channels expressed in mammalian cells open when a negative pressure is applied to the patch pipette in the inside-out and cell-attached configuration or when a convex curvature of the plasma membrane is induced by addition of the crenator TNP (Maingret et al., 1999a). Interestingly, disruption of the actin cytoskeleton results in strongly enhanced open probability and the threshold of mechanical stimulation drops from -70 to -20 mmHg (Maingret et al., 1999a). In a recent study, purified TRAAK was reconstituted in liposomes and recorded in the inside-out configuration. TRAAK channel activity could be evoked by application of positive and negative pipette pressure, suggesting a direct mechanism of mechanical gating without the involvement of tethers (Brohawn et al., 2014). Similar to TREK-1, TRAAK has a low threshold of activation (0.5–4 nN • m^{-1}), suggestive of a broad mechanosensory ability.

In summary, there is good evidence that the K_{2P} channels TREK-1 and TRAAK have inherent mechanosensitive properties. Both channels were successfully reconstituted into artificial liposomes by two independent groups and showed low thresholds for mechanical activation

(Berrier et al., 2013; Brohawn et al., 2014). Although matters are less convincing for TREK-2, the patch-clamp experiments and the high similarity of TREK-2 with TREK-1 suggest a similar gating mechanism of TREK-2. Interestingly, truncation of the carboxyl terminus of either one of the three K_{2P} channels abolishes mechanogating, clearly demonstrating that their C-terminus is essential for sensing the mechanical stimulation (Honore et al., 2002; Maingret et al., 2002).

Transient receptor potential channels

The TRP are members of a superfamily of hexahelical cation channels. Both termini face the inside of the cell and the single pore domain is thought to be located between segments five and six. TRPs can be further subdivided into the subfamilies canonical TRPs (TRPCs), melastatin-related TRPs (TRPMs), vanilloid TRPs (TRPVs), polycystin TRPs (TRPPs), mucolipin TRPs (TRPMLs), ankyrin TRPs (TRPAs, only one family member), NompC-like TRP (TRPNs) and yeast TRPs (TRPYs). TRP channels are usually non-selective for various cations and are expressed in neuronal and non-neuronal cells with various roles in sensory functions like hearing, vision, taste, olfaction and thermosensation (Clapham et al., 2001; Montell, 2005). The subunits arrange into homo- and heterotetramers and can be activated by various modes including activation of PLC-activating receptors, chemical or thermal activation, or modulation of intracellular calcium concentrations. In recent years, several TRPs have been suggested as mechanically activated channels.

Yeast transient receptor potential channels

Yeast releases calcium from their vacuole into the yeast cytoplasm on osmotic shock. The underlying calcium-permeable channel is thought to be TRPY1, since recordings of TRPY1-deficient vacuole showed that no calcium was released upon hyperosmotic or mechanical challenge (Palmer et al., 2001; Zhou et al., 2003). Whether TRPY1 is activated directly or indirectly through mechanical stress is unsettled, but TRPY1-like function could be restored in TRPY1-deficient yeast using the fungal homologues TRPY2 or TRPY3 (Zhou et al., 2005). Due to the evolutionary distance of fungal and yeast TRPYs, the authors suggest a rather direct mode of activation, because binding of the distant fungal homologue to endogenous linking proteins in yeast seems less likely. Interestingly, an aromatic residue Y458 in the sixth transmembrane domain close to the internal lipid interface of the membrane was crucial for the mechanosensitivity of TRPY1 (Zhou et al., 2007). Moreover, indole and other aromatic compounds were shown to activate TRPY1 likely by altering the innate forces in the lipid bilayer (John Haynes et al., 2008). It was also reported that a C-terminal cytosolic 30 residues stretch renders TRPY1 less sensitive to stretch. In a more recent paper, the TM5-TM6 core of TRPY1 was uncoupled from the N-terminal TM1-TM4 by strategic peptide insertions that block the

covalent core-periphery interactions (Su et al., 2011). The authors suggest that membrane tension pulls on TM5-TM6, expanding the core and opening the TRPY1 gate. In summary, the patch-clamp experiments of yeast vacuoles provide good evidence that TRPY1 is inherently mechanoperceptive. However, the results should be confirmed by independent groups. Additionally, mechanical gating of TRPY1 should be examined by reconstitution of TRPY1 in artificial bilayers, which was already successfully done by Wada et al. (1987).

Vanilloid transient receptor potential channels

The TRPV channel family consists of six mammalian members (TRPV1 to TRPV6) that are sensitive to heat, protons and lipid mediators including the TRPV1-activating vanilloid capsaicin. TRPV channels have a diverse tissue distribution, while particularly TRPV1 is highly expressed in sensory neurons. TRPV channels can be activated by warm temperatures, acidic pH and chemical compounds like 4α-phorbol 12,13-didecanoate, citrate, AA and 5',6'-epoxyeicosatrienoic acid (EET). The first evidence of a mammalian mechanosensitive TRP channel came from studies of the TRPV4 homologue OSM-9 in the nematode *C. elegans* (Colbert et al., 1997). OSM-9 was shown to be expressed in ciliated sensory neurons in the frontal end of the worm. Worms deficient of OSM-9 were impaired in their ability to response to high osmolarity, nose touch and odorant molecules. Remarkably, substitution of OSM-9 with the mammalian TRPV4 rescued the phenotypes of the worms (Liedtke et al., 2000) indicating some functional similarity. TRPV4 expressed in heterologous systems could be activated by hypotonic stimuli (Liedtke et al., 2000) and fluid shear stress (Gao et al., 2003; Hartmannsgruber et al., 2007) while hypertonicity decreased channel activity (Strotmann et al., 2000). Mice lacking TRPV4 showed reduced regulation of serum osmolarity and sensitivity to noxious mechanical stimuli (Mizuno et al., 2003; Suzuki et al., 2003) indicating that TRPV4 is indeed osmo- and shearsensitive, although it cannot be activated by membrane stretch (Strotmann et al., 2000). More recent evidence suggests that TRPV4 is not directly activated by mechanical stimuli but depends on PLA_2, which generates AA – and cytochrome P450 epoxygenase, which metabolizes AA to EET (Vriens et al., 2005). Both metabolites are known activators of TRPV4. Most likely, the direct mechanosensor in this system is an isoform of PLA_2, while TRPV4 is activated downstream of PLA_2. Supportive evidence comes from a study showing that Deg/ENaC rather than TRPV4 is the mechanosensor in ciliated sensory neurons in worms (Geffeney et al., 2011).

Close homologues of TRPV4, TRPV1 and TRPV2 were also thought to be mechanosensitive (ONeil Heller 2005). TRPV1 is expressed in bladder epithelium, where it is essential for mechanically-regulated bladder function (Birder et al., 2002). Furthermore, TRPV1 expression is high in sensory and osmosensitive neurons. In the hypothalamus, a splice variant of TRPV1 is essential to osmosensitivity of neurons in the organum vasculosum laminae terminalis and

supraoptic nucleus. Neurons isolated from TRPV1$^{-/-}$ mice failed to appropriately respond to hypertonic solution (Ciura and Bourque, 2006; Sharif Naeini et al., 2006). Additionally, TRPV1-deficient mice did not respond to hypertonicity-induced thirst and arginine-vasopressin release, suggesting an involvement of TRPV1 in osmosensing. However, evidence showing an inherent mechanosensitivity apart from the osmosensing characteristic is still lacking.

TRPV2 is expressed in aorta, mesenteric and cerebral basilar arteries. Consistent with the localization pattern, TRPV2 has been proposed to function as a stretch-sensor in VSMCs (Muraki et al., 2003) and has been implicated in membrane stretch-evoked response during axon outgrowth (Shibasaki et al., 2010). In aortic VSMCs, knock-down of TRPV2 reduced cell-swelling-activated non-selective cation currents (Muraki et al., 2003). Additionally, TRPV2 could be activated by membrane stretch in the cell-attached configuration when overexpressed in Chinese-hamster-ovary K1 cells (Muraki et al., 2003). However, its slow activation time may also imply the involvement of second messengers.

Altogether, it seems likely that TRPV channels are osmosensitive but mechanical activation of TRPV1, TRPV2 and TRPV4 channels probably involves the generation of second messengers like AA and EET that might be generated through mechanical activation of PLA_2.

NompC-like transient receptor potential channels

Mutational studies with *Drosophila melanogaster* touch-insensitive larvae that developed into profoundly uncoordinated adults have led to the discovery of the new ion channel TRPN that is essential for mechanosensory transduction (Walker et al., 2000). TRPN was highly expressed in mechanosensory organs of *Drosophila* and *C. elegans* and change-of-function mutations resulted in the alteration of the mechanotransducing currents (Walker et al., 2000). In *Drosophila*, TRPN1 forms heteromeric channel complexes with the two TRPV homologues *Inactive* and *Nanchung*. *Inactive* and *Nanchung*-mutant flies are deaf, because they lack sound-evoked field potentials in the antennal nerve (Gong et al., 2004; Kim et al., 2003). *Inactive* and *Nanchung* are thought to act downstream of the primary mechanotransducers and amplify subthreshold transducer depolarizations (Delmas and Coste, 2013). Lehnert and coworkers (2013) used a noninvasive method for monitoring sound-evoked transducer signals (Lehnert et al., 2013). Interestingly, mechanical transduction currents in hair cells were abolished by deleting either *inactive* or *nanchung* but persisted in the absence of TRPN1. The authors suggest that transduction and active amplification are genetically separable processes in *Drosophila* hearing and that TRPN1 is necessary for active amplification of sound-evoked motion.

This hypothesis is supported by earlier findings in the zebrafish *Danio rerio*. Reduction of TRPN1 in zebrafish led to hearing defects and impaired mechanotransduction-dependent endocytic events (Sidi et al., 2003). However, TRPN accounted only for roughly 90% of the

mechanically-induced currents, supporting the hypothesis that TRPN1 acts as an amplifier of mechanical stimuli and not as mechanosensory element.
In *C. elegans*, the TRPN1 homologue TRP-4 was implicated in proprioception, since loss of TRP-4 resulted in defective locomotion and body bending (Li et al., 2006), however no mechanism regarding the gating of TPRN1 were revealed.
In summary, the role of TRPN channels as mechanosensitive ion channels is still obscure. Although TRPN1 homologues are expressed in mechanosensory cells of diverse species, loss of TRPN1 does not necessarily lead to loss of mechanosensory function. Rather than being an intrinsically mechanoperceptive channel, TRPN seems to amplify signals sensed by a mechanosensor of yet unknown identity. Mammalian homologues of TRPN have not been identified.

Ankyrin transient receptor potential channels

Another study with *Drosophila* mutants has revealed the TRPA1 homologue *painless* as essential protein for noxious stimuli and heat (Tracey et al., 2003). Flies deficient of TRPA1 did not steer away from noxious stimulation but showed normal behavior to gentle touch. In *C. elegans*, TRPA1 is expressed in several sensory neurons including those that mediate cessation of foraging after gentle nose touch (Kindt et al., 2007). *C. elegans* worms with mutated TRPA1 showed impaired mechanosensory behaviors related to nose-touch responses and foraging. In mammals, TRPA1 encodes the unusual TRP family member TRPA1 that can be activated by noxious cold, pungent natural chemicals including mustard oil, and by several environmental irritants (Bandell et al., 2004). TRPA1 contains a long N-terminus with 29 ankyrin repeats. Ankyin repeats are motifs with a conserved backbone and variable residues that mediate specific protein-protein interactions. Performing immunohistochemistry, TRPA1 expression was found in the tips of cilia in vertebrate hair cells (Corey et al., 2004). Reduction of TRPA1 protein expression diminished transduction currents and uptake of channel-permeable fluorescent dye (Corey et al., 2004). Based on these findings, TRPA1 appeared a strong candidate for the transduction channel in hair cells. This is supported by evidence showing that suction can activate *C. elegans* TRPA1 expressed in mammalian cells (Kindt et al., 2007). The threshold of activation was estimated to be approximately 45 mmHg. Additionally, TRPA1 could be activated by the amphiphilic substance TNP and by the tarantula toxin GsMTx-4 (Hill and Schaefer, 2007). However, several more recent findings argue against TRPA1 as the transduction channel in hair cells. First, mechanical transduction currents of hair cells were not affected by the TRPA1 activator (Jordt et al., 2004). Second, membrane stretch failed to activate TRPA1 proteins heterologously expressed in renal fibroblast COS cells (CV-1 in Origin with SV40 genes) of African green monkey *Chlorocebus sabaeus* recorded in the cell-attached patch configuration (Sharif-Naeini

et al., 2008). Third, TRPA1-deficient mice showed normal transduction currents in hair cells and balance of TRPA1$^{-/-}$ mice was unimpaired (Bautista et al., 2006; Kwan et al., 2006). However, TRPA1$^{-/-}$ mice displayed behavioral deficits in response to mustard oil, to cold and to punctate mechanical stimuli suggesting an indirect role of TRPA1 in mechanotransduction (Brierley et al., 2011; Kwan et al., 2006; Lennertz et al., 2012).

Polycystin transient receptor potential channels

Autosomal dominant polycystic kidney disease (ADPKD) is a very common inherited disease caused by mutations in *polycystic kidney disease (pkd)* genes *pkd1* and *pkd2*. *Pkd1* and *pkd2* encode two proteins of the TRPP family TRPP1 and TRPP2 respectively. The much larger TRPP1 (polycystin-1, PKD1) is an eleven transmembrane containing protein that has a C-terminal TRP-like channel domain, although it does most likely not form an ion channel itself (Hanaoka et al., 2000). TRPP2 (alternative names: polycystin-2, PKD2) proteins form a non-selective large conductance cation channel family that is largely expressed in kidney, heart and blood vessels. Functional analysis of TRPP2 as an ion channel came initially from heterologous studies in chinese hamster ovary (CHO) cells. It was demonstrated that TRPP2 alone did not reach the plasma membrane but was retained in the endoplasmic reticulum (ER) unless co-expressed with TRPP1 (Hanaoka et al., 2000). Naturally occurring mutations in either TRPP1 or TRPP2 eliminated their interaction resulting in loss of channel activity of TRPP2 due to its retention at the ER. Later studies using oocytes (Vassilev et al., 2001), HEK293 cells (Pelucchi et al., 2006) or purified TRPP2 in cell-free systems (Gonzalez-Perrett et al., 2001) confirmed that TRPP2 can indeed function as an ion channel at the plasma membrane. However, TRPP2 expression at the plasma membrane is strictly regulated in several ways including regulation by posttranslational modifications, glucogen synthase kinase 3 activity, epidermal growth factor receptor activation and interactions with other channel subunits like TRPC1 (Tsiokas et al., 1999) and TRPV4 (Kottgen et al., 2008; Ma et al., 2011; Tsiokas et al., 2007). TRPP2 expression has been found in the primary cilium of kidney epithelial cells (Luo et al., 2003; Nauli et al., 2003; Pazour et al., 2002). An N-terminal motif is responsible for trafficking of TRPP2 to the cilia which is independent of TRPP1 expression (Geng et al., 2006). Because cilia behave as sensory organelles in the olfactory bulb and vision system, it is thought that primary cilia in the kidney have a similar mechanosensory function in the detection of kidney fluid flow (Tsiokas et al., 2007). Indeed, Nauli et al. (2013) proved that epithelial cells require their cilia in order to sense fluid flow. In addition, the group showed that epithelial cells respond to shear stress with increased intracellular calcium concentrations through activation of TRPP1 and TRPP2 via a PLC-independent mechanism. Cells without functional TRPP1 showed no response to fluid shear stress (Nauli et al., 2003) while cells in which TRPP2 was blocked with an antibody raised against internal epitope of TRPP2, blocked

about 50% of fluid-flow-induced increase in intracellular calcium. While this study underlines the importance of TRPP1 in fluid shear sensing, there is no report on the mechanosensitivity of TRPP2 alone or in combination with other subunits. It is possible that TRPP1 functions as the actual sensor while adherent subunits including TRPP2, TRPC1 or TRPV4 transduce the stimuli. This hypothesis is supported by findings showing that the N-terminal region of TRPP1 can be stretched when force is applied (Qian et al., 2005). Another possibility is that TRPP2 assembles with an auxiliary subunit to form a mechanosensitive channel complex. This question has been addressed by a study showing that TRPP2/TRPV4 complexes are needed for sensing the fluid shear stress in epithelial kidney cells (Kottgen et al., 2008). A functional interaction of TRPP2 with TRPV4 was confirmed by expression of TRPP2 and TRPV4 in oocytes. In line with previous findings, TRPP2 alone was not susceptible to cell swelling while TRPV4 was. However, co-expression of TRPP2 with TRPV4 did result in larger cell-swelling mediated currents compared to currents seen with single TRPV4 expression (Kottgen et al., 2008). These findings could indicate a mechanosensory role of TRPP2 in complex with TRPV4, but additional investigation is needed.

In striking contrast to the hypothesis of TRPP2 channel complexes functioning as mechanosensors are findings of Sharif-Naeini and coworkers (2009) who suggested that TRPP2 inhibits the endogenous stretch-activated channel in VSMCs. In arterial myocytes and COS cells, reduction of TRPP1 resulted in suppressed stretch-activated channel activity. This suppression was likely mediated by excessive free TRPP2, because additional suppression of TRPP2 fully reversed mechanosensitive channel activity. Similar results were found in resistance arteries of TRPP1-deficient mice that showed reduced myogenic tone. The inhibition of the stretch-activated channel was not dependent on TRPC1, TRPC6 or TRPV4 but was largely effected by the actin cytoskeleton. Disruption of F-actin fibers enhanced mechanically induced endogenous channel activity and could restore the TRPP2-mediated suppression in COS cells. These findings indicate that TRPP1/TRPP2 ratio regulates pressure sensing and argue against a direct mechanosensory role of TRPP2 in arterial myocytes. In summary, there is little evidence pointing to a direct mechanogating property of TRPP2 channels so far, but stringent experimental data are still missing, leaving the role of TRPP2 in mechanosensitivity ill-defined.

Mucolipid transient receptor potential channels

TRPML3 is mostly expressed in inner ear and hair cells. TRPML3 was shown to localize to cytoplasmic compartments of hair cells and to the plasma membrane of stereocilia, suggesting a role of TRPML3 in mechanical hair cell conductance. Likewise, a mutation in TRPML3 causing a constitutively active cation channel conformation was found in varitint-waddler mice, which are deaf and show progressive disorganization of hair cell cilia (Grimm et al., 2007). Due

to the importance of TRPM3 in the organization of hair cell cilia, TRPML3 was suggested to be mechanosensitive. However, TRPML3 primarily localizes to early- and late-endosomes as well as lysosomes (Venkatachalam et al., 2006). Therefore, it seems more likely that TRPML3 is involved in vesicle trafficking rather than being a directly mechanogated channel itself.

Melastin transient receptor potential channels

TRPM channels have eight subfamily members (TRPM1 to TRPM8) and are widely expressed in excitable and non-excitable cells where they perform diverse functions ranging from detection of cold, taste, redox state and pH to control of magnesium homeostasis and cell proliferation or death (for review see Zholos, 2010). In the TRPM family, the family members TRPM3, TRPM4 and TRPM7 have been considered as mechanosensitive ion channels.

TRPM3 is expressed in kidney and brain and has at least 12 isoforms. Full-length TRPM3 was responsive to hypotonic cell swelling when overexpressed in HEK293 cells (Grimm et al., 2003). However, mechanisms of channel opening are still missing.

TRPM4 is a calcium- and voltage-dependent channel that is expressed in multiple tissues including arterial smooth muscle cells and endothelium. A current with similar conductance, ion selectivity and calcium dependence as overexpressed TRPM4 was found in cerebral artery myocytes. Knock-down of TRPM4 in those arteries resulted in attenuated pressure-induced myocyte depolarization and myogenic constriction (Earley et al., 2004). Additionally, overexpressed TRPM4 in HEK293 cells could be activated by negative pressure through the patch pipette. Mechanical activation of TRPM4 via stretch possibly depended on rise in intracellular calcium concentration following activation of ryanodine receptors (Morita et al., 2007). In this way, TRPM4 activation can contribute to the depolarization and concomitant vasoconstriction of intact cerebral arteries following mechanical stimulation. However, TRPM4-deficient mice had a normal myogenic response, arguing against a role of TRPM4 as direct mechanosensor important for myogenic vasoconstriction (Mathar et al., 2010). Interestingly, blood pressure levels of TRPM4 mice were elevated, which was likely a consequence of TRPM4-dependent excessive catecholamine release from chromaffin cells. Catecholamine contributes to increased sympathetic tone, explaining the high blood pressure levels observed in TRPM4-deficient mice. In conclusion, because of the strong calcium-dependency of TRPM4, activation of TRPM4 is likely subsequent to activation of calcium-permeable or calcium-release mechanisms like ryanodine receptor activation or TRPC6 activation. Therefore, TRPM4 activation through stretch activation is probably indirect and requires intracellular calcium as well as phosphorylation-dependent mechanisms.

TRPM7 forms a magnesium-dependent non-selective cation outward rectifying channel expressed in a wide variety of tissues including kidney and vascular smooth muscles. Interestingly, TRPM7 has a kinase activity in its own C-terminus that regulates TRPM7 channel

activity (Runnels et al., 2002). TRPM7 was suggested to be important in volume regulation because of its stretch and swelling sensitivity. Oancea et al. (2006) showed that TRPM7 channels translocated to the plasma membrane in response to laminar flow in a exocytosis-mediated pathway. In this way, fluid flow increased endogenous TRPM7 current amplitudes in VSMCs but not in endothelial cells, suggesting that TRPM7 is involved in vessel wall injury. These data are in contrast to findings from Numata and colleagues (2007), who indicated that heterologous expression of TRPM7 in HEK293 cells augments channel activity upon shear stress and cell swelling even under the conditions where exocytotic events can hardly take place. Moreover, in excised patches, membrane stretch stimulated single channel activity of TRPM7. The present research group also demonstrated activation of an endogenous magnesium- and gadolinium-sensitive non-selective cation channel in epithelial cells, that could be opened upon membrane stretch and osmotic cell swelling in cell-attached and inside-out recordings (Numata et al., 2007b). The channel identity was concluded to be TRPM7, because reduction of TRPM7 proteins by siRNAs led to abolition of stretch-activated channel activity. However, single channel conductance found in these experiments does not match the single-conductance found in heterologous expression systems (Sharif-Naeini et al., 2008), arguing against direct mechanoperceptive properties of TRPM7. Likewise, another study suggested that TRPM7 senses alteration of cytosolic concentrations of free magnesium, magnesium-nucleotides and a further unidentified factor upon hypoosmotically-induced cell swelling rather than mechanically induced membrane stretch (Bessac and Fleig, 2007). Therefore activation of TRPM7 is considered indirectly and depends on intercalation of TRPM7 proteins to the plasma membrane upon mechanical stimulation.

Canonical transient receptor potential channels

TRPC channels are widely expressed in different mammalian tissues like vascular smooth muscle, lung, kidney, and brain, where they participate in central cell physiological processes including development, proliferation and differentiation (for review see Dietrich et al., 2006 or Venkatachalam and Montell, 2007). The mechanical properties of several TRPC channels including TRPC1, TRPC5 and TRPC6 have been examined over the years.

The research group of Hamill (2005) proposed an intrinsic mechanosensitivity of TRPC1. They solubilized frog oocytes membranes and reconstructed the isolated proteins in liposomes and evaluated the stretch-activated currents (Maroto et al., 2005). Reconstitution of TRPC1 in oocytes resulted in highly increased stretch-activated current densities, whereas TRPC1 knock-down in oocytes attenuated endogenous stretch-activated currents. Similar results were found in CHO-K1 cells heterologously expressing TRPC1. However, subsequent studies could not confirm an intrinsic mechanosensitivity of TRPC1 (Dietrich et al., 2007; Gottlieb et al., 2008). TRPC1 expression is predominantly high in cerebral arteries and thoratic aorta

compared to the other TRPC channels. However, TRPC1$^{-/-}$ mice showed no obvious phenotype and demonstrated normal myogenic vasoconstriction. Additionally, smooth muscle cells from cerebral arteries isolated from TRPC1-deficient mice were as responsive to hypoosmotic swelling and inflation as their wild type controls (Dietrich et al., 2007). Importantly, the authors excluded up-regulation of other TRPC channels in the TRPC1$^{-/-}$ mice, excluding genetic compensation mechanisms. In accord with this notion is a study from Hamill and coworkers (2008) who revised mechanosensitivity of TRPC1 by showing that the stretch-activated currents were not higher in control cells compared to TRPC1 overexpressing cells (Gottlieb et al., 2008). Rather, the present authors suggested that the endogenous stretch-activated currents seen in those cells resulted from activation of endogenous TREK-1. Another issue arguing against mechanoperceptive properties of TRPC1 channels regards the subcellular localization of TRPC1. Most of the TRPC1 channels seem to be ER-retained unless co-expressed with other TRPC subunits, questioning the relevance of overexpression studies with TRPC1 (Alfonso et al., 2008; Storch et al., 2012a). Based on the reports showing that TRPC1 is not expressed in the plasma membrane and is not responsible for stretch-activated currents in liposomes, cell systems or myogenic arteries, TRPC1 cannot be considered an inherent mechanosensitive channel.

TRPC5 is widely expressed in the central and peripheral nervous system and at lower levels in many other tissues such as gonads, lung, heart, adrenal gland, endothelium, kidney and vascular and gastric smooth muscle (Beech, 2007b). TRPC5 channel activation is generally subsequent to PLC-dependent receptor activation. Interestingly, TRPC5 is a sensor of important signaling phospholipids. For example, TRPC5 channels can be activated by depletion of PIP_2 levels surrounding the channel (for review see Beech, 2007). The lipid sensitivity and the presence of TRPC5 in baroreceptors (Glazebrook et al., 2005)—the peripheral nerve endings involved in sensing arterial pressure—prompted Gomis et al. (2008) to investigate TRPC5 as mechanically gated channel. Whole-cell recordings of HEK293 cells heterologously expressing TRPC5 revealed TRPC5 currents upon application of hypotonic bath solution and positive pressure through the patch pipette. Additionally, the mechanically induced currents were sensitive to inhibition by GsMTx-4. In PIP_2-depleted cells, the currents evoked with hypotonic solution were reduced supporting the dependence of TRPC5 on PIP_2. However, it should be noted that mechanically activated TRPC5 currents opened with a considerate delay time of several seconds, suggesting a rather indirect activation of TRPC5 channels that most likely depends on formation of second messengers. A recent report from the same research group shows that activation of TRPC5 is likely secondary to cell swelling-induced $G_{q/11}$PCR activation, which in turn enhances the activation of TRPC5 by regulating this channel's membrane trafficking (Jemal et al., 2014). Therefore, TRPC5 can only be considered

as mechanotransducing channel while the mechanical stimulus is perceived by other mechanosensors like GPCRs.

Another TRPC channel is controversially discussed as being mechanosensitive. TRPC6 is a double rectifying non-selective cation channel highly expressed in lung, brain, kidney with particular high expression in vascular smooth muscle cells. TRPC6 channels are directly activated by the second messenger diacylglycerol (DAG) (Hofmann et al., 1999). TRPC6 was postulated to be a mechanosensitive ion channel in arteries that is important in maintaining myogenic tone (Welsh et al., 2002). Welsh et al. (2002) examined cerebral artery smooth muscle cell depolarization and constriction caused by elevated intraluminar pressure after knock-down of TRPC6. Knock-down of TRPC6 in cerebral VSMCs suppressed depolarization and vasoconstriction. Additionally, TRPC6 knock-out reduced cell swelling-induced current amplitudes in isolated myocytes. Supporting intrinsic mechanoperceptive properties of TRPC6, Spassova et al. (2006) reported that TRPC6 could be activated independently of PLC by mechanically and osmotically induced membrane stretch in a GsMTx-4-sensitive manner. The threshold pressure needed to open TRPC6 was roughly 80 mmHg in membrane patches of CHO-K1 cells—a value close to the pressure needed to rupture most cell membranes—questioning the physiological relevance of mechanically gated TRPC6 channels. Indeed, similar to TRPC1, stretch activation of homomeric TRPC6 could neither be confirmed in transiently transfected COS cells (Gottlieb et al., 2008), nor in HEK293 cells (Mederos y Schnitzler et al., 2008). Instead, TRPC6 activation seems to be the result of agonist-independent mechanical activation of $G_{q/11}$PCRs with subsequent build-up of the TRPC6 activator DAG (Mederos y Schnitzler et al., 2008). In line with this hypothesis are findings from TRPC6-deficient mice that have an elevated blood pressure and increased myogenic constriction, a phenotype inconsistent with the loss of a channel essential for maintaining myogenic tone (Dietrich et al., 2005). The increased myogenic constriction is likely the result of molecular compensation mechanism in TRPC6-deficient cells: $TRPC6^{-/-}$ smooth muscle cells overexpress TRPC3, which has a higher basal affinity compared to TRPC6. Consequently, smooth muscle cells of TRPC6-deficient mice have higher basal cation entry resulting in more depolarized membrane potentials. These findings are inconsistent with TRPC6 being an intrinsic mechanosensor. However, Huber and coworkers (2006) suggested that TRPC6 might be a directly mechanosensitive in the kidney, because TRPC6 interacts with podocyte-specific protein podocin—a homologue of the PDZ-containing protein MEC-2 (Huber et al., 2006). Since the homologue of podocin MEC-2 is part of a mechanosensitive multi-protein ion channel complex in *C. elegans,* it was suggested that TRPC6 in complex with other slit-membrane proteins including podocin could form a mechanosensitive ion channel complex (Huber et al., 2007). A recent study claimed that a TRPC6 mutation found in patients with focal and segmental glomerulosclerosis renders the channel insensitive to hypotonically induced

membrane stretch (Wilson and Dryer, 2014). However, this study has several methodic drawbacks. First, cell swelling was induced by diluting isotonic bath solution with water. This results in reduced calcium concentrations that might already be sufficient to cause TRPC6 channel activation. Second, no chloride channel blockers were used in this study suggesting that the effects seen under cell swelling might be caused by endogenous VRAC channel activation. This could explain why no characteristic double rectifying TRPC6 current-voltage relationships were seen under cell swelling.
In summary, there is good evidence that TRPC6 is not inherently mechanosensitive in most cell systems. However, it is intriguing to investigate a putative mechanosensitive TRPC6/podocin channel complex in podocytes.

Purinergic channels

Purinergic (P_2X) channels form a family of non-selective cation channels with seven family members (P_2X_1–P_2X_7) that open in response to extracellular ATP. The N- and C-termini of purinergic channel face the inside of the cell and three channel subunits are needed to form a functional ion channel. P_2X channels are distinct from the P_2Y family which are purinergic GPCRs, and are widely expressed in a variety of tissues. Activation of purinergic receptors results in increased intracellular calcium levels, thereby regulating diverse cellular functions (for review see North, 2002). Purinergic channels are not directly mechanogated because the latency time for mechanical activation lies within a few seconds and is therefore comparatively slow. P_2X channels are rather thought to be activated due to mechanically induced release of ATP. Extracellular ATP binds to P_2Y and P_2X receptors on the same or neighboring cell. ATP release is a common mechanism in many cell types including bone osteoblast (Ke et al., 2003), lung fibroblast (Murata et al., 2014), airway and tubular epithelial (Homolya et al., 2000; Jensen et al., 2007) and aortic endothelial cells (Yamamoto et al., 2000) as well as neurons (Xia et al., 2012). In general, there are several different ways how ATP can leave the cell: Through ATP-permeable channels like connexin and pannexin hemichannels, through adenine nucleotide transporters of yet unknown identity, and through fusion of ATP-loaded vesicles with the plasma membrane. Although released ATP can act on all expressed P_2 receptors in the cell, a special role for P_2X_4 was found in shear-stress-mediated calcium influx into endothelial cells (Kessler et al., 2011; Yamamoto et al., 2000). Kessler et al. (2011) showed that fluid shear stress did not activate HEK293 cells heterologously expressing P_2X_4 channels. However, subsequent stimulation of P_2X_4 with ATP did result in diminished desensitization. These results indicate that shear stress might directly influence P_2X_4 channels.
Altogether, P_2X_4 channels are not directly mechanogated but form mechanotransducing structures in several cell systems that are likely activated by mechanically induced ATP release.

8. Mechanoresponse – downstream signaling

Ultimately, mechanical stimuli lead to downstream cellular signaling and adaptation processes that are not *per se* force-dependent. A common rapid response mechanism is the feedback to mechanosensitive structures that initiated the response in the first place as is the case for integrin-mediated and cadherin-mediated adhesions, that enlarge and tighten in response to tension (for review see Schwartz and DeSimone, 2008).

Apart from the more rapid adaptation, force additionally activates more sustained signaling pathways like formation of stress fibers through GTPase RhoA thereby controlling cell morphology as well as transcriptional network processing. Other cascades regulate development, cell morphology, migration, differentiation or proliferation.

For instance, the mechanical signaling determines the stem cell lineage commitment and specification of mesenchymal cells. Mesenchymal stem cells can differentiate into a range of anchorage-dependent mesenchymal tissues, including bone, cartilage, fat, tendon, muscle, and marrow stroma (adipocytic, chondrocytic, or osteocytic lineages). Lower plating density and therefore decreased local pressure and adhesion contacts alter the cell shape and their differentiation (Pittenger et al., 1999). Importantly, differentiation is dependent on actomyosin generated tension, highlighting the importance of mechanical cues in driving cell fate decisions (for review see Schwartz and DeSimone, 2008).

Another example highlights the role of mechanoresponse in the kidney. Podocytes undergo a variety of mechanically mediated adaptations including adhesion remodeling, actin cytoskeleton rearrangement and transcriptional processing. Podocytes are highly specialized visceral epithelial cells lining the Bowman's capsule that wrap the capillaries of the glomerulus. Blood pressure in the glomerular capillaries as well as shear stress resulting from fluid flow through the slit diaphragm and over the apical site of the podocytes constantly generates high mechanical stress. High pressure induces calcium influx and causes a reorganization of the actin cytoskeleton through a Rho-dependent pathway (Endlich et al., 2001). Additionally, calcium influx into podocytes is known to modulate gene expression through a calcineurin- and nuclear factor of activated T-cells (NFAT) transcription factor-dependent pathway (Kuwahara et al., 2006). NFAT also regulates apoptosis in podocytes (Wang et al., 2011) but whether mechanical stimulation causes apoptosis in podocytes is controversial (Endlich et al., 2001; Huang et al., 2012). In addition to activation of NFAT, stretch-mediated influx of calcium also regulates slit-membrane protein adhesions via nephrin and neph-proteins (Miceli et al., 2010) and could possibly regulate the calcium-dependent attachment of podocytes to the glomerular basal membrane via integins (Sachs et al., 2012). All these adaptations allow podocytes to dynamically regulate kidney filtration and counteract high pressure situations. Failure to

balance high pressure situations would result in podocytes damage, loss of podocytes ultimately resulting in filtration deficiencies like proteinuria.

II Aim of this study

Since the discovery of the first mechanosensitive structures, many attempts have been made to unravel the identity of mammalian proteins sensing mechanical stimulation. Because several mechanosensitive structures respond to mechanical stimulation with non-selective ion channel conductivity, TRPC channels have been suggested as mechanotransducing elements in a variety of cell systems. The data regarding the direct mechanosensitivity of these channels is conflicting and has been questioned several times. Therefore, the following questions are addressed in this thesis:

1. Can TRPC1 be activated by mechanical stimulation in heterologous cell systems?
   a) Is TRPC1 expressed in the plasma membrane?
   b) What is the role of endogenous TRPC1?

2. *How are TRPC4 and TRPC5 channels activated subsequent to activation of GPCRs?
   a) What is the function of the C-terminal PKC-phosphorylation site within the VTTRL motif?
   b) How do NHERF proteins contribute to the regulation of TRPC4 and TRPC5 activation?
   c) Is the activation of TRPC4 and TRPC5 lipid-dependent?

   *the key findings and discussion of this project can be found on the pages 116-128

3. What is the identity and contribution of $G_{q/11}$PCRs on myogenic tone?
   a) Which $G_{q/11}$PCRs are expressed in arterial smooth muscle cells of small resistance arteries?
   b) Do the expressed $G_{q/11}$PCRs contribute to myogenic tone?
   c) How are the $G_{q/11}$PCRs activated?

4. Are TRPC channels mechanosensitive in podocytes?
   a) If not, what are the molecular correlates for mechanosensitive elements in podocytes?
   b) How are the mechanosensitive elements regulated regarding composition of the plasma membrane and dependence on the cytoskeleton?
   c) Does mechanical activation result in disease-associated F-actin reorganization?

III Results

The following section encompasses the findings that can be found in the following publications:

1. Publication: TRPC1 calcium permeability in heteromeric channel complexes

Storch U, Forst AL, Philipp M, Gudermann T, Mederos y Schnitzler M. Transient receptor potential channel 1 (TRPC1) reduces calcium permeability in heteromeric channel complexes. J Biol Chem. 2012 Jan 27;287(5):3530-40.

2. Publication: Novel role of mechanosensitive AT1B receptors in myogenic vasoconstriction

Blodow S, Schneider H, Storch U, Wizemann R, Forst AL, Gudermann T, Mederos y Schnitzler M. Novel role of mechanosensitive AT1B receptors in myogenic vasoconstriction. Pflugers Arch. 2014 Jul;466(7):1343-53.

3. Publication: Podocyte purinergic P2X4 channels are mechanotransducers that mediate cytoskeletal disorganization

Forst AL, Olteanu V, Mollet G, Wlodkowski T, Schaefer F, Dietrich A, Reiser J, Gudermann T, Mederos y Schnitzler M, Storch U. Podocyte purinergic P2X4 channels are mechanotransducers that mediate cytoskeletal disorganization. J Am Soc Nephrol. 2015 Jul 9. pii: ASN.2014111144. [published ahead of print]

1. Publication: Storch et al. (2012)

TRPC1 calcium permeability in heteromeric channel complexes.

Storch U, Forst AL, Philipp M, Gudermann T, Mederos y Schnitzler M.

J Biol Chem. 2012 Jan 27;287(5):3530-40.

Author's contribution to this work:
AL.F. designed and performed experiments and analyzed the data from the following experiments: Western Blot Analysis, G/F-actin assay and Scratch assay. Additionally, AL.F. generated shRNA constructs and monoclonal stabile cell lines.
U.S., T.G., and M.MyS. designed and supervised the study. U.S. and M.P. performed electrophysiological experiments. U.S. performed intracellular calcium recordings and cloned shRNA. M.P. and M.MyS. performed mutagenesis. U.S., M.P. and M.MyS. analyzed data. U.S., T.G., and M.MyS. wrote the manuscript.

THE JOURNAL OF BIOLOGICAL CHEMISTRY VOL. 287, NO. 5, pp. 3530–3540, January 27, 2012

Transient Receptor Potential Channel 1 (TRPC1) Reduces Calcium Permeability in Heteromeric Channel Complexes[S]

Received for publication, July 15, 2011, and in revised form, December 7, 2011 Published, JBC Papers in Press, December 8, 2011, DOI 10.1074/jbc.M111.283218

Ursula Storch[‡], Anna-Lena Forst[‡], Maximilian Philipp[§], Thomas Gudermann[‡1], and Michael Mederos y Schnitzler[‡]

From the [‡]Walther-Straub-Institute for Pharmacology and Toxicology, Ludwig-Maximilians University, 80336 Munich, Germany and the [§]Institute for Pharmacology and Toxicology, Marburg University, 35032 Marburg, Germany

Specific biological roles of the classical transient receptor potential channel 1 (TRPC1) are still largely elusive. To investigate the function of TRPC1 proteins in cell physiology, we studied heterologously expressed TRPC1 channels and found that recombinant TRPC1 subunits do not form functional homomeric channels. Instead, by electrophysiological analysis TRPC1 was shown to form functional heteromeric, receptor-operated channel complexes with TRPC3, -4, -5, -6, and -7 indicating that TRPC1 proteins can co-assemble with all members of the TRPC subfamily. In all TRPC1-containing heteromers, TRPC1 subunits significantly decreased calcium permeation. The exchange of select amino acids in the putative pore-forming region of TRPC1 further reduced calcium permeability, suggesting that TRPC1 subunits contribute to the channel pore. In immortalized immature gonadotropin-releasing hormone neurons endogenously expressing TRPC1, -2, -5, and -6, down-regulation of TRPC1 resulted in increased calcium permeability and elevated basal cytosolic calcium concentrations. We did not observe any involvement of TRPC1 in store-operated cation influx. Notably, TRPC1 suppressed the migration of gonadotropin-releasing hormone neurons without affecting cell proliferation. Conversely, in TRPC1 knockdown neurons, specific migratory properties like distance covered, locomotion speed, and directionality were increased. These findings suggest a novel regulatory mechanism relying on the expression of TRPC1 and the subsequent formation of heteromeric TRPC channel complexes with reduced calcium permeability, thereby fine-tuning neuronal migration.

The classical transient receptor potential (TRPC)[2] channel subfamily comprises seven members (TRPC1–7) that are regarded as non-selective, calcium-permeable cation channels involved in a wide range of physiological events that require calcium (Ca^{2+}) signaling. To date, it is broadly accepted that the general activation mechanism of TRPC channels is contingent upon receptor-mediated phospholipase C activation independent of protein kinase C activity and the depletion of internal calcium stores (1). However, channel activation subsequent to store depletion is also discussed for some TRPC family members (summarized by Ref. 2). TRPC channels are widely expressed in different mammalian tissues like vascular smooth muscle, lung, kidney, and brain, and they have been identified to participate in central cell physiological processes (3). In the nervous system, for example, TRPC channels are involved in neuronal development, proliferation, and differentiation (4, 5), and a growing body of evidence indicates that TRPC channels are involved in neurological diseases (6).

For TRPC1 channels, an involvement in stretch-induced (7) and in store-operated calcium (SOC) influx is discussed (8–10). Previous investigations of TRPC1 gene-deficient mice indicated that TRPC1 was neither involved in store-operated cation influx in vascular smooth muscle cells and in platelets (11, 12) nor in pressure-induced cation influx (11). However, a contribution of TRPC1 to SOC in neurons is still a moot issue. Moreover, a detailed analysis of the specific role of TRPC1 for receptor-operated calcium influx in neurons has not been conducted.

Although numerous publications demonstrate that TRPC1 channels are involved in many intracellular processes like smooth muscle contraction, stem cell differentiation and endothelial cell permeability, salivary gland secretion, growth cone movement, neuronal differentiation, and glutamate-mediated neurotransmission (8, 9, 13), TRPC1 gene-deficient mice did not exhibit an obvious phenotype (11). Furthermore, the specific role of TRPC1 channels for neuronal migration in the developing brain is still elusive.

Based on the finding that TRPC1 is able to form receptor-operated heterotetrameric channel complexes with other TRPC channel subunits (14), we investigated the role of TRPC1 alone and in heteromeric channel complexes for receptor-operated calcium influx in a heterologous expression system as well as in neurons. We observed that upon incorporation into heteromeric channel complexes TRPC1 subunits contribute to the channel pore and decrease calcium permeation. As a consequence the presence of TRPC1 in immortalized immature GnRH neurons suppresses neuronal migration without affecting cell proliferation, thus highlighting a novel regulatory mechanism based on the formation of heteromeric TRPC channel complexes with reduced calcium permeability.

EXPERIMENTAL PROCEDURES

Cell Culture—Human embryonic kidney (HEK293) cells were maintained in Earl's minimal essential medium (Invitrogen), CHO-K1 cells were cultured in Ham's F-12 medium (Invitrogen), and immortalized murine gonadotropin releasing

[S] This article contains supplemental Figs. S1–S7.

[1] To whom correspondence should be addressed: Walther-Straub-Institute for Pharmacology and Toxicology, Ludwig-Maximilians University, Goethestrasse 33, 80336 Munich, Germany. Tel.: 49-89-218075700; Fax: 49-89-218075701; E-mail: thomas.gudermann@lrz.uni-muenchen.de.

[2] The abbreviations used are: TRPC, transient receptor potential; SOC, store-operated calcium; GnRH, gonadotropine releasing hormone; qPCR, quantitative real-time PCR; M_5R, muscarine M_5 receptor; CCh, carbachol; EGFP, enhanced GFP; GTPγS, guanosine 5′-3-*O*-(thio)triphosphate.

hormone (GnRH) neurons (Gn11 cells) (15) were maintained in Dulbecco's modified Eagle's medium (DMEM, Invitrogen) supplemented with 10% fetal calf serum (FCS, Invitrogen), 100 units ml^{-1} penicillin, and 100 $\mu g\ ml^{-1}$ streptomycin and 2 mM glutamine at 37 °C in a humidified atmosphere with 5% CO_2. Monoclonal TRPC1 knockdown and control Gn11 cell lines were cultured in DMEM additionally containing 800 $\mu g\ ml^{-1}$ Geneticin (Invitrogen).

Mutagenesis—For amino acid exchanges from glutamate to glutamine at positions 581 and 582, mutations in TRPC1 were introduced by site-directed mutagenesis using the QuikChange system (Stratagene, La Jolla, CA). All cDNA constructs used in the present work were confirmed by sequencing.

Generation of shRNA—To investigate the role of TRPC1 in Gn11 cells, RNA interference was used (16). For this, shRNA was transiently expressed via a pSuper NeoGFP expression vector. shRNA targeting murine TRPC1, murine TRPC5 and murine TRPC6 was designed according to Reynolds *et al.* (17) with additional testing of the three-dimensional structure of the mRNA target sequence to ensure optimal efficacy of RNA interference (18). As a control, unrelated shRNA was expressed. The DNA sequence was 5′-ACT TAA GTC GTC TGA AAC T-3′ for the TRPC1-specific construct, 5′-ATC AAA TAT CAC CAG AAA G-3′ for the TRPC5-specific construct, 5′-TCG AGG ACC AGC ATA CAT G-3′ for the TRPC6-specific construct, and 5′-TTT GAT TTG CGA AGG TTT T-3′ for the unrelated construct. shRNA constructs targeting TRPC5 and TRPC6 were expressed employing a pSuper NeoGFP expression vector with GFP being exchanged to JRed by subcloning. For transient transfections, either TransIT (Mirus Bio LLC, Madison) or the NEON device (Invitrogen) was used according to the manufacturer's protocol. The efficiency of the shRNA construct was tested using quantitative real-time polymerase chain reaction and Western blot analysis. All shRNA constructs used had no effect on the TRPC expression profile of Gn11 cells.

Quantitative Real-time Polymerase Chain Reaction (qPCR) Analysis—Total RNA from Gn11 cells was isolated using the Tri Reagent (Sigma). First-strand synthesis was carried out with random hexamers as primers using REVERTAID reverse transcriptase (Fermentas, Sankt Leon-Roth, Germany). The following primers pairs were used for the amplification of specific fragments from the first-strand synthesis: TRPC1, C1for (5′-GAT GTG TCT TTG CCC AAG C-3′), C1rev (5′-CTG GAC TGG CCA GAC ATC TAT-3′), TRPC2, C2for (5′-ACT TCA CTA CAT ATG ATC TGG GTC AC-3′), C2rev (5′-CAC GTC CAG GAA GTT CCA C-3′), TRPC3, C3for (5′-TTA ATT ATG GTC TGG GTT CTT GG-3′), C3rev (5′-TCC ACA ACT GCA CGA TGT ACT-3′), TRPC4, C4for (5′-AAG GAA GCC AGA AAG CTT CG-3′), C4frev (5′-CCA GGT TCC TCA TCA CCT CT-3′), TRPC5, C5for (5′-GCT GAA GGT GGC AAT CAA AT-3′), C5rev (5′-AAG CCA TCG TAC CAC AAG GT-3′), TRPC6, C6for (5′-ACT GGT GTG CTC CTT GCA G-3′), C6rev (5′-GAG CAG CCC CAG GAA AAT-3′), TRPC7, C7for (5′-CCC AAA CAG ATC TTC AGA GTG A-3′), C7rev (5′-TGC ATT CGG ACC AGA TCA T-3′), voltage-gated N-type calcium channel, $Ca_vN$for (5′-CCA GGA ACC TCC TTT GGA AT-3′), Ca_vNrev (5′-AAA CCA CCA GGT TCC TCA GA-3′), voltage-gated PQ-type calcium channel, $Ca_vPQ$for (5′-CTG ACA TCG CGT CTG TGG-3′), Ca_vPQrev (5′-CGC ATT CTT CTC TCC TTC TTG-3′), and three references, hypoxanthin phosphoribosyltransferase 1, Hprt1for (5′-TCC TCC TCA GAC CGC TTT T-3′), Hprt1rev (5′-CCT GGT TCA TCA TCG CTA ATC-3′), tyrosine 3-monooxygenase/tryptophan 5-monooxygenase activation protein, ζ-polypeptide, Ywhazfor (5′-TAA AAG GTC TAA GGC CGC TTC-3′), Ywhazrev (5′-CAC CACA CGC ACG ATG AC-3′), and succinate dehydrogenase complex, subunit A, Sdhafor (5′-CCC TGA GCA TTG CAG AAT C-3′), Sdharev (5′-TCT TCT CCA GCA TTT GCC TTA-3′) giving predicted product sizes of 127 bp for TRPC1, 111 bp for TRPC2, 91 bp for TRPC3, 92 bp for TRPC4, 90 bp for TRPC5, 101 bp for TRPC6, 94 bp for TRPC7, 100 bp for Ca_vN, 100 bp for Ca_vPQ, 90 bp for Hprt1, 60 bp for Ywhaz, and 70 bp for Sdha. Real-time polymerase chain reaction (RT-PCR) was performed using the master mix from the Absolute QPCR SYBR Green Mix kit (Abgene, Epsom, UK). Ten picomoles of each primer pair and 0.2 μl of the first-strand synthesis was added to the reaction mixture, and PCR was carried out in a light-cycler apparatus (Light-Cycler 480, Roche Applied Science) using the following conditions: 15 min of initial activation and 45 cycles of 12 s at 94 °C, 30 s at 50 °C, 30 s at 72 °C, and 10 s at 80 °C each. Fluorescence intensities were recorded after the extension step at 80 °C after each cycle to exclude fluorescence of primer dimers melting lower than 80 °C. All primers were tested by using diluted complementary DNA (cDNA) from the first-strand synthesis (10−1000×) to confirm linearity of the reaction and to determine particular efficiencies. Data were calculated as percentage of mean expression of the three references. Samples containing primer dimers were excluded by melting curve analysis and identification of the products by agarose gel electrophoresis. Crossing points were determined by the software program. All experiments were performed in quadruplets, and experiments were repeated at least three times.

Detection of TRPC1 Protein—To confirm the efficiency of TRPC1 shRNA, CHO-K1 cells were stably transfected with HA-tagged mouse TRPC1 (NM_011643). Cells were transiently transfected with different shRNAs using the NEON device (Invitrogen) as described by the manufacturer. Two days after transfection, cells were lysed for 10 min in radioimmune precipitation assay buffer (50 mM Tris, pH 7.5, 200 mM NaCl, 1% Triton X-100, 0.25% deoxycholate, 1 mM EDTA, 1 mM EGTA, and freshly added protease inhibitors (Fermentas)) on ice and centrifuged for half an hour at maximum speed. Supernatant was placed in SDS sample buffer, boiled for 5 min, and subjected to gel electrophoresis on a 12% SDS-PAGE gel. Proteins were transferred onto PVDF membranes as described by manufacturer (Bio-Rad). After transfer, blots were blocked with 1× RotiBlock (Roth, Karlsruhe, Germany) and incubated with primary mouse anti-HA (Sigma) or mouse anti-GAPDH antibody (Sigma) in combination with secondary anti-mouse antibody (Promega, Mannheim, Germany) to determine the expression of TRPC1. The experiment was repeated three more times with comparable results.

Electrophysiology—HEK293 cells were transfected with cDNAs coding for human TRPC1 (NM_003304), TRPC3 (NM_001130698), TRPC6 (NM_004621), and TRPC7 (NM_

020389), mouse TRPC5 (NM_009428), and rat TRPC4β1 (NM_001083115) with the original cDNA coding for the rat type-5 muscarinic (M_5R) acetylcholine receptor in pcDNA3 using TransIT (Mirus Bio LLC) reagent unless mentioned otherwise. TRPC1 in pcDNA3 and in pRK5 (Genentech) with an N-terminal HA-tag and TRPC3 and TRPC7 in pcDNA3 were additionally co-transfected with the enhanced green fluorescent protein (EGFP) reporter plasmid. TRPC1, TRPC4β1, TRPC5, and TRPC6 were also present in pIRES2-EGFP (Clontech, Palo Alto, CA). Gn11 cells were either transiently transfected with shRNA against TRPC1 or unrelated control shRNA or were used as stable shRNA against TRPC1 or unrelated shRNA-expressing cells. Conventional whole-cell patch clamp recordings were carried out at 23 °C 48 h after transfection. Cells were superfused with the standard bath solution (Na^+_{div}) containing 140 mM NaCl, 5 mM CsCl, 1 mM $MgCl_2$, 2 mM $CaCl_2$, 10 mM glucose, 10 mM HEPES (pH 7.4 with NaOH) supplemented with mannitol to 300 mosmol kg^{-1}. Gn11 cells were superfused with the standard bath solution plus 50 μM 5-nitro-2-(3-phenyl-propylamino)-benzoate to suppress chloride conductance. For the determination of calcium permeabilities, a divalent-free sodium extracellular solution (Na^+, 130 mM NaCl, 50 mM mannitol, and 10 mM HEPES, pH 7.4) and a monovalent-free calcium solution (Ca^{2+}, 10 mM $CaCl_2$ and 150 mM *N*-methyl-D-glucamine-Cl, pH 7.4) were applied. The protocol for whole-cell measurements was the following; 1) superfusion with $Na^+_{div,}$ solution, 2) when current activation occurred, application of Ca^{2+} solution for 60 s, and 3) application of Na^+ solution. In the case of receptor stimulation, 100 μM carbachol was added in Na^+_{div}, in Ca^{2+}, and in Na^+ solution. Permeability ratios (P_{Ca}/P_{Na}) were determined using the following equation (19),

$$\frac{P_{div}}{P_{Na}} = \frac{e^{((RP_{div} - RP_{Na}) R^{-1}T^{-1}F)}\,[Na]_o\,(1 + e^{(RP_{div}\,R^{-1}T^{-1}F)}}{4[div]_o} \qquad \text{(Eq. 1)}$$

where $[Na]_o$ represents the extracellular sodium ion concentration, $[div]_o$ represents the extracellular calcium concentration, RP_{Na} represents the reversal potential (E_{rev}) of the sodium current, RP_{div} represents the E_{rev} of the calcium current, R represents the gas constant, T represents the absolute temperature, and F represents the Faraday constant.

The pipette solution contained 130 mM cesium methanesulfonate, 10 mM CsCl, 9.4 mM NaCl, 0.2 mM Na_3GTP, 1 mM $MgCl_2$, 3.949 mM $CaCl_2$, 10 mM BAPTA (100 nM free Ca^{2+}), and 10 mM HEPES (pH 7.2 with CsOH), resulting in an osmolality of 294 mosmol kg^{-1}. Data were collected with an EPC10 patch clamp amplifier (HEKA, Lambrecht, Germany) using the Pulse software. Current voltage relations were obtained from triangular voltage ramps from −100 to +60 mV with a slope of 0.4 V s^{-1} applied at a frequency of 1 Hz. Data were acquired at a frequency of 5 kHz after filtering at 1.67 kHz. The IV curves and the current amplitudes were always extracted at maximal currents.

Determination of Intracellular Calcium Concentrations and Mn^{2+} Quenching—Intracellular free calcium was determined in Gn11 cells and Gn11 cells stably expressing shRNA against TRPC1 or unrelated control shRNA. Cells were loaded for 15–30 min with fura-2-acetoxymethyl ester (5 μM; Molecular Probes Inc., Eugene, OR) in HEPES-buffered saline containing 140 mM NaCl, 5 mM KCl, 1 mM $MgCl_2$, 2 mM $CaCl_2$, 5 mM glucose, 10 mM HEPES (pH 7.4 with NaOH) at 37 °C. Coverslips were mounted on the stage of a monochromator-equipped (Polychrome V, TILL-Photonics, Martinsried, Germany) inverted microscope (Olympus IX 71 with an UPlanSApo 20×/0.85 oil immersion objective). Fluorescence was recorded with a 14-bit EMCCD camera (iXON3 885, Andor, Belfast, UK). Fura-2 fluorescence was excited at 340 and 380 nm. Intracellular free calcium concentrations were calculated as described previously (20). For imaging experiments, Gn11 cells were seeded on coverslips. Cells were continuously superfused at room temperature with HEPES-buffered saline. For store depletion experiments, Gn11 cells were superfused with calcium-free HEPES-buffered saline containing 2 mM EGTA and 10 μM cyclopiazonic acid for at least 10 min. Subsequently HEPES-buffered saline containing 2 mM Ca^{2+} and 10 μM cyclopiazonic acid was added, and calcium influx was monitored. Finally 5 μM Gd^{3+} was added to block unselective cation channels.

Mn^{2+} quench experiments were conducted 48 h after transfection of HEK293 cells. Transfected HEK293 cells were loaded for 30 min with fura-2-acetoxymethyl ester in HEPES-buffered saline. The fluorescence of fura-2 and enhanced yellow fluorescence protein was excited at 340, 360, 380, and 500 nm. Fura-2 was not excited at 500 nm, and enhanced YFP contributed negligibly to fluorescence excited at 340–380 nm. Cells were continuously superfused at room temperature with HEPES-buffered saline. In Mn^{2+} quench experiments, 200 μM $MnCl_2$ was applied. Mn^{2+} quench was calculated and normalized as described previously (21).

Scratch Assay—Gn11 cells were stably transfected with TRPC1 and control shRNA. Down-regulation of TRPC1 was confirmed with qPCR. To analyze motility of Gn11 cells, 5×10^5 cells were plated in DMEM plus 10% FCS in a 10-cm plastic dish at least 32 h before the experiment. To initiate migration of cells, the cell layer was scratched six times per well with a yellow pipette tip and marked with a perpendicular line on the outside of the dish. Dishes were washed twice with PBS, then normal growth medium was gently added. A picture of the scratch was taken at 5× magnification using an inverse microscope (Axiovert 40 CFL, Zeiss, Göttingen, Germany) immediately after and 16 h after scratch. Migrated cells were counted using the ImageJ software. All experiments were carried out at least in triplicate, and all results are reported as -fold increase of migrated cells compared with control Gn11 cells stably expressing unrelated shRNA.

Videomicroscopy—20.000–40.000 Gn11 cells stably transfected with shRNA against TRPC1 or control shRNA were seeded in 35-mm culture dishes with glass bottoms (FluoroDish, WPI, Berlin, Germany) 24 h before the experiment. Dishes were mounted on an inverse microscope (Axiovert 40 CFL, Zeiss). Using a digital camera (AxioCamICc1, Zeiss) with the AxioVision 4.8.2 software (Zeiss), movies of Gn11 cells were acquired at a 10× magnification by shooting single photographs every 30 s for a period of 16 h. During the experiments, cells were maintained in culture medium and held at 37 °C in a

humidified atmosphere with 5% CO_2. Analysis of the migratory properties was done with the AxioVision software.

G-actin/F-actin Assay—We used Western blot quantification to determine the amount of filamentous actin (F-actin) *versus* free globular actin (G-actin) as described previously (22). Briefly, 300,000 Gn11 cells stably transfected with either shRNA against TRPC1 or control shRNA were seeded in a 6-well dish 1 day before harvesting cells at 37 °C with 750 μl of freshly prepared lysis buffer (50 mM PIPES, pH 6.9, 50 mM NaCl, 5 mM $MgCl_2$, 5 mM EGTA, 5% (v/v) glycerol, 0.1% Nonidet P40, 0.1% Triton X-100, 0.1% Tween 20, 0.1% 2-mercaptoethanol, 0.001% Antifoam C, 1 mM ATP, and protease inhibitor mixture (Fermentas)). Lysis buffer for the F-actin-positive control sample additionally contained 1 μM phalloidin (Sigma), whereas the G-actin positive control sample contained 10 μM cytochalasin D (Sigma). Cells were incubated for 10 min at 37 °C and centrifuged for 5 min at 2000 rpm to pellet unbroken cells. The homogenate was ultracentrifuged at 100,000 × *g* for 1 h at 37 °C. After centrifugation, the supernatant containing soluble G-actin was transferred to a new tube, whereas the pellet containing the F-actin fraction was resuspended to the same volume as the supernatant using ice-cold water plus 10 μM cytochalasin D and left on ice for 1 h to dissociate F-actin. Samples were analyzed using SDS-PAGE electrophoresis, blotted onto a PVDF membrane, and analyzed with anti-actin antibody (Sigma).

Statistical Analysis—Data are presented as the S.E. Unless stated otherwise, data were compared by a paired or unpaired Student's *t* test if a Gaussian distribution was confirmed by applying a Shapiro-Wilk (normality) test, and significance was accepted at $p < 0.05$. *, $p < 0.05$; **, $p < 0.01$; ***, $p < 0.001$, *n.s.*, $p > 0.05$.

RESULTS

TRPC1 Suppresses Calcium Permeability in Heteromeric Channel Complexes with TRPC4 and -5 but Is Not Able to Form Functional Receptor-operated Homomeric Channels—To investigate whether TRPC1 is able to form functional homomeric channel complexes, we first used a heterologous expression system and performed patch clamp recordings in the whole-cell configuration with HEK293 cells overexpressing recombinant TRPC1 and the G_q-protein-coupled muscarinic M_5 receptor (M_5R). Receptor activation by carbachol (100 μM) in the bath solution (Fig. 1, *A* and *B*) as well as by GTPγS (200 μM) infusion through the patch pipette (supplemental Fig. S1, *A* and *B*) failed to activate cation currents in TRPC1 overexpressing HEK293 cells. Current densities at ±60 mV and current-voltage relationships (IVs) were not different between TRPC1-expressing and control cells (EGFP and receptor co-expressing and untransfected HEK293 cells). Identical observations were made when recombinant TRPC1 was expressed in CHO-K1 cells (supplemental Fig. S1, *D* and *E*). To obtain more detailed information about the biophysical properties of TRPC1 overexpressing cells, we analyzed ion permeabilities using an external solution containing 10 mM Ca^{2+}. However, calcium permeability in TRPC1 overexpressing cells did not differ from control cells (Fig. 1*C* and supplemental Fig. S1*C*). Because it has been reported that reduction of the phosphatidylinositol 4,5-bisphosphate content of the plasma membrane activates certain TRPC channels (23, 24), we analyzed whether TRPC1 is also regulated by phosphatidylinositol 4,5-bisphosphate depletion using wortmannin (20 μM), an inhibitor of phosphoinositide 3-kinases causing phosphatidylinositol 4,5-bisphosphate depletion at high concentrations. Incubation with wortmannin had no effect on endogenous cation currents and did not change the calcium permeability of TRPC1-expressing cells as compared with untransfected cells (supplemental Fig. S1, *F–I*). Taken together, these findings indicate that homomeric recombinant TRPC1 is incapable of forming functional receptor-operated channels despite its high mRNA expression level (supplemental Fig. S2).

Because co-expression of TRPC1 together with TRPC4 or TRPC5 results in receptor-operated heteromeric channel complexes with characteristic channel properties (25), we sought to define the specific contribution of TRPC1 to the biophysical properties of heteromeric channel complexes. Co-expression of TRPC1 with TRPC4 or TRPC5 and M_5R in HEK293 cells resulted in rapidly developing inward and outward currents evoked by agonist stimulation with carbachol or by GTPγS infusions showing altered biophysical properties compared with cells expressing TRPC4 or TRPC5 alone (Fig. 1, *D* and *E*). In physiological bath solution current voltage curves exhibited significantly larger outward and smaller inward currents mirrored by increased current ratios at ±60 mV (Fig. 1*F*). Furthermore, in a bath solution containing 10 mM Ca^{2+}, reversal potentials of heteromeric channels were significantly shifted toward more negative potentials, indicating that TRPC1 reduces the calcium permeability of heteromeric channel complexes containing TRPC4 and TRPC5 (Fig. 1, *G–I*).

TRPC1 Is Pore-forming Subunit in Heteromeric Channel Complexes and Reduces Calcium Permeabilities When Co-assembled with TRPC3/6 and -7—Next, we investigated whether co-expression with TRPC1 would also modify channel properties of the members of the diacylglycerol-sensitive subfamily TRPC3, -6, and -7. Notably, receptor-activated currents in TRPC3/1 and TRPC7/1 and M_5R co-expressing cells were characterized by significantly increased ratios of outward to inward currents at ±60 mV when compared with cells expressing TRPC3 or TRPC7 and M_5R (Fig. 2, *A* and *C*). In addition, slope conductances at ±55 mV (determined at current amplitudes of −200 pA and +1 nA) were significantly different. In physiological bath solution no differences were observed between TRPC6/1- and TRPC6-expressing cells (Fig. 2*B*) although both TRPC subunits were highly expressed at the mRNA level (supplemental Fig. S2). However, application of 10 mM Ca^{2+} to the bath always resulted in a leftward shift of reversal potentials of TRPC1-co-expressing cells reflecting a significantly reduced calcium permeability (Fig. 2, *E* and *F*) that was not noted in TRPM7/TRPC1-co-expressing cells (supplemental Fig. S3). These findings indicate a potential function of TRPC1 as a modulator of calcium permeabilities of heteromeric TRPC channel complexes.

To sort out the mechanism by which TRPC1 alters calcium permeabilities, we asked whether TRPC1 functions as a pore-forming subunit in heteromeric channel complexes. Amino acid exchanges from glutamate to glutamine at positions 581 and 582 in the putative pore region of TRPC1 resulted in a

TRPC1 Reduces Calcium Permeability

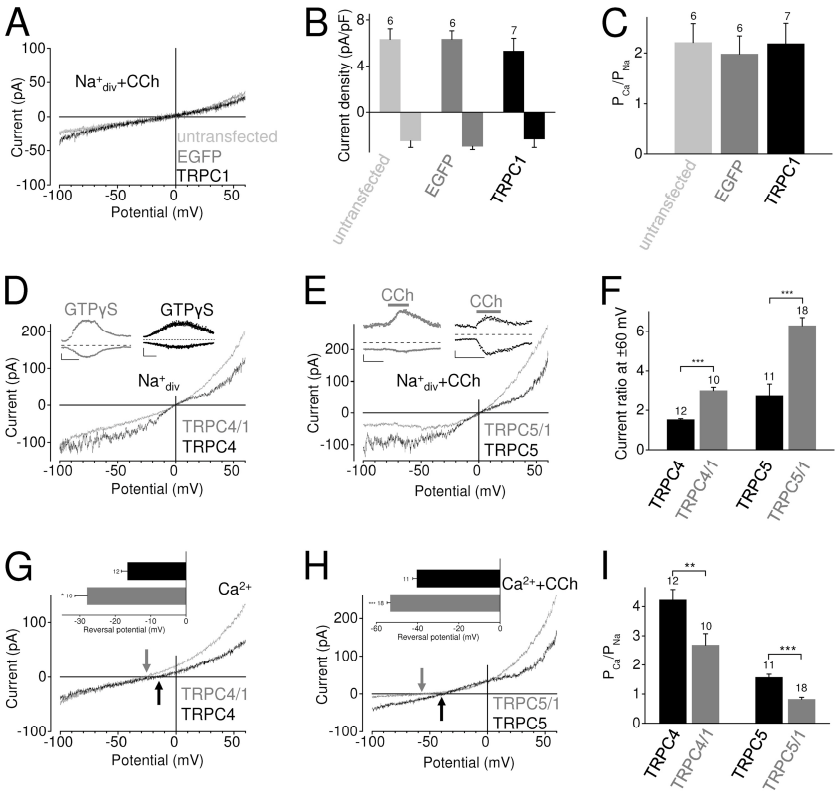

FIGURE 1. **TRPC1 attenuates calcium permeability in heteromeric channel complexes with TRPC4 and 5, but TRPC1 *per se* cannot form functional receptor-operated homomeric channel complexes.** *A–I*, shown are whole-cell recordings from untransfected HEK293 cells and HEK293 cells expressing EGFP alone or TRPC1 and the muscarinic M_5R (*A–C*) or expressing TRPC4 or TRPC5 alone or in combination with TRPC1 and M_5R (*D–I*). TRPC4-expressing cells were activated by infusions of 200 μM GTPγS through the patch pipette (*D*) and TRPC5-expressing cells by receptor stimulations with 100 μM carbachol (*E*). Exemplary IV curves in standard bath solution (Na^+_{div}) (*D*) and (Na^+_{div}+*CCh*) (*A* and *E*) and in 10 mM Ca^{2+} solution (Ca^{2+}) (*G*) and in (Ca^{2+}+*CCh*) (*H*) are shown. *D* and *E*, *insets* in *D* and *E* show current time courses at ±60 mV, 0 current levels (*stippled lines*), *time scale bars* (100 s), and *current scale bars* (50 pA). *G* and *H*, *arrows* indicate reversal potentials. *Insets* in *G* and *H* show the analysis of reversal potentials determined in 10 mM Ca^{2+} solution. *B*, analysis of current densities at ±60 mV is shown. *C* and *I*, analysis of calcium permeabilities is shown. *F*, analysis of current ratios determined at holding potentials of ±60 mV is shown. indicate the number of cells measured. *pF*, picofarads; **, $p < 0.01$; ***, $p < 0.001$.

significantly reduced calcium permeability when co-expressed with TRPC5 (Fig. 2, *G* and *H*). This pair of glutamic acid residues is only present in the putative pore region of TRPC1 but not in other TRPCs. The simultaneous exchange of both glutamates had no additional effect. These findings indicate that in heteromeric channel complexes TRPC1 proteins are involved in the formation of the pore region. Moreover, to determine changes of cation permeability by a different approach, basal entry of extracellular divalent cations was analyzed by measuring the quenching of the fura-2 fluorescence by influx of extracellular Mn^{2+}. A pronounced quench of fura-2 fluorescence was observed in TRPC3-expressing cells (Fig. 2*I*), reflecting this channel high basal activity of about 50% (21). In TRPC3- and TRPC1-co-expressing cells, fura-2 quenching was significantly reduced, indicating a decrease of divalent cation influx. Co-expression of the TRPC1 mutant $TRPC1^{E582Q}$ reduced Mn^{2+} quenching even further demonstrating that under basal conditions cation entry through homomeric TRPC3 channels is significantly reduced in the presence of TRPC1. To test whether the reduced divalent cation influx in TRPC1-co-expressing cells was based on altered ion channel expression levels, we performed additional qPCR experiments (supplemental Fig. S4). mRNA expression levels of recombinant TRPC1 and TRPC3 were not significantly different, suggesting that the reduced divalent cation influx observed was most likely not caused by different TRPC expression levels. These findings affirm that TRPC1 is a pore-forming subunit in heteromeric TRPC channel complexes thereby reducing the calcium permeability.

TRPC1 Attenuates Calcium Permeability in GnRH Neurons Thereby Reducing Basal Intracellular Calcium Concentrations—We wondered whether endogenously expressed TRPC1 would also impact calcium permeation. To this end, immortalized murine GnRH-releasing neurons (Gn11 cells), originally derived from the olfactory bulb at embryonic state day 11.5, were investigated because they prominently express TRPC1 as detected by quantitative RT-PCR analysis (Fig. 3*A*). TRPC2, TRPC5, and TRPC6 were expressed less abundantly. In addition, the expression pattern of voltage-gated calcium channels (Ca_vs) was examined showing that these neurons only express Ca_vs of the PQ- but not of the N-type, most likely due to their immature nature. To define the specific role of TRPC1 in these

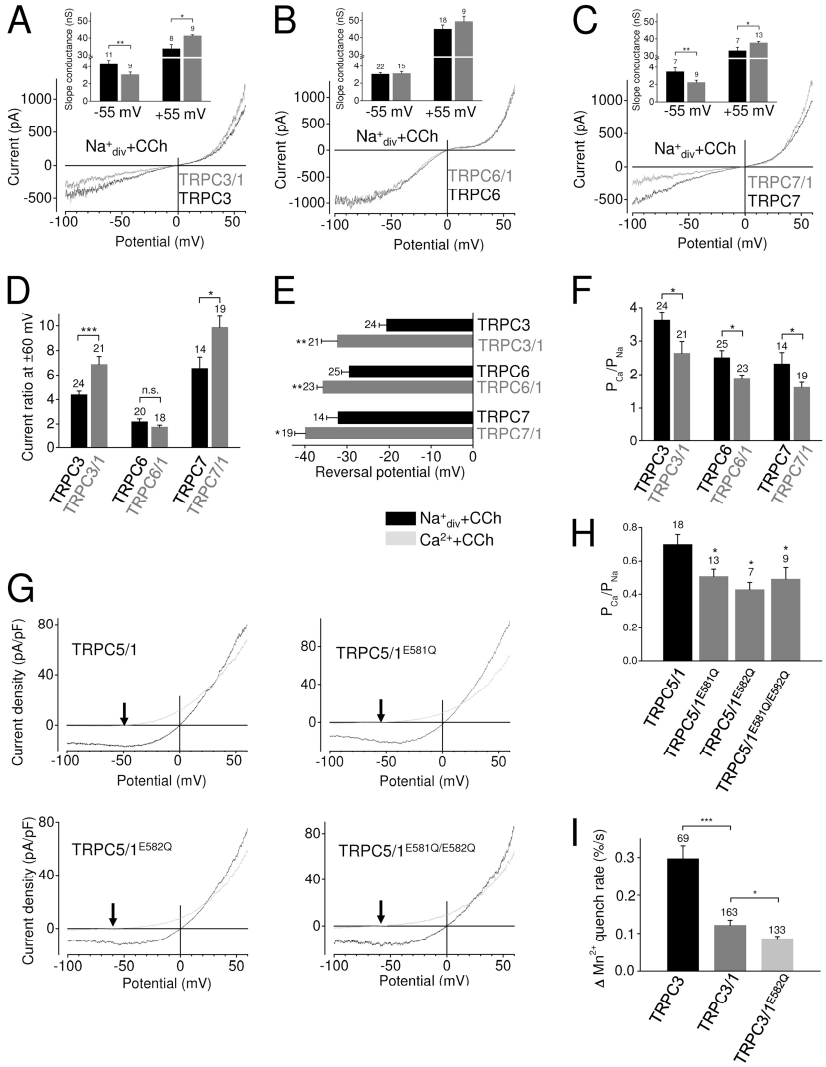

FIGURE 2. **TRPC1 is a pore-forming subunit in heteromeric channel complexes and suppresses the calcium permeability of TRPC3/6/7 channel complexes.** *A–H*, whole-cell recordings are shown of HEK293 cells expressing TRPC3, TRPC6, or TRPC7 alone or in combination with TRPC1 together with M_5R (*A–C*) or of HEK293 cells co-expressing TRPC5 and TRPC1 or TRPC1 mutant channels with amino acid exchanges from glutamate to glutamine at positions 581 (E581Q) and 582 (E582Q) or both (E581Q/E582Q) in combination with the M_5R (*G* and *H*). *A–C*, typical carbachol-induced IV curves measured in standard bath solution ($Na^+_{div}+CCh$) are displayed. *Insets* show the slope conductance determined during voltage changes from −50 to −60 mV (−55 mV) and from +50 to +60 mV (+55 mV). Only measurements with inwards currents of −200 ± 10 pA at −60 mV and outward currents of 1 ± 0.02 nA at +60 mV were included in the calculations. *nS*, nano Siemens. *D*, analysis of the ratios between outward and inward currents at ±60 mV is shown. *E*, analysis of the reversal potentials determined during application of 10 mM Ca^{2+} solution in the presence of carbachol is shown. *F*, analysis of the respective calcium permeabilities is shown. *G*, current density-voltage relationships of carbachol-induced currents in standard bath solution ($Na^+_{div}+CCh$) and in 10 mM Ca^{2+} solution ($Ca^{2+}+CCh$) are displayed. The *arrows* indicate the reversal potentials in Ca^{2+} solution in the presence of carbachol. *H*, shown is analysis of the calcium permeabilities. The *numbers over the bars* indicate the number of cells measured. *I*, analysis of Mn^{2+} quenching experiments with fura-2-loaded HEK293 cells expressing recombinant TRPC3 alone and TRPC3/TRPC1 as well as TRPC3/TRPC1^{E582Q} in the presence of 200 μM extracellular Mn^{2+}. Each indicated transfection shows the normalized Mn^{2+} quench rate expressed as percentages over time. *Numbers above the bars* indicate the number of cells measured of six independent experiments for each indicated transfection. *, $p < 0.05$; **, $p < 0.01$; ***, $p < 0.001$.

neuronal cells, channel expression was suppressed using an shRNA approach. TRPC1 expression was significantly reduced to 13.1 ± 9.4% by a specific shRNA directed against TRPC1 when compared with wild-type cells (Fig. 3*B*), whereas unrelated control shRNA had no effect on TRPC1 expression. Additionally, the efficiency of TRPC1 knockdown was tested on the protein level by Western blot analysis. Because of the lack of specific antibodies against endogenous TRPC1 proteins in Gn11 neurons, CHO-K1 cells stably expressing N- and C-terminal-tagged TRPC1 (HA-mTRPC1-HA) were used, and TRPC1 was detected by an anti-HA antibody. Transient transfections with shRNA against TRPC1 resulted in disappearance of the TRPC1 band, whereas the expression of control shRNA had no effect (Fig. 3*C*), demonstrating that the shRNA used

TRPC1 Reduces Calcium Permeability

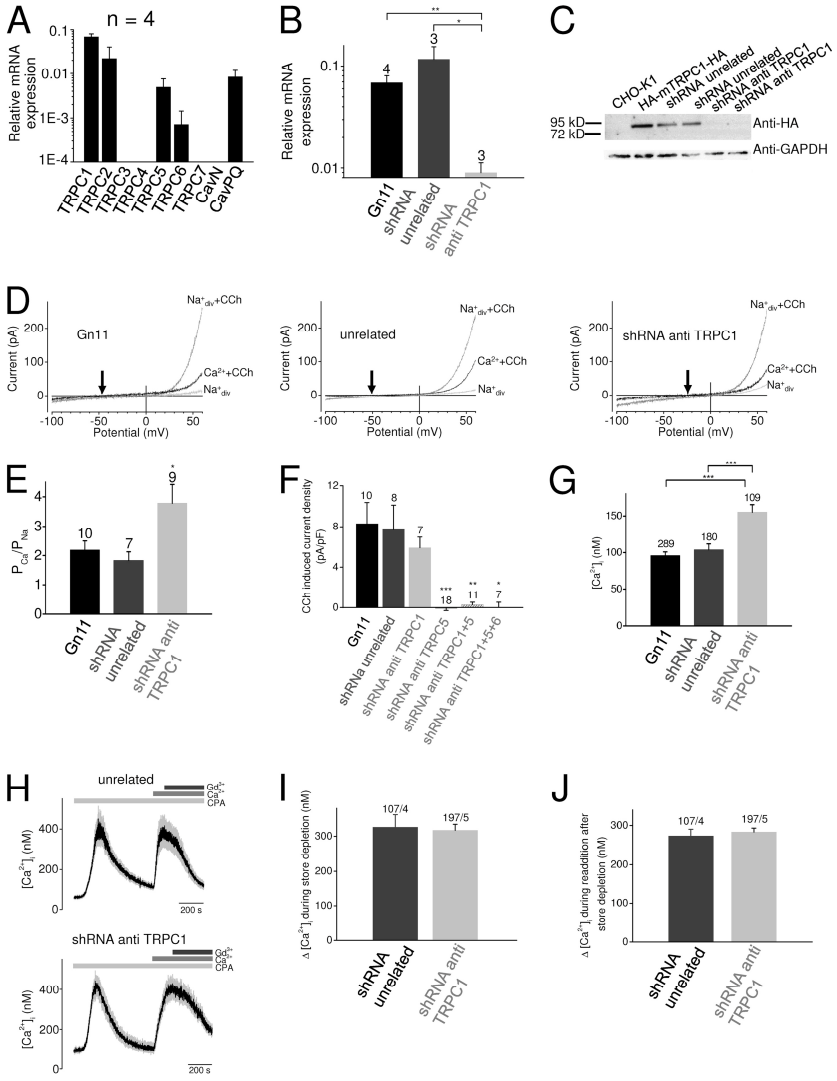

FIGURE 3. **TRPC1 reduces the calcium permeability and the cytosolic calcium concentrations in Gn11 neurons without affecting the store-operated calcium influx.** *A*, shown is relative mRNA expression analysis of TRPC channels and voltage-gated N-type and PQ-type calcium channels in Gn11 cells. *B*, analysis of the relative mRNA TRPC1 expression in Gn11 wild-type cells and in monoclonal Gn11 cell lines stably expressing unrelated control shRNA (*shRNA unrelated*) and shRNA targeting TRPC1 (*shRNA anti-TRPC1*). The *numbers over the bars* indicate the number of independent experiments each determined as quadruplets. *C*, Western blot analysis of CHO-K1 cells and of CHO-K1 cells stably expressing HA-tagged TRPC1 (*CHO-K1 HA-mTRPC1-HA*) alone or in combination with unrelated control shRNA or shRNA targeting TRPC1. *D* and *E*, whole-cell measurements of Gn11 wild-type cells and of Gn11 cells transiently transfected with unrelated shRNA (*shRNA unrelated*) and with shRNA targeting TRPC1 (*shRNA anti-TRPC1*) with exemplary IV relationships before and during agonist stimulation with CCh in standard bath solution and in 10 mM Ca^{2+} solution in the presence of carbachol (*D*). The *arrows* indicate the reversal potentials in Ca^{2+} solution. *E*, shown is analysis of the respective calcium permeabilities. *F*, shown is current density analysis of Gn11 cells, Gn11 cells expressing unrelated shRNA, shRNA targeting TRPC1 or TRPC5, and Gn11 cells co-expressing shRNA targeting TRPC1 and TRPC5 or TRPC1, TRPC5, and TRPC6. Outward current densities at +60 mV are displayed, and basal current densities before agonist stimulation with carbachol are subtracted. Significant differences in comparison to wild-type, unrelated, and TRPC1 knockdown Gn11 cells are highlighted by an *asterisk*. *Numbers over the bars* indicate the number of cells measured. *G*, shown is analysis of fluorescence measurements of the basal cytosolic-free calcium concentrations $[Ca^{2+}]_i$ of fura-2-loaded Gn11 wild-type cells and of Gn11 cells stably expressing unrelated shRNA or shRNA against TRPC1 (TRPC1 knockdown). The *numbers over the bars* indicate the numbers of measured cells from four to six independent experiments. *H*, shown are exemplary time courses of two individual experiments with 12 fura-2-loaded control or TRPC1 knockdown Gn11 cells each are displayed. Time courses of the 12 cells are averaged. Changes of $[Ca^{2+}]_i$ in fura-2-loaded Gn11 cells were monitored after store depletion by 10 μM cyclopiazonic acid (*CPA*) in calcium-free, EGTA-buffered bath solution. Calcium influx after store depletion was induced by the addition of 2 mM Ca^{2+}. Application of 10 μM Gd^{3+} is displayed. *I*, shown are maximal increases of $[Ca^{2+}]_i$ during store depletion, and maximal calcium $[Ca^{2+}]_i$ answers after the readdition of 2 mM Ca^{2+} (*J*) are shown. Basal $[Ca^{2+}]_i$ was subtracted. The *first number over the bars* indicates the number of cells measured, and the *second number* indicates the number of independent experiments. *, $p < 0.05$; **, $p < 0.01$; ***, $p < 0.001$.

strongly suppresses TRPC1 expression. Next, whole-cell patch clamp measurements were performed with wild-type Gn11 cells and Gn11 cells expressing either unrelated control shRNA or shRNA directed against TRPC1. Current increases were induced by application of 100 μM carbachol or 1 μM bradykinin (data not shown). Interestingly, transient (Fig. 3, *D* and *E*) as

well as stable overexpression of shRNA against TRPC1 (supplemental Fig. S5) resulted in a significantly increased calcium permeability indicating that endogenously expressed TRPC1 proteins also reduce the overall calcium permeability in Gn11 neurons.

To analyze the molecular identity of the carbachol-induced cation currents in Gn11 cells, we performed additional whole-cell measurements with TRPC1 knockdown Gn11 cells transiently transfected with shRNA targeting murine TRPC5 and/or murine TRPC6. shRNA constructs targeting mouse TRPC5 and mouse TRPC6 were generated and tested for their efficiency performing quantitative qPCR and Western blot analysis (supplemental Fig. S6). In Gn11 cells stably expressing TRPC5 shRNA, the relative TRPC5 mRNA expression was markedly reduced (reduction of 76.6 ± 7.7% compared with WT Gn11 cells and 89.7 ± 3.4% compared with control cells expressing unrelated shRNA), whereas in Gn11 cells stably expressing TRPC6 shRNA, the relative TRPC6 mRNA expression was reduced to a smaller extent (reduction of relative mRNA expression of 54.3 ± 21.9% compared with WT Gn11 cells and 77.8 ± 10.6% compared with control cells expressing unrelated shRNA). However, in performing qPCR analysis we observed that TRPC6 mRNA expression levels are very low, close to the detection limit. Therefore, we performed Western blot analysis with CHO-K1 cells stably overexpressing HA-tagged mouse TRPC6 to monitor TRPC6 expression on the protein level. Co-expression of shRNA against TRPC6 markedly reduced TRPC6 expression (supplemental Fig. S6C), indicating that the generated shRNA against TRPC6 is effective. shRNA against TRPC5 or TRPC6 had no effect on the TRPC expression profile of Gn11 cells (data not shown). Interestingly, knockdown of TRPC1 resulted in a minor insignificant decrease of outward currents, whereas shRNA targeting TRPC5 caused a significant suppression of carbachol-induced cation currents (Fig. 3*F*). Knockdown of TRPC1 and TRPC5 resulted in a similar current reduction. Additional shRNA targeting of TRPC6 had no additional effect, indicating that TRPC6 is not relevant for carbachol-induced cation currents in Gn11 cells. Furthermore, TRPC2, which is mainly expressed in the vomeronasal organ, did not participate in receptor-operated cation currents. These results indicate that in Gn11 neuron receptor-operated cation currents are mainly mediated by heteromeric TRPC1 and TRPC5 channel complexes. Furthermore, these results strongly suggest that endogenous TRPC1 in Gn11 neurons is not able to form functional homomeric receptor-operated cation channel complexes.

To analyze the impact of calcium permeability on the global free intracellular calcium concentration ($[Ca^{2+}]_i$), Gn11 neurons were loaded with the fluorescent dye fura-2, and $[Ca^{2+}]_i$ was determined. We observed that $[Ca^{2+}]_i$ was significantly increased by 51.6 ± 9.2 nM when TRPC1 knockdown and control cells were compared (Fig. 3*G*), thus supporting the notion that TRPC1 is a regulator of the intracellular calcium concentration.

Because TRPC1 is regarded as a key player for store-operated calcium influx (8–10), we monitored changes of $[Ca^{2+}]_i$ in fura-2-loaded Gn11 neurons after performing established maneuvers to assess store-operated calcium entry. After store depletion in a calcium-free bath solution by 10 μM cyclopiazonic acid, an inhibitor of calcium ATPases in intracellular calcium stores, for more than 10 min, 2 mM Ca^{2+} was added to the bath and resulted in a rapid calcium influx. The calcium release component did not differ between TRPC1 knockdown and control cells (Fig. 3, *H* and *I*), and subsequent store-operated calcium influx was also not different (Fig. 3*J*). The addition of Gd^{3+} at the end of the procedure led to a decrease of $[Ca^{2+}]_i$ in both cases. These findings strongly suggest that TRPC1 is not a relevant component of store-operated calcium channels in GnRH neurons.

TRPC1 Is Involved in Migration of GnRH Neurons—GnRH neurons originate from the olfactory bulb from where they migrate to the hypothalamus to fully differentiate and to lose their migratory properties during development. To shed light on the role of TRPC1 as a calcium suppressor in Gn11 neurons, which are immature and still have the ability to migrate, we performed scratch assays. Interestingly, TRPC1 knockdown cells showed significantly enhanced motility compared with wild-type and control cells (Fig. 4, *A* and *B*). This increased migratory property was independent of the concentration of fetal calf serum, and it could not be further increased by agonist stimulation with carbachol, bradykinin, or endothelin-1. Additionally, we examined cell proliferation (supplemental Fig. S7) and apoptosis (data not shown) as alternative explanations for the apparent increased motility of TRPC1 knockdown neurons in scratch assays. We did not observe any differences in cell proliferation between control shRNA-expressing Gn11 and TRPC1 knockdown cells. However, untransfected Gn11 wild-type cells exhibited a slight increase in cell proliferation. Furthermore, TRPC1 had no effect on apoptosis (data not shown).

Because polymerization and depolymerization of actin are important determinants of cell motility (26), we investigated the F-actin/G-actin ratio by quantification of Western blots of cellular fractions of filamentous actin (F-actin) *versus* free globular-actin (G-actin) (Fig. 4, *C* and *D*). Phalloidin, which prevents depolymerization of F-actin, and cytochalasin D, which binds to G actin and prevents polymerization, were used as positive controls for F- and G-actin, respectively. Although there were no significant differences between F- and G-actin fractions in Gn11 and in control cells, TRPC1 knockdown cells showed a significantly increased G-actin fraction demonstrating that the enhanced motility of TRPC1 knockdown neurons is associated with a marked reorganization of the actin cytoskeleton. Taken together, these results suggest that TRPC1 knockdown cells exhibiting increased cytosolic calcium concentrations show increased cell motility, pointing to a specific role of TRPC1 for the migration of Gn11 neurons.

Moreover, performing time lapse videomicroscopy, we noted that TRPC1 knockdown and control Gn11 neurons significantly differed in terms of specific migratory properties like distance covered, migration speed, and directionality. TRPC1 knockdown cells changed direction less frequently, thereby covering a greater effective distance from start to end. Additionally, these cells moved with a higher speed, thus traveling a greater total distance, *e.g.* path length (Fig. 4, *E* and *F*). Additionally, the ratio of the total path length and the effective distance covered was decreased in TRPC1 knockdown cells, sug-

TRPC1 Reduces Calcium Permeability

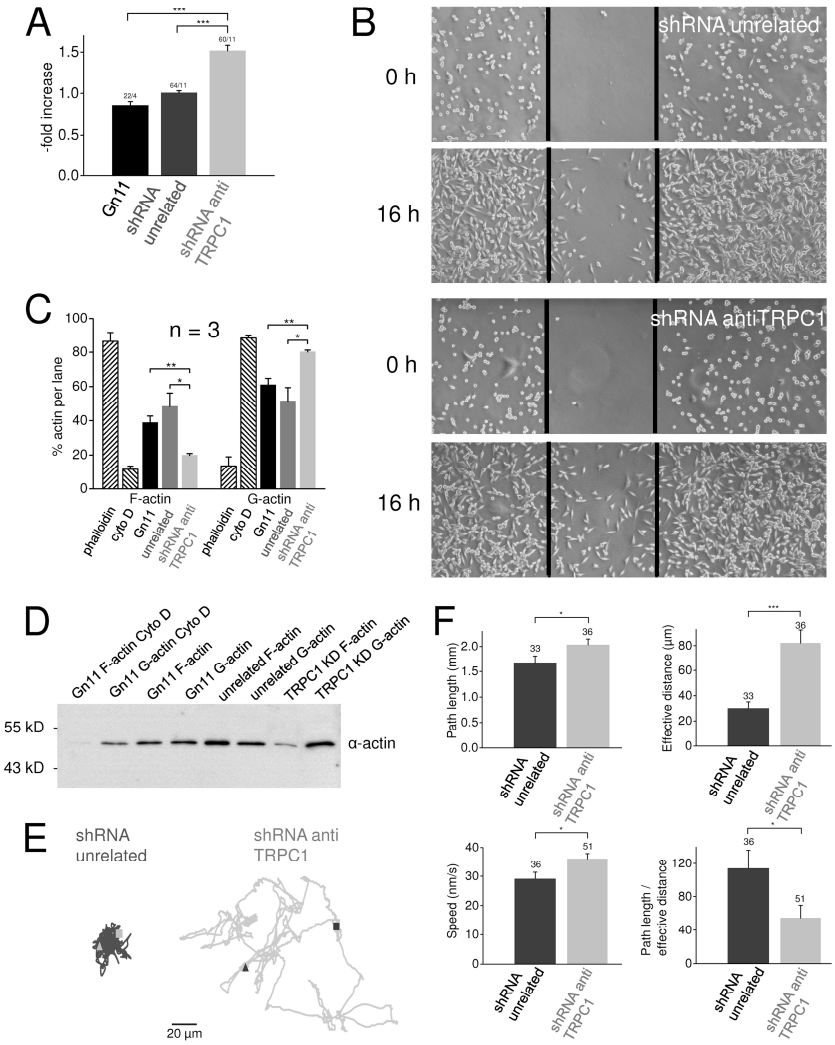

FIGURE 4. **TRPC1 reduces migration and motility of GnRH neurons.** *A*, shown is analysis of scratch assays with wild-type Gn11 cells and with Gn11 cells stably expressing unrelated shRNA or shRNA against TRPC1. *B*, a representative illustration of the migratory behavior of Gn11 cell lines in scratch assay right after scratch and after 16 h is shown. The *black lines* indicate the scratch performed with a yellow pipette tip. *C* and *D*, shown is analysis of the F-actin/G-actin assay with phalloidin as a positive control for F-actin, preventing F-actin depolymerization, and with cytochalasin D (*cyto D*) as a positive control for G-actin, preventing G-actin polymerization. *D*, a representative Western blot is displayed. *E* and *F*, translocation analysis of migrating Gn11 neurons with time laps movies is shown. *E*, exemplary trajectories of unrelated shRNA and shRNA against TRPC1 expressing Gn11 cells are shown. The *triangles* display the start, and the *squares* indicate the end of the movement. *F*, shown are the analysis of total path length, effective distance from start to end, speed, and the quotient between the total path length, and the effective distance displaying the degree of changes of direction. *Numbers over bars* indicate the number of measured cells. *, $p < 0.05$; **, $p < 0.01$; ***, $p < 0.001$.

gesting a lower degree of changes of direction. These findings provide strong evidence in favor of the concept that suppression of TRPC1 expression enhances neuronal motility.

DISCUSSION

The present study reveals that TRPC1 alone is not able to form functional homotetrameric, receptor-operated channels in heterologous expression systems. Instead, we made the observation that TRPC1 proteins are not only able to assemble to heteromeric receptor-operated channel complexes with TRPC4 and -5 (14, 25) but also form heteromeric complexes with all members of the diacylglycerol-sensitive subfamily TRPC3, -6, and -7, suggesting that TRPC1 is rather promiscuous in terms of heteromultimerization with other TRPC channels. Although interaction of TRPC1 with TRPC3/6/7 was previously not detected using co-immunoprecipitation or FRET analysis (27–29), we took advantage of a highly sensitive electrophysiological approach and found that TRPC1 functionally interacts with TRPC3, -6, or -7 to form receptor-operated channel complexes with distinct biophysical properties. Our data are in line with the findings of other groups showing heterotetramerization of TRPC1/3 or TRPC1/7 or of TRPC1/5/6 (14, 30–34).

To date there is still controversy about the issue as to whether TRPC1 is able to form functional homomeric channels. In our study the lack of agonist-, GTPγS-, or phosphatidylinositol 4,5-bisphosphate depletion-induced currents in TRPC1 overexpressing cells suggests that at least in the heterologous expression system employed by us, TRPC1 proteins *per se* are unable to form functional homomeric channels in the plasma membrane. This might be explained by their inability for homotetramerization or by intracellular localization of TRPC1 homomers, preventing insertion into the plasma membrane (35–37). However, at present we cannot rule out that homomeric TRPC1 channels are not gated by typical TRPC activators. However, we noted that amino acid exchanges from glutamate to glutamine at positions 581 and 582 in the putative pore-forming region of TRPC1 further reduced the calcium permeability of heteromeric channel complexes, indicating that TRPC1 is not an accessory (β) subunit of heteromeric channel complexes but that TRPC1 is involved in the formation of the channel pore.

There is still controversy about the role of TRPC1 for store-operated Ca^{2+} entry. Our previous studies with vascular smooth muscle cells of TRPC1 gene-deficient mice showed that TRPC1 is not involved in SOC (11). Likewise, Potier *et al.* (38) showed that SOC in vascular smooth muscle cells was independent of TRPC1 but was mediated by STIM1 and Orai1. So far, the role of TRPC1 for SOC in neurons is largely unknown. Applying an established store-depletion protocol, we did not observe an involvement of TRPC1 in SOC in Gn11 neurons. However, it was shown recently that TRPC1 is involved in SOC-dependent migration in transformed renal epithelial cells (MDCK-F cells) as a model to study tumor cell migration (39). Interestingly, Fabian *et al.* (39, 40) demonstrated that knockdown of TRPC1 by shRNA in MDCK-F cells resulted in a decrease of cytosolic $[Ca^{2+}]_i$ thereby impairing motility and directed migration. These findings contrast with our results but might be explained by different cell systems used and by a different TRPC channel expression levels of renal epithelial cells compared with neurons.

In this study Gn11 neurons were chosen as a model to study the cell physiological role of TRPC1 because of their pronounced TRPC1 expression. Furthermore, mRNA analysis revealed expression of TRPC2, -5, and -6 at lower levels. However, Gn11 cells were previously described to express all TRPC subtypes by immunochemistry (41), but recently the same group only detected TRPC1, -2, and -5 in these cells by mRNA analysis (42). Regarding the extraordinarily high expression level of TRPC1 and the select expression profile of other TRPC subtypes, Gn11 cells turned out to be an excellent model to study TRPC1 heteromers. Because Strübing *et al.* (14) had shown that heteromeric channel complexes consisting of TRPC4/5–3/6 can only assemble in the presence of TRPC1 and occur only in the embryonic brain during development but not in the adult brain, it was very likely that heteromeric TRPC channel complexes also occur in Gn11 neurons derived from embryonic brain. We could verify our experimental data obtained by expression of recombinant TRPC1 in a heterologous expression system by performing knockdown of TRPC1 in Gn11 neurons by an shRNA approach that did not impinge on the expression profile of other TRPC channels. Interestingly, TRPC1 knockdown Gn11 cells showed a significantly increased calcium permeability supporting the notion that endogenously expressed TRPC1 likewise functions as a suppressor of calcium permeability.

Ariano *et al.* (42) recently showed that TRPC channels are involved in calcium-dependent migration of Gn11 neurons. Here we identified TRPC1 as a specific regulator of the free cytosolic calcium concentration in Gn11 neurons controlling neuronal migration. Specific knockdown of TRPC1 in Gn11 cells resulted in increased $[Ca^{2+}]_i$ and in enhanced motility verified with three different approaches; 1) scratch assay, 2) time lapse microscopy, 3) determination of the G-actin/F-actin ratio. Although Ariano *et al.* (42) used unspecific TRP channel blockers like SKF96365 and La^{3+} and an antibody against the predicted pore-forming region of TRPC1, we performed specific down-regulation of TRPC1. Using the TRPC1 antibody to deactivate TRPC1, Ariano *et al.* (42) reduced the migration of Gn11 cells, which is contrary to our findings with knockdown of TRPC1 by shRNA. These conflicting results might be explained by a blockade of all heteromeric TRPC1 containing channels by the antibody thus resulting in decreased calcium influx and reduced calcium-dependent cell motility. Our knockdown approach by specific shRNAs ensured that other TRPC protein subtypes can still form functional channels allowing for calcium influx. Consequently, calcium influx was not impaired, and calcium permeability and free cytosolic $[Ca^{2+}]_i$ were increased. However, in line with Ariano *et al.* (42), we did not observe any effect of TRPC1 on proliferation.

Zaninetti *et al.* (43) have demonstrated that migration of Gn11 cells is dependent on calcineurin and nuclear factor of activated T-cells (NFAT). Therefore, we propose the following pathway. Down-regulation of TRPC1 in Gn11 cells increases the calcium permeability leading to a rise in cytosolic $[Ca^{2+}]_i$, thereby activating calmodulin, which subsequently activates calcineurin. Calcineurin in turn dephosphorylates nuclear factor of activated T-cells and induces translocation into the nucleus, thereby enhancing the transcription of genes pertinent to increased cell migration.

To summarize, our results provide several lines of evidence to support the new concept that in immortalized immature GnRH neurons TRPC1 suppress neuronal migration, thus highlighting a novel regulatory mechanism based on the formation of heteromeric TRPC channel complexes with reduced calcium permeability.

Acknowledgments—We thank Eva Braun, Ernst Bernges, Elisabeth Topoll, and Joanna Zaisserer for excellent technical assistance. We are grateful to Sally Radovick and Davide Lovisolo for providing Gn11 cells. We thank Alexander Dietrich and Meike Fahlbusch for supplying and cloning HA-mTRPC1-HA cDNA and Hermann Kalwa for assistance in the design of shRNA constructs. We are indebted to Alexander Liebstein (Zeiss) who made the AxioVision software available to us and to Christoph Klingner for initial help with time lapse microscopy.

REFERENCES

1. Hofmann, T., Obukhov, A. G., Schaefer, M., Harteneck, C., Gudermann, T., and Schultz, G. (1999) Direct activation of human TRPC6 and TRPC3 channels by diacylglycerol. *Nature* **397,** 259–263
2. Salido, G. M., Sage, S. O., and Rosado, J. A. (2009) TRPC channels and

store-operated Ca^{2+} entry. *Biochim. Biophys. Acta* **1793,** 223–230
3. Wu, L. J., Sweet, T. B., and Clapham, D. E. (2010) International union of basic and clinical pharmacology. LXXVI. Current progress in the mammalian TRP ion channel family. *Pharmacol. Rev.* **62,** 381–404
4. Bollimuntha, S., Selvaraj, S., and Singh, B. B. (2011) Emerging roles of canonical TRP channels in neuronal function. *Adv. Exp. Med. Biol.* **704,** 573–593
5. Cui, K., and Yuan, X. (2007) in *TRP Ion Channel Function in Sensory Transduction and Cellular Signaling Cascades* (Liedke, W. B., and Heller, S., eds) Chapter 4, CRC Press, Boca Raton, FL
6. Selvaraj, S., Sun, Y., and Singh, B. B. (2010) TRPC channels and their implication in neurological diseases. *CNS Neurol. Disord. Drug Targets* **9,** 94–104
7. Maroto, R., Raso, A., Wood, T. G., Kurosky, A., Martinac, B., and Hamill, O. P. (2005) TRPC1 forms the stretch-activated cation channel in vertebrate cells. *Nat. Cell Biol.* **7,** 179–185
8. Beech, D. J. (2005) TRPC1. Store-operated channel and more. *Pflugers Arch.* **451,** 53–60
9. Ambudkar, I. S., Ong, H. L., Liu, X., Bandyopadhyay, B. C., Bandyopadhyay, B., and Cheng, K. T. (2007) TRPC1. The link between functionally distinct store-operated calcium channels. *Cell Calcium* **42,** 213–223
10. Yuan, J. P., Kim, M. S., Zeng, W., Shin, D. M., Huang, G., Worley, P. F., and Muallem, S. (2009) TRPC channels as STIM1-regulated SOCs. *Channels* **3,** 221–225
11. Dietrich, A., Kalwa, H., Storch, U., Mederos y Schnitzler, M., Salanova, B., Pinkenburg, O., Dubrovska, G., Essin, K., Gollasch, M., Birnbaumer, L., and Gudermann, T. (2007) Pressure-induced and store-operated cation influx in vascular smooth muscle cells is independent of TRPC1. *Pflugers Arch.* **455,** 465–477
12. Varga-Szabo, D., Authi, K. S., Braun, A., Bender, M., Ambily, A., Hassock, S. R., Gudermann, T., Dietrich, A., and Nieswandt, B. (2008) Store-operated Ca^{2+} entry in platelets occurs independently of transient receptor potential (TRP) C1. *Pflugers Arch.* **457,** 377–387
13. Rychkov, G., and Barritt, G. J. (2007) TRPC1 Ca^{2+}-permeable channels in animal cells. *Handb. Exp. Pharmacol.* **179,** 23–52
14. Strübing, C., Krapivinsky, G., Krapivinsky, L., and Clapham, D. E. (2003) Formation of novel TRPC channels by complex subunit interactions in embryonic brain. *J. Biol. Chem.* **278,** 39014–39019
15. Radovick, S., Wray, S., Lee, E., Nicols, D. K., Nakayama, Y., Weintraub, B. D., Westphal, H., Cutler, G. B., Jr., and Wondisford, F. E. (1991) Migratory arrest of gonadotropin-releasing hormone neurons in transgenic mice. *Proc. Natl. Acad. Sci. U. S. A.* **88,** 3402–3406
16. Brummelkamp, T. R., Bernards, R., and Agami, R. (2002) A system for stable expression of short interfering RNAs in mammalian cells. *Science* **296,** 550–553
17. Reynolds, A., Leake, D., Boese, Q., Scaringe, S., Marshall, W. S., and Khvorova, A. (2004) Rational siRNA design for RNA interference. *Nat. Biotechnol.* **22,** 326–330
18. Yiu, S. M., Wong, P. W., Lam, T. W., Mui, Y. C., Kung, H. F., Lin, M., and Cheung, Y. T. (2005) Filtering of ineffective siRNAs and improved siRNA design tool. *Bioinformatics* **21,** 144–151
19. Lewis, C. A. (1979) Ion concentration dependence of the reversal potential and the single channel conductance of ion channels at the frog neuromuscular junction. *J. Physiol.* **286,** 417–445
20. Grynkiewicz, G., Poenie, M., and Tsien, R. Y. (1985) A new generation of Ca^{2+} indicators with greatly improved fluorescence properties. *J. Biol. Chem.* **260,** 3440–3450
21. Dietrich, A., Mederos y Schnitzler, M., Emmel, J., Kalwa, H., Hofmann, T., and Gudermann, T. (2003) *N*-Linked protein glycosylation is a major determinant for basal TRPC3 and TRPC6 channel activity. *J. Biol. Chem.* **278,** 47842–47852
22. Tang, D. D., Zhang, W., and Gunst, S. J. (2005) The adapter protein CrkII regulates neuronal Wiskott-Aldrich syndrome protein, actin polymerization, and tension development during contractile stimulation of smooth muscle. *J. Biol. Chem.* **280,** 23380–23389
23. Trebak, M., Lemonnier, L., DeHaven, W. I., Wedel, B. J., Bird, G. S., and Putney, J. W., Jr. (2009) Complex functions of phosphatidylinositol 4,5-bisphosphate in regulation of TRPC5 cation channels. *Pflugers Arch.* **457,** 757–769
24. Otsuguro, K., Tang, J., Tang, Y., Xiao, R., Freichel, M., Tsvilovskyy, V., Ito, S., Flockerzi, V., Zhu, M. X., and Zholos, A. V. (2008) Isoform-specific inhibition of TRPC4 channel by phosphatidylinositol 4,5-bisphosphate. *J. Biol. Chem.* **283,** 10026–10036
25. Strübing, C., Krapivinsky, G., Krapivinsky, L., and Clapham, D. E. (2001) TRPC1 and TRPC5 form a novel cation channel in mammalian brain. *Neuron* **29,** 645–655
26. Machesky, L. M., and Insall, R. H. (1999) Signaling to actin dynamics. *J. Cell Biol.* **146,** 267–272
27. Hofmann, T., Schaefer, M., Schultz, G., and Gudermann, T. (2002) Subunit composition of mammalian transient receptor potential channels in living cells. *Proc. Natl. Acad. Sci. U. S. A.* **99,** 7461–7466
28. Goel, M., Sinkins, W. G., and Schilling, W. P. (2002) Selective association of TRPC channel subunits in rat brain synaptosomes. *J. Biol. Chem.* **277,** 48303–48310
29. Brownlow, S. L., and Sage, S. O. (2005) Transient receptor potential protein subunit assembly and membrane distribution in human platelets. *Thromb. Haemost.* **94,** 839–845
30. Lintschinger, B., Balzer-Geldsetzer, M., Baskaran, T., Graier, W. F., Romanin, C., Zhu, M. X., and Groschner, K. (2000) Coassembly of Trp1 and Trp3 proteins generates diacylglycerol- and Ca^{2+}-sensitive cation channels. *J. Biol. Chem.* **275,** 27799–27805
31. Liu, X., Bandyopadhyay, B. C., Singh, B. B., Groschner, K., and Ambudkar, I. S. (2005) Molecular analysis of a store-operated and 2-acetyl-*sn*-glycerol-sensitive non-selective cation channel. Heteromeric assembly of TRPC1-TRPC3. *J. Biol. Chem.* **280,** 21600–21606
32. Zagranichnaya, T. K., Wu, X., and Villereal, M. L. (2005) Endogenous TRPC1, TRPC3, and TRPC7 proteins combine to form native store-operated channels in HEK-293 cells. *J. Biol. Chem.* **280,** 29559–29569
33. Wu, X., Zagranichnaya, T. K., Gurda, G. T., Eves, E. M., and Villereal, M. L. (2004) A TRPC1/TRPC3-mediated increase in store-operated calcium entry is required for differentiation of H19–7 hippocampal neuronal cells. *J. Biol. Chem.* **279,** 43392–43402
34. Saleh, S. N., Albert, A. P., and Large, W. A. (2009) Activation of native TRPC1/C5/C6 channels by endothelin-1 is mediated by both PIP_3 and PIP_2 in rabbit coronary artery myocytes. *J. Physiol.* **587,** 5361–5375
35. Berbey, C., Weiss, N., Legrand, C., and Allard, B. (2009) Transient receptor potential canonical type 1 (TRPC1) operates as a sarcoplasmic reticulum calcium leak channel in skeletal muscle. *J. Biol. Chem.* **284,** 36387–36394
36. Wang, W., O'Connell, B., Dykeman, R., Sakai, T., Delporte, C., Swaim, W., Zhu, X., Birnbaumer, L., and Ambudkar, I. S. (1999) Cloning of Trp1β isoform from rat brain. Immunodetection and localization of the endogenous Trp1 protein. *Am. J. Physiol.* **276,** C969–C979
37. Uehara, K. (2005) Localization of TRPC1 channel in the sinus endothelial cells of rat spleen. *Histochem. Cell Biol.* **123,** 347–356
38. Potier, M., Gonzalez, J. C., Motiani, R. K., Abdullaev, I. F., Bisaillon, J. M., Singer, H. A., and Trebak, M. (2009) Evidence for STIM1- and Orai1-dependent store-operated calcium influx through ICRAC in vascular smooth muscle cells. Role in proliferation and migration. *FASEB J.* **23,** 2425–2437
39. Fabian, A., Fortmann, T., Dieterich, P., Riethmüller, C., Schön, P., Mally, S., Nilius, B., and Schwab, A. (2008) TRPC1 channels regulate directionality of migrating cells. *Pflugers Arch.* **457,** 475–484
40. Fabian, A., Fortmann, T., Bulk, E., Bomben, V. C., Sontheimer, H., and Schwab, A. (2011) Chemotaxis of MDCK-F cells toward fibroblast growth factor-2 depends on transient receptor potential canonical channel 1. *Pflugers Arch.* **461,** 295–306
41. Dalmazzo, S., Antoniotti, S., Ariano, P., Gilardino, A., and Lovisolo, D. (2008) Expression and localization of TRPC channels in immortalised GnRH neurons. *Brain Res.* **1230,** 27–36
42. Ariano, P., Dalmazzo, S., Owsianik, G., Nilius, B., and Lovisolo, D. (2011) TRPC channels are involved in calcium-dependent migration and proliferation in immortalized GnRH neurons. *Cell Calcium* **49,** 387–394
43. Zaninetti, R., Tacchi, S., Erriquez, J., Distasi, C., Maggi, R., Cariboni, A., Condorelli, F., Canonico, P. L., and Genazzani, A. A. (2008) Calcineurin primes immature gonadotropin-releasing hormone-secreting neuroendocrine cells for migration. *Mol. Endocrinol.* **22,** 729–736

Supplementary Figure 1

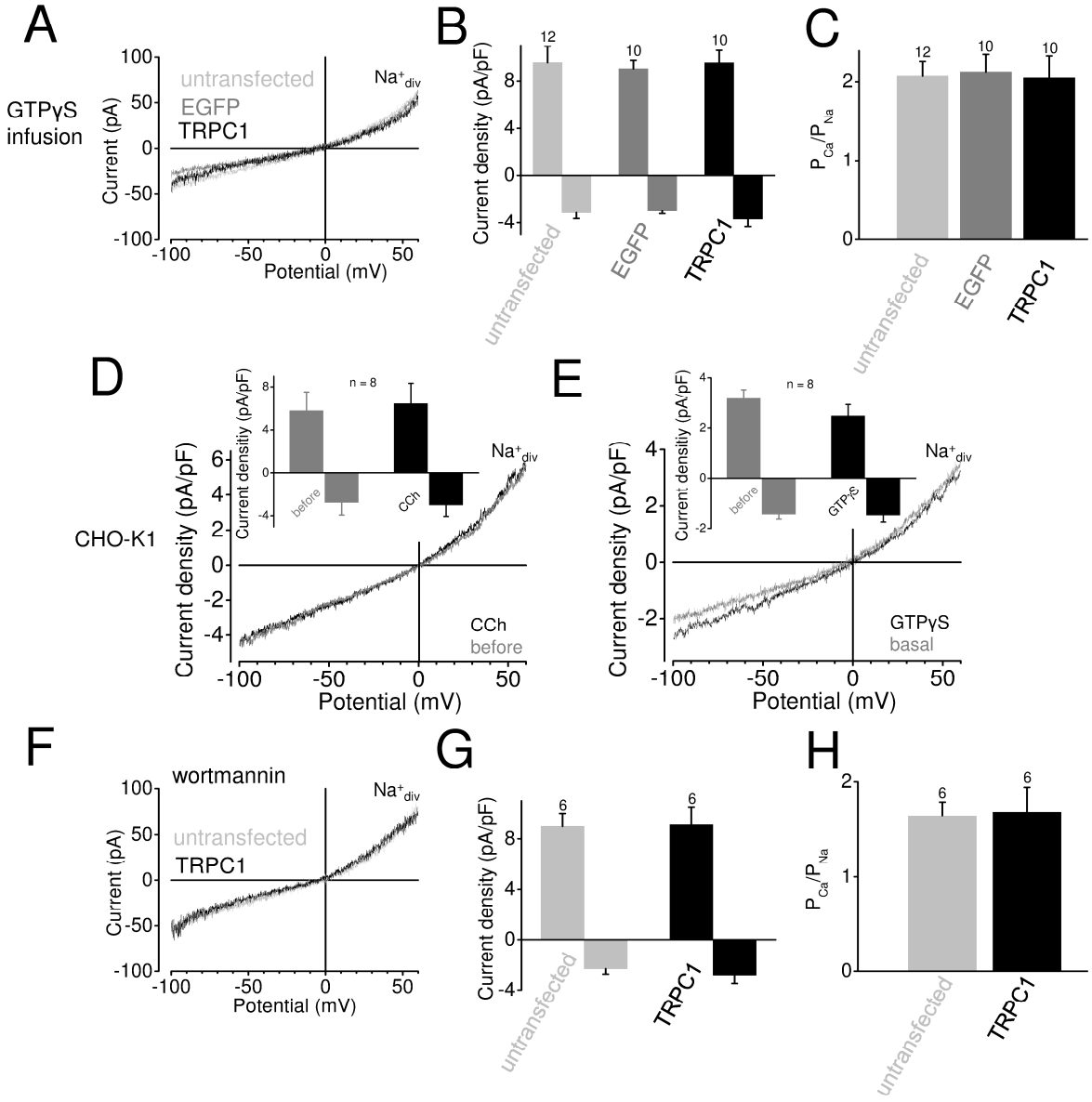

Supplementary Figure S1: TRPC1 is not able to form functional homomeric channels. (*A-H*) Whole-cell recordings from untransfected HEK293 cells and HEK293 cells expressing EGFP alone or TRPC1 and the muscarinic M_5 receptor (M_5R) (*A-C and F-H*) and CHO-K1 cells over-expressing TRPC1 and the M_5R (*D,E*). GTPγS (200 µM) infusions (*A-C,E*), agonist stimulation with 100 µM carbachol "CCh" (*D*) and application of wortmannin (20 µM) (*F,G*) are displayed. Exemplary IV curves (*A,D-F*) in standard bath solution (Na^+_{div}) are shown. Analysis of current densities (*B,D,E,G*) and of calcium permeabilities (*C,H).* The numbers over the bars indicate the number of cells measured.

Supplementary Figure 2

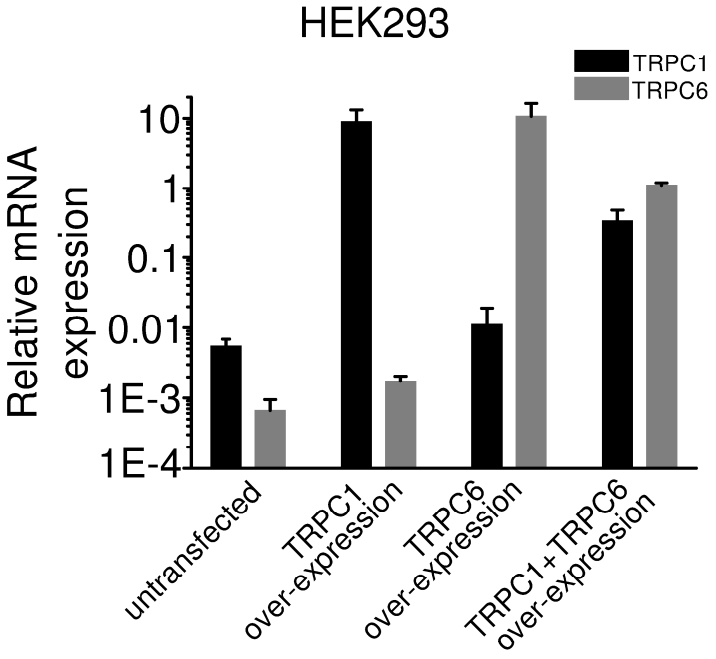

Supplementary Figure S2: Expression levels of TRPC1 and TRPC6 in untransfected and in transiently transfected HEK293 cells. Analysis of three independent quantitative qPCR approaches with untransfected, human TRPC1, human TRPC6 and human TRPC1/ human TRPC6 expressing HEK293 cells. The following primers pairs were used for the amplification of specific fragments from the first strand synthesis: TRPC1, C1for: 5'-ATG GCG CTGA AGG ATGT G-3' and C1rev: 5'-TCC TCC AAA ATC TTT TTA ACC ATA TAA-3', TRPC6, C6for: 5'-ATT TAC TGG TTT GCT CCA TGC-3' and C6rev: 5'-GCA GTC CCA GAA AAA TGG TG-3' and three references hypoxanthin phosphoribosyltransferase 1, Hprt1for (5'-TGA CCT TGA TTT ATT TTG CAT ACC-3'), Hprt1rev (5'-CGA GCA AGA CGT TCA GTC CT-3'), tyrosine 3-monooxygenase/tryptophan 5-monooxygenase activation protein, zeta polypeptide, Ywhazfor (5'-GAT CCC CAA TGC TTC ACA AG-3'), Ywhazrev (5'-TGC TTG TTG TGA CTG ATC GAC-3') and succinate dehydrogenase complex, subunit A, Sdhafor (5'-GGA CCT GGT TGT CTT TGG TC-3'), Sdharev (5'-CCA GCG TTT GGT TTA ATT GG-3') giving predicted product sizes of 113 bp for TRPC1, 103 bp for TRPC6, 102 for Hprt1, 130 for Ywhaz and 93 for Sdha.

Supplementary Figure 3

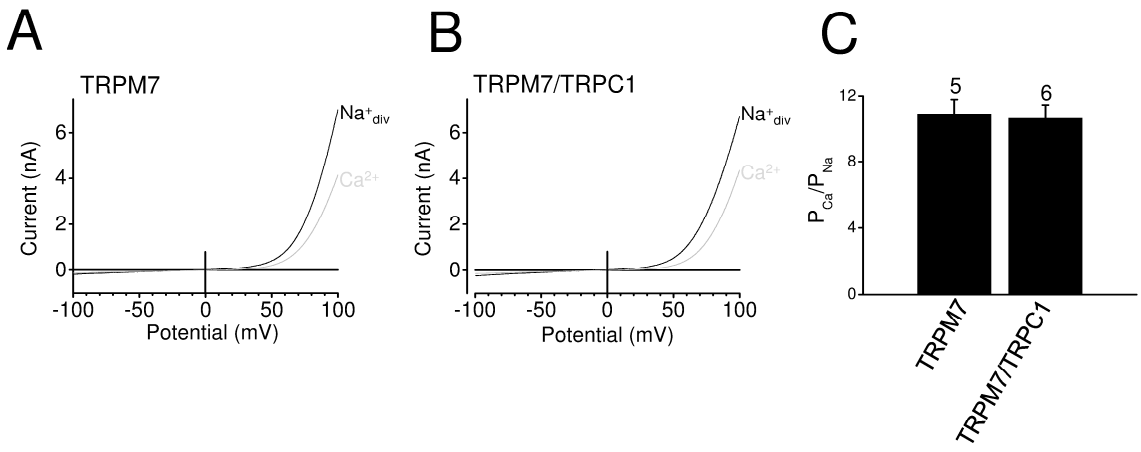

Supplementary Figure S3: TRPC1 is not able to co-assemble with TRPM7. Whole-cell recordings from HEK293 cells expressing TRPM7 alone (*A*) or TRPM7 and TRPC1 (*B*). Current activation was induced by using the following intracellular solution: 130 mM CsCl, 0.635 mM $CaCl_2$ (5.5 nM calculated free [Ca^{2+}]), 10 mM BAPTA, 1 mM HEDTA, and 10 mM HEPES, pH 7.2. IV relations were recorded during voltage ramps from –100 to +100 mV with a slope of 0.5 V/s applied at a frequency of 2 Hz. Exemplary IV relationships in standard bath solution and in 10 mM Ca^{2+} solution (*A,B*) are shown. (*C*) Analysis of the respective calcium permeabilities. The numbers over the bars indicate the number of cells measured.

Supplementary Figure 4

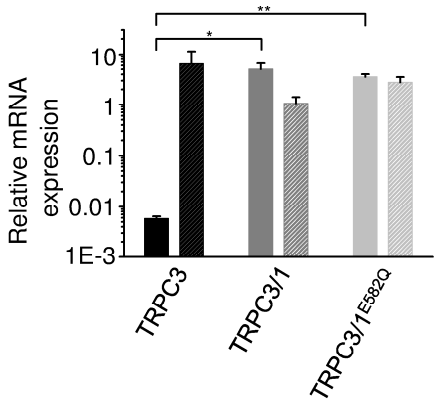

Supplementary Figure S4: qPCR analysis of HEK293 cells transfected with TRPC3 alone, with TRPC3 and TRPC1 and with TRPC3 and the TRPC1 mutant TRPC1^{E582Q}. Analysis of three independent qPCR experiments using human TRPC1 and TRPC3 primers. Relative TRPC1 (*left bars,* uncolored) and relative TRPC3 (*right bars,* shaded) mRNA expression.

Supplementary Figure 5

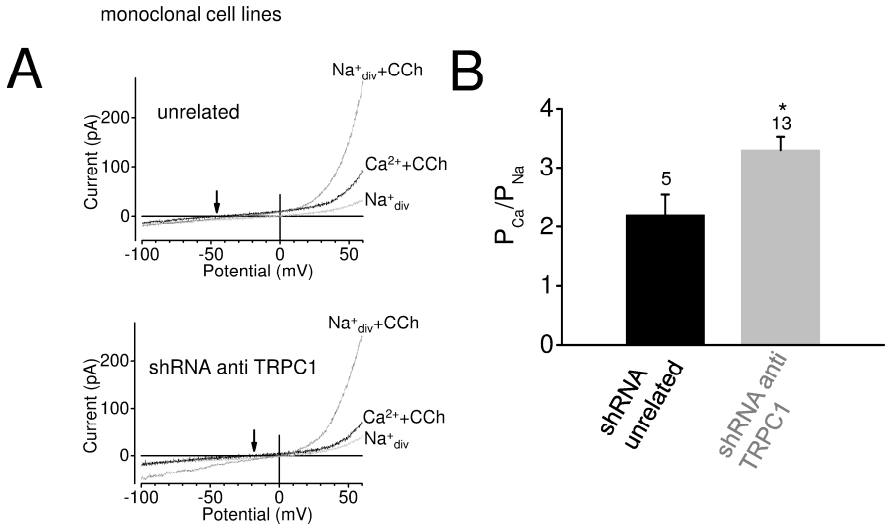

Supplementary Figure S5: Knock-down of TRPC1 in Gn11 cells increases calcium permeability. (*A*,*B*) Whole-cell measurements of monoclonal cell lines of Gn11 cells stably transfected with unrelated shRNA and with shRNA targeting TRPC1 with exemplary IV relationships before and during agonist stimulation with carbachol (CCh) and in 10 mM Ca^{2+} solution (*A*). (*B*) Analysis of the respective calcium permeabilities.

Supplementary Figure 6

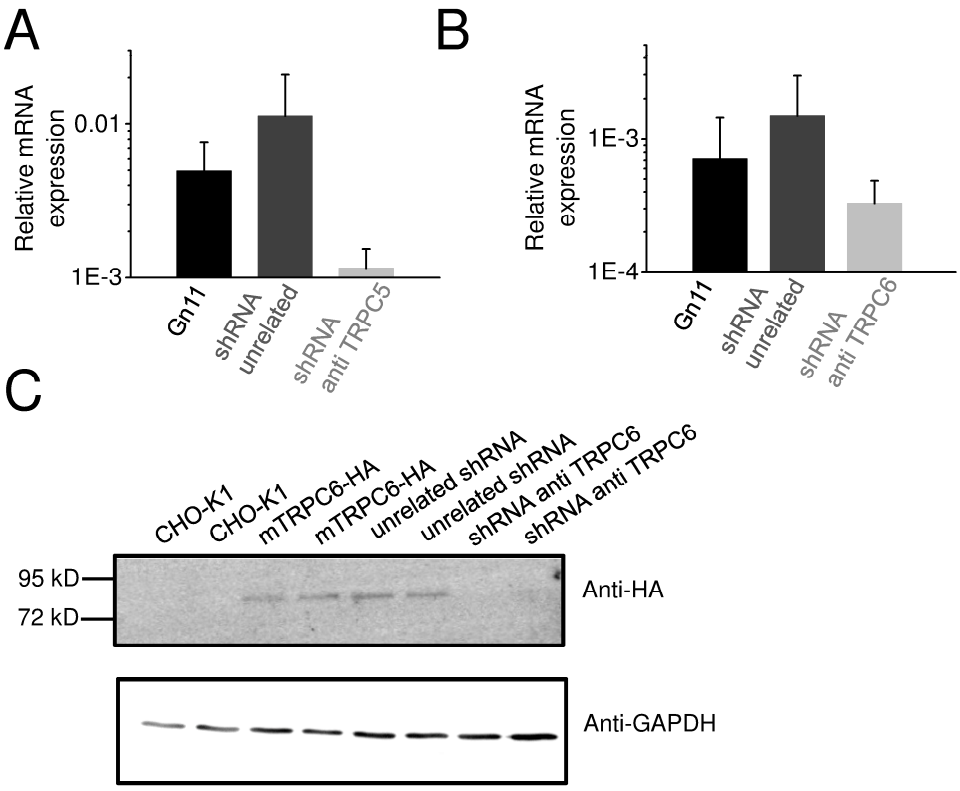

Supplementary Figure S6: Efficiency testing of shRNA targeting mouse TRPC5 and TRPC6. (A,B) Analysis of the relative TRPC5 (A) and TRPC6 (B) mRNA expression in Gn11 wild-type cells and in Gn11 cell lines expressing unrelated control shRNA "shRNA unrelated" or shRNA targeting TRPC5 "shRNA anti TRPC5" (A) or TRPC6 "shRNA anti TRPC6" (B) of three independent experiments each determined in quadruplicates. (C) Western blot analysis of CHO-K1 cells and of CHO-K1 cells stably expressing HA-tagged mouse TRPC6 "mTRPC6-HA" alone, in combination with unrelated control shRNA or with shRNA targeting TRPC6.

Supplementary Figure 7

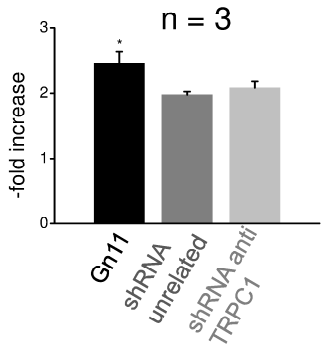

Supplementary Figure S7: Knock-down of TRPC1 in Gn11 cells did not affect proliferation. Analysis of proliferation assays with polyclonal Gn11 wild-type cells and with monoclonal cell lines of Gn11 cells stably transfected with unrelated shRNA and with shRNA targeting TRPC1.

Supplementary Material and Methods

Proliferation assay

To analyze the effect of TRPC1 knock down on proliferation ability of migrating Gn11 cells, CellTiter 96 AQueous One Solution Cell Proliferation Assay (Promega) was used according to the manufacturer's description. $2x10^4$ Gn11 cells were seeded in normal growth medium in a 96-well plate and viable cell number was measured right after and 24 hours after seeding of cells. All experiments were performed in triplicate and results are shown as fold increase of cell number compared to wild type Gn11 cells.

2. Publication: Blodow et al. (2014)

Novel role of mechanosensitive AT_{1B} receptors in myogenic vasoconstriction.

Blodow S, Schneider H, Storch U, Wizemann R, Forst AL, Gudermann T, Mederos y Schnitzler M.

Pflügers Arch. 2014 Jul;466(7):1343-53.

Author's contribution to this work:

AL.F. designed and generated AT_{1A} and AT_{1B} constructs and isolated vasucular smooth muscle cells.

S.B., H.S., and R.W. performed myogenic tone measurements and analyzed the data. S.B. and H.S. performed quantitative RT-PCRs. S.B. recorded intracellular calcium. M.MyS. and U.S. designed experiments and analyzed the data. M.MyS., U.S. and T.G. wrote the manuscript and supervised the study.

Pflugers Arch - Eur J Physiol (2014) 466:1343–1353
DOI 10.1007/s00424-013-1372-3

ION CHANNELS, RECEPTORS AND TRANSPORTERS

Novel role of mechanosensitive AT_{1B} receptors in myogenic vasoconstriction

Stephanie Blodow · Holger Schneider · Ursula Storch · Richard Wizemann · Anna-Lena Forst · Thomas Gudermann · Michael Mederos y Schnitzler

Received: 12 September 2013 / Revised: 26 September 2013 / Accepted: 27 September 2013 / Published online: 8 October 2013

Abstract Myogenic vasoconstriction is an inherent property of vascular smooth muscle cells (VSMCs) of resistance arteries harboring ill-defined mechanosensing and mechanotransducing elements. G protein-coupled receptors (GPCRs) are discussed as mechanosensors in VSMCs. In this study, we sought to identify and characterize the role and impact of GPCRs on myogenic vasoconstriction. Thus, we analyzed mRNA expression levels of GPCRs in resistance versus preceding conduit arteries revealing a significant enrichment of several GPCRs in resistance vessels. Selective pharmacological blockade of the highly expressed GPCRs in isolated murine mesenteric arteries ex vivo decreased myogenic vasoconstriction. In particular, candesartan and losartan most prominently suppressed myogenic tone, suggesting that AT_1 receptors play a central role in myogenic vasoconstriction. Analyzing angiotensinogen$^{-/-}$ mice, a relevant contribution of locally produced angiotensin II to myogenic tone could be excluded. Investigation of $AT_{1A}{}^{-/-}$ and $AT_{1B}{}^{-/-}$ murine mesenteric arteries revealed that AT_{1B}, but not AT_{1A}, receptors are key components of myogenic regulation. This notion was supported by examining fura-2-loaded isolated $AT_{1A}{}^{-/-}$ and $AT_{1B}{}^{-/-}$ VSMCs. Our results indicate that in VSMCs, AT_{1B} receptors are more mechanosensitive than AT_{1A} receptors even at comparable receptor expression levels. Furthermore, we demonstrate that the mechanosensitivity of GPCRs is agonist-independent and positively correlates with receptor expression levels.

Keywords Myogenic tone · Angiotensin II AT_1 receptors · Mechanosensitivity · G protein-coupled receptors · Resistance arteries

Abbreviations
GPCRs G protein-coupled receptors
VSMCs Vascular smooth muscle cells

Introduction

Small resistance arteries and arterioles have the intrinsic property to constrict in response to an elevated intraluminal pressure, a phenomenon known as myogenic vasoconstriction or Bayliss effect [2, 6]. This autoregulation determines basal vascular tone and peripheral vascular resistance and regulates capillary hydrostatic pressure and organ perfusion. Consequently, impaired myogenic responsiveness is encountered in various pathological states such as systemic hypertension, anaphylactic shock, diabetes mellitus, and stroke [12].

Myogenic vasoconstriction is generally assumed to be an intrinsic property of vascular smooth muscle cells (VSMCs) displaying the intrinsic property to sense mechanical stress without involvement of the endothelium [3] and neuronal innervation [2, 6]. Until now, the molecular identity of mechanosensors engaging in signaling cascades pertinent to myogenic vasoconstriction still remains largely elusive. Several proteins have been discussed as potential mechanosensors including cell adhesion proteins, membrane-bound enzymes, as well as cation channels of the transient receptor potential (TRP) channel family (summarized in [18, 20, 24, 26]).

Stephanie Blodow, Holger Schneider, and Ursula Storch have contributed equally to this work.

S. Blodow · H. Schneider · U. Storch · R. Wizemann · A.-L. Forst · T. Gudermann · M. Mederos y Schnitzler
Walther-Straub-Institute of Pharmacology and Toxicology, Ludwig Maximilians University of Munich, Goethestr. 33, 80336 Munich, Germany

T. Gudermann (✉) · M. Mederos y Schnitzler (✉)
DZHK (German Centre for Cardiovascular Research), Munich Heart Alliance, Munich, Germany
e-mail: thomas.gudermann@lrz.uni-muenchen.de
e-mail: mederos@lrz.uni-muenchen.de

Recently, the $G_{q/11}$ protein-coupled angiotensin II AT_1 receptor (AT_1R) was identified as a mechanosensor activated by mechanical cues without participation of agonists [16, 21, 32, 38] and was shown to be involved in myogenic vasoconstriction [16]. HIowever, the function of G protein-coupled receptors (GPCRs) as mechanosensors in resistance arteries has recently been challenged [1].

Furthermore, it could not be rigorously ruled out that locally produced angiotensin II might be required for myogenic vasoconstriction in situ. Our previous studies suggest that the signaling cascade culminating in myogenic vasoconstriction is initiated by a distinct active conformation of intrinsically mechanosensitive receptors [32] entailing G protein activation resulting in gating of classical TRP channels and resultant cation influx, membrane depolarization, and subsequent opening of voltage-gated calcium channels. The influx of contractile calcium then brings about vasoconstriction of resistance arteries [15, 16].

Apart from AT_1Rs, several other GPCRs like the bradykinin B_2, dopamine D_5, endothelin ET_A, parathyroid hormone type 1, histamine H_1, muscarinic M_5, formyl peptide 1, and vasopressin V_{1A} receptor were also identified as mechanosensitive signaling proteins (summarized in [26]). However, the relative importance of these or other mechanosensitive GPCRs for myogenic vasoconstriction still remains largely unexplored. Therefore, we set out to systematically analyze the contribution of select GPCRs on myogenic tone. In this regard, both murine AT_1R isoforms, AT_{1A} and AT_{1B}, were investigated.

The mechanosensitivity of resistance arteries has been shown to depend on receptor density: Firstly, overexpression of AT_1Rs in non-mechanosensitive VSMCs derived from the aorta, a conduit artery, endowed these cells with mechanosensitivity; secondly, VSMCs from renal resistance arteries and arterioles, endogenously expressing high levels of AT_1Rs, are mechanosensitive; and thirdly, in HEK293 cells overexpressing AT_1Rs, there was a linear correlation between receptor density and cellular calcium responses to a defined mechanical stimulus [16]. In line with these observations, AT_1R protein expression in small resistance arteries was several times higher than in conduit arteries [17, 22]. Therefore, we identified GPCRs enriched in resistance arteries and thoroughly assessed their impact on myogenic tone.

Methods

Ethical approval

All experiments and procedures were approved by the governmental oversight authority, District Government of Upper Bavaria (Germany).

Analysis of myogenic tone in mesenteric arteries

After decapitation of anesthetized male mice, the mesentery was removed and transferred to cold (4 °C), oxygenated (carbogen 95 % O_2 and 5 % CO_2) physiological salt solution (PSS) with the following composition (in mM): 119 NaCl, 25 $NaHCO_3$, 4.7 KCl, 1.2 KH_2PO_4, 1.2 $MgSO_4$, 1.6 $CaCl_2$, and 11.1 glucose (pH 7.6 with NaOH and pH 7.4 after purging by carbogen). Mesenteric arteries were exempt from fat, and third- and fourth-order branches were cannulated on extended borosilicate glass pipettes (GB120T-8P, Science Products, Hofheim, Germany) filled with PSS, allowing application of intravascular pressure. Cannulated vessels were mounted onto a pressure myograph (DMT 111P, DMT, Aarhus, Denmark), and outer vessel diameters were determined using video microscopy using MyoView software (DMT, Aarhus). Measurements were performed with continuous superfusion at 37 °C. Viability of the vessels was tested by applying 60 mM potassium chloride solution with the following composition (in mM): 63.7 NaCl, 25 $NaHCO_3$, 60 KCl, 1.2 KH_2PO_4, 1.2 $MgSO_4$, 1.6 $CaCl_2$, and 11.1 glucose (pH 7.6 with NaOH). Only arteries showing a contraction of at least 30 % were further investigated. To analyze the vascular response, the outer vessel diameter was monitored in response to stepwise increases in intravascular pressure from 5 to 80 mmHg in 2-min steps and from 90 to 120 mmHg in 5-min steps. The first stepwise pressure increase resulted in vessel sensitization. The second pressure ladder was used for analysis to determine myogenic tone, and the third which was performed in calcium-free PSS solution with 3 mM EDTA served as a reference to determine maximal passive dilatative diameters which were used for normalization using the following formula:

$$\text{Myogenic tone } (\%) = 100\frac{\text{Diameter}_{\text{Ca-free}} - \text{Diameter}_{\text{PSS or PSS with drugs}}}{\text{Diameter}_{\text{Ca-free}}}.$$

In some experiments, isolated blood vessels were superfused with the ACE inhibitor captopril or the indicated receptor antagonists or inverse agonists for 30 min subsequent to the first pressure ladder and during the second pressure ladder. Isolated arteries had maximal passive diameters of 140.3±2.8 μm at 40 mmHg and 170.2±3.3 μm at 120 mmHg (n=119 of 111 mice). The outer diameters of the vessels at 5 mmHg determined at the beginning of the second pressure ladder reflecting the initial basal vessel tone were not significantly different between each experimental group and between $AT_{1A}^{-/-}$, $AT_{1B}^{-/-}$, and $Agt^{-/-}$ and their control vessels with a mean diameter of all vessels of 100.5±2.3 μm (n=119 of 111 mice). In addition, repeated pressure steps from 40 to 120 mmHg were performed to analyze the kinetics of vasoconstriction (n=11 of 4 mice). Thus, three pressure steps to 120 mmHg for 5 min were performed to induce vessel sensitization. The mean of the following three pressure increases to

120 mmHg was used for analysis. Statistics was done using Student's *t* test between gene-deficient mice and their wild-type controls having the same genetic background.

Mice used in this study

The following mice were analyzed in this study: AT_{1A} receptor gene-deficient ($AT_{1A}^{-/-}$) mice [14] and angiotensinogen ($Agt^{-/-}$) mice [28] in FVB/N genetic background (from Michael Bader, Max Delbrück Center for Molecular Medicine, Berlin) and AT_{1B} receptor gene-deficient ($AT_{1B}^{-/-}$) mice [19] in C57BL/6J genetic background (from Thomas Coffman, Division of Nephrology, Department of Medicine, Duke University and Durham VA Medical Centers, Durham, NC, USA). As wild-type controls, FVB/N for $AT_{1A}^{-/-}$ and $Agt^{-/-}$ mice and C57BL/6J for $AT_{1B}^{-/-}$ mice were used. Control mice were from the same strains as gene-deficient mice. Quantitative real-time polymerase chain reaction (RT-PCR) experiments with mesenteric and cerebral arteries and pharmacological blocking experiments with receptor antagonists were performed using FVB/N wild-type mice ($n=68$ and $n=52$, respectively). C57BL/6J wild-type mice were used for experiments with captopril. For myogenic tone measurements, only male mice older than 12 weeks were used with a mean age of 112.6±2.5 days and a weight of 29.9±0.3 g ($n=115$).

Preparation of vascular smooth muscle cells

Single mesenteric smooth muscle cells were enzymatically isolated from mesenteric arteries of mice as described in detail elsewhere [9]. Renal VSMCs were non-enzymatically isolated using the sieve method [16] and cultivated for 5 days in vitro.

Determination of intracellular calcium concentrations

Intracellular free calcium was determined with fura-2 acetoxymethyl ester (5 μM; Molecular Probes Inc., Eugene, OR, USA) loaded mesenteric and renal VSMCs as described in detail elsewhere [25]. Cells were continuously superfused with an isotonic bath solution containing (in mM) NaCl 55, KCl 5, $CaCl_2$ 2, HEPES 10, glucose 10, and $MgCl_2$ 1 (pH 7.4 with NaOH) which was supplemented with mannitol to 300 mOsm kg^{-1}. The hypoosmotic solution had the same salt concentration without added mannitol resulting in an osmolality of 149 to 152 mOsm kg^{-1}. In these experiments, 1 μM losartan was used.

Quantitative qPCR analysis

Total RNA from indicated vessel segments was isolated using the Tri Reagent (Sigma, Munich, Germany). First strand synthesis was carried out with random hexamers as primers, using REVERTAID reverse transcriptase (Fermentas, Sankt Leon-Roth, Germany). The following primer pairs were used for the amplification of specific fragments from the first strand synthesis: endothelin ET_A receptor, $ET_A$for (tgtgagcaagaaattcaaaaattg), ET_Arev (atgaggcttttggactggtg); endothelin ET_B receptor, $ET_B$for (cggtatgcagattgctttga), ET_Brev (aacagagagcaaacacgagga); angiotensin II AT_{1A} receptor, $AT_{1A}$for (actcacagcaaccctccaag), AT_{1A}rev (ctcagacactgttcaaaatgcac); angiotensin II AT_{1B} receptor, $AT_{1B}$for (cagtttcaacctctacgccagt), AT_{1B}rev (gggtggacaatggctaggta); vasopressin V_{1A} receptor, $V_{1A}$for (gggataccaatttcgtttgg), V_{1A}rev (aagccagtaacgccgtgat); α_{1A} adrenoceptor, $\alpha_{1A}$for (ctgaaggtccgcttctcct), α_{1A}rev (gccctggagcttcgtttat); α_{1B} adrenoceptor, $\alpha_{1B}$for (ttcttcatcgctctcccact), α_{1B}rev (gggttgaggcagctgttg); α_{1D} adrenoceptor, $\alpha_{1DE}$for (tttttcttcgtcctgcctct), α_{1D}rev (agcgggttcacacagctatt); α_{2A} adrenoceptor, $\alpha_{2A}$for (tagaactgacttttcttccgttctc), α_{2A}rev (aacatacacgctcttcttcaagc); α_{2B} adrenoceptor, $\alpha_{2B}$for (gctgcccttgaactcacaa), α_{2B}rev (cagccagcagatggttacaa); β_2 adrenoceptor, $\beta_2$for (gaagattccacgcccaaa), $\beta_2$rev (cttggaggaccttcggagt); and three references hypoxanthin phosphoribosyltransferase 1, Hprt1for (tcctcctcagaccgctttt), Hprt1rev (cctggttcatcatcgctaatc); tyrosine 3-monooxygenase/tryptophan 5-monooxygenase activation protein, zeta polypeptide, Ywhazfor (taaaaggtctaaggccgcttc), Ywhazrev (caccacacgcacgatgac); and succinate dehydrogenase complex, subunit A, Sdhafor (ccctgagcattgcagaatc), Sdharev (tcttctccagcatttgcctta) giving predicted product sizes of 72 bp for ET_A, 92 bp for ET_B, 62 bp for AT_{1A}, 75 for AT_{1B}, 66 bp for V_{1A}, 68 bp for α_{1A}, 107 bp for α_{1B}, 110 bp for α_{1D}, 60 bp for α_{2A}, 113 bp for α_{2B}, 90 bp for Hprt1, 60 bp for Ywhaz, and 70 bp for Sdha. RT-PCR was performed using the master mix from the Absolute QPCR SYBR Green Mix kit (Abgene, Epsom, UK). Ten picomoles of each primer pair and 0.2 μl of the first strand synthesis were added to the reaction mixture, and PCR was carried out in a LightCycler apparatus (LightCycler 480, Roche, Mannheim, Germany) using the following conditions: 15 min initial activation and 45 cycles of 12 s at 94 °C, 30 s at 50 °C, 30 s at 72 °C, and 10 s at 80 °C each. Fluorescence intensities were recorded after the extension step at 80 °C after each cycle to exclude fluorescence of primer dimers melting lower than 80 °C. All primers were tested by using diluted complementary DNA (cDNA) from the first strand synthesis (10–1,000×) to confirm linearity of the reaction and to determine particular efficiencies. Data were calculated as percentage of the geometric mean expression of the three references which showed the highest tissue-independent transcription stability [31]. Samples containing primer dimers were excluded by melting curve analysis and identification of the products by agarose gel electrophoresis. Crossing points were determined by the software program. For each qPCR experiment, tissue and vessel preparations from 3 to 4 mice were pooled and mRNA levels were measured in quadruplets. At least three independent qPCRs experiments were performed. One bar equates to 11–16 mice. Only male mice older than 12 weeks were used.

Wilcoxon rank-sum test [33] was used for analysis of mRNA expression levels.

Statistical analysis

Data are presented as means ± standard error of the mean (s.e.m.). Unless stated otherwise, data were compared by a paired or unpaired Student's *t* test, if a Gaussian distribution was confirmed by applying a Shapiro–Wilk (normality) test. Significance was accepted at $P<0.05$ ($^{*}P<0.05$, $^{**}P<0.01$, $^{***}P<0.001$, n.s. $P>0.05$). Myogenic tone was fitted using the Hill equation.

Results

mRNA expression levels of GPCRs are increased in small resistance compared to conduit arteries

Since previous findings suggested that the mechanosensitivity of GPCRs correlates with receptor density [16], quantitative RT-PCR was employed to determine whether select GPCRs—namely $G_{q/11}$ protein-coupled AT_{1A}, AT_{1B}, vasopressin V_{1A}, endothelin ET_A and ET_B, adrenergic α_{1A}, α_{1B}, and α_{1D} receptors; $G_{i/o}$ protein-coupled adrenergic α_{2A} and α_{2B} receptors; and G_s protein-coupled adrenergic β_2 receptors—were enriched in resistance arteries. The aforementioned receptors are all known to modify smooth muscle contractility. mRNA expression was compared between conduit and small resistance arteries from consecutive vessel segments of FVB/N wild-type mice. We investigated cerebral and mesenteric arteries. To assess the purity of mesenteric artery preparations, mRNA expression levels of the fat marker adiponectin [10] were determined (Fig. 1a) showing low expression in Aa. mesentericae (4.7 %) and in A. mesenterica superior (0.8 %) preparations, indicating that the isolated vessels were sufficiently devoid of surrounding fat tissue.

Notably, mRNA expression of AT_{1B}, α_{1A}, and α_{2A} receptors was significantly increased, but AT_{1A} and α_{1D} receptor expression was reduced in myogenic cerebral resistance arteries as compared to the preceding conduit artery A. carotis communis (Fig. 1b). In addition, mesenteric resistance arteries exhibited elevated mRNA expression of AT_{1B}, ET_A, ET_B, and α_{1A} but decreased α_{1B} receptor expression relative to A. mesenterica superior (Fig. 1c). The relative mRNA expression depicted as an expression ratio between resistance and their preceding conduit arteries reveals that AT_{1B}, V_{1A}, ET_A and ET_B, α_{1A} and α_{2A} receptor expression is increased (Fig. 1d) with a predominant expression of AT_{1B} receptors. Interestingly, the percentage of AT_{1B}R versus AT_{1A}R mRNA expression was substantially higher in small resistance arteries (>96 %) than in conduit arteries (Fig. 1e), pointing to a distinct function of AT_{1B}Rs in small resistance arteries. A very similar GPCR expression pattern was observed in C57BL6/J wild-type mice.

Myogenic response is reduced by pharmacological blockade of highly expressed GPCRs

To investigate whether the highly expressed GPCRs are involved in myogenic vasoconstriction, pressure myography of isolated mesenteric artery segments from wild-type mice exhibiting a pronounced myogenic responsiveness was performed in the presence and absence of specific receptor blockers (antagonists or inverse agonists) at maximal inhibitory concentrations. In the presence or absence of the blockers, maximal high potassium-induced vasoconstrictions revealed no differences between the analyzed arteries (data not shown), ruling out toxic side effects. First, relcovaptan, a selective V_{1A} receptor antagonist, and RX821002, a selective inverse agonist of α_{2A} and α_{2B} receptors, were tested (Fig. 2a, b). Incubation of mesenteric arteries with relcovaptan or RX821002 did not significantly decrease myogenic vasoconstriction, indicating that V_{1A} as well as α_{2A} and α_{2B} receptors do not significantly contribute to myogenic tone. On the contrary, BQ123, a selective ET_A receptor antagonist, and prazosin, a selective α_{1A}, α_{1B}, and α_{1D} receptor inverse agonist [37] (Fig. 2c, d), reduced myogenic tone significantly. These findings are suggestive of a role of ET_A and α_1 receptors for myogenic vasoconstriction.

Targeting both AT_{1A} and AT_{1B} receptors by administering the AT_1 receptor blockers [30] losartan and candesartan reduced myogenic vasoconstriction even more prominently (Fig. 2e–g). Figure 2f shows exemplary vessel diameter time courses at indicated pressure steps of wild-type mesenteric arteries in the presence or absence of 10 μM losartan and the subsequent incubation with calcium-free bath solution resulting in maximal vessel dilatations. Increasing the losartan concentration from 1 up to 30 μM resulted in pronounced reduction of myogenic tone, causing an absolute reduction of -13.6±1.7 % at 100 to 120 mmHg (Fig. 2e, h) which equates to a relative decrease of myogenic tone of 45.8±9.5 %. These findings indicate that 10 μM losartan is a submaximal concentration for effective AT_1R blockade in these artery segments. A further increase in candesartan concentrations from 1 to 10 μM had no additional effect, suggesting that 1 μM candesartan is the maximally inhibitory concentration (Fig. 2g, h).

Calculating the reduction of myogenic tone at pressure ranges from 70 to 90 mmHg and from 100 to 120 mmHg shows that blockade of AT_{1A} and AT_{1B} receptors had the greatest impact on myogenic response (Fig. 2h). Likewise, depicting receptor mRNA expression levels in small resistance mesenteric arteries as *n*-fold increase over conduit artery expression versus reduction of myogenic tone induced by specific drugs normalized to maximal myogenic

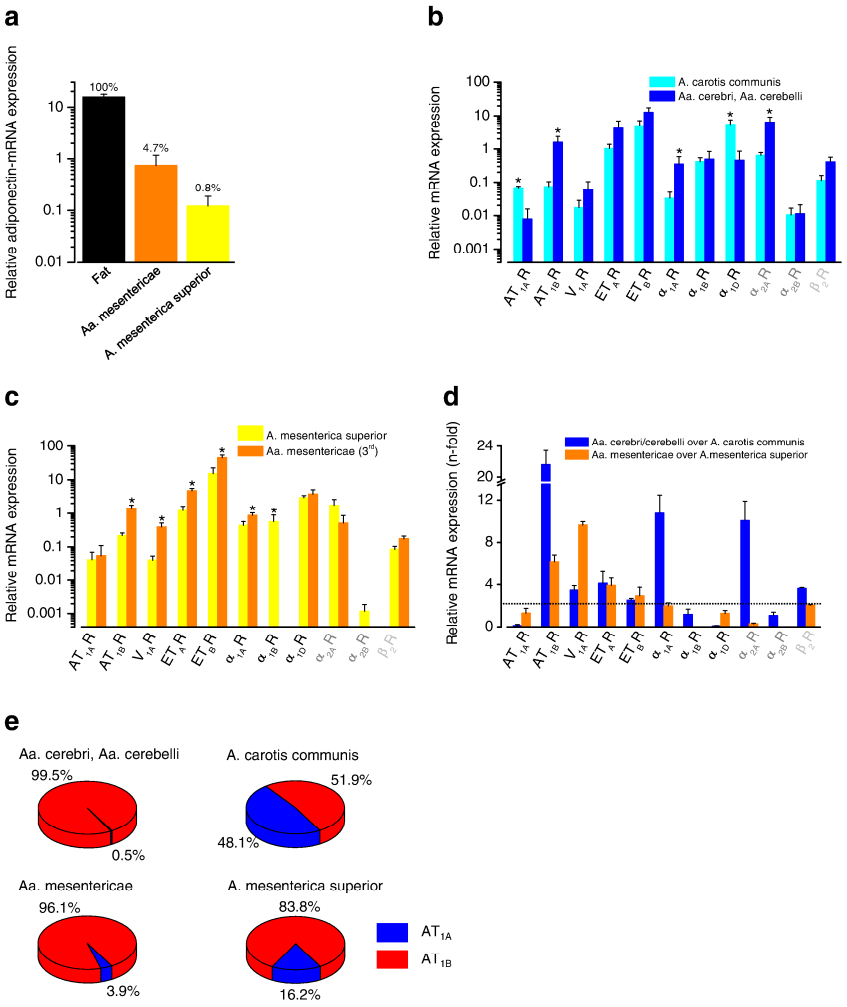

Fig. 1 mRNA expression levels of GPCRs in resistance compared to conduit arteries. Summary of relative mRNA expression levels determined by quantitative RT-PCR from a least three independent experiments. **a** Relative mRNA expression levels of the fat marker adiponectin in fat tissue and in indicated isolated mesenteric arteries. **b–d** Relative mRNA expression levels of selected $G_{q/11}$ (*black*), $G_{i/0}$ (*gray*), and G_{s-} (*light gray*) protein-coupled receptors in cerebral (**b**) and mesenteric (**c**) arteries. Cerebral and mesenteric conduit arteries are displayed in *blue* and *yellow*; cerebral and mesenteric small resistance arteries are depicted in *dark blue* and *orange*, respectively. **d** Analysis of mRNA expression in resistance arteries as n-fold over mRNA expression in conduit arteries. Cerebral arteries are displayed in *blue* and mesenteric arteries in *orange*. The *dotted line* indicates twofold expression. **e** Analysis of AT_{1A} (*blue*) and AT_{1B} (*red*) receptor expression in percentage in cerebral (*top*) and mesenteric (*bottom*) conduit (*right*) and resistance (*left*) arteries

tone seen in control arteries (Fig. 2i) suggests a correlation between receptor mRNA expression levels and the contribution of a given receptor to myogenic vasoconstriction. Of note, a dominant role of AT_{1A} and AT_{1B} receptors for myogenic vasoconstriction is underscored by reductions of around 50 % as compared to control arteries. Although highly expressed, blockade of V_{1A} receptors did not result in a significant reduction of myogenic tone (Fig. 2a). This is in line with previous findings that V_{1A} receptors were much less mechanosensitive than heterologously expressed AT_1, ET_A, M_5, and H_1 receptors [16]. In summary, our findings point to a key role of AT_1Rs in myogenic vasoconstriction and lend further credence to the notion that the density of mechanosensitive G_qPCRs is correlated with their impact on myogenic vasoconstriction.

Myogenic vasoconstriction is independent of endogenous angiotensin II production

Although previous data already suggested agonist-independent GPCR activation by membrane stretch [16, 38], a participation of endogenously produced angiotensin II in myogenic vasoconstriction could not be completely ruled out. To rigorously address this issue, angiotensinogen gene-deficient ($Agt^{-/-}$) mice were investigated. In line with previous assumptions, myogenic vasoconstriction was not significantly different in these mice compared to wild-type controls, demonstrating that locally produced angiotensin II is not involved in myogenic vasoconstriction (Fig. 3a). Interestingly, additional administration of 10 μM losartan significantly reduced myogenic vasoconstriction (Fig. 3a, b) equivalent to a

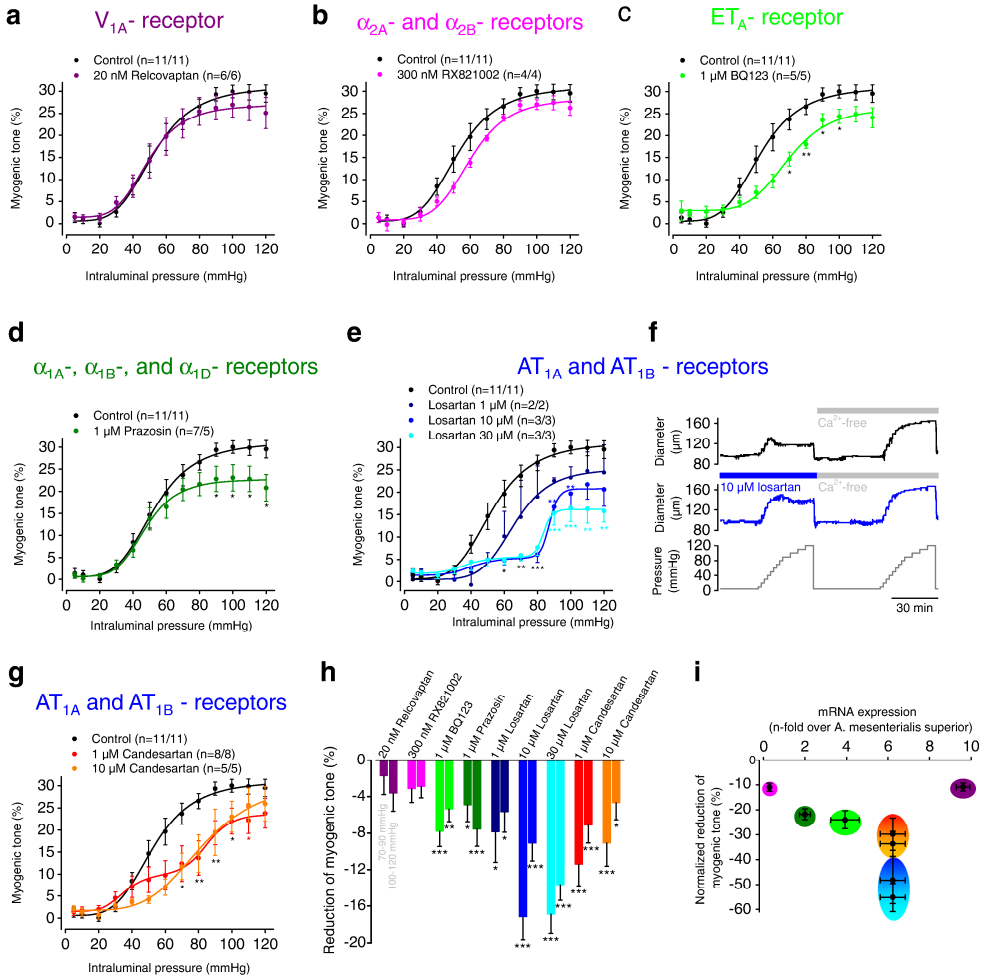

Fig. 2 Pharmacological blocking of highly expressed GPCRs reduces myogenic response. **a**–**e**, **g** Myogenic tone of wild-type mesenteric arteries normalized to the maximal passive vasodilatation by Ca^{2+}-free solution at increasing intraluminal pressures from 5 to 120 mmHg in the presence (*colored line*) or absence (*black line*) of selective receptor antagonists or inverse agonists. Pharmacological blocking of V_{1A} (**a**); α_{2A} and α_{2A} (**b**); ET_A (**c**); α_{1A}, α_{1B}, and α_{1D} (**d**); and AT_{1A} and AT_{1B} (**e**–**g**) receptors is shown. *Numbers in parentheses* display the numbers of individual measurements and the numbers of mice. **f** Exemplary time courses of vessel diameter measurements during the second and third pressure ladder with indicated pressure steps (*bottom*) of wild-type arteries in the presence (*blue*, *middle*) or absence (*black*, *top*) of 10 μM losartan. Incubations with losartan (*blue bar*) and calcium-free solution (*gray bar*) are indicated. **h** Summary of the absolute reduction of myogenic tone by receptor blockers at pressure ranges from 70 to 90 mmHg (*left bars*) and from 100 to 120 mmHg (*right bars*) compared to the control. **i** Summary of the reduction of myogenic tone at pressure ranges from 70 to 120 mmHg normalized to the control and plotted against the mRNA expression levels of Aa. mesentericae as n-fold over mRNA expression of A. mesenterica superior. Blockade of V_{1A} (*violet*); α_{2A} and α_{2B} (*magenta*); ET_A (*light green*); α_{1A}, α_{1B}, and α_{1D} (*dark green*); and AT_{1A} and AT_{1B} receptors (with losartan (*blue*) and with candesartan (*orange*)) is displayed

relative decrease of maximal myogenic tone of about 33 % at 110 to 120 mmHg. This reduction most probably reflects the fraction of agonist-independent mechanical AT_{1A}/AT_{1B} receptor activation in response to membrane stretch. Maximal high potassium chloride (KCl)-induced vasoconstrictions of $Agt^{-/-}$ arteries were unaffected by losartan and even higher than control vessels (Fig. 3a, inset), clearly demonstrating that the viability of these arteries was not impaired. However, postnatal survival of these male mice was compromised with a survival rate up to 6 months of 48 %. Furthermore, AT_{1A} and AT_{1B} receptor mRNA expression levels were similar to wild-type vessels (data not shown). To rule out uncontrolled compensatory effects and to mimic the scenario in $Agt^{-/-}$ mice, wild-type arteries

were incubated with the ACE inhibitor captopril (1 μM) to prevent local angiotensin II production. High KCl-induced maximal vasoconstriction did not differ in the absence and presence of captopril, showing that all vessels were comparably viable (Fig. 3c, inset). Captopril did not affect myogenic vasoconstriction (Fig. 3c), yet additional blockade of AT_1Rs with 10 μM losartan resulted in a significant reduction of myogenic tone over a wide pressure range (Fig. 3b). This reduction was not significantly different from the 10 μM losartan-induced reduction in wild-type arteries (Fig. 2e). These results provide strong support for the notion that AT_1Rs are mechanically activated and the endogenous agonist angiotensin II is not essentially involved in myogenic tone. Altogether, these findings entertain the notion that agonist-independent AT_1R activation plays a role for myogenic vasoconstriction.

Myogenic vasoconstriction is impaired in AT_{1B} but not in AT_{1A} receptor gene-deficient mice

Because our pharmacological approach indicated a prominent role of AT_1Rs for myogenic vasoconstriction, AT_1R gene-deficient mice were analyzed next. Notably, myogenic vasoconstriction of AT_{1A} receptor gene-deficient ($AT_{1A}^{-/-}$) mice was not reduced over a pressure range from 5 to 120 mmHg (Fig. 4a), ruling out an indispensable contribution of AT_{1A}Rs to myogenic vasoconstriction. However, further increasing the intravascular pressure up to 160 mmHg resulted in a significant reduction of myogenic tone in $AT_{1A}^{-/-}$ but not in control arteries (Fig. 4a inset, c), indicating that AT_{1A}Rs are mechanically activated only at high intravascular pressures. Interestingly, 1 μM candesartan to inhibit the remaining AT_{1B}Rs considerably reduced myogenic tone over a broad pressure range (Fig. 4b, c).

Next, AT_{1B} receptor gene-deficient ($AT_{1B}^{-/-}$) mice were investigated. Indeed, $AT_{1B}^{-/-}$ arteries showed a significantly reduced myogenic tone at a pressure range from 60 to 120 mmHg (Fig. 4d, f). Additional application of 1 μM candesartan to inhibit AT_{1A}Rs resulted only in a minor further decrease at intravascular pressures from 30 to 60 mmHg when compared to untreated $AT_{1B}^{-/-}$ arteries (Fig. 4e, f). Moreover, maximal KCl-induced vasoconstrictions showed no significant differences between gene-deficient arteries and their respective wild-type controls (data not shown), suggesting that all vessels were comparably viable. Moreover, mRNA expression levels of the aforementioned select array of GPCRs (see Fig. 1) were similar in $AT_{1A}^{-/-}$ and $AT_{1B}^{-/-}$ isolated murine mesenteric arteries compared to their wild-type controls, and AT_{1B} or AT_{1A} receptor mRNA expression was also unchanged (data not shown). Altogether, these findings support the notion that AT_{1B} and not AT_{1A} receptors have a predominant role for myogenic vasoconstriction.

Kinetics of myogenic vasoconstriction is lowered in $AT_{1B}^{-/-}$ arteries

For a more detailed analysis of the kinetics of myogenic vasoconstriction in $AT_{1B}^{-/-}$ arteries, a modified protocol similar to [7] was employed characterized by repeated pressure steps from 40 to 120 mmHg. $AT_{1B}^{-/-}$ arteries showed a slower kinetics of vasoconstriction (Fig. 5a) with a time constant of −133±8 s for $AT_{1B}^{-/-}$ compared to −60±10 s for wild-type arteries (Fig. 5b) and reached 90 % of maximal vasoconstriction after 317±17 s and of 188±21 s, respectively (Fig. 5c). Furthermore, the extent of myogenic vasoconstriction was less pronounced in $AT_{1B}^{-/-}$ arteries compared to controls. These findings can be interpreted to mean that AT_{1B}Rs not only are essential for the magnitude of myogenic vasoconstriction, but also determine the kinetics of the myogenic response.

In VSMCs, AT_{1B} receptors are more mechanosensitive than AT_{1A} receptors

To investigate whether the dominant role of AT_{1B}Rs in resistance arteries was a direct consequence of the increased AT_{1B}R expression compared to AT_{1A}Rs or whether AT_{1B}Rs are more mechanosensitive than AT_{1A}Rs, we isolated single VSMCs and performed calcium imaging with fura-2. Firstly, freshly isolated VSMCs from $AT_{1A}^{-/-}$ and $AT_{1B}^{-/-}$ isolated murine mesenteric arteries were used. Hypoosmotically induced cell swelling caused calcium transients that were significantly higher in $AT_{1A}^{-/-}$ VSMCs (Fig. 6a, b), indicating that $AT_{1A}^{-/-}$ VSMCs might be more mechanosensitive. In both cell types, losartan significantly reduced stretch-induced calcium responses. In addition, we compared mRNA expression levels of AT_{1A}Rs in $AT_{1B}^{-/-}$ to those of AT_{1B}Rs in $AT_{1A}^{-/-}$ VSMCs (Fig. 6c). In line with wild-type isolated murine mesenteric arteries (see Fig. 1c), AT_{1B}R expression was significantly higher than AT_{1A}R expression, suggesting that the increased mechanosensitivity of $AT_{1A}^{-/-}$ VSMCs might depend on the 5.6-fold higher AT_{1B}R density.

To analyze this in more detail, we next used renal VSMCs from $AT_{1A}^{-/-}$ and $AT_{1B}^{-/-}$ mice cultivated for five days in vitro. These cells showed smaller calcium increases upon hypoosmotic cell swelling (Fig. 6d) than freshly isolated mesenteric VSMCs. However, calcium transients induced by hypotonic cell swelling were higher in $AT_{1A}^{-/-}$ than in $AT_{1B}^{-/-}$ VSMCs (Fig. 6e), indicating that $AT_{1A}^{-/-}$ VSMCs were more mechanosensitive. Furthermore, losartan significantly suppressed hypoosmotically induced calcium increases to similar values in both cell types (Fig. 6d, e). Interestingly, in contrary to mesenteric VSMCs, mRNA expression levels of AT_{1A}Rs and AT_{1B}Rs in $AT_{1B}^{-/-}$ and $AT_{1A}^{-/-}$ renal VSMCs were not significantly different (Fig. 6f). Given that at similar

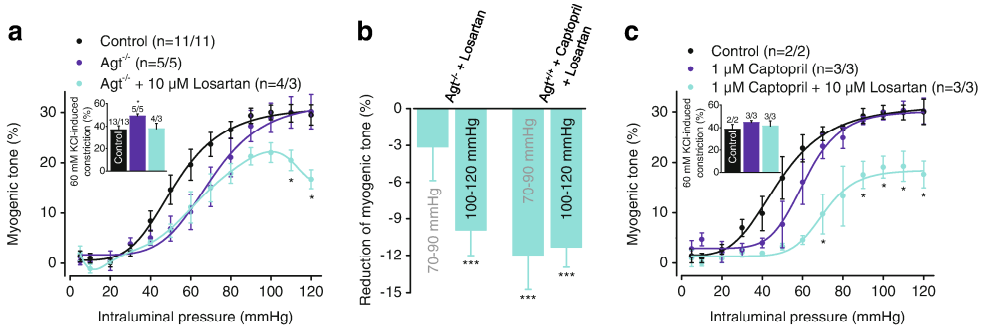

Fig. 3 Myogenic tone is independent from endogenous AII production. **a** Myogenic tone of mesenteric arteries from wild-type (control) and angiotensinogen gene-deficient ($Agt^{-/-}$) mice normalized to the maximal passive vasodilatation by Ca^{2+}-free solution at increasing intraluminal pressures from 5 to 120 mmHg in the presence (*cyan line*) or absence (*black* and *violet line*) of losartan. Significance was tested in comparison to untreated $Agt^{-/-}$ and wild-type arteries. The *insert* shows the summary of KCl-induced vasoconstrictions in wild-type (control, *black*), untreated $Agt^{-/-}$ vessels (*violet*), and losartan-treated $Agt^{-/-}$ vessels (*cyan*). Significance was tested in comparison to $Agt^{-/-}$ arteries. **b** Summary of losartan-induced absolute reduction of myogenic tone of $Agt^{-/-}$ arteries and of wild-type arteries ($Agt^{+/+}$) treated with captopril at two different pressure ranges. **c** Myogenic tone of isolated murine mesenteric arteries from wild-type mice in the absence (control, *black*) or presence of captopril (*violet*) and in the presence of captopril and losartan (*cyan*). Significance was tested in comparison to captopril-treated wild-type arteries. The *insert* shows the summary of KCl-induced vasoconstrictions. *Numbers over bars* indicate the numbers of arteries measured and the numbers of mice

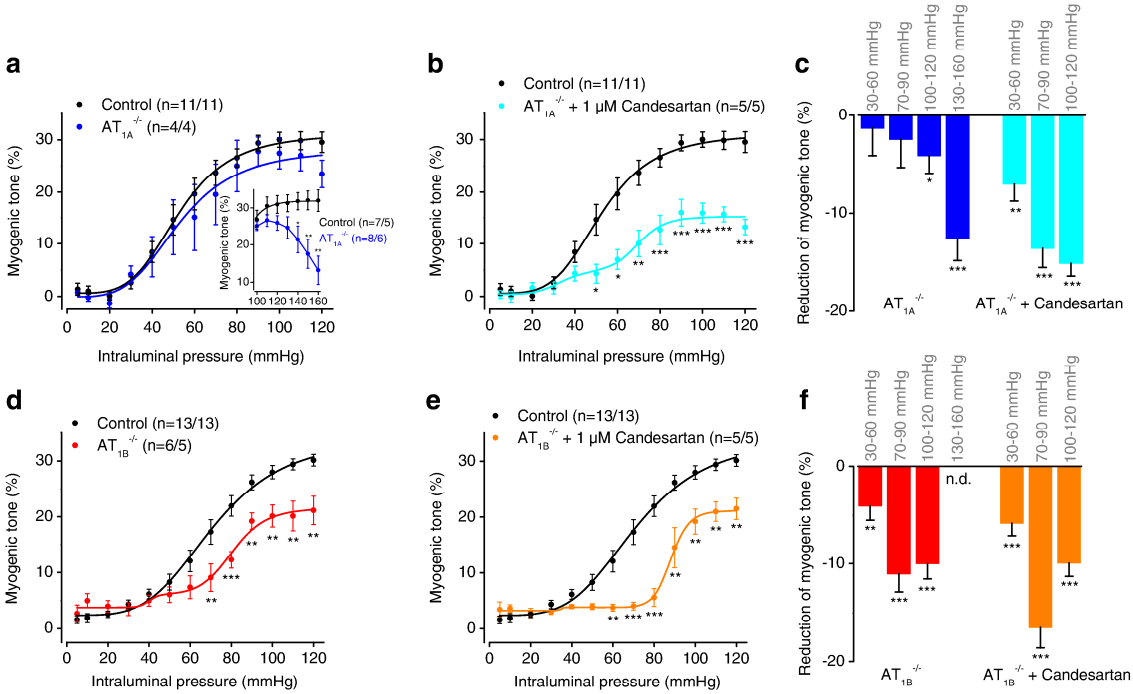

Fig. 4 Myogenic vasoconstriction is impaired in AT_{1B} but not in AT_{1A} receptor gene-deficient mice. **a**, **b** Myogenic tone of mesenteric arteries from wild-type (control, *black*) and AT_{1A} receptor gene-deficient ($AT_{1A}^{-/-}$) mice in the presence (**b**) and absence (**a**) of candesartan at increasing intraluminal pressures from 5 to 120 mmHg. **a** *Insert* shows further increased intraluminal pressures from 100 to 160 mmHg. **c** Summary of the absolute reduction of myogenic tone compared to control arteries of $AT_{1A}^{-/-}$ arteries in the presence (*light blue*) and absence (*dark blue*) of candesartan. **d**, **e**, Myogenic tone of mesenteric arteries from wild-type (control, *black*) and AT_{1B} receptor gene-deficient ($AT_{1B}^{-/-}$) mice in the presence (**e**) and absence (**d**) of candesartan. **f** Summary of the absolute reduction of myogenic tone compared to control arteries of $AT_{1B}^{-/-}$ arteries in the presence (*orange*) and absence (*red*) of candesartan. *Numbers in parentheses* indicate the number of measurements and the number of mice

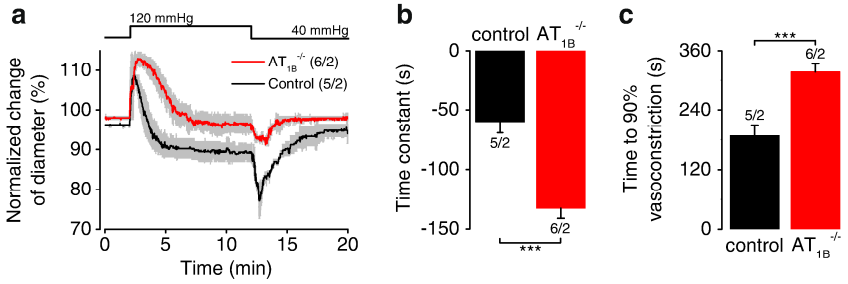

Fig. 5 Kinetics of myogenic vasoconstriction is lowered in $AT_{1B}^{-/-}$ arteries. **a** Vessel diameter time courses normalized to the diameter at 40 mmHg intraluminal pressure of control (*black*) and $AT_{1B}^{-/-}$ (*red*) arteries. For each experiment, vessel diameters of three sequential pressure steps from 40 to 120 mmHg for 10 min and in reverse were averaged. *Numbers in parentheses* display the number of experiments and the number of mice. Summary of time constant (**b**) and time to 90 % of maximal vasoconstriction (**c**) of control (*black bars*) and $AT_{1B}^{-/-}$ (*red bars*) isolated murine mesenteric arteries. *Numbers over bars* indicate the number of measurements and the number of mice

receptor expression levels $AT_{1A}^{-/-}$ VSMCs were still more sensitive to membrane stretch than $AT_{1B}^{-/-}$ VSCMs, these findings suggest that AT_{1B}Rs per se are more mechanosensitive than AT_{1A}Rs.

Discussion

Our findings provide experimental evidence to support the notion that AT_1Rs are key components in the signaling cascade leading to myogenic vasoconstriction. Among the GPCRs analyzed, AT_{1B}, V_{1A}, ET_A, ET_B, α_{1A}, α_{1B}, α_{1D}, and α_{2B} receptors were significantly enriched in small resistance arteries. However, pharmacological blockade of V_{1A} and α_2 receptors was without functional effects, suggesting that, although highly expressed, these receptors are not crucial for myogenic vasoconstriction. On the contrary, the highly expressed ET_A and α_{1A}, α_{1B}, and α_{1D} receptors contributed to myogenic vasoconstriction. Of note, the reduction or myogenic vasoconstriction induced by application of selective

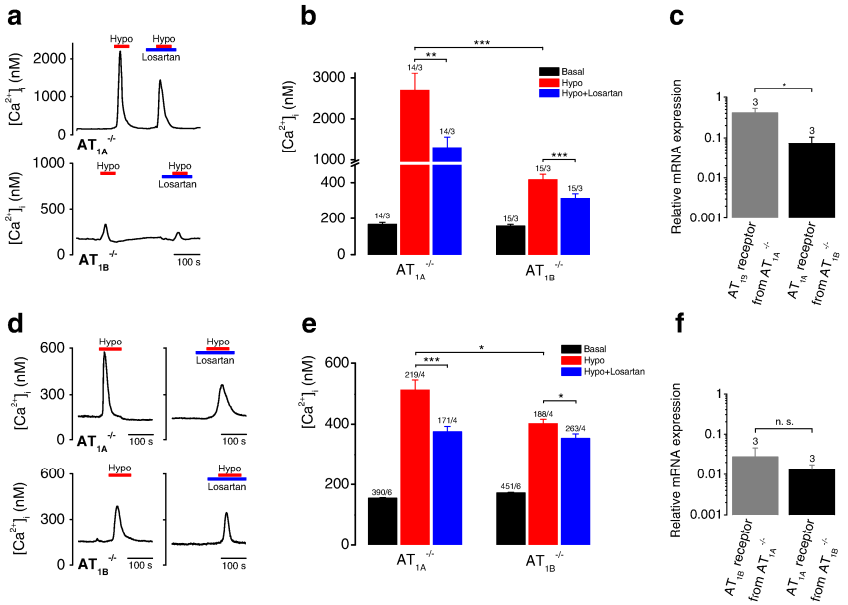

Fig. 6 In VSMCs, AT_{1B} receptors are more mechanosensitive than AT_{1A} receptors. **a**, **f**, **d**, **e** Fluorimetric calcium measurements with fura-2-loaded freshly isolated mesenteric VSMCs (**a**–**c**) and with renal VSMCs cultivated for 5 days in vitro (**d**–**f**) from $AT_{1A}^{-/-}$ and $AT_{1B}^{-/-}$ mice. **a**, **d**, Exemplary time courses of the intracellular calcium concentration. Application of hypoosmotic solution (150 mOsm kg^{-1}) "Hypo" and of losartan is indicated. **b**, **e** Summary of the intracellular calcium concentrations before (basal, *black bars*) and during application of hypoosmotic solution in the absence (*red bars*) and presence (*blue bars*) of 1 μM losartan. **e** *Numbers over bars* indicate the number of measured cells and the number of mice. **c**, **f**, Summary of relative mRNA expression levels determined by quantitative RT-PCR of freshly isolated mesenteric VSMCs (**c**) and renal VSMCs (**f**). *Numbers over bars* indicate the number of independent experiments

receptor antagonists was much less pronounced than that resulting from blocking AT_1Rs. BQ123 caused suppressions of myogenic tone at middle, prazosin at high, and losartan and candesartan at middle to high intraluminal pressures, suggesting that these receptors may be tuned to different pressure ranges to cover the whole physiologically relevant spectrum. All experiments were performed with mesenteric resistance arteries because these arteries showed reliable and pronounced myogenic tone of about 30 % similar to cerebral resistance arteries.

In contrast to humans, rodents possess two distinct AT_1R isoforms, AT_{1A} and AT_{1B} that engage the same signaling cascades [29, 34]. These subtypes cannot be rigorously discriminated pharmacologically [5, 23]. However, we observed high mRNA expression levels of $AT_{1B}Rs$ in resistance arteries commensurate with previous studies [35, 36]. The lack of specific antibodies to discriminate between both receptor subtypes [13] has hitherto seriously hampered the determination of subtype fractions at the protein level. Therefore, specific physiological roles which can unequivocally be ascribed to $AT_{1B}Rs$ have remained largely elusive so far. Surprisingly, $AT_{1B}^{-/-}$ mice showed normal blood pressure [4] but reduced myogenic responsiveness. In contrast, $AT_{1A}^{-/-}$ mice exhibited lowered blood pressure [14, 27] but normal myogenic vasoconstriction. Furthermore, in efferent renal arterioles of $AT_{1A}^{-/-}$ mice, the response to angiotensin II was attenuated [11], and interestingly, $AT_{1B}^{-/-}$ but not $AT_{1A}^{-/-}$ mice showed impaired thirst sensing and drinking behavior [8], suggesting non-exchangeable, distinct functions of the receptor isoforms. However, since the mechanosensitivity of AT_1R critically depends on receptor density [16], an explanation for the dominant role of $AT_{1B}Rs$ for myogenic vasoconstriction may be based on substantially increased expression levels. Calcium measurements in renal $AT_{1A}^{-/-}$ and $AT_{1B}^{-/-}$ VSMCs that exhibit similar mRNA expression levels of both receptor isoforms indicate, however, that $AT_{1B}Rs$ are more mechanosensitive than $AT_{1A}Rs$. A detailed comparison of these receptors at the molecular level may allow to reveal structural characteristics that are responsible for the distinct mechanosensing properties.

To rigorously rule out an involvement of endogenously produced angiotensin II on myogenic vasoconstriction—as expected from previous studies [16, 38] – we investigated $Agt^{-/-}$ mice which showed unaltered myogenic tone but have a lowered blood pressure [28], indicating that the ligand angiotensin II is not essentially involved in myogenic vasoconstriction, whereas the cognate AT_1Rs are of central importance, thus entertaining the notion that agonist-independent mechanical AT_1R activation is centrally involved in myogenic vasoconstriction. Our findings demonstrate for the first time that ligand-independent activation of mechanosensitive GPCRs is responsible for up to 50 % of myogenic vasoconstriction, highlighting that such a percentage of myogenic vasoconstriction occurs without involvement of mechanosensitive ion channels.

The human AT_1R appears to combine several properties of the murine AT_1R subtypes in one protein, i.e., regulation of blood pressure, myogenic vasoconstriction, and local blood flow. A deeper understanding of the cellular and molecular mechanisms responsible for myogenic vasoconstriction may help identify new and verify known pharmacological targets to tackle common diseases like systemic hypertension, diabetes, and stroke.

Acknowledgments We thank Ernst Bernges, Laura Danner, and Joanna Zaisserer for excellent technical assistance. We are grateful to Michael Bader and Thomas Coffman for providing AT_{1A}, AT_{1B} receptor and Agt gene-deficient mice. This work was supported by grants from the Deutsche Forschungsgemeinschaft (DFG).

References

1. Anfinogenova Y, Brett SE, Walsh MP, Harraz OF, Welsh DG (2011) Do TRPC-like currents and G protein-coupled receptors interact to facilitate myogenic tone development? Am J Physiol Heart Circ Physiol 301(4):H1378–H1388
2. Bayliss WM (1902) On the local reactions of the arterial wall to changes of internal pressure. J Physiol 28:220–231
3. Bevan JA, Laher I (1991) Pressure and flow-dependent vascular tone. Faseb J 5(9):2267–2273
4. Chen X, Li W, Yoshida H, Tsuchida S, Nishimura H, Takemoto F, Okubo S, Fogo A, Matsusaka T, Ichikawa I (1997) Targeting deletion of angiotensin type 1B receptor gene in the mouse. Am J Physiol 272(3 Pt 2):F299–F304
5. Chiu AT, Dunscomb J, Kosierowski J, Burton CR, Santomenna LD, Corjay MH, Benfield P (1993) The ligand binding signatures of the rat AT1A, AT1B and the human AT1 receptors are essentially identical. Biochem Biophys Res Commun 197(2):440–449
6. Davis MJ, Hill MA (1999) Signaling mechanisms underlying the vascular myogenic response. Physiol Rev 79(2):387–423
7. Davis MJ, Sikes PJ (1990) Myogenic responses of isolated arterioles: test for a rate-sensitive mechanism. Am J Physiol 259(6 Pt 2): H1890–H1900
8. Davisson RL, Oliverio MI, Coffman TM, Sigmund CD (2000) Divergent functions of angiotensin II receptor isoforms in the brain. J Clin Invest 106(1):103–106
9. Dietrich A, Mederos y Schnitzler M, Gollasch M, Gross V, Storch U, Dubrovska G, Obst M, Yildirim E, Salanova B, Kalwa H, Essin K, Pinkenburg O, Luft FC, Gudermann T, Birnbaumer L (2005) Increased vascular smooth muscle contractility in $TRPC6^{-/-}$ mice. Mol Cell Biol 25(16):6980–6989
10. Galic S, Oakhill JS, Steinberg GR (2009) Adipose tissue as an endocrine organ. Mol Cell Endocrinol 316(2):129–139
11. Harrison-Bernard LM, Cook AK, Oliverio MI, Coffman TM (2003) Renal segmental microvascular responses to ANG II in AT1A receptor null mice. Am J Physiol Renal Physiol 284(3):F538–F545
12. Hill MA, Meininger GA, Davis MJ, Laher I (2009) Therapeutic potential of pharmacologically targeting arteriolar myogenic tone. Trends Pharmacol Sci 30:363–374
13. Hoffmann A, Cool DR (2005) Characterization of two polyclonal peptide antibodies that recognize the carboxy terminus of angiotensin

II AT1A and AT1B receptors. Clin Exp Pharmacol Physiol 32(11): 936–943
14. Ito M, Oliverio MI, Mannon PJ, Best CF, Maeda N, Smithies O, Coffman TM (1995) Regulation of blood pressure by the type 1A angiotensin II receptor gene. Proc Natl Acad Sci U S A 92(8):3521–3525
15. Mederos y Schnitzler M, Storch U, Gudermann T (2011) AT1 receptors as mechanosensors. Curr Opin Pharmacol 11(2):112–116
16. Mederos y Schnitzler M, Storch U, Meibers S, Nurwakagari P, Breit A, Essin K, Gollasch M, Gudermann T (2008) Gq-coupled receptors as mechanosensors mediating myogenic vasoconstriction. EMBO J 27(23):3092–3103
17. Nickenig G, Strehlow K, Roeling J, Zolk O, Knorr A, Bohm M (1998) Salt induces vascular AT1 receptor overexpression in vitro and in vivo. Hypertension 31(6):1272–1277
18. Nilius B, Honore E (2012) Sensing pressure with ion channels. Trends Neurosci 35(8):477–486. doi:10.1016/j.tins.2012.04.002
19. Oliverio MI, Kim HS, Ito M, Le T, Audoly L, Best CF, Hiller S, Kluckman K, Maeda N, Smithies O, Coffman TM (1998) Reduced growth, abnormal kidney structure, and type 2 (AT2) angiotensin receptor-mediated blood pressure regulation in mice lacking both AT1A and AT1B receptors for angiotensin II. Proc Natl Acad Sci U S A 95(26):15496–15501
20. Pedersen SF, Nilius B (2007) Transient receptor potential channels in mechanosensing and cell volume regulation. Methods Enzymol 428: 183–207. doi:10.1016/S0076-6879(07)28010-3
21. Rakesh K, Yoo B, Kim IM, Salazar N, Kim KS, Rockman HA (2010) beta-Arrestin-biased agonism of the angiotensin receptor induced by mechanical stress. Sci Signal 3(125):ra46
22. Ruan X, Wagner C, Chatziantoniou C, Kurtz A, Arendshorst WJ (1997) Regulation of angiotensin II receptor AT1 subtypes in renal afferent arterioles during chronic changes in sodium diet. J Clin Invest 99(5):1072–1081
23. Saavedra JM (1999) Emerging features of brain angiotensin receptors. Regul Pept 85(1):31–45
24. Sharif-Naeini R, Dedman A, Folgering JH, Duprat F, Patel A, Nilius B, Honore E (2008) TRP channels and mechanosensory transduction: insights into the arterial myogenic response. Pflugers Arch 456(3):529–540. doi:10.1007/s00424-007-0432-y
25. Storch U, Forst AL, Philipp M, Gudermann T, Mederos y Schnitzler M (2012) Transient receptor potential channel 1 (TRPC1) reduces calcium permeability in heteromeric channel complexes. J Biol Chem 287(5):3530–3540. doi:10.1074/jbc.M111.283218
26. Storch U, Mederos y Schnitzler M, Gudermann T (2012) G protein-mediated stretch reception. Am J Physiol Heart Circ Physiol 302(6): H1241–H1249
27. Sugaya T, Nishimatsu S, Tanimoto K, Takimoto E, Yamagishi T, Imamura K, Goto S, Imaizumi K, Hisada Y, Otsuka A et al (1995) Angiotensin II type 1a receptor-deficient mice with hypotension and hyperreninemia. J Biol Chem 270(32):18719–18722
28. Tanimoto K, Sugiyama F, Goto Y, Ishida J, Takimoto E, Yagami K, Fukamizu A, Murakami K (1994) Angiotensinogen-deficient mice with hypotension. J Biol Chem 269(50):31334–31337
29. Tian Y, Baukal AJ, Sandberg K, Bernstein KE, Balla T, Catt KJ (1996) Properties of AT1a and AT1b angiotensin receptors expressed in adrenocortical Y-1 cells. Am J Physiol 270(5 Pt 1): E831–E839
30. Van Liefde I, Vauquelin G (2009) Sartan-AT1 receptor interactions: in vitro evidence for insurmountable antagonism and inverse agonism. Mol Cell Endocrinol 302(2):237–243. doi:10.1016/j.mce.2008.06.006
31. Vandesompele J, De Preter K, Pattyn F, Poppe B, Van Roy N, De Paepe A, Speleman F Accurate normalization of real-time quantitative RT-PCR data by geometric averaging of multiple internal control genes. Genome Biol 3(7), RESEARCH0034
32. Yasuda N, Miura S, Akazawa H, Tanaka T, Qin Y, Kiya Y, Imaizumi S, Fujino M, Ito K, Zou Y, Fukuhara S, Kunimoto S, Fukuzaki K, Sato T, Ge J, Mochizuki N, Nakaya H, Saku K, Komuro I (2008) Conformational switch of angiotensin II type 1 receptor underlying mechanical stress-induced activation. EMBO Rep 9(2):179–186
33. Yuan JS, Reed A, Chen F, Stewart CN Jr (2006) Statistical analysis of real-time PCR data. BMC Bioinforma 7:85
34. Zhou J, Ernsberger P, Douglas JG (1993) A novel angiotensin receptor subtype in rat mesangium. Coupling to adenylyl cyclase. Hypertension 21(6 Pt 2):1035–1038
35. Zhou Y, Chen Y, Dirksen WP, Morris M, Periasamy M (2003) AT1b receptor predominantly mediates contractions in major mouse blood vessels. Circ Res 93(11):1089–1094
36. Zhou Y, Dirksen WP, Chen Y, Morris M, Zweier JL, Periasamy M (2005) A major role for AT1b receptor in mouse mesenteric resistance vessels and its distribution in heart and neuroendocrine tissues. J Mol Cell Cardiol 38(4):693–696
37. Zhu J, Taniguchi T, Takauji R, Suzuki F, Tanaka T, Muramatsu I (2000) Inverse agonism and neutral antagonism at a constitutively active alpha-1a adrenoceptor. Br J Pharmacol 131(3):546–552. doi:10.1038/sj.bjp.0703584
38. Zou Y, Akazawa H, Qin Y, Sano M, Takano H, Minamino T, Makita N, Iwanaga K, Zhu W, Kudoh S, Toko H, Tamura K, Kihara M, Nagai T, Fukamizu A, Umemura S, Iiri T, Fujita T, Komuro I (2004) Mechanical stress activates angiotensin II type 1 receptor without the involvement of angiotensin II. Nat Cell Biol 6(6):499–506

3. Publication: Forst et al. (2015)

Podocyte purinergic P_2X_4 channels are mechanotransducers that mediate cytoskeletal disorganization.

Forst AL, Olteanu V, Mollet G, Wlodkowski T, Schaefer F, Dietrich A, Reiser J, Gudermann T, Mederos y Schnitzler M, Storch U.

J Am Soc Nephrol. 2015 Jul 9. pii: ASN.2014111144.
[published ahead of print]

Author's contribution to this work:
AL.F. designed and performed experiments and analyzed the data from the following experiments: Culturing of mouse podocyte cell line, electrophysiological recordings, Western Blot analysis, ATP-release assay, stretching and staining of podocytes. AL.F. isolated and maintained primary podocytes and performed calcium recordings and analyzed the data. AL.F., U.S. and M.MyS. wrote the manuscript.
V.O. isolated and maintained primary podocytes and carried out quantitative RT-PCRs. G.M., F.S., T.W., and A.D. contributed mice strains. J.R. contributed constructs and helped with the design of the study. M.MyS. and U.S. designed experiments and analyzed data. U.S., M.MyS. and T.G. supervised the study.

BASIC RESEARCH www.jasn.org

Podocyte Purinergic $P2X_4$ Channels Are Mechanotransducers That Mediate Cytoskeletal Disorganization

Anna-Lena Forst,* Vlad Sorin Olteanu,* Géraldine Mollet,† Tanja Wlodkowski,‡ Franz Schaefer,‡ Alexander Dietrich,* Jochen Reiser,§ Thomas Gudermann,*‖ Michael Mederos y Schnitzler,*‖ and Ursula Storch*

*Walther-Straub-Institute of Pharmacology and Toxicology, University of Munich, Munich, Germany; †INSERM U1163, Laboratory of Hereditary Kidney Diseases, Imagine Institute, Paris, France; ‡Division of Pediatric Nephrology, Heidelberg University Center for Pediatrics and Adolescent Medicine, Heidelberg, Germany; §Department of Medicine, Rush University Medical Center, Chicago, Illinois; and ‖DZHK (German Centre for Cardiovascular Research), Munich Heart Alliance, Munich, Germany

ABSTRACT

Podocytes are specialized, highly differentiated epithelial cells in the kidney glomerulus that are exposed to glomerular capillary pressure and possible increases in mechanical load. The proteins sensing mechanical forces in podocytes are unconfirmed, but the classic transient receptor potential channel 6 (TRPC6) interacting with the MEC-2 homolog podocin may form a mechanosensitive ion channel complex in podocytes. Here, we observed that podocytes respond to mechanical stimulation with increased intracellular calcium concentrations and increased inward cation currents. However, TRPC6-deficient podocytes responded in a manner similar to that of control podocytes, and mechanically induced currents were unaffected by genetic inactivation of TRPC1/3/6 or administration of the broad-range TRPC blocker SKF-96365. Instead, mechanically induced currents were significantly decreased by the specific P2X purinoceptor 4 ($P2X_4$) blocker 5-BDBD. Moreover, mechanical $P2X_4$ channel activation depended on cholesterol and podocin and was inhibited by stabilization of the actin cytoskeleton. Because $P2X_4$ channels are not intrinsically mechanosensitive, we investigated whether podocytes release ATP upon mechanical stimulation using a fluorometric approach. Indeed, mechanically induced ATP release from podocytes was observed. Furthermore, 5-BDBD attenuated mechanically induced reorganization of the actin cytoskeleton. Altogether, our findings reveal a TRPC channel-independent role of $P2X_4$ channels as mechanotransducers in podocytes.

J Am Soc Nephrol 27: ●●●–●●●, 2015. doi: 10.1681/ASN.2014111144

Podocytes are unique visceral epithelial cells lining the inner part of the Bowman capsule, where they are important regulators of the kidney filtration barrier. Podocytes contain a cell body and so-called foot processes, which allow for protein-protein interactions with adjacent interdigitated foot processes, thereby forming the slit membrane.[1,2] Slit-membrane proteins, such as nephrin or Neph1–3, as well as slit-membrane–associated proteins, such as podocin, synaptopodin, CD2-associated protein (CD2AP), and the transient receptor potential channel 6 (TRPC6), are tightly regulated to ensure proper function of the podocyte filtration barrier. Hypertension and the resulting increase in glomerular pressure are believed to result in podocyte damage, leading to proteinuria.[3] Glomerular

Received November 26, 2014. Accepted June 10, 2015.

Published online ahead of print. Publication date available at www.jasn.org.

Correspondence: Dr. Michael Mederos y Schnitzler, or Dr. Ursula Storch, Walther Straub Institute for Pharmacology and Toxicology, Ludwig Maximilians University of Munich, Goethestr. 33, 80336 Munich, Germany. Email: mederos@lrz.uni-muenchen.de or ursula.storch@lrz.uni-muenchen.de.

hypertension–provoked hypertrophy, foot process effacement, and detachment of podocytes are well characterized in animal models.[4–6] There is also evidence for a damaging effect of hypertension in humans.[7]

Until now, it has been completely unknown how podocytes sense the changes in glomerular pressure. It was postulated that TRPC6 channels involved in the pathogenesis of familial FSGS[8,9] may serve as mechanosensors in podocytes.[2,10,11] However, at least in overexpression systems, TRPC6 itself was not inherently mechanosensitive.[12–14] TRPC6 was shown to be expressed at the slit membrane,[8,9] where it interacts with the podocyte-specific protein podocin.[10] Because the podocin homolog MEC-2 is part of a mechanosensitive multiprotein ion channel complex in *Caenorhabditis elegans,* it was suggested that TRPC6 in complex with other slit-membrane proteins (including podocin) could form a mechanosensitive ion channel complex.[2] Of note, in our previous studies, $G_{q/11}$-protein–coupled receptors ($G_{q/11}$PCRs) and not TRPC6 channels shaped up as mechanosensors in vascular smooth muscle cells[13,15] contributing to myogenic vasoconstriction. There is still growing evidence for an inherent mechanosensitivity of G-protein–coupled receptors (GPCRs) in other tissues and organs (summarized by Storch *et al.*[16]). Furthermore, many other proteins, including structural proteins and various ion channels, have been discussed as potential mechanosensors.[17] Because the mechanosensory and -transducing elements in podocytes are still largely elusive, we sought to analyze the role of TRPC6 and GPCRs as potential mechanosensors in podocytes and at uncovering novel candidates for mechanosensors or -transducers in podocytes. Deeper insight into the mechanisms leading to mechanically induced podocyte damage may be instrumental in devising targeted treatments for podocyte injuries, as seen in hypertensive nephropathy.[18]

RESULTS

Mechanical Membrane Stretch Induces Inwardly Rectifying Currents and Intracellular Calcium Increases in Podocytes

To analyze the mechanosensory and -transduction properties of podocytes, we used isolated murine podocytes, which express several podocyte-specific proteins, such as nephrin and podocin (Supplemental Figure 1). Quantitative RT-PCR was used to determine the expression of the podocyte markers nephrin, podocin, Neph1–3, synaptopodin, and CD2AP (Figure 1A) and of all TRPC channels exception TRPC7 (Figure 1B). Next, fluorometric calcium measurements with fura-2–loaded podocytes were performed. As a mechanical stimulus, cell swelling with hypoosmotic bath solution was deployed, resulting in transient calcium increases (Figure 1, C and D). Whole-cell measurements showed that podocytes responded to cell swelling with hypoosmotic bath solution with significantly increased inwardly rectifying cation currents (Figure 1, E and F); this finding indicates that podocytes are mechanosensitive. Because hypotonic cell swelling might trigger additional unspecific effects apart from exerting membrane stretch by increasing the cell volume, we next applied a positive pipette pressure of 30 cmH_2O; this led to transient cation current increases with a similar current density voltage relationship, as observed upon hypoosmotic cell swelling (Figure 1, G and H). Similar results were obtained by analyzing conditionally immortalized murine podocytes[19] that responded to hypoosmotic cell swelling and positive pipette pressure in a similar manner (Supplemental Figure 2, A–D).

Because it is hypothesized that in podocytes TRPC6 in complex with slit-membrane proteins (SMPs) is mechanosensitive, we analyzed isolated podocytes from TRPC6 gene-deficient ($Trpc6^{-/-}$) mice.[20] Interestingly, $Trpc6^{-/-}$ podocytes showed similar inwardly rectifying currents as observed in control podocytes (Figure 1, I–K), suggesting that TRPC6 is not essential for mechanosensation or -transduction. Moreover, the reconstitution of a potentially mechanosensitive ion channel complex by coexpressing TRPC6 together with the SMPs podocin, CD2AP, and nephrin in human embryonic kidney 293 (HEK293) cells was unsuccessful because TRPC6 current did not increase upon mechanical stimulation (Supplemental Figure 2, E and F), while subsequent stimulation with the TRPC6 activator oleoyl-2-acetyl-glycerol, a membrane-permeable diacylglycerol analogue, augmented TRPC6 currents. Taken together, these data argue against TRPC6 as a mechanosensor in podocytes. To rule out the involvement of other TRPC channels, C57BL/6 podocytes were incubated with the broad-range TRPC channel blocker SKF-96365 (10 μM), which had no effect on mechanically induced cation current increases (Supplemental Figure 2, G and H). Moreover, podocytes isolated from TRPC1/3/6 triple gene–deficient ($Trpc1/3/6^{-/-}$) mice were analyzed in the presence and absence of 10 μM SKF-96365. Mechanical stimulation caused similar cation currents as monitored in control podocytes (Figure 1, L–N), indicating that TRPC channels are not essentially involved in mechanosensation or mechanotransduction in podocytes.

$G_{q/11}$-PCRs Are Not Mechanosensors in Podocytes

In cardiac and vascular smooth muscle, $G_{q/11}$PCRs and particularly angiotensin II (AT_1) receptors (AT_1Rs) were identified as direct mechanosensors.[13,15,21] Moreover, there is evidence that overexpression of AT_1Rs causes proteinuria,[22] and AT_1R antagonists and angiotensin-converting enzyme inhibitors are protective for podocytes and can improve proteinuria.[23,24] Therefore, we analyzed the role of $G_{q/11}$PCRs as potential mechanosensors in podocytes. Performing quantitative RT-PCR, we documented the expression of several $G_{q/11}$PCRs known to play a role in the kidney, including endothelin type A and type B, AT_{1A}, AT_{1B}, and AT_2 and vasopressin $(V)_{1A}$, V_{1B}, and V_2 receptors (Figure 2A). Inhibition of all $G_{q/11}$ proteins by the selective $G_{q/11}$ protein inhibitor YM-254890, preventing the exchange of guanosine diphosphate for guanosine triphosphate during $G\alpha_{q/11}$ activation,[25] did not suppress mechanically induced currents (Figure 2, B and C) or

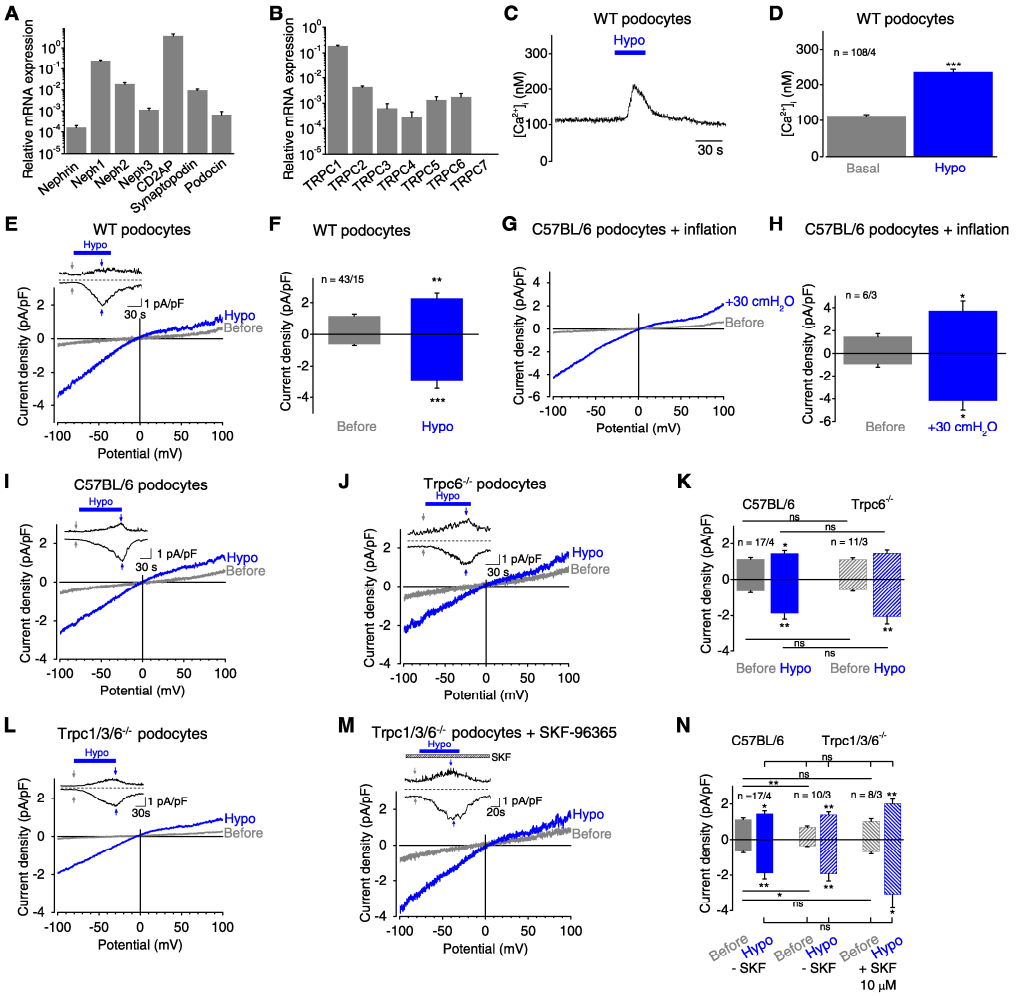

Figure 1. Mechanical membrane stretch induces inwardly rectifying currents and intracellular calcium increases in podocytes. (A and B) Relative mRNA expression levels of selected podocyte marker proteins (A) and TRPC channels (B) in primary podocytes determined by quantitative PCR analysis from three independent experiments. (C) Exemplary time courses of the intracellular calcium concentration $[Ca^{2+}]_i$ of fura-2–loaded podocytes. Application of hypoosmotic bath solution "Hypo" is indicated. (D) Summary of $[Ca^{2+}]_i$ before (gray bar) and during (blue bar) application of hypoosmotic bath solution. Numbers indicate the numbers of measured cells and of independent experiments. (E–N) Electrophysiologic whole-cell measurements of wild-type (WT) (E), C57BL/6 (G and I), TRPC6 gene-deficient ($Trpc6^{-/-}$) (J), and TRPC1/3/6 gene-deficient ($Trpc1/3/6^{-/-}$) (L and M) podocytes in the presence (M) or absence (L) of the nonselective TRPC blocker SKF-96365 with exemplary current density voltage (CDV) relationships. CDVs are displayed before (gray) and during (blue) application of hypoosmotic bath solution "Hypo" and of positive pipette pressure of 30 cmH_2O "inflation" (G). Insets show current density time courses at holding potentials of ±100 mV. Stippled lines represent zero current. Blue bars indicate application of hypoosmotic solution. Arrows represent the time points of depicted CDV traces. (F, H, K, and N) Summary of current densities before (gray and gray hatched bars) and during application of hypoosmotic bath solution or of positive pipette pressure (blue and blue hatched bars) of respective control (solid bars) and gene-deficient podocytes (hatched bars) at ±100 mV. Numbers display the numbers of measured cells and of independent experiments. Nonsignificant (ns) differences are indicated. $*P<0.05$; $**P<0.01$; $***P<0.001$; ns $P>0.05$.

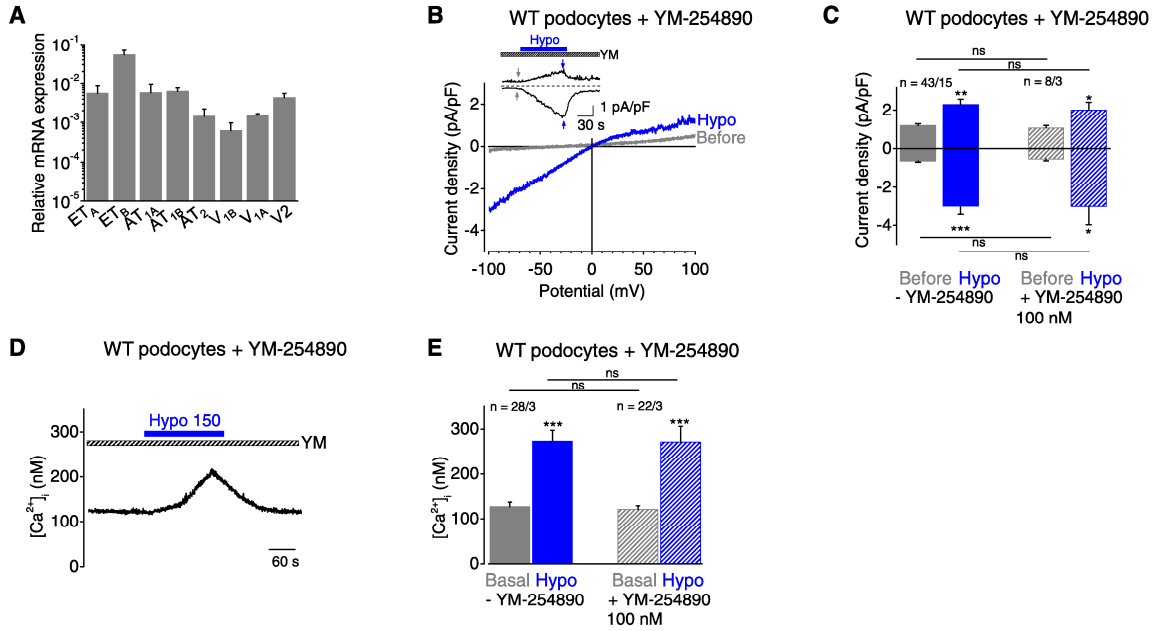

Figure 2. $G_{q/11}$-PCRs are not mechanosensors in podocytes. (A) Relative mRNA expression levels of selected GPCRs in primary podocytes determined by quantitative PCR analysis from three independent experiments. (B) Exemplary CDV relationships of podocytes preincubated with the $G_{q/11}$-inhibitor YM-254890 (100 nM) for 30 minutes before (gray) and during (blue) cell swelling. Insets show current density time courses at ±100 mV. Stippled lines represent zero current. Application of hypoosmotic solution is indicated. Arrows represent the time points of depicted CDV traces. (C) Summary of current densities before (gray and gray hatched bars) and during (blue and blue hatched bars) the application of hypoosmotic solution of control podocytes (solid bars) and podocytes preincubated with YM-254890 (hatched bars) determined at holding potentials of ±100 mV. Numbers display the number of measured cells and of independent experiments. (D) Exemplary time course of the $[Ca^{2+}]_i$ of fura-2–loaded podocytes in the presence of YM-25489. Application of hypoosmotic bath solution "Hypo" is indicated. (E) Summary of $[Ca^{2+}]_i$ before (gray and gray hatched bar) and during (blue and blue hatched bar) application of hypoosmotic bath solution in the presence or absence of YM-25489. Numbers indicate the numbers of measured cells and of independent experiments. Nonsignificant differences (ns) are indicated. *P<0.05; **P<0.01; ***P<0.001; ns P>0.05.

intracellular calcium increases (Figure 2, D–F). This finding indicates that $G_{q/11}$PCRs are not involved in mechanosensation in podocytes.

ATP Application and Mechanical Membrane Stretch Cause Similar Purinergic Currents in Podocytes

Interestingly, mechanically induced cation currents in podocytes share properties with purinergic (P_2X) channels, such as nonselectivity and inward rectification.[26,27] Performing quantitative RT-PCR, we observed expression of all seven P_2X channel subunits (P_2X_1–P_2X_7) in podocytes. P_2X_2 and P_2X_4 showed highest mRNA expression levels, which were 15- to 17-fold higher compared with P_2X_5, exhibiting the third highest mRNA expression level (Figure 3A). Expression of the $G_{q/11}$-coupled P_2Y_1 receptor was also detected. Surprisingly, 100 μM ATP gave rise to inward currents with marked inward rectification (Figure 3, B and C), similar to mechanically induced currents. Further, ATP application provoked transient calcium increases in fura-2–loaded podocytes (Figure 3, D and E). ATP-induced currents slowly inactivated in the presence of ATP (Figure 3, B and D) with an inactivation constant of τ=40.8±7.2 seconds calculated at a holding potential of −100 mV. Homomeric P_2X channels consisting of three P_2X subunits can be distinguished by their current inactivation time within milliseconds (P_2X_1 and P_2X_3), within several seconds (P_2X_2 and P_2X_4), and by little and no inactivation (P_2X_5 and P_2X_7, respectively).[27] Therefore, our estimated inactivation constant in podocytes points to P_2X_2 and P_2X_4 channels.

To test whether mechanical stimulation as well as ATP activates P_2X channels, we first applied 50 μM suramin blocking P_2X_1, P_2X_2, P_2X_3 P_2X_5, and P_2X_6 channels.[28] Suramin did not significantly reduce mechanically induced currents in podocytes (Figure 3, F and G). Furthermore, suramin did not suppress subsequent hypoosmotically induced calcium transients in fura-2–loaded podocytes (Figure 3, H and I) compared with untreated cells; this finding indicates that P_2X_4 or P_2X_7 channels might be involved. Of note, the first hypoosmotic stimulus served as a control, illustrating the

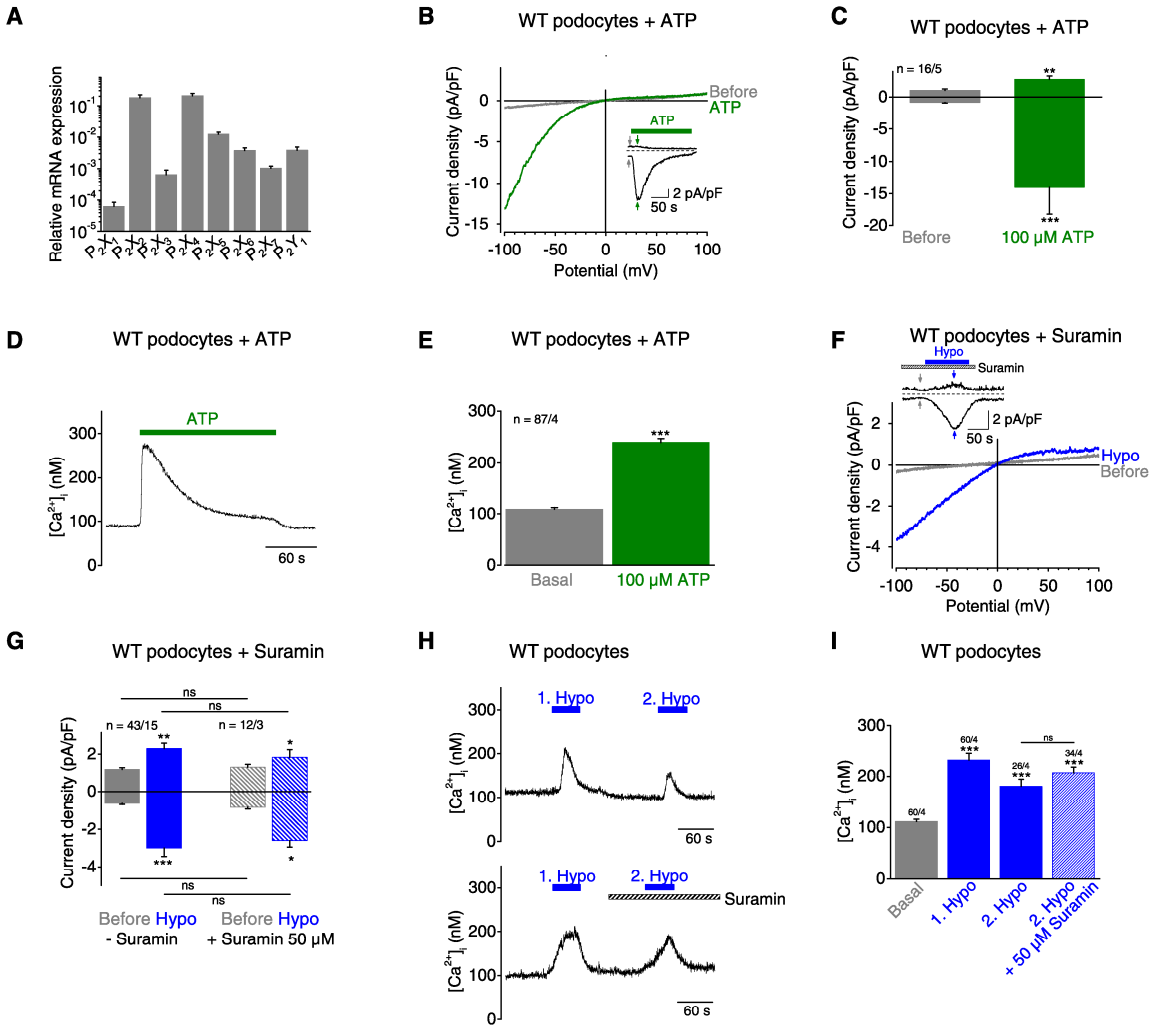

Figure 3. ATP application and mechanical membrane stretch cause similar P_2X currents in podocytes. (A) Relative mRNA expression levels of selected GPCRs of primary podocytes determined by quantitative PCR analysis from three independent experiments. (B, C, F, G) Electrophysiologic whole-cell measurements of podocytes. (B and F) Exemplary CDV relationships before (gray) and during (green) application of 100 μM ATP and of hypoosmotic solution "Hypo" in the presence of 50 μM suramin (blue) are displayed. Insets show current density time course at $\pm$100 mV. Stippled lines represent zero current. Application of ATP is indicated. Arrows represent the time points of depicted CDV traces. (C and G) Summary of current densities before (gray bars) and during (green bars) application of ATP and of hypoosmotic solution in the presence (blue hatched bars) and absence (blue bars) of suramin at $\pm$100 mV. (D and E) Fluorimetric calcium measurements with fura-2–loaded podocytes. (D) Exemplary time course of intracellular calcium concentration $[Ca^{2+}]_i$ with application of 100 μM ATP is displayed. (E) Summary of $[Ca^{2+}]_i$ before (gray bar) and during (green bar) application of ATP. Numbers indicate the numbers of measured cells and of independent experiments. (F and G) Electrophysiologic whole-cell measurements of podocytes. (H and I) Fluorimetric calcium measurements with fura-2–loaded podocytes. (H) Exemplary time courses of $[Ca^{2+}]_i$ in the presence (lower panel) and absence (upper panel) of 50 μM suramin during the second hypoosmotic stimulation. Applications of hypoosmotic solution and of suramin are indicated. (I) Summary of $[Ca^{2+}]_i$ before (gray bars) and during application of hypoosmotic solution in the presence (blue hatched bar) and absence (blue bars) of suramin. Numbers indicate the numbers of measured cells and of independent experiments. Nonsignificant differences (ns) are indicated. *P<0.05; **P<0.01; ***P<0.001; ns P>0.05.

comparability of the cells. In light of the slow inactivation kinetics characteristic of P_2X_2 and P_2X_4 channels and the lack of any suramin effect, these findings suggest that the currents evoked by mechanical stimulation are mainly mediated by P_2X_4 channels. Moreover, 50 μM suramin uncouples G proteins from receptors,[29] additionally indicating that GPCRs including P_2Y receptors are not involved in mechanical responses of podocytes.

P_2X_4 Channels in Podocytes Are Activated upon Mechanical Stimulation

To ascertain mechanically induced P_2X_4 channel activation in podocytes, we applied the nonselective P_2X channel blocker trinitrophenyl (TNP)-ATP (75 μM) affecting all homomeric P_2X channels except P_2X_7[27] (Figure 4, A and B) and the selective P_2X_4 blocker 5-BDBD[30] (10 μM) (Figure 4, C and D). Both blockers significantly reduced mechanically induced currents, indicating that P_2X_4 is crucially involved in the mechanical response of podocytes. This notion was further supported by analyzing conditionally immortalized podocytes, which likewise showed significantly suppressed currents in the presence of 10 μM 5-BDBD (Supplemental Figure 3, A and B). However, mechanically induced currents and intracellular calcium increases (Supplemental Figure 3, C and D) were not fully suppressed, which may be caused by the specific assembly of endogenous heteromeric P_2X channels with distinct properties.

To verify the prominent role of P_2X_4 channels, the selective P_2X_4 potentiator ivermectin was applied to fura-2–loaded podocytes. In the presence of 50 μM ivermectin mechanically induced calcium transients were significantly higher compared with the respective initial calcium response (Figure 4, E and F), whereas in the absence of ivermectin the second calcium response was always smaller (Figure 3, H [upper panel] and I). Altogether, these pharmacologic interventions identified P_2X_4 as a key component of the mechanotransduction process in podocytes. As a crucial proof-of-principle, isolated podocytes from P_2X_4 gene-deficient ($P_2X_4^{-/-}$) mice[31] were investigated. Indeed, $P_2X_4^{-/-}$ podocytes were devoid of mechanically induced current increases (Figure 4G) compared with their respective wild-type controls (Figure 4, H and I), confirming the cardinal role of $P_2X_4^{-/-}$. Of note, ATP-induced currents were also significantly reduced in $P_2X_4^{-/-}$ compared with wild-type podocytes (Figure 4, J–L). The current inactivation constant was 40.4±5.0 seconds in $P_2X_4^{-/-}$ similar to that seen in $P_2X_4^{+/+}$ control cells; this finding points to slow inactivating P_2X_2 currents activated by ATP in $P_2X_4^{-/-}$ podocytes. Altogether, these findings provide strong evidence for an essential involvement of P_2X_4 channels in the mechanical responsiveness of podocytes.

Mechanical Stimulation of Podocytes Causes ATP Release Leading to Subsequent P_2X_4 Channel Activation

To analyze whether P_2X_4 channels in podocytes are mechanosensors or mechanotransducers, we performed whole-cell measurements with HEK293 cells overexpressing P_2X_2, P_2X_4, or both channel subunits together. Hypoosmotic cell swelling did not activate P_2X channels (Supplemental Figure 4, A–C) in cells overexpressing P_2X_4, P_2X_2, or combinations thereof in the presence or absence of the SMPs podocin, CD2AP, and nephrin (Figure 5, A and B, and Supplemental Figure 4, D and E), suggesting that P_2X channels are not inherently mechanosensitive. The involvement of the actin cytoskeleton in mechanosensation of podocytes was analyzed by incubation of podocytes with 5 μM cytochalasin D for 20 minutes at 37°C to disrupt actin fibers. This measure had no effect on hypoosmotically induced current responses in podocytes (Figure 5, C and D), indicating that the actin cytoskeleton *per se* is not crucial for mechanical activation in podocytes. Next, 8 nM jasplakinolide[32] was administered for 20 minutes at 37°C to induce actin polymerization, resulting in significant reduction of mechanically induced currents (Figure 5, E and F). This finding suggests that stabilization of the actin cytoskeleton might prevent ATP release. This is in congruence with previous findings in PC12 cells showing impaired vesicle release by jasplakinolide.[33,34] Of note, 200 nM jasplakinolide, a frequently used concentration in other cells, did not significantly suppress mechanically induced currents (Supplemental Figure 5, A and B), indicating that this concentration results in disruption rather than stabilization of the actin cytoskeleton, as seen in other cells.[35,36] Moreover, applying 10 μM thiocolchicine for 2 hours at 37°C to prevent microtubule assembly did not affect mechanically induced current increases (Supplemental Figure 5, C and D). Altogether, these findings are compatible with the notion that mechanically induced release of prestored ATP-filled vesicles is impaired by actin cytoskeleton stabilization, but not by microtubule disassembly or actin cytoskeleton disruption.

To analyze whether P_2X channels are indeed activated by ATP released from podocytes upon mechanical stimulation, podocytes were treated with the ATP-converting enzyme apyrase, which rapidly converts ATP to AMP. Preincubation for 30 minutes at 37°C and addition of apyrase to all bath solutions completely abolished mechanically induced current increases (Figure 5, G and H). To measure ATP release from podocytes, we performed fluorescence photometry. Perfusion of cells with hypoosmotic bath solution (Figure 5I) and subsequent application of increasing ATP concentrations (Figure 5J) used for calibration purposes resulted in fluorescence increases at 450 nm, corresponding to 419±133 nM ATP (n=9). To further analyze the mechanism of ATP release in podocytes, we applied N-ethylmaleimide, an unspecific SNARE protein blocker that disables vesicular fusion, because podocytes express SNARE proteins.[37] Incubation of podocytes with 2 mM N-ethylmaleimide for 2 minutes was sufficient to completely prevent hypoosmotically induced current increases (Figure 5, K and L), compatible with the notion that podocytes release ATP upon mechanical stimulation *via* fusion of ATP-loaded vesicles to the plasma membrane. Altogether, these findings strongly point to mechanically induced ATP release in podocytes.

Mechanically Induced P_2X_4 Channel Activation Is Podocin and Cholesterol Dependent and Is Crucial for Reorganization of the Actin Cytoskeleton

Exocytosis is inhibited by depletion of cholesterol[38] distributed in lipid rafts in the podocyte cell membrane[39] and is thought to play a role in the pathomechanism of podocyte injuries.[40] To analyze whether cholesterol is involved in mechanically induced P_2X_4 activation, cells were preincubated with fluvastatin

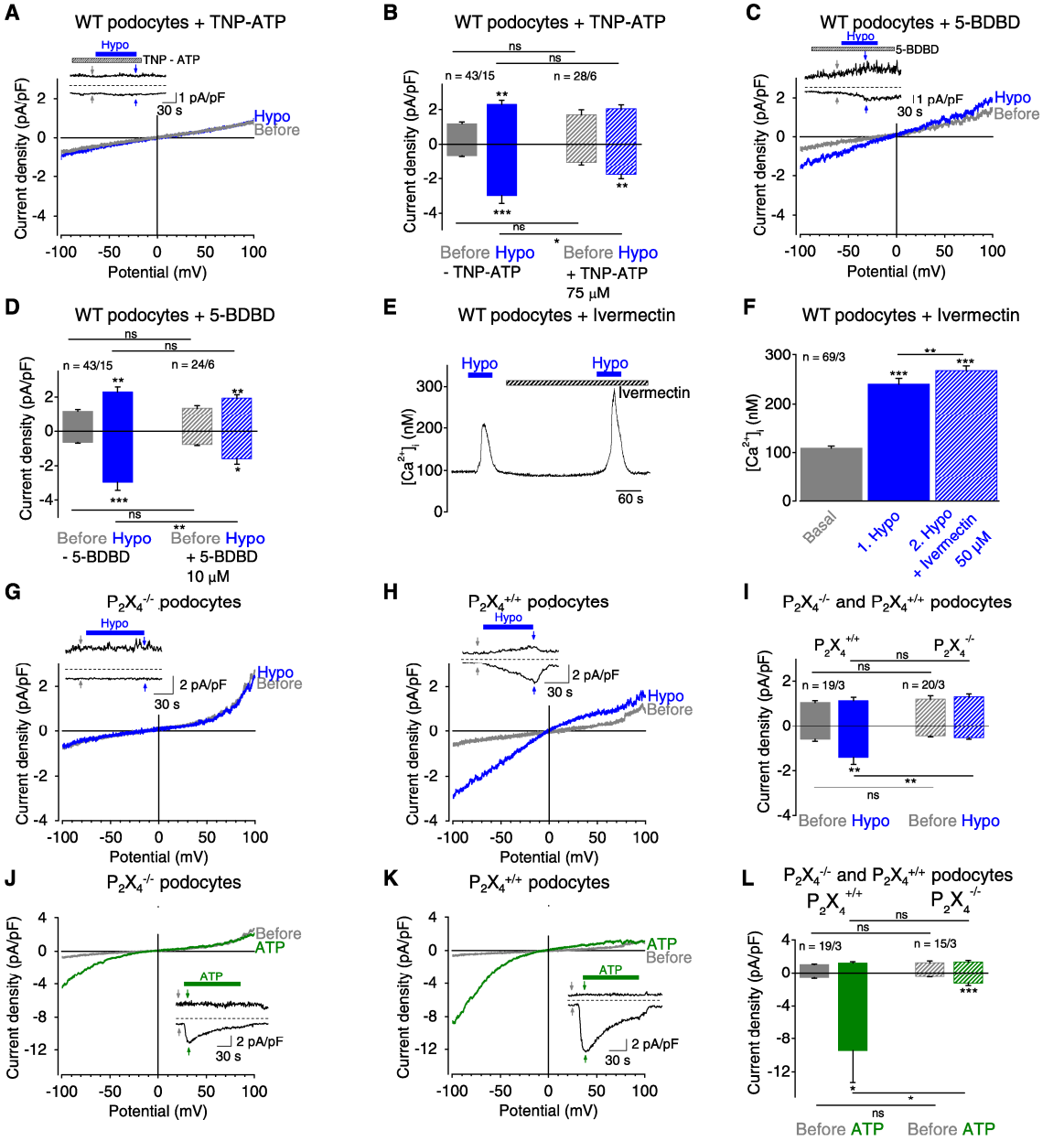

Figure 4. P_2X_4 channels in podocytes are activated upon mechanical stimulation. (A–D) Electrophysiologic whole-cell measurements of podocytes. (A and C) Exemplary CDV relationships before (gray) and during (blue) application of hypoosmotic solution in the presence of 75 μM TNP-ATP (A) and of 10 μM 5-BDBD (C). Insets show current density time courses at ±100 mV. Stippled lines represent zero current. Applications of hypoosmotic solution and of TNP-ATP (A) or of 5-BDBD (C) are indicated. Arrows represent the time points of depicted CDV traces. (B and D) Summaries of current densities before (gray and gray hatched bars) and during application of hypoosmotic solution (blue and blue hatched bars) in the presence and absence of TNP-ATP (B) or of 5-BDBD (D) determined at holding potentials of ±100 mV. (E and F) Fluorimetric calcium measurements with fura-2–loaded podocytes. (E) Exemplary time courses of $[Ca^{2+}]_i$ and applications of hypoosmotic solution and of 50 μM ivermectin are indicated. (F) Summary of $[Ca^{2+}]_i$ before (gray bar) and during application of hypoosmotic solution in the presence (blue hatched bar) and absence (blue bar) of ivermectin. Numbers indicate the numbers of measured cells and of independent experiments. (G–L) Electrophysiologic whole-cell measurements of $P_2X_4^{-/-}$ and of $P_2X_4^{+/+}$ control

(10 μM)[41] for 24 hours at 37°C to prevent cholesterol production and with the cholesterol-binding agent methyl-β-cyclodextrin (10 mM) for 10 minutes at 37°C. Interestingly, ATP-induced currents in cholesterol-depleted podocytes were still observed in fluvastatin and methyl-β-cyclodextrin–treated podocytes, although they were suppressed by a factor of 2.9 and 3.4, respectively (Figure 6, A and B, and Supplemental Figure 6, A and B). However, mechanically induced inward currents were nearly completely suppressed and typical inwardly rectifying P_2X currents were abolished (Figure 6, C and D, and Supplemental Figure 6, A and B), suggesting that cholesterol is essential for mechanical P_2X_4 activation. Of note, slight current increases were still seen in methyl-β-cyclodextrin–treated podocytes evoked by membrane stretch, probably reflecting the presence of other cation channels (Supplemental Figure 6, C and D).

Furthermore, podocin is known to bind to cholesterol and to potentiate diacylglycerol induced TRPC6 currents in an ion channel complex.[42] Therefore, we next analyzed the involvement of podocin in mechanical P_2X_4 activation. To this end, podocin knockdown podocytes isolated from *Nphs2*$^{flox/flox}$, *Cre*$^{+/+}$ mice[31,43] were used and tested for successful *in vitro* podocin downregulation according to Western blot analysis (Supplemental Figure 7). Interestingly, mechanically induced currents were completely abolished in podocin knockdown podocytes compared with respective control podocytes (Figure 6, E–G), whereas ATP-induced currents were unchanged (Supplemental Figure 8). Altogether, these findings indicate that podocin and cholesterol together determine mechanically induced P_2X_4 channel activation in podocytes.

Disorganization of the actin cytoskeleton, which is important for podocyte structure and function, damages podocytes.[44–46] To investigate whether mechanically induced P_2X activation affects the actin cytoskeleton, podocytes were seeded onto silicone membranes and subjected to cyclic tensile strain for 2 hours. After F-actin staining, the actin fiber organization in stretched and nonstretched podocytes was analyzed by categorizing the observed actin structures into four groups (Figure 6H): presence of well defined parallel actin stress fibers representing the physiologic state, actin structure formations displaying the disorganized state (characterized by the presence of actin-rich centers [ARCs] known to be evoked by membrane stretch[47]), ring-like actin fiber structures, and nondefinable actin structures (termed "others", which do not fit in one of the categories but also reflects actin dysregulation). Nonstretched podocytes showed 55.3% parallel stress fibers; in stretched podocytes the percentage of podocytes with ARCs was increased 4-fold, ring-like structures 1.6-fold, and noncategorizable actin fiber formation 1.4-fold, whereas the percentage of podocytes with parallel stress fibers was decreased by a factor of 3 (Figure 6I). These findings illustrate a highly significant ($P<0.001$) reorganization of the actin cytoskeleton. Incubation of nonstretched podocytes with the P_2X_4 blocker 5-BDBD had no significant effect on actin fiber organization ($P>0.6$). Interestingly, actin disorganization by membrane stretch could be partially rescued by 5-BDBD, which significantly reduced the percentage of cells showing ARCs to 64% and increased the number of cells with parallel actin stress fibers to 177% compared with untreated stretched podocytes ($P<0.01$). This result points to a protective effect of 5-BDBD in mechanically stressed podocytes. Furthermore, in the presence of 5-BDBD, nonstretched and stretched podocytes showed significant differences ($P<0.01$) with regard to increased actin disorganization and loss of parallel actin stress fibers. Interestingly, the nonselective TRPC channel blocker SKF-96365 had no protective effect on actin cytoskeleton reorganization in mechanically stressed podocytes, suggesting that TRPC channels are not involved. Altogether, these findings strongly indicate that P_2X_4 channels play a crucial role for mechanically induced actin skeleton reorganization contributing to podocyte damage.

DISCUSSION

Proper podocyte function is of utmost importance for the maintenance of the filtration barrier. Several mutations *(e.g.,* in podocin, CD2AP, nephrin, PLCε, and TRPC6, summarized by Machuca *et al.*[48]) are known causes for podocyte damage. However, very little is known about mechanically induced podocyte injury. A mechanosensitive TRPC6/podocin channel complex was assumed in podocytes,[10] similar to the mechanosensitive degenerin and epithelial Na^+ channel complex in *Caenorhabditis elegans.*

However, as shown here, reconstitution of the postulated channel complex by coexpressing TRPC6 and the SMPs podocin, CD2AP, and nephrin failed to give rise to mechanically induced TRPC6 currents. Moreover, Trpc6$^{-/-}$ podocytes were still mechanosensitive, demonstrating that TRPC6 is neither a mechanosensor nor mechanotransducer in podocytes, contrasting with observations by Wilson *et al.*[49] One reason for the discrepancy observed might be the use of

podocytes. (G, H, J, K) Exemplary CDV relationships of $P_2X_4^{-/-}$ (G and J) and of $P_2X_4^{+/+}$ control podocytes (H and K) before (gray) and during application of hypoosmotic solution (blue) or of 100 μM ATP (green). Insets show current density time courses at $\pm$100 mV. Stippled lines represent zero current. Application of hypoosmotic solution and of ATP is indicated. Arrows represent the time points of depicted CDV traces. (I and L) Summaries of current densities before (gray and gray hatched bars) and during application of hypoosmotic solution (blue and blue hatched bars) (I) or of 100 μM ATP (green and green hatched bars) (L) of $P_2X_4^{-/-}$ and $P_2X_4^{+/+}$ control podocytes determined at $\pm$100 mV. Numbers indicate the numbers of measured cells and of independent experiments. Nonsignificant differences (ns) are indicated. *$P<0.05$; **$P<0.01$; ***$P<0.001$; ns $P>0.05$.

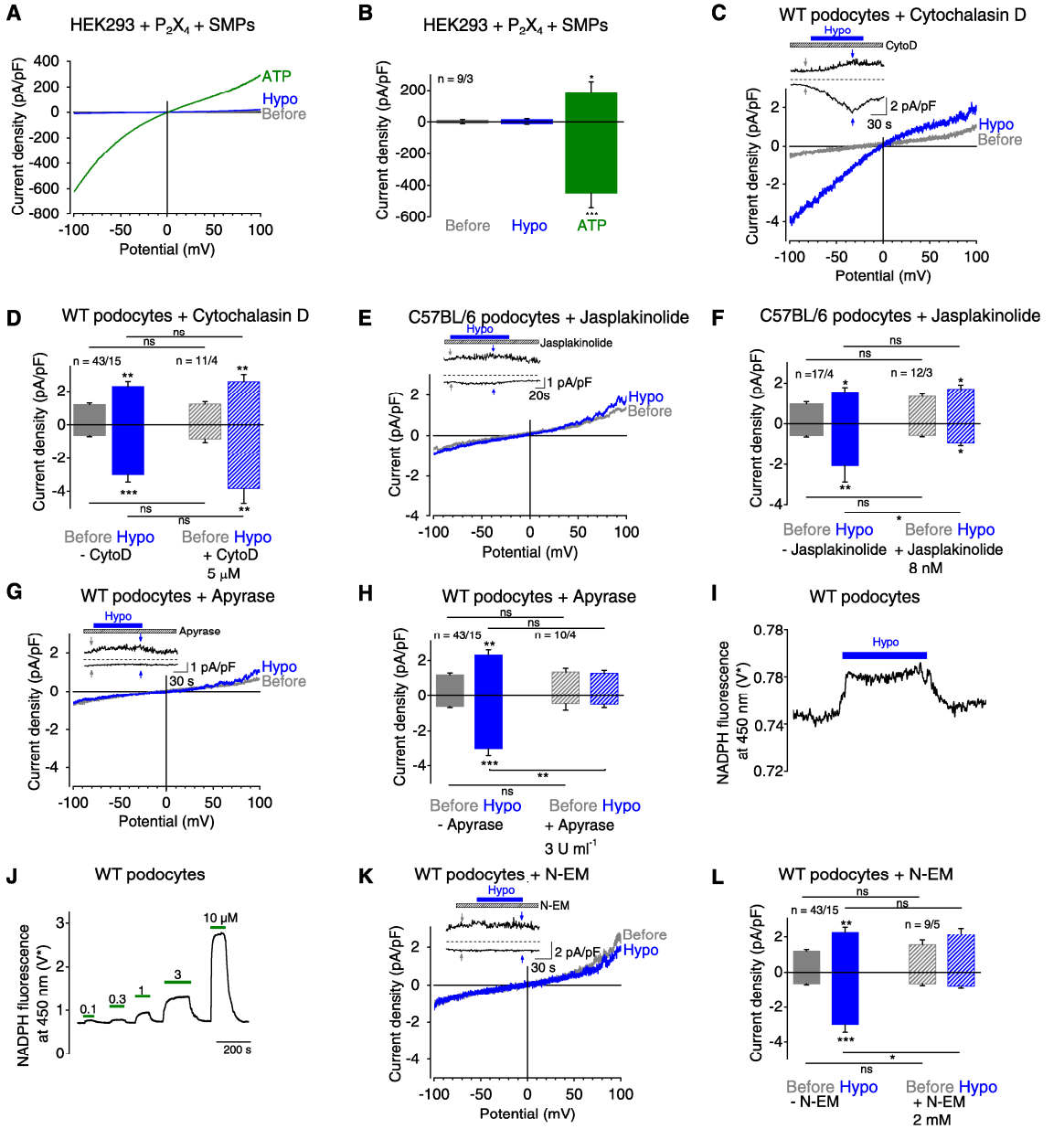

Figure 5. Mechanical stimulation of podocytes causes ATP release leading to subsequent P_2X_4 channel activation. (A–H, K, and L) Electrophysiologic whole-cell measurements of HEK293 cells (A and B) and podocytes (C–H, K, and L). (A) Exemplary CDV relationships of HEK293 cells overexpressing P_2X_4 and the SMPs podocin, nephrin, and CD2AP before (gray) and during (blue) application of hypoosmotic solution and of 100 μM ATP (green). (B) Summary of current densities before (gray bars) and during (blue bar) application of hypoosmotic bath solution and of ATP (green bar) at ±100 mV. Numbers display the number of measured cells and of independent experiments. (C, E, G, K) Exemplary CDV relationships of podocytes before (gray) and during (blue) application of hypoosmotic solution in the presence of 5 μM cytochalasin D (C), 8 nM jasplakinolide (E), 3 U/ml apyrase (G), and 2 mM N-ethylmaleimide (N-EM) (K). Insets show current density time courses at ±100 mV. Stippled lines represent zero current. Application of hypoosmotic solution and of cytochalasin D (C), jasplakinolide (E), of apyrase (G) and of N-EM (K) is indicated. Arrows represent the time points of depicted CDV traces. (D, F, H, L) Summaries of current densities before (gray and gray hatched bars) and during (blue and blue hatched bars) application of hypoosmotic solution in the presence or absence of cytochalasin D, jasplakinolide, apyrase and N-EM determined at ±100 mV.

Trpc6$^{-/-}$ podocytes in our study compared with the use of small interfering RNA against TRPC6. Moreover, different bath solutions were used in the latter study; these solutions were devoid of the chloride channel blockers 5-nitro-2-(3-phenylpropylamino) benzoic acid (NPPB) and 4,4′-diisothiocyanatostilbene-2,2′-disulphonic acid (DIDS). Thus, volume-regulated chloride channels may have contributed to the currents measured by Wilson *et al.*[49] However, in our study we did not obtain experimental evidence supporting a role of other TRPC channels for mechanosensation or mechanotransduction after analyzing Trpc1/3/6$^{-/-}$ podocytes and by applying the nonselective TRPC channel blocker SKF-96365 on wild-type and Trpc1/3/6$^{-/-}$ podocytes. Genetic inactivation of TRPC channels and pharmacologic blockade had no effect on mechanically induced inwardly rectifying currents. Furthermore, we could exclude $G_{q/11}$PCRs as mechanosensors in podocytes, although several GPCRs were expressed in these cells. Instead, our findings point to a key role of P_2X_4 channels for the mechanical responsiveness of podocytes.

ATP evoked similar inwardly rectifying currents in podocytes, as induced by membrane stretch with slow inactivation kinetics pointing to P_2X_2 and P_2X_4 channels, which were found to be highly expressed on the mRNA level. These findings are at odds with observations by Roshanravan and Dryer,[50] who described ATP-induced TRPC6 channel activations. This discrepancy might also be explained by the use of different bath solutions without addition of chloride channel blockers, which were always present throughout our experiments in order to isolate cation currents. However, the inactivation constant of about 41 seconds we determined in podocytes was markedly higher than that observed in the analysis of homomeric P_2X channels.[27] This may be explained by the formation of endogenous heteromeric channel complexes with adapter proteins. This could also explain the incomplete suppression of mechanically induced currents of about 65%–75% by 5-BDBD and TNP-ATP. However, using a pharmacologic approach, we could verify a key role of P_2X_4 channels for the mechanical response of podocytes. As a crucial test, $P_2X_4^{-/-}$ podocytes were analyzed; this showed a complete suppression of mechanically induced currents, clearly demonstrating the essential role of P_2X_4 channels as mechanotransducers mediating mechanically induced cation influx in podocytes.

Interestingly, two studies show that P_2X_4 channels are sensitive to shear stress in endothelial cells and in oocytes without mechanistic explanation.[51,52] However, we demonstrate for the first time that P_2X_4 channels are mechanotransducers in podocytes activated by ATP released upon mechanical stimulation. Using a fluorescence approach to monitor cell swelling induced ATP accumulation in the bath solution, we determined a concentration of about 400 nM, which should be sufficient for P_2X activation considering dilution in the bath solution and the occurrence of high local ATP concentrations near the cell membrane. Moreover, apyrase abolished stretch-induced currents and using N-ethylmaleimide (N-EM) we obtained initial evidence that ATP might be released by vesicle fusion *via* the SNARE complex. Furthermore, heterologously expressed P_2X channels were not directly mechanosensitive even in the presence of SMPs. Altogether, our findings strongly argue for an indirect mechanosensitivity of P_2X channels.

Interestingly, in our study disruption of the actin cytoskeleton did not affect mechanosensation of podocytes, in contrast to the mechanosensitive degenerin and epithelial Na^+ channel protein complex in *C. elegans*, because treatment with cytochalasin D was without effect. Instead, mechanosensation of podocytes was inhibited by stabilization of the actin cytoskeleton, possibly caused by impairment of mechanically induced ATP release. Disassembly of microtubules had no effect on ATP release. Moreover, we found cholesterol to be critically involved in mechanical responsiveness of podocytes because cholesterol depletion by fluvastatin and methyl-β-cyclodextrins completely suppressed mechanically induced P_2X_4 currents. Interestingly, cholesterol depletion only abolished mechanically but not ATP-induced P_2X_4 currents. Thus, cholesterol, which is important for exocytosis and for formation of lipid rafts in the slit diaphragm, is essential for mechanical responsiveness of podocytes probably as a regulator of ATP release. Moreover, our findings with podocin knockdown podocytes show that podocin also regulates mechanical P_2X_4 channel activation. In podocin knockdown podocytes, mechanically induced P_2X_4 currents were completely suppressed, indicating that podocin is primarily involved in an upstream mechanosensing process independent of the formation and function of TRPC6/podocin complexes in the plasma membrane.[10] Altogether, we can demonstrate that cholesterol and podocin play dominant roles for mechanical responsiveness of podocytes.

There is evidence for an ATP-induced reorganization of the cytoskeleton in macrophages and mammary tumor cells.[53,54] Beyond that, our findings demonstrate that mechanically induced P_2X_4 activation *via* ATP release plays a key role for the reorganization of the actin cytoskeleton in podocytes, indicating that mechanical P_2X_4 activation might be crucial for the pathomechanism leading to hypertension-induced podocyte damage. We found that nonstretched podocytes exhibited a 6% frequency of podocytes with ARCs; this is similar to

Numbers indicate the numbers of measured cells and of independent experiments. (I and J) Photometric determination of ATP release from podocytes during hypoosmotic stimulation by measuring ATP-dependent conversion of NADP to NADPH. *Voltage of the transimpedance amplifier from the photodiode. (I) Exemplary trace of NADPH fluorescence at 450 nm with application of hypoosmotic solution (blue bar) is displayed. (J) Subsequent calibration curve with application of increasing ATP concentrations (green bars). *$P<0.05$; **$P<0.01$; ***$P<0.001$; ns $P>0.05$.

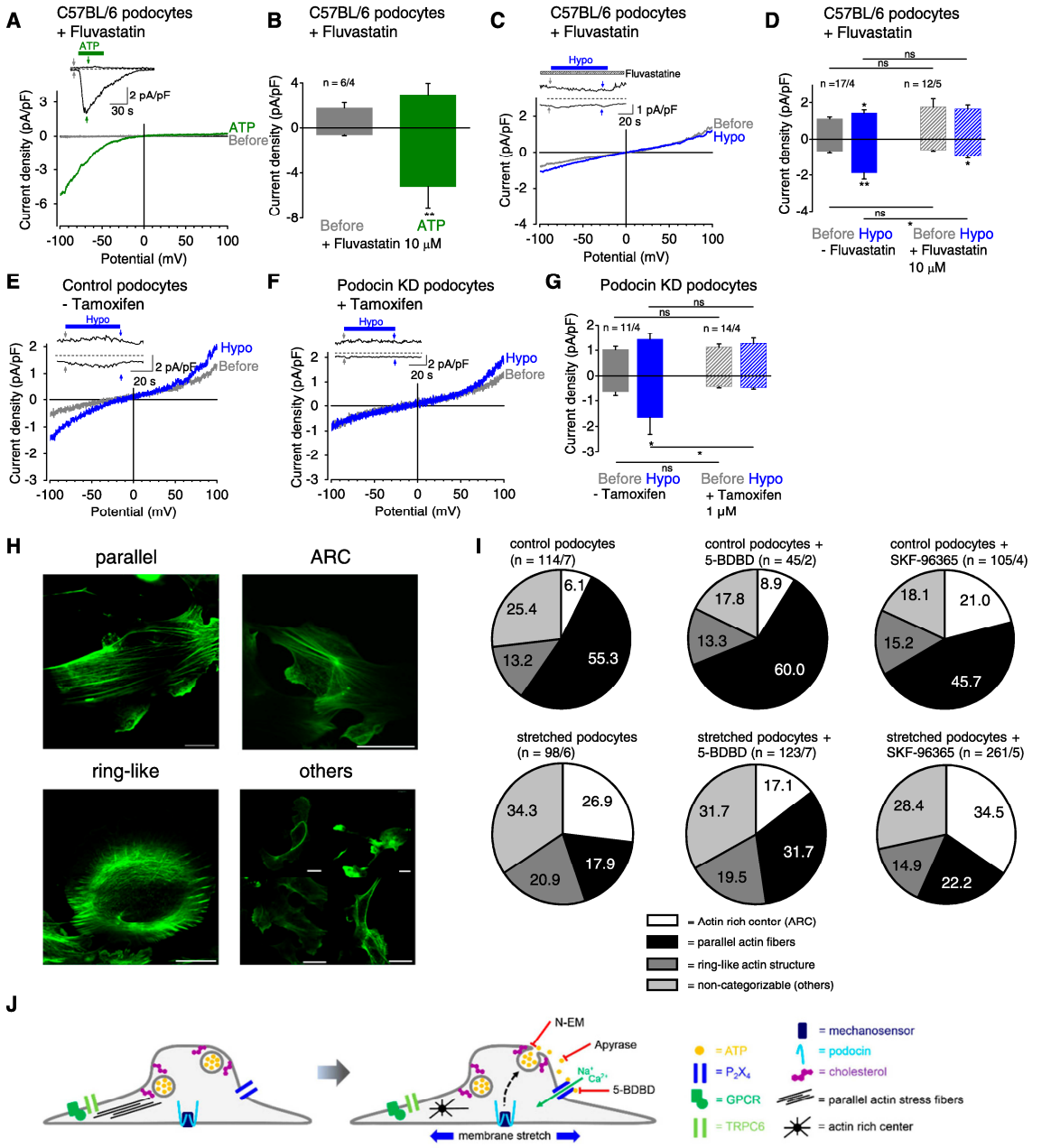

Figure 6. Mechanically induced P_2X_4 channel activation is podocin and cholesterol dependent and is crucial for reorganization of the actin cytoskeleton. (A– G) Electrophysiologic whole-cell measurements of podocytes treated with fluvastatin (A–D) and of podocin knockdown (KD) and respective control podocytes (E–G). (A and C) Exemplary CDV relationships before (gray) and during (green) application of 100 μM ATP and of hypoosmotic solution (blue) in the presence of 10 μM fluvastatin. Insets show current density time courses at $\pm$100 mV. Stippled lines represent zero current. Application of hypoosmotic solution, ATP, and fluvastatin is indicated. Arrows represent the time points of depicted CDV traces. (B and D) Summaries of current densities before (gray bar) and during (green bar) application of ATP (B) or of hypoosmotic solution (blue bar) (D) in the presence of fluvastatin at $\pm$100 mV. Numbers indicate the numbers of measured cells and of independent experiments. (E and F) Exemplary CDV relationships before (gray) and during (blue) application of hypoosmotic solution of *Nphs2*$^{flox/flox}$,*Cre*$^{+/+}$ podocytes not treated with tamoxifen (control podocytes, E) and treated

Endlich and colleagues' study,[47] which reported a frequency of about 15%. Interestingly, we observed a significant increase in podocytes with ARCs of about 27% after 2 hours compared with an increase of about 50% monitored after 24 hours, as shown by others.[47] This finding indicates that reorganization of the actin cytoskeleton is a fast process. Remarkably, cyclic membrane stretch caused significant reorganization of the actin cytoskeleton, which could be rescued by the selective P_2X_4 blocker 5-BDBD while the nonselective TRPC channel blocker SKF-96365 had no effect. Altogether, we postulate a novel role of P_2X_4 channels as mechanotransducers in podocytes regulated by podocin and cholesterol and activated by membrane stretch-induced ATP release *via* the SNARE complex, finally resulting in reorganization of the actin cytoskeleton (summarized in Figure 6H). This signaling pathway may contribute to mechanically induced podocyte injury and open up novel strategies for nephroprotection in conditions such as hypertension.

CONCISE METHODS

Mice Used in the Study

If not stated otherwise, we used wild-type mice with the BKS.Cg-Dock7m$^{+/+}$ background and with the C57BL/6 background obtained from Jackson Laboratory. $P_2X_4^{-/-}$ mice in C57BL/6 background were provided from GlaxoSmithKline and from Manfred Frick (Ulm, Germany). To induce podocin knockdown in cultured podocytes, inducible podocin knockdown (*Nphs2*$^{flox/flox}$,*Cre*$^{+/+}$) mice were used in C57BL/6 background developed in the laboratory of Corinne Antignac (Paris, France).[31,43] Trpc6$^{-/-}$ and Trpc1/3/6$^{-/-}$ mice were in C57BL/6 background. All experiments and procedures were approved by the governmental oversight authority, district government of Upper Bavaria (Germany).

Materials

We used 1-Oleoyl-2-acetyl-sn-glycerol (Calbiochem), DIDS (Invitrogen), 5-BDBD (Tocris), Suramin (Tocris), TNP-ATP (Tocris), Normacin (Invivogen), and YM-254890 (Taiho Pharmaceutical). Unless otherwise stated, all other materials were obtained from Sigma-Aldrich.

Electrophysiologic Whole-Cell Recordings

Conventional whole-cell patch-clamp recordings were performed to analyze isolated podocytes and HEK293 cells transfected with cDNA coding for TRPC6 (NM_004621), nephrin (AAF91087.1), podocin (NM_130456.3) and CD2-associated protein (CD2AP, NM_009847.3) and P_2X_4 (AF089751) using Genejuice (EMD Millipore) reagent. All measurements were carried out at room temperature. Bath solutions contained (in mM): 110 NaCl, 0.1 $CaCl_2$, 1 $MgCl_2$, 10 HEPES (adjusted to pH 7.40 with NaOH), and 10 glucose supplemented with mannitol to 300 mOsm/kg. Hypoosmotic solution contained no mannitol, which resulted in an osmolality of 240 mOsm/kg. For podocyte measurements, all bath solutions additionally contained 100 μM NPPB and 300 μM DIDS to block chloride channels. Patch pipettes were made of borosilicate glass (Science Products, Hofheim, Germany) and had resistances of 1.9–3.6 MΩ when filled with the standard intracellular solution containing (in mM): 9.4 NaCl, 120 CsCl, 3.949 $CaCl_2$, 0.2 Na_3-GTP, 10 HEPES (pH 7.2 with CsOH), and 10 BAPTA, resulting in 100 nM free Ca^{2+}. The liquid junction potential was 4.0 mV and corrected by the PatchMaster software. Data were collected with an EPC10 patch-clamp amplifier (HEKA, Lambrecht, Germany) using PatchMaster v2×52 software. Current voltage relationships were obtained from voltage ramps from −100 to 100 mV with a slope of 0.5 V/s at a frequency of 2 Hz. Data were acquired at a frequency of 5 kHz after filtering at 1.67 kHz. Measurements with basal inward current densities at −100 mV higher than −2.00 pA/pF for wild-type podocytes and −1.55 pA/pF for C57BL/6 podocytes were regarded as leak currents and were not further analyzed.

Podocytes Used in the Study

Primary podocytes were isolated from the kidneys of 3- to 4-week-old mice using a conventional sieving approach[55,56] with some modifications. Kidneys were mechanically disrupted in 200 ml Ham's F12 medium containing 10% fetal calf serum (FCS, Invitrogen), 100 U/ml penicillin, 100 mg/ml streptomycin, and 2 mM glutamine using a set of steel sieves with a pore size of 100, 75, 50, and 36 μm (Retsch, Haan, Germany) coated by Ham's F12 medium containing 50% FCS (Invitrogen) at room temperature. Freshly isolated cells from the final fraction were centrifuged for 5 minutes at 200 *g* and cultured in Ham's

with 1 μM tamoxifen to induce podocin knockdown (podocin KD podocytes, F). Insets show current density time courses at ±100 mV. Stippled lines represent zero current. Application of hypoosmotic solution is indicated. Arrows represent the time points of depicted CDV traces. (G) Summary of current densities before (gray and gray hatched bars) and during (blue and blue hatched bars) application of hypoosmotic solution at ±100 mV. Numbers indicate the numbers of measured cells and of independent experiments. (H) Exemplary fluorescence pictures of actin fiber distribution of podocytes after subjection to radial tensile strain for 2 hours representing four categories: parallel stress fibers "parallel," presence of ARCs, ring-like actin structure, and nondefinable actin structure ("others"). Actin fibers were stained with Alexa Fluor-488 phalloidin. Scale bar is 20 μm. (I) Frequency distribution of the four categories of stretched and nonstretched podocytes in the presence and absence of 10 μM 5-BDBD and of 10 μM SKF-96365. Numbers indicate percentage. Numbers in parentheses show numbers of podocytes and numbers of independent experiments. (J) Schematic model of mechanically induced P_2X_4 activation in podocytes. TRPC6 and GPCRs do not appear to be involved in the induction of ionic currents by mechanical membrane stretch. Podocin may participate in the function of a hitherto unidentified mechanosensor. Mechanical membrane stretch causes cholesterol-dependent ATP release by vesicle fusion *via* the SNARE complex. ATP subsequently activates P_2X_4 channels, resulting in disorganization of the actin cytoskeleton, which might contribute to the pathomechanism leading to hypertension-induced podocyte injury. Pharmacologic interventions with N-EM, which prevents vesicle fusion, with apyrase causing ATP degradation and of the selective P_2X_4 channel blocker 5-BDBD, are displayed. *P<0.05; **P<0.01; ns P>0.05.

F12 medium supplemented with 10% FCS, 2 mM glutamine, 100 U/ml penicillin, 100 μg/ml streptomycin, 100 μg/ml normocin, 5 μg/ml transferrin, 5 ng/ml natriumselenite, 100 nM hydrocortisone, and 5 μg/ml recombinant human insulin (Sigma-Aldrich, Taufkirchen, Germany) in a humidified atmosphere with 5% CO_2. Enrichment of podocytes was >95% as assessed by cell morphology, staining with an antipodocin antibody (Sigma-Aldrich) and by expression of nephrin, synapotopodin, and Wilms tumor protein (WT1), which is described in detail elsewhere.[57] Cell membrane capacity was used as another selection criterion for podocytes. Cell membrane capacity was estimated to be 71.2±2.3 pF (n=362) for primary podocytes; thus, there was no significant difference to conditionally immortalized murine podocytes, which had cell membrane capacities of 63.4±3.3 pF (n=52). Primary podocytes were analyzed after the first cell passage approximately 10 days after isolation. Conditionally immortalized murine podocytes were cultured as described in detail elsewhere.[19]

Determination of Intracellular Calcium Concentrations

Intracellular free calcium concentration was determined in isolated podocytes using 5 μM fura-2 acetoxymethyl ester (Sigma-Aldrich) as described in detail elsewhere.[58] In brief, cells were mounted on the stage of a monochromator-equipped (Polychrome V; TILL-Photonics, Martinsried, Germany) inverted microscope (Olympus IX 71 with an UPlanSApo 20×/0.85 oil immersion objective). Fluorescence was recorded with a 14-bit EMCCD camera (iXON 885; Andor, Belfast, UK). Fura-2 fluorescence was excited at 340 and 380 nm. Intracellular free calcium concentrations were calculated as described previously.[59] During imaging, cells were continuously superfused at room temperature with an isotonic bath solution containing (in mM) the following: 55 NaCl, 5 KCl, 2 $CaCl_2$, 1 $MgCl_2$, 10 HEPES (pH 7.40), and 10 glucose, supplemented with mannitol to 300 mOsm/kg. The hypoosmotic bath solution had the same salt concentration without added mannitol, resulting in an osmolality of 149–152 mOsm/kg.

Quantitative RT-PCR Analysis

Total RNA was isolated using the Tri Reagent (Sigma-Aldrich, Munich, Germany). First-strand synthesis was carried out with random hexamer primers, using REVERTAID reverse transcription (Fermentas, Sankt Leon-Roth, Germany). For detailed information and primers, see the Supplemental Material. The Wilcoxon rank-sum test was used for analysis of mRNA expression levels. All experiments were performed in quadruplets, and experiments were repeated at least three times.

Determination of Extracellular ATP Concentrations Using NADP Conversion

To measure ATP release from podocytes, photometry was performed by turning to account ATP-dependent conversion of NADP to NADPH in the presence of the enzymes hexokinase and glucose-6-phosphate dehydrogenase and of the substrates glucose and NADP, which resulted in an increased fluorescence emission at 450 nm. Quantification of ATP was essentially done as previously described.[60] Podocytes were seeded onto a glass coverslip 24 hours before analysis. For analysis of ATP, cells were superfused with (*1*) isotonic bath solution (in mM: 110 NaCl, 0.1 $CaCl_2$, 1 $MgCl_2$, 10 HEPES [pH 7.40], and 10 glucose supplemented with mannitol to 300 mOsm/kg) additionally containing 2 mM NADP, 2 U/ml hexokinase, and 2 U/ml glucose-6-phosphate-dehydrogenase or (*2*) hypoosmotic solution without the supplementation of mannitol, resulting in about 240 mOsm/kg. NAPDH was excited with Polychrome V (TillPhotonics) at 340 nm, and emission was measured as voltage of the transimpedance amplifier from the photodiode at 450 nm. Data were collected by EPC10 amplifier (HEKA Lambrecht, Germany) with the Patchmaster software (HEKA). Hypoosmotic solution was applied, resulting in fluorescence increases, which were quantified by subsequently measuring different increasing ATP concentrations in isotonic bath solution for calibration.

Mechanical Membrane Stretch Using FlexCell Tension System

Cyclic radial tensile strains were applied to podocytes using the Flexcell Tension System (FX-5000T; Flexcell International Corp.). A total of 200,000 podocytes were seeded onto collagene-coated silicon membranes (BioFlex Culture Plate; Flexcell International Corp.) 24 hours before cells were subjected to cyclic 10% radial tensile strain with a frequency of 0.5 Hz for 2 hours. Thereafter, cells were fixated with 4% paraformaldehyde for 30 minutes at 4°C. Actin was labeled by 20-minute incubation of cells with Alexa Fluor 488–tagged phalloidin (Invitrogen). Subsequently, fluorescence pictures were taken using confocal microscopy with a Leica TCS SP5 using an HCX PL APO CS 63.0×/1.40 ultraviolet oil immersion objective. Probes were excited with 488 nm while emission was measured at 515±10 nm. Reorganization of the cytoskeleton was quantified using the chi-squared test for analysis of sample distribution.

Statistical Analyses

Data are presented as mean±SEM. Unless stated otherwise, data were compared by a paired or unpaired t test if a Gaussian distribution was confirmed by applying a Shapiro-Wilk (normality) test. Calcium measurements were analyzed using the one-way ANOVA with Bonferroni *post hoc* means comparison. Significance was accepted at $P<0.05$. For statistical analysis the software Origin 7.5 and 8.0 (OriginLab Corporation, Northampton, MA) was used. Chi-squared analysis was done with Excel 2013 (Microsoft Corporation, Redmond, WA).

ACKNOWLEDGMENTS

We thank Joanna Zaißerer and Laura Danner for excellent technical assistance. We are grateful to GlaxoSmithKline and Manfred Frick (Ulm, Germany) for providing $P_2X_4^{-/-}$ mice, Lutz Birnbaumer for providing $Trpc3^{-/-}$ mice, and for critically reading the manuscript, Maike Fahlbusch and Jana Demleitner for providing $Trpc6^{-/-}$ podocytes, and Natsuko Kayakiri (Taiho Pharmaceutical) for providing YM-254890. This study was supported by Deutsche Forschungsgemeinschaft SFB/TRR152.

DISCLOSURES

J.R. is cofounder and president of TRISAQ, a biopharmaceutical company aimed at developing kidney protective therapeutics. He stands to gain royalties from issued and pending patents relevant to treating kidney disease. None of the other authors report any conflict of interests.

REFERENCES

1. Huber TB, Benzing T: The slit diaphragm: A signaling platform to regulate podocyte function. *Curr Opin Nephrol Hypertens* 14: 211–216, 2005
2. Huber TB, Schermer B, Benzing T: Podocin organizes ion channel-lipid supercomplexes: Implications for mechanosensation at the slit diaphragm. *Nephron, Exp Nephrol* 106: e27–e31, 2007
3. Endlich N, Endlich K: The challenge and response of podocytes to glomerular hypertension. *Semin Nephrol* 32: 327–341, 2012
4. Kreisberg JI, Karnovsky MJ: Focal glomerular sclerosis in the fawn-hooded rat. *Am J Pathol* 92: 637–652, 1978
5. Kretzler M, Koeppen-Hagemann I, Kriz W: Podocyte damage is a critical step in the development of glomerulosclerosis in the uninephrectomised-desoxycorticosterone hypertensive rat. *Virchows Archiv* 425: 181–193, 1994
6. Kriz W, Hosser H, Hähnel B, Simons JL, Provoost AP: Development of vascular pole-associated glomerulosclerosis in the Fawn-hooded rat. *J Am Soc Nephrol* 9: 381–396, 1998
7. Bidani AK, Griffin KA: Long-term renal consequences of hypertension for normal and diseased kidneys. *Curr Opin Nephrol Hypertens* 11: 73–80, 2002
8. Reiser J, Polu KR, Möller CC, Kenlan P, Altintas MM, Wei C, Faul C, Herbert S, Villegas I, Avila-Casado C, McGee M, Sugimoto H, Brown D, Kalluri R, Mundel P, Smith PL, Clapham DE, Pollak MR: TRPC6 is a glomerular slit diaphragm-associated channel required for normal renal function. *Nat Genet* 37: 739–744, 2005
9. Winn MP, Conlon PJ, Lynn KL, Farrington MK, Creazzo T, Hawkins AF, Daskalakis N, Kwan SY, Ebersviller S, Burchette JL, Pericak-Vance MA, Howell DN, Vance JM, Rosenberg PB: A mutation in the TRPC6 cation channel causes familial focal segmental glomerulosclerosis. *Science* 308: 1801–1804, 2005
10. Huber TB, Schermer B, Müller RU, Höhne M, Bartram M, Calixto A, Hagmann H, Reinhardt C, Koos F, Kunzelmann K, Shirokova E, Krautwurst D, Harteneck C, Simons M, Pavenstädt H, Kerjaschki D, Thiele C, Walz G, Chalfie M, Benzing T: Podocin and MEC-2 bind cholesterol to regulate the activity of associated ion channels. *Proc Natl Acad Sci U S A* 103: 17079–17086, 2006
11. El Hindi S, Reiser J: TRPC channel modulation in podocytes-inching toward novel treatments for glomerular disease. *Pediatr Nephrol* 26: 1057–1064, 2011
12. Gottlieb P, Folgering J, Maroto R, Raso A, Wood TG, Kurosky A, Bowman C, Bichet D, Patel A, Sachs F, Martinac B, Hamill OP, Honore E: Revisiting TRPC1 and TRPC6 mechanosensitivity. *Pflugers Archiv* 455: 1097–1103, 2008
13. Mederos y Schnitzler M, Storch U, Meibers S, Nurwakagari P, Breit A, Essin K, Gollasch M, Gudermann T: Gq-coupled receptors as mechanosensors mediating myogenic vasoconstriction. *EMBO J* 27: 3092–3103, 2008
14. Sharif-Naeini R, Folgering JH, Bichet D, Duprat F, Delmas P, Patel A, Honoré E: Sensing pressure in the cardiovascular system: Gq-coupled mechanoreceptors and TRP channels. *J Mol Cell Cardiol* 48: 83–89, 2010
15. Blodow S, Schneider H, Storch U, Wizemann R, Forst AL, Gudermann T, Mederos y Schnitzler M: Novel role of mechanosensitive AT1B receptors in myogenic vasoconstriction. *Pflugers Archiv* 466: 1343–1353, 2014
16. Storch U, Mederos y Schnitzler M, Gudermann T: G protein-mediated stretch reception. *Am J Physiol Heart Circ Physiol* 302: H1241–H1249, 2012
17. Mederos y Schnitzler M, Storch U, Gudermann T: AT1 receptors as mechanosensors. *Curr Opin Pharmacol* 11: 112–116, 2011
18. Mennuni S, Rubattu S, Pierelli G, Tocci G, Fofi C, Volpe M: Hypertension and kidneys: Unraveling complex molecular mechanisms underlying hypertensive renal damage. *J Hum Hypertens* 28: 74–79, 2014
19. Mundel P, Reiser J, Zúñiga Mejía Borja A, Pavenstädt H, Davidson GR, Kriz W, Zeller R: Rearrangements of the cytoskeleton and cell contacts induce process formation during differentiation of conditionally immortalized mouse podocyte cell lines. *Exp Cell Res* 236: 248–258, 1997
20. Dietrich A, Mederos Y Schnitzler M, Gollasch M, Gross V, Storch U, Dubrovska G, Obst M, Yildirim E, Salanova B, Kalwa H, Essin K, Pinkenburg O, Luft FC, Gudermann T, Birnbaumer L: Increased vascular smooth muscle contractility in TRPC6-/- mice. *Mol Cell Biol* 25: 6980–6989, 2005
21. Zou Y, Akazawa H, Qin Y, Sano M, Takano H, Minamino T, Makita N, Iwanaga K, Zhu W, Kudoh S, Toko H, Tamura K, Kihara M, Nagai T, Fukamizu A, Umemura S, Iiri T, Fujita T, Komuro I: Mechanical stress activates angiotensin II type 1 receptor without the involvement of angiotensin II. *Nat Cell Biol* 6: 499–506, 2004
22. Hoffmann S, Podlich D, Hähnel B, Kriz W, Gretz N: Angiotensin II type 1 receptor overexpression in podocytes induces glomerulosclerosis in transgenic rats. *J Am Soc Nephrol* 15: 1475–1487, 2004
23. Delles C, Jacobi J, John S, Fleischmann I, Schmieder RE: Effects of enalapril and eprosartan on the renal vascular nitric oxide system in human essential hypertension. *Kidney Int* 61: 1462–1468, 2002
24. Ziai F, Ots M, Provoost AP, Troy JL, Rennke HG, Brenner BM, Mackenzie HS: The angiotensin receptor antagonist, irbesartan, reduces renal injury in experimental chronic renal failure. *Kidney Int Suppl* 57: S132–S136, 1996
25. Takasaki J, Saito T, Taniguchi M, Kawasaki T, Moritani Y, Hayashi K, Kobori M: A novel Galphaq/11-selective inhibitor. *J Biol Chem* 279: 47438–47445, 2004
26. Coddou C, Yan Z, Obsil T, Huidobro-Toro JP, Stojilkovic SS: Activation and regulation of purinergic P2X receptor channels. *Pharmacol Rev* 63: 641–683, 2011
27. North RA: Molecular physiology of P2X receptors. *Physiol Rev* 82: 1013–1067, 2002
28. North RA, Surprenant A: Pharmacology of cloned P2X receptors. *Annu Rev Pharmacol Toxicol* 40: 563–580, 2000
29. Chung WC, Kermode JC: Suramin disrupts receptor-G protein coupling by blocking association of G protein alpha and betagamma subunits. *J Pharmacol Exp Ther* 313: 191–198, 2005
30. Balazs B, Danko T, Kovacs G, Koles L, Hediger MA, Zsembery A: Investigation of the inhibitory effects of the benzodiazepine derivative, 5-BDBD on P2X4 purinergic receptors by two complementary methods. *Cell Physiol Biochem* 32: 11–24, 2013
31. Mollet G, Ratelade J, Boyer O, Muda AO, Morisset L, Lavin TA, Kitzis D, Dallman MJ, Bugeon L, Hubner N, Gubler MC, Antignac C, Esquivel EL: Podocin inactivation in mature kidneys causes focal segmental glomerulosclerosis and nephrotic syndrome. *J Am Soc Nephrol* 20: 2181–2189, 2009
32. Bernstein BW, Bamburg JR: Actin-ATP hydrolysis is a major energy drain for neurons. *J Neurosci* 23: 1–6, 2003
33. Ng YK, Lu X, Levitan ES: Physical mobilization of secretory vesicles facilitates neuropeptide release by nerve growth factor-differentiated PC12 cells. *J Physiol* 542: 395–402, 2002
34. Wang J, Richards DA: Spatial regulation of exocytic site and vesicle mobilization by the actin cytoskeleton. *PLoS ONE* 6: e29162, 2011
35. Bubb MR, Spector I, Beyer BB, Fosen KM: Effects of jasplakinolide on the kinetics of actin polymerization. An explanation for certain in vivo observations. *J Biol Chem* 275: 5163–5170, 2000
36. Ou GS, Chen ZL, Yuan M: Jasplakinolide reversibly disrupts actin filaments in suspension-cultured tobacco BY-2 cells. *Protoplasma* 219: 168–175, 2002
37. Coward RJ, Welsh GI, Koziell A, Hussain S, Lennon R, Ni L, Tavaré JM, Mathieson PW, Saleem MA: Nephrin is critical for the action of insulin on human glomerular podocytes. *Diabetes* 56: 1127–1135, 2007
38. Lang T: SNARE proteins and 'membrane rafts'. *J Physiol* 585: 693–698, 2007
39. Orci L, Singh A, Amherdt M, Brown D, Perrelet A: Microheterogeneity of protein and sterol content in kidney podocyte membrane. *Nature* 293: 646–647, 1981

40. Fornoni A, Merscher S, Kopp JB: Lipid biology of the podocyte—new perspectives offer new opportunities. *Nat Rev Nephrol* 10: 379–388, 2014
41. Li J, Fountain SJ: Fluvastatin suppresses native and recombinant human P2X4 receptor function. *Purinergic Signal* 8: 311–316, 2012
42. Schermer B, Benzing T: Lipid-protein interactions along the slit diaphragm of podocytes. *J Am Soc Nephrol* 20: 473–478, 2009
43. Bugeon L, Danou A, Carpentier D, Langridge P, Syed N, Dallman MJ: Inducible gene silencing in podocytes: A new tool for studying glomerular function. *J Am Soc Nephrol* 14: 786–791, 2003
44. Faul C, Asanuma K, Yanagida-Asanuma E, Kim K, Mundel P: Actin up: regulation of podocyte structure and function by components of the actin cytoskeleton. *Trends Cell Biol* 17: 428–437, 2007
45. Mathieson PW: Podocyte actin in health, disease and treatment. *Nephrol Dial Transplant* 25: 1772–1773, 2010
46. Endlich N, Endlich K: Stretch, tension and adhesion—adaptive mechanisms of the actin cytoskeleton in podocytes. *Eur J Cell Biol* 85: 229–234, 2006
47. Endlich N, Kress KR, Reiser J, Uttenweiler D, Kriz W, Mundel P, Endlich K: Podocytes respond to mechanical stress in vitro. *J Am Soc Nephrol* 12: 413–422, 2001
48. Machuca E, Benoit G, Antignac C: Genetics of nephrotic syndrome: Connecting molecular genetics to podocyte physiology. *Hum Mol Genet* 18[R2]: R185–R194, 2009
49. Wilson C, Dryer SE: A mutation in TRPC6 channels abolishes their activation by hypoosmotic stretch but does not affect activation by diacylglycerol or G protein signaling cascades. *Am J Physiol Renal Physiol* 306: F1018–F1025, 2014
50. Roshanravan H, Dryer SE: ATP acting through P2Y receptors causes activation of podocyte TRPC6 channels: Role of podocin and reactive oxygen species. *Am J Physiol Renal Physiol* 306: F1088–F1097, 2014
51. Kessler S, Clauss WG, Fronius M: Laminar shear stress modulates the activity of heterologously expressed P2X(4) receptors. *Biochim Biophys Acta* 1808: 2488–2495, 2011
52. Yamamoto K, Korenaga R, Kamiya A, Ando J: Fluid shear stress activates Ca(2+) influx into human endothelial cells via P2X4 purinoceptors. *Circ Res* 87: 385–391, 2000
53. Pfeiffer ZA, Aga M, Prabhu U, Watters JJ, Hall DJ, Bertics PJ: The nucleotide receptor P2X7 mediates actin reorganization and membrane blebbing in RAW 264.7 macrophages via p38 MAP kinase and Rho. *J Leukoc Biol* 75: 1173–1182, 2004
54. Pubill D, Dayanithi G, Siatka C, Andrés M, Dufour MN, Guillon G, Mendre C: ATP induces intracellular calcium increases and actin cytoskeleton disaggregation via P2x receptors. *Cell Calcium* 29: 299–309, 2001
55. Mundel P, Reiser J, Kriz W: Induction of differentiation in cultured rat and human podocytes. *J Am Soc Nephrol* 8: 697–705, 1997
56. Schlondorff D: Preparation and study of isolated glomeruli. *Methods Enzymol* 191: 130–140, 1990
57. Kalwa H, Storch U, Demleitner J, Fiedler S, Mayer T, Kannler M, Fahlbusch M, Barth H, Smrcka A, Hildebrandt F, Gudermann T, Dietrich A: Phospholipase C epsilon (PLCε) induced TRPC6 activation: a common but redundant mechanism in primary podocytes. *J Cell Physiol* 230: 1389–1399, 2015
58. Storch U, Forst AL, Philipp M, Gudermann T, Mederos y Schnitzler M: Transient receptor potential channel 1 (TRPC1) reduces calcium permeability in heteromeric channel complexes. *J Biol Chem* 287: 3530–3540, 2012
59. Grynkiewicz G, Poenie M, Tsien RY: A new generation of Ca2+ indicators with greatly improved fluorescence properties. *J Biol Chem* 260: 3440–3450, 1985
60. Corriden R, Insel PA, Junger WG: A novel method using fluorescence microscopy for real-time assessment of ATP release from individual cells. *Am J Physiol Cell Physiol* 293: C1420–C1425, 2007

This article contains supplemental material online at http://jasn.asnjournals.org/lookup/suppl/doi:10.1681/ASN.2014111144/-/DCSupplemental.

Supplemental Figure 1

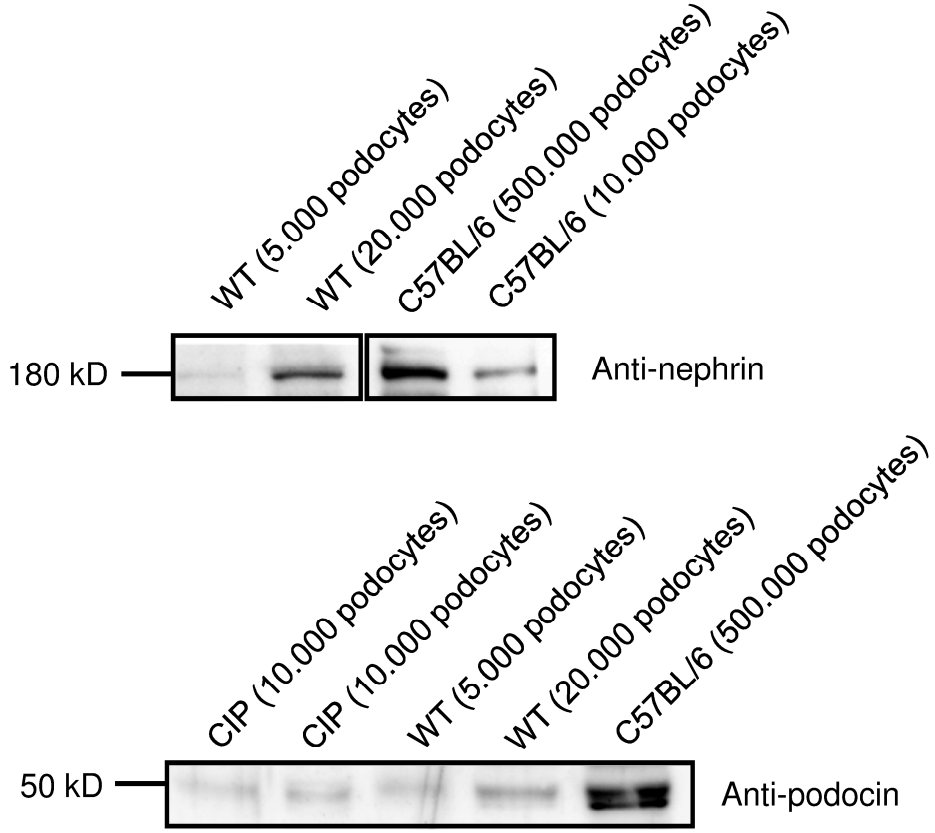

Supplemental Figure 1: Nephrin and podocin are expressed in podocytes on the protein level. Western blot analysis of isolated primary WT and C57BL/6 podocytes and of conditionally immortalized podocytes (CIPs) using guinea-pig anti-nephrin antibodies and rabbit anti-podocin antibodies. Numbers in a parentheses indicate approximate numbers of isolated cells.

Supplemental Figure 2

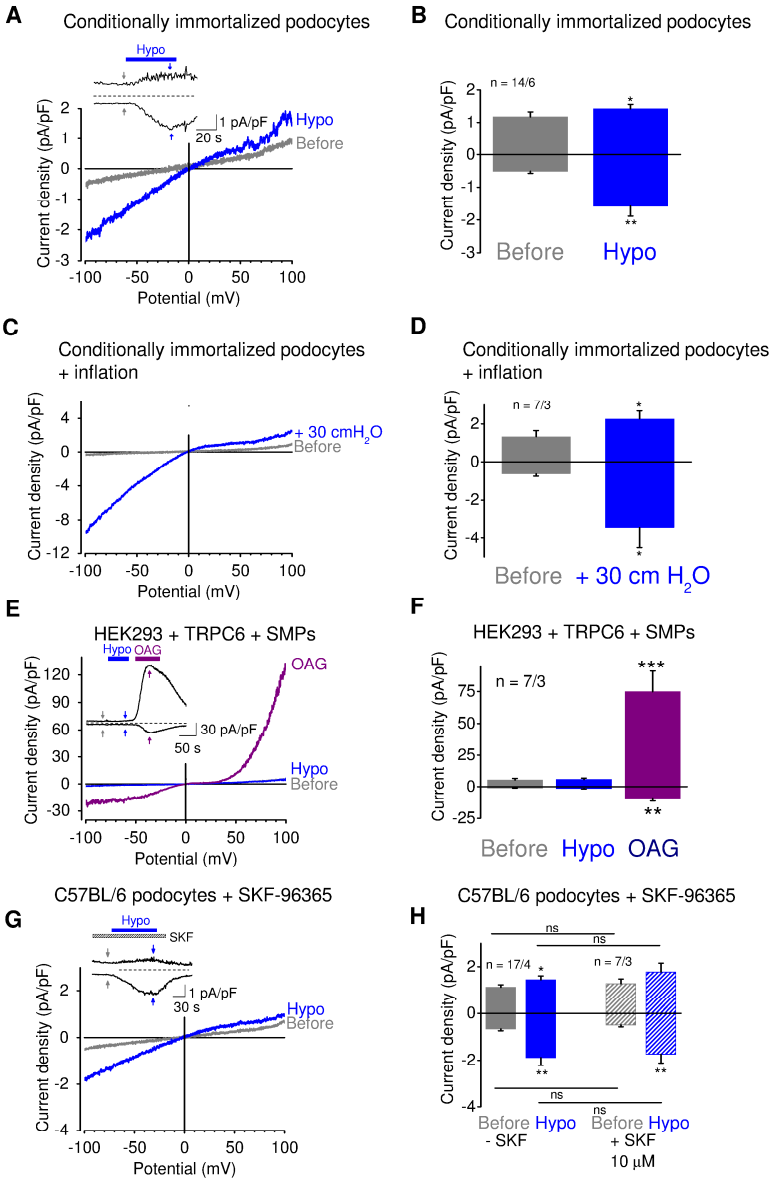

Supplemental Figure 2: Conditionally immortalized podocytes are mechanosensitive and TRPC channels are not mechanotransducing elements in podocytes. (A-D, G and H) Electrophysiological whole-cell measurements of conditionally immortalized murine podocytes (A-D) and of C57BL/6 podocytes in the presence of SKF-96365 (G and H) Exemplary CDV relationships before (grey) and during application of hypoosmotic bath solution (blue) (A, G) and of positive pipette pressure (G). Insets show current density time courses at ±100 mV. Stippled line represents zero current. Bars indicate presence of hypoosmotic solution and of SKF-96365 (hatched bar). Arrows represent the time points of depicted CDV traces. (B, D, H) Summary of current densities before (gray and gray hatched bars) and during application of hypoosmotic bath solution (blue and blue hatched bars) (B, H) or positive pipette pressure (D) in the absence (solid bars) and presence of SKF-96365 (hatched bars) at ±100 mV. Numbers display the number of measured cells and of independent experiments. (E and F) Whole-cell measurements of HEK293 cells over-expressing human TRPC6 and the slit membrane proteins (SMPs) podocin, nephrin and CD2AP with exemplary CDV relationships in the before (grey) and during (blue) hypoosmotic bath solution “Hypo” and in the presence of 100 µM OAG (violet). Insets show current density time courses at ±100 mV. Stippled line represents zero current. Bars indicate application of hypoosmotic solution and of OAG. Arrows represent the time points of depicted CDV traces. (F) Summary of current densities before (gray bars) and during application of hypoosmotic bath solution (blue bar) and of OAG (violet bar) at ±100 mV. Numbers display the number of measured cells and of independent experiments.

Supplemental Figure 3

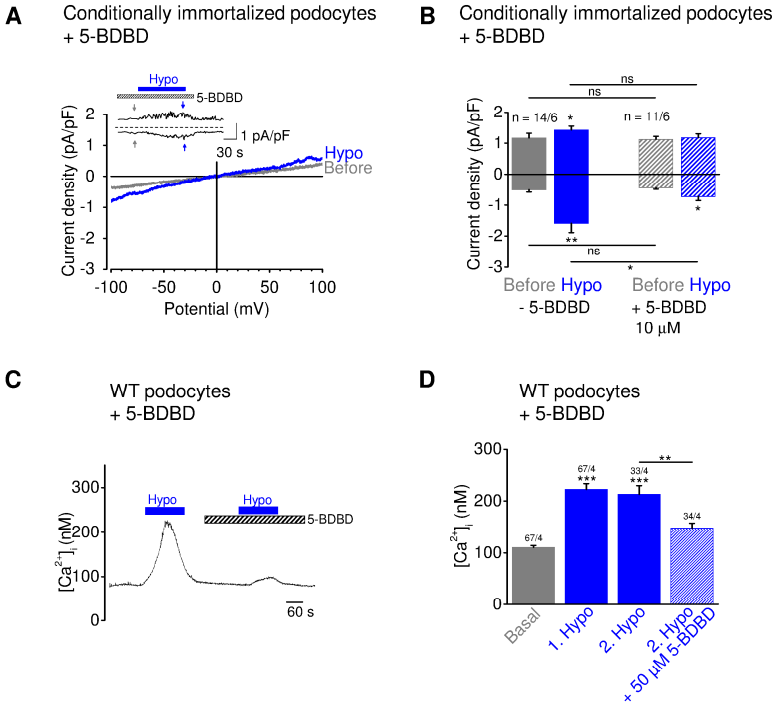

Supplemental Figure 3: P_2X_4 channel blocker 5-BDBD suppresses cell swelling induced calcium increases. (A and B) Electrophysiological whole-cell measurements of conditionally immortalized murine podocytes. (A) Exemplary current density voltage (CDV) relationships before (grey) and during application of hypoosmotic bath solution "Hypo" (blue) in the presence of 10 µM 5-BDBD. Insets show current density time courses at ±100 mV. Stippled line represents zero current. Bars indicate application of hypoosmotic solution and of 5-BDBD (hatched bar). Arrows represent the time points of depicted CDV traces. (B) Summary of current densities before (gray and gray hatched bars) and during application of hypoosmotic bath solution (blue and blue hatched bars) of podocytes in the absence (solid bars) or presence of 5-BDBD (hatched bars) at ±100 mV. Numbers display the number of measured cells and of independent experiments. (C) Representative intracellular calcium concentration trace of fura-2 loaded podocytes repeatedly stimulated with hypoosmotic solution in the presence of absence of 5-BDBD. Applications of hypoosmotic solution (blue bars) and of 5-BDBD (striped bar) are indicated. (D) Summary of calcium concentrations before (gray bar) and during the first application of hypoosmotic solution (blue bar "1. Hypo") and during the second application of hypoosmotic solution "2. Hypo" in the presence (blue striped bar) or absence (blue bar) of 5-BDBD.

Supplemental Figure 4

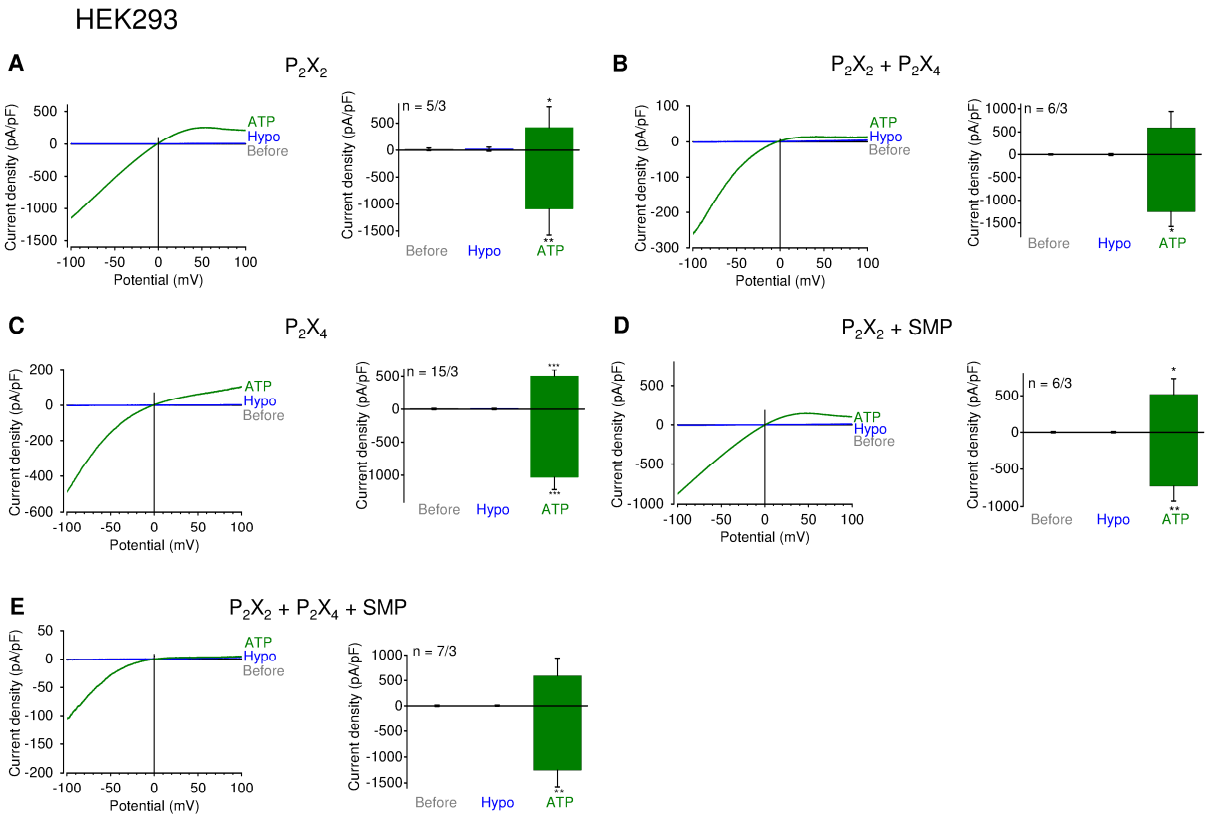

Supplemental Figure 4: Over-expressed P_2X channels are not mechanosensitive. (A-E, left panels) Representative current density voltage relationships of whole-cell recordings of HEK293T cell transiently over-expressing P_2X_2 (A), P_2X_2 and P_2X_4 (B), P_2X_4 (C), P_2X_2 and the slit membrane proteins (SMP) podocin, nephrin and CD2AP (D) or P_2X_2, P_2X_4 and SMP (E) before and during application of hypoosmotic solution and during application of 100 µM ATP (green). (A-E, right panels) Summary of current densities before (gray bars), during the application of hypoosmotic solution (blue bars) and during application of ATP (green bars). Numbers indicate the number of measured cells and of independent experiments.

Supplemental Figure 5

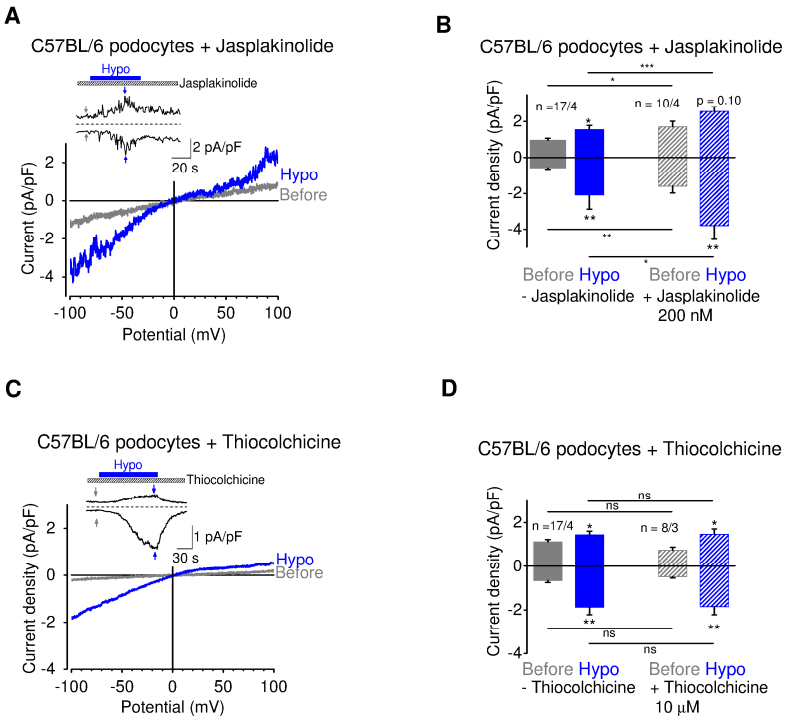

Supplemental Figure 5: Influence of the cytoskeleton on mechanosensation of podocytes (A, C) Representative current density voltage (CDV) relationships of whole-cell recordings of C57BL/6 podocytes treated with 200 nM jasplakinolide (A) or with 10 µM thiochochicine (C) before (gray) and during application of hypoosmotic solution (blue). Insets show current density time courses at ±100 mV. Stippled line represents zero current. Bars indicate application of hypoosmotic solution. Arrows represent the time points of depicted CDV traces. (B, D) Summary of current densities before (gray and gray hatched bars), during the application of hypoosmotic solution (blue and blue hatched bars) of control cells (solid bars) and of podocytes treated with jasplakinolide (B) and with thiocholcicine (D) (hatched bars). Numbers indicate the number of measured cells and of independent experiments.

Supplemental Figure 6

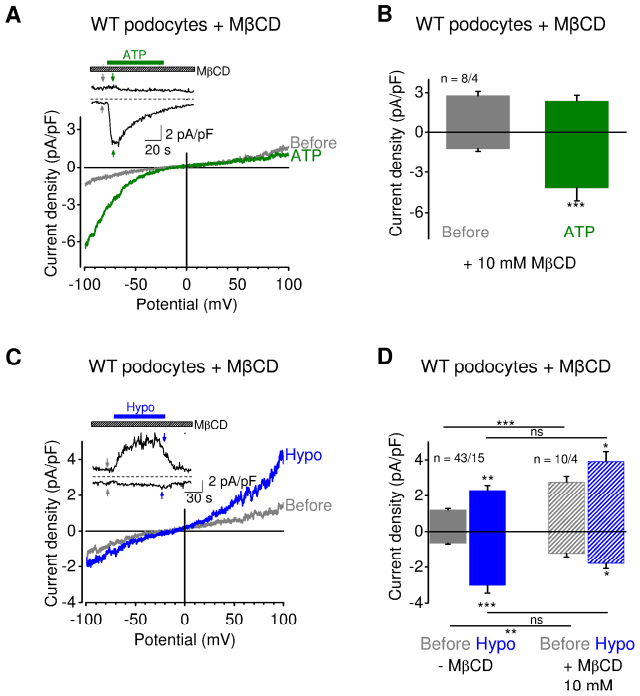

Supplemental Figure 6: Cholesterol depletion abolishes mechanically induced inwardly rectifying cation currents in podocytes. (A-D) Electrophysiological whole-cell measurements of podocytes treated with 10 mM methyl-β-cyclodextrine (MβCD). (A and C) Exemplary current density voltage (CDV) relationships before (grey) and during application of 100 µM ATP (A) (green) and of hypoosmotic solution (blue) (C) in the presence of 10 mM MβCD. Insets show current density time courses at ±100 mV. Stippled lines represent zero current. Application of hypoosmotic solution, of ATP and of MβCD is indicated. Arrows represent the time points of depicted CDV traces. (B and D) Summaries of current densities before (grey and gray hatched bars) and during application of ATP (green bar) (B) or of hypoosmotic solution (blue and blue hatched bars) (D) in the absence (solid bars) and presence of MβCD (hatched bars) at ±100 mV. Numbers indicate the numbers of measured cells and of independent experiments.

Supplemental Figure 7

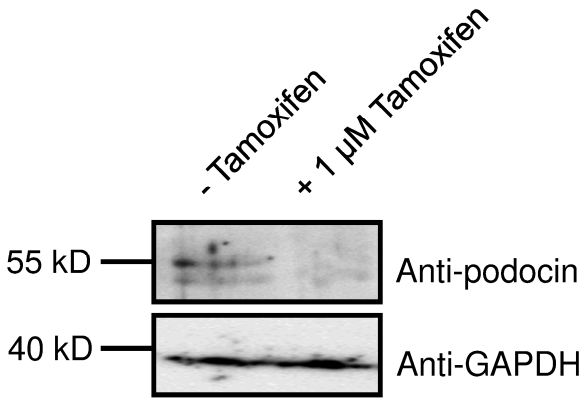

Supplemental Figure 7: Tamoxifen induced podocin down-regulation in podocytes from *Nphs2*$^{flox/flox}$,*Cre*$^{+/+}$ mice. Exemplary western blot showing expression of podocin in podocytes isolated from *Nphs2*$^{flox/flox}$,*Cre*$^{+/+}$ mice treated with 1 µM tamoxifen and untreated control podocytes. Probe was isolated from approximately 2000 primary podocytes.

Supplemental Figure 8

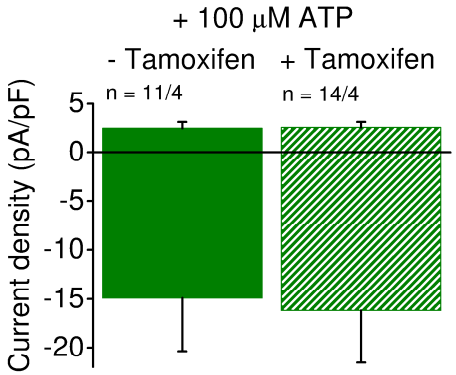

Supplemental Figure 8: ATP-induced currents are similar in podocin knock-down and control podocytes. Summary of ATP-induced current density increases at ±100 mV in podocin knock-down (green hatched bar) and control podocytes (green bar). Numbers indicate the numbers of measured cells and of independent measurements.

Supplemental Material and Methods

Quantitative Real-time Polymerase Chain Reaction (qPCR) analysis

Total RNA from primary mouse podocytes was isolated using the Trizol Reagent (Qiagen). First-strand synthesis was carried out with random hexamers as primers using REVERTAID reverse transcriptase (Fermentas, Sankt Leon-Roth, Germany). The following primers pairs were used for the amplification of specific fragments from the first-strand synthesis: TRPC1, C1for (GATGTGTCTTTGCCAAGC), C1rev (CTGGACTGGCCAGACATCTAT); TRPC2, C2for (ACTTCACTACATATGATCTGGGTCAC), C2rev (CACGTCCAGGAAGTTCCAC); TRPC3, C3for (TTAATTATGGTCTGGGTTCTTGG), C3rev (TCCACAACTGCACGATGTACT); TRPC4, C4for (AAGGAAGCCAGAAAGCTTCG), C4frev (CCAGGTTCCTCATCACCTCT); TRPC5, C5for (GCTGAAGGTGGCAATCAAAT), C5rev (AAGCCATCGTACCACAAGGT); TRPC6, C6for (ACTGGTGTGCTCCTTGCAG), C6rev (GAGCAGCCCCAGGAAAAT); TRPC7, C7for (CCCAAACAGATCTTCAGAGTGA), C7rev (TGCATTCGGACCAGATCA); nephrin, Nephrinfor (CCATCCTCCCAGAGATGTTC), Nephrinrev (TTCTCCATGTCGTCCAGGTT); Neph1, Neph1for (CAGTGCCAACCTTTCTACGTC), Neph1rev (TGTTTGCACTGTGGTTGACA); Neph2, Neph2for (GCTTCTTCCTCTTCAGTCAAGG), Neph2rev (GCTGTCCTGACACCACCAC); Neph3, Neph3for (ATCCACTTGGGCCGTAGA), Neph3rev (AGAGAGGTGGCTGCAGATG); CD2AP, CD2APfor (GAAGGGGAGATTATCCATTTGA), CD2APrev (TCCTTCTTTACCGTTCAGTTCAC); Synaptopodin, Synpofor (GTAGCCAGGTGAGCCAAGG), Synporev (TTTTCGGTGAAGCTTGTGC); podocin, Podofor (CCATCTGGTTCTGCATAAAGG), Podorev (CCAGGACCTTTGGCTCTTC); endothelin receptor type A, $Et_A$for (TGTGAGCAAGAAATTCAAAAATTG), ET_Arev (ATGAGGCTTTTGGACTGGTG); endothelin receptor type B, $ET_B$for (CGGTATGCAGATTGCTTTGA), ET_Brev (AACAGAGAGCAAACACGAGGA); angiotensin II type 1a receptor, $AT_{1A}$for (ACTCACAGCAACCCTCCAAG), AT_{1A}rev (CTCAGACACTGTTCAAAATGCAC); angiotensin II type 1b receptor, $AT_{1B}$for (CAGTTTCAACCTCTACGCCAGT), AT_{1B}rev (GGGTGGACAATGGCTAGGTA); angiotensin II type 2 receptor, $AT_2$for (TGTTCTGACCTTCTTGGATGC), AT_2rev (GCCAGGTCAATGACTGCTATAACT); arginine vasopressine V1 type A receptor, $V_{1a}$for (GGGATACCAATTTCGTTTGG), V_{1a}rev (AAGCCAGTAACGCCGTGAT); arginine vasopressine V1b receptor, $V_{1b}$for (TGATGTGGGACCTGATACCTAGT), V_{1b}rev (CCATCCTGTGGTAAGGGTGA); arginine vasopressine receptor type 2, $V_2$for (GACAGGTGTGCCGCTCAT), V_2rev (GAGAGCTAGGGGACGAAAGG); P_2X_1, $P_2X_1$for (TCCGAAGCCTTGCTGAGA); P_2X_1rev (GGTTTGCAGTGCCGTACAT); P_2X_2, $P_2X_2$for (CTTCACAGAACTGGCACACAA), P_2X_2rev (TATTTGGGGTTGCACTCTGA); P_2X_3, $P_2X_3$for (AGCATCCGTTTCCCTCTCTT), P_2X_3rev (TTTATGTCCTTGTCGGTGAGG); P_2X_4, $P_2X_4$for (CCAACACTTCTCAGCTTGGAT), P_2X_4rev (TGGTCATGATGAAGAGGGAGT); P_2X_5, $P_2X_5$for (CACAGTCATCAACATTGGTTCC), P_2X_5 (AGGTAGATAAGTACCAGGTCACAGAAG); P_2X_6, $P_2X_6$for (CCTGGACACGAAAGGCTCT), P_2X_6rev (CACCAGTGATTGGCTGTCC); P_2X_7, $P_2X_7$for (TCTTCCGACTAGGGGACATC), P_2X_7rev (TACCCATGATTCCTCCCTGA); P_2Y_1, $P_2Y_1$for (GCAGTCCAGTCTTTGGCTAGA), P_2Y_1rev (AGTTTCAACCTTTCCATACCACA); and three references, hypoxanthin phosphoribosyltransferase 1, Hprt1for (TCCTCCTCAGACCGCTTTT), Hprt1rev (CCTGGTTCATCATCGCTAATC), tyrosine 3-monooxygenase/tryptophan 5-monooxygenase activation protein, ζ-polypeptide, Ywhazfor (TAAAAGGTCTAAGGCCGCTTC), Ywhazrev (CACCACACGCACGATGAC), and succinate dehydrogenase complex, subunit A, Sdhafor (CCCTGAGCATTGCAGAATC), Sdharev (TCTTCTCCAGCATTTGCCTTA) giving predicted product sizes of 127 bp for TRPC1, 111 bp for TRPC2, 91 bp for TRPC3, 92 bp for TRPC4, 90 bp for TRPC5, 101 bp for TRPC6, 94 bp for TRPC7, 76 bp for Nephrin, 86 bp for Neph1, 78 bp for Neph2, 74 bp for Neph 3, 81 bp for CD2AP, 93bp for synaptopodin, 94 bp for podocin, 72 bp for ETA, 92 bp for ETB, 62 bp for AT1A, 75 for AT1B, 66 bp for V1A, 75 bp for V1B, 92 bp for V2, 76 bp for AT2, 90 bp for Hprt1, 60 bp for Ywhaz and 70 bp for Sdha. Real-time polymerase chain reaction (RT-PCR) was performed using the master mix from the Absolute QPCR SYBR Green Mix kit (Abgene, Epsom, UK).

Supplemental Material and Methods

Quantitative Real-time Polymerase Chain Reaction (qPCR) analysis (2)

Ten picomoles of each primer pair and 0.2 µl of the first-strand synthesis was added to the reaction mixture, and PCR was carried out in a light-cycler apparatus (Light-Cycler 480, Roche Applied Science) using the following conditions: 15 min of initial activation and 45 cycles of 12 s at 94 °C, 30 s at 50 °C, 30 s at 72 °C, and 10 s at 80 °C each. Fluorescence intensities were recorded after the extension step at 80 °C after each cycle to exclude fluorescence of primer dimers melting lower than 80 °C. All primers were tested by using diluted complementary DNA (cDNA) from the first-strand synthesis (10–1000×) to confirm linearity of the reaction and to determine particular efficiencies. Data were calculated as percentage of the geometric mean expression of the three references (Hprt1, Ywhaz and Sdha) which showed the highest tissue-independent transcription. Samples containing primer dimers were excluded by melting curve analysis and identification of the products by agarose gel electrophoresis. Crossing points were determined by the software program. All experiments were performed in quadruplets, and experiments were repeated at least three times.

IV Discussion

This section discusses characteristics of several cation channels including TRPC1, TRPC6 and P_2X_4 and their role in mechanosensitivity based on the three publications in the results chapter of this thesis and the relevant literature. The section “Biophysical characterization and mechanosensitivity of TRPC1” focusses on the paper from Storch et al. (2012), “Mechanosensitive elements in smooth muscle cells: Role of AT_{1B}“ reviews the findings from Blodow et al. (2014) while “Mechanosensitive elements in podocytes: Role of P_2X channels” discusses the findings found in Forst et al. (2015).

Additionally, the most recent findings of our group on the activation characteristics of TRPC4 and TRPC5 channels are discussed in the section “Biophysical characterization of TRPC4 and TRPC5”, which have been submitted to Nature Cell Biology but have not yet been published (Storch et al., 2015).

Biophysical characterization and mechanosensitivity of TRPC1

TRPC1 channels are expressed in a variety of tissues, including vascular smooth muscles, lung, kidney and brain, where they contribute to a wide range of biological functions that include proliferation, arterial contraction, salivary gland secretion, neurotransmission, growth cone turning, neuronal differentiation and transcription control. Till date, it has been generally accepted that the general activation mechanism of TRPC1 is subsequent to receptor mediated PLC activation. TRPC1 has at least five different splice variants (α, β, γ, δ and ε) but only three (α, β, and ε) are known to be translated into functional proteins (Ong et al., 2013; Sakura and Ashcroft, 1997) and isoform specific activation might be possible. The TRPC1β protein lacks 34 amino acids in the third ankyrin repeat while TRPC1ε carries a seven amino acid deletion downstream of the first membrane spanning helix compared to the longer TRPC1α isoform (see Figure 7).

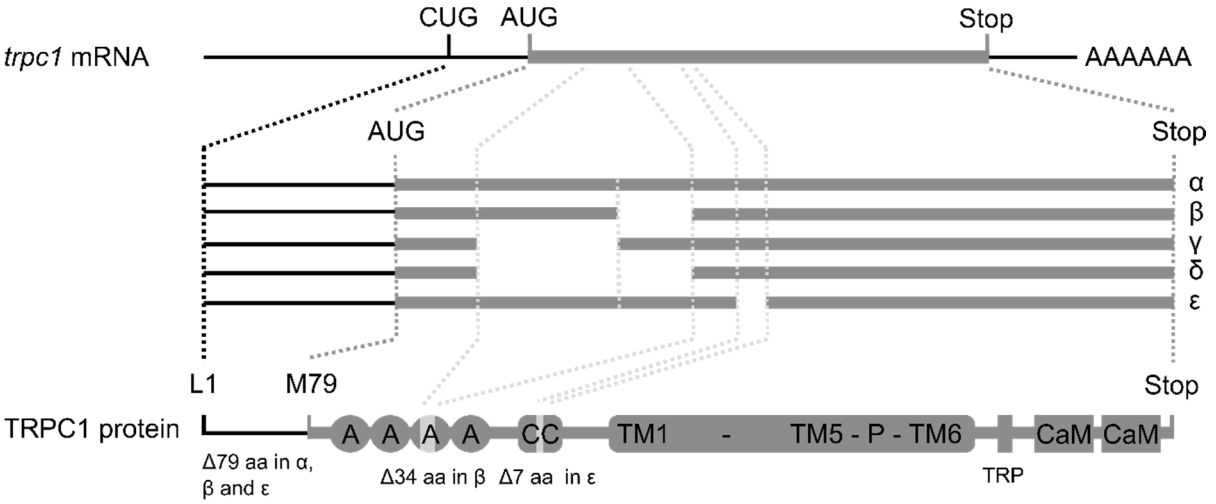

Figure 7: Schema of the different mouse *trpc1* slice variants and their respective translated TRPC1 isoforms. The *trpc1* gene is transcribed into several different *trpc1* mRNAs including splice variants α, β, γ, δ and ε, but only splice variants α, β, and ε are translated into a functional TRPC1 protein. Additionally, the alternative start codon CUG results in the extended TRPC1 protein. In the TRPC1 protein, L1 indicates the first amino acid (aa) found in the extended murine TRPC1 isoform, M79 indicates the start codon AUG common to the TRPC1α, β, and ε. TRPC1 proteins contain four ankyrin repeats (A), and one coiled-coiled domain (CC) in their N-terminal region. Transmembrane domains (TM1 to TM6) and the pore region (P) as well as the TRP box and two calmodulin-binding sites (CaM) are indicated. Human TRPC1 proteins are 16 amino acids shorter compared to mouse TRPC1 due to a downstream ATG codon. The alternative CUG start codon is conserved among most species and can also be found in human *trpc1* mRNA. Translation starting from this CUG codon would result in an 83 amino acid N-terminal extension.

Although accumulating results clarify the functional properties of TRPC1, discrimination between the splice variants is rare. Recent reports suggest that stimulation of the longer TRPC1α isoform in complex with TRPC4 results in higher current amplitudes as compared to the shorter TRPCβ protein (Kim et al., 2014). On the other hand, TRPC1ε seems unique among all TRPC1 isoforms in its ability to amplify store-operated currents. This newly identified isoform could explain why several groups have reported that TRPC1 channels are activated upon depletion of internal calcium stores (summarized in Salida et al., 2009 and Yuan et al., 2009), while others found no involvement of TRPC1 in store depletion (Dietrich et al., 2007).
Apart from receptor-mediated activation and activation upon internal store depletion, TRPC1 has been suggested to be activated by membrane stretch (Maroto et al., 2005). Other groups, however, could not confirm these findings, leaving the activation mechanisms of TRPC1 proteins to be ill defined (Dietrich et al., 2007; Gottlieb et al., 2008).
In order to understand the contradictory data regarding TRPC1 proteins, human TRPC1β was analyzed in heterologous expression systems with a highly sensitive electrophysiological approach (Storch et al., 2012). In contrast to what has been previously reported, TRPC1β alone did not form functional homotetrameric receptor-operated channels. Agonist-, GTPγS-, or PIP_2 depletion-induced currents were never observed in all TRPC1-expressing systems employed by us. It can be concluded from this phenomenon that TRPC1β forms no functional channel in the plasma membrane, although it is impossible to distinguish whether TRPC1 does not assemble into homotetramers or is retained in subcellular structures like the endoplasmic reticulum. Previous studies with fluorescently-tagged TRPC1 demonstrated that functional homotetrameric TRPC1 channels are mostly present in the cytoplasm (Alfonso et al., 2008). Based on this study and our own observations, it can be concluded that functional TRPC1 homomers exist but are retained in the ER, which could explain the lack of TRPC1 currents observed in our study. However, it should be noted that the lack of TRPC1 currents in our study can also be explained by the inability of TRPC1 to react to the typical TRPC activators employed by us, although previous reports have shown that TRPC1 can be activated by stimulation of the PLC cascade after GPCR activation (Alfonso et al., 2008; Zhu et al., 1996).
Although homomeric TRPC1 seems incapable of insertion into the plasma membrane, TRPC1-mediated currents could be observed when TRPC1 was co-expressed with other TRPC subunits (Storch et al., 2012). Surprisingly, TRPC currents could be measured regardless of the co-transfected TRPC subunit (TRPC3, -4, -5, -6, and -7). Previous studies showed that TRPC1 co-assembles with TRPC4 and TRPC5, but no interaction between TRPC1 and the diacyglycerol-sensitive subfamily TRPC3, -6, and -7 have been found in previous studies that used Förster resonance energy transfer (FRET) (Brownlow and Sage, 2005; Goel et al., 2002; Hofmann et al., 2002). In all TRPC1-containing heteromers, the presence of TRPC1 subunits altered the biophysical properties of the channel units by significantly decreasing calcium

permeation (Storch et al., 2012). To assure that TRPC1 is part of the channel pore, two TRPC1 pore-mutants E581Q and E582Q were generated. Both glutamic acid residues are present in the putative pore region of TRPC1 and are not present in other TRPCs. Mutating either one of the glutamic acids was sufficient to impair calcium permeation of the TRPC1-containing heteromers, while simultaneous exchange of both glutamates had no additional effect. This suggests that TRPC1 subunits contribute to pore formation, thereby altering the calcium permeation properties of heteromeric TRPC channels. See Table 1 for an overview of the biophysical properties of TRPC1β-containing TRPC heteromeric channels. Since TRPC1 channels have been discussed as store-operated channels (SOC) that open in response to depletion of internal stores, the contribution of TRPC1 to SOC activity in immortalized murine GnRH-releasing neurons (Gn11 cells) was investigated (Storch et al., 2012). These cells were used for our study because of their prominent TRPC1 expression as detected by quantitative RT-PCR. It should be noted that the primers used to detect TRPC1 mRNA detected all the above-mentioned TRPC1 isoforms and do not provide insight into the expression profile of specific TRPC1 isoforms. Altered SOC activity was not observed when TRPC1 levels using TRPC1-specific shRNA were reduced. This suggests that TRPC1 does not contribute to SOC activity in Gn11 cells. Similar results were observed in previous studies that used vascular smooth muscle cells deficient in TRPC1 (Dietrich et al., 2007). Instead of TRPC1, the calcium release-activated calcium channel protein 1 (Orai1) in the plasma membrane is activated by stromal interaction molecule 1 (STIM1), an ER calcium sensor, to mediate store-operated calcium entry (Potier et al., 2009). While some groups postulated that SOC activity depends on Orai1 and STIM1 alone and is independent of TRPC1 (Potier et al., 2009), other investigators reported interaction of some TRPC channels including TRPC1 with Orai1 and STIM1 *in vitro* ((Lee et al., 2014); reviewed in (Cheng et al., 2013)). The discrepancies regarding TRPC1 channel activation might be explained by a recent report that identified an extended form of mouse TRPC1 in early pre-osteoclasts (Ong et al., 2013). The newly identified functional splice variant called TRPC1ε bears a seven amino acid deletion downstream of the first membrane-spanning helix. It should be noted that mouse TRPC1 contains an earlier ATG start codon that results in a 16 amino acid extension compared to human TRPC1. For a comparison between the human and mouse TRPC1 proteins see supplementary Table 2. Heterologous expression of mouse TRPC1ε in HEK293 cells revealed that it physically interacts with Orai1 and that expression of TRPC1ε amplifies SOC activity (Ong et al., 2013). Additionally, Ong et al. (2013) identified the alternative TRPC1 start codon CUG upstream of the published AUG resulting in a 78 amino acid extension. The extension harbors a cluster of positively charged amino acids that might block the negatively charged pore domain of the channel.

Channel	IV	Composition	Calcium permeation P_{Ca}/P_{Na}	Reversal potential (mV)
TRPC1	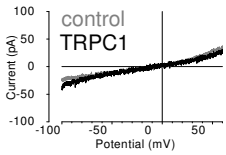	Control: C1:	2.21 ± 0.37 2.19 ± 0.40 (ns)	-35 ± 4 -38 ± 4 (ns)
TRPC3/TRPC1	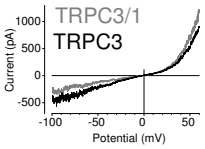	C3: C3/C1:	3.61 ± 0.25 2.64 ± 0.35 (*)	-18 ± 2 -23 ± 5 (**)
TRPC4/TRPC1	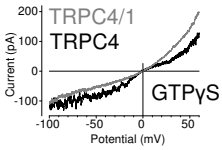	C4: C4/C1:	4.23 ± 0.36 2.77 ± 0.34 (**)	-16 ± 2 -26 ± 2 (*)
TRPC5/TRPC1	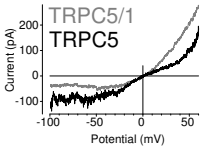	C5: C5/C1: C5/C1^{E581Q}: C5/C1^{E582Q}: C5/C1$^{E581Q/E582Q}$:	1.57 ± 0.11 0.82 ± 0.07 (***) 0.45 ± 0.04 (*) 0.38 ± 0.04 (*) 0.43 ± 0.06 (*)	-40 ± 2 -53 ± 2 (***) -60 ± 2 (*) -60 ± 2 (*) -61 ± 3 (*)
TRPC6/TRPC1	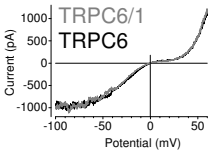	C6: C6/C1:	2.63 ± 0.25 1.79 ± 0.13 (*)	-25 ± 2 -32 ± 3 (**)
TRPC7/TRPC1	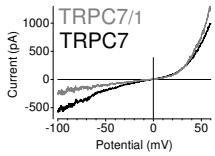	C7: C7/C1:	2.33 ± 0.33 1.62 ± 0.14 (*)	-44 ± 3 -40 ±3 (*)

Table 1: Overview of the biophysical properties of TRPC1β-containing TRPC channels and their respective calcium permeations as measured in whole cell recordings of HEK293. The current-voltage relationships (IVs) of the homo- and heteromeric TRPC channels are depicted, as well as the calcium permeation properties and reversal potentials. For the determination of IVs, cells were transfected with the type-5 muscarinic acetylcholine receptor and TRPC channels and measured in the whole-cell configuration. Typical carbachol- or guanosine 5'-O-[gamma-thio]triphosphate (GTPγS)-induced IV curves are displayed. For the determination of calcium permeabilities, a divalent-free sodium extracellular solution (Na^+, 130 mM NaCl, 50 mM mannitol, and 10 mM HEPES, pH 7.4) and a monovalent-free calcium solution (Ca^{2+}, 10 mM $CaCl_2$ and 150 mM N-methyl-D-glucamine-Cl, pH 7.4) were applied. The reversal potentials were measured in the presence of an activator and 10 mM calcium in the bath solution. Black asterisks in parentheses indicate significant differences between heteromers containing TRPC1β compared to respective homomers without TRPC1. Red asterisks in parentheses indicate significant differences between heteromers containing mutant TRPC1 compared to respective heteromers containing wild type TRPC1.

The alternative CUG start codon is conserved among most species and can also be found in human *trpc1* mRNA. Translation starting from this CUG codon would result in an 83 amino acid N-terminal extension. Ong et al. (2013) functionally characterized the newly found TRPC1 proteins by measuring currents observed after store depletion (I_{SOC}) of HEK293 cells' heterologous co-expression of each TRPC1 isoform with Orai1 and STIM1. Interestingly, single expression of either isoform was insufficient to produce any current but required co-expression with Orai1 and STIM1 confirming the observations made in our own study (Storch et al., 2012). The newly identified extended TRPC1 proteins modified the ionic selectivity of the I_{SOC} currents mediated by Orai1, or possibly TRPC1/Orai1 channels and may thereby help to fine-tune I_{SOC} currents. In contrast, expression of TRPC1ε was unique among all TRPC1 isoforms in its ability to amplify store-operated currents, suggesting isoform-specific functions. These newly identified TRPC1 proteins may explain the discrepancies observed in the function of TRPC1 proteins: The extended TRPC1 may represent the real native protein better than the shorter form used in some overexpression studies and might be able to translocate to the plasma membrane in contrast to its shorter isoforms. On the other hand, the TRPC1ε isoform might be responsible for TRPC1-dependent SOC currents observed by some researchers. However, it should be mentioned that the expression profile of the newly identified TRPC1 isoforms is still largely elusive and requires further investigation.

Apart from SOC activity, the role of endogenous TRPC1 as a calcium suppressor in murine gonadotropin-releasing hormone-releasing Gn11 neurons was investigated (Storch et al., 2012). Down-regulation of all TRPC1 isoforms using shRNA resulted in increased calcium permeation properties in Gn11 cells similar to the results found in HEK293 cells heterologously expressing TRPC1β/TRPC complexes. Gn11 neurons were originally derived from the olfactory bulb at embryonic day 11.5. At this stage of development, GnRH-releasing cells have the capability to migrate to the hypothalamus to fully differentiate, thereby losing their migratory properties. Gn11 cells in culture also show high migratory properties. The migratory ability of Gn11 was tested using scratch assays. As expected, wild type and Gn11 cells transfected with control shRNA did migrate to the space left by the scratch. Interestingly, TRPC1 knock-down cells showed enhanced migration compared to wild type and control cells. This effect was due to the enhanced motility of cells since TRPC1 knock-down did not alter proliferation and apoptosis levels. Moreover, TRPC1 knock-down and control Gn11 cells differed in terms of migratory properties such as distance covered, migration speed and directionality. TRPC1 knock-down cells moved with higher speed and changed direction less frequently allowing them to cover a greater effective distance. The increased migratory ability of TRPC1 knock-down cells was due to the increased G-actin levels, demonstrating that the enhanced motility of TRPC1 knock-down neurons is associated with a marked reorganization of the actin cytoskeleton. Taken together, the results in the study from Storch and colleagues (2012)

suggest that TRPC1 expression in Gn11 cells suppresses calcium permeation properties in these cells and thereby limiting migration.

However, these findings are in contrast to earlier reports with a polarized renal epithelial cell line. In renal cell systems TRPC1 knock-down by shRNA resulted in suppressed calcium entry and impaired motility and migration (Fabian et al., 2011; Fabian et al., 2008). These findings can be explained by a different TRPC expression profile or expression of a different TRPC1 isoform as discussed above.

It has been previously shown that Gn11 migration is dependent on calcineurin and NFAT (Zaninetti et al., 2008). On the basis of earlier reports and on our own observations, we postulate that TRPC1β regulates neuronal migration in the following way (see Figure 8):

1. TRPC1β assembles with other TRPC in the plasma membrane and reduces the calcium permeation properties of functional TRPC channel subunits resulting in lower intracellular calcium concentrations upon TRPC channel activation.
2. Intracellular calcium activates the calcium-dependent protein calmodulin, which in turn activates the phosphatase calcineurin.
3. Activated calcineurin dephosphorylates NFAT, which subsequently translocates to the nucleus.
4. Nuclear NFAT drives NFAT-dependent transcription and translation of migration-regulating proteins.

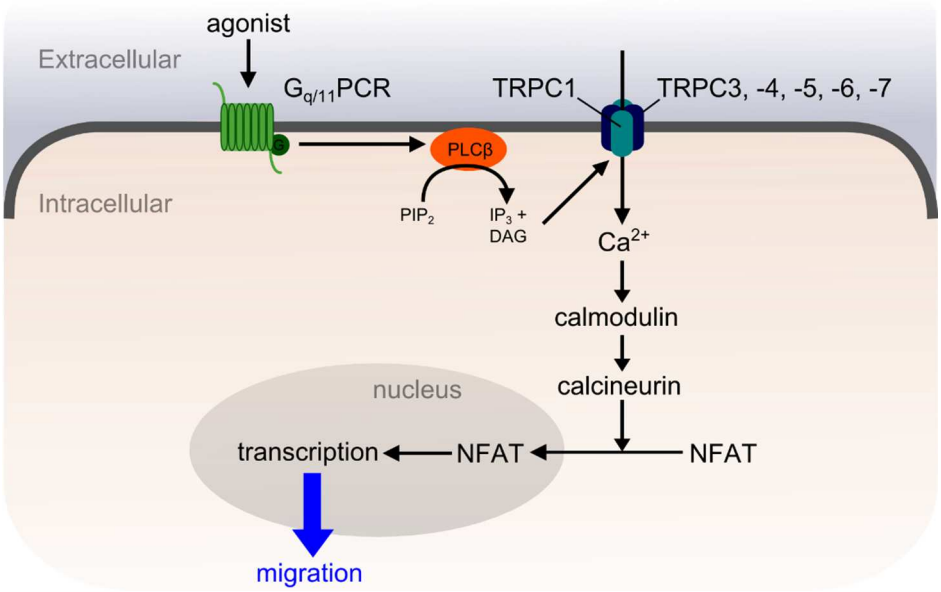

Figure 8: TRPC1 channel activation in neuronal cell systems. TRPC1 *per se* is only present in the plasma membrane in TRPC3, -4, -5, -6, -7 containing heterotetramers. TRPC heteromers are activated upon receptor-mediated PLC activation that results in increased intracellular calcium concentrations. Intracellular calcium activates calmodulin, which in turn activates the phosphatase calcineurin. Calcineurin dephosphorylates nuclear factor of activated T-cells (NFAT), which translocalizes to the nucleus. Nuclear NFAT drives NFAT-controlled transcription and translation of migratory proteins.

Altogether, the results presented in the study from Storch et al. (2012) support the notion that TRPC1β homomers are located in the cytoplasm of the cells while TRPC1β-containing heteromeric TRPC complexes can form functional channel subunits in the plasma membrane. In the plasma membrane, TRPC1β contributes to pore formation of heterotetrameric TRPC channels which effectively reduce calcium permeation. Since functional TRPC1β homomers are not present in the plasma membrane, a stretch-induced activation of TRPC1β channels seems to be highly unlikely. However, it cannot be ruled out that other isoforms might form homomers in the plasma membrane that might be sensitive to membrane stretch. Our findings were confirmed in neuronal Gn11 cells. It was shown that TRPC1 proteins in their function as calcium suppressors control neuronal migration while no evidence of TRPC1 contributing to SOC activity was found. The presented data highlights the promiscuous role of TRPC1 in various cell functions, but further research is needed to unravel the role of the different TRPC1 isoforms and their role in SOC activity.

Biophysical characterization of TRPC4 and TRPC5

TRPC5 channels are widely expressed in the central nervous system and are involved in amygdala function and fear-related behavior (Riccio et al., 2009). In hippocampal neurons, TRPC5 also regulates hippocampal neurite length and growth cone morphology (Greka et al., 2003). Lower TRPC5 expression levels can be found in the kidney, where TRPC5 activation seems protective against renal failure (Schaldecker et al., 2013; Tian et al., 2010). TRPC5 and its close family member TRPC4 are activated through activation of $G_{q/11}$PCRs and receptor tyrosine kinases (Schaefer et al., 2000). Activation of these channels seems to require PLC-mediated conversion of PIP_2 to DAG and IP_3 although neither IP_3 nor DAG alone is sufficient to cause channel activation. On the contrary, TRPC4 and -5 channels are rather inhibited by DAG or its membrane-permeable analogue OAG (Venkatachalam et al., 2003) in contrast to the DAG-sensitive subfamily members TRPC3, -6 and -7 (Hofmann et al., 1999). A DAG-mediated activation of TRPC5 currents has only been observed in heterologous studies with suppressed PKC activity (Venkatachalam et al., 2003). It has been suggested that the mechanism of TRPC4 and -5 activation depends on PLC-mediated depletion of PIP_2 in proximity to TRPC4 and -5 channels. Indeed, PIP_2 depletion is sufficient to cause TRPC4 and -5 channel activation (Flemming et al., 2006).

In contrast to the DAG-sensitive subfamily, TRPC5 and its close family member TRPC4 contain the C-terminal Na^+/H^+ exchanger regulatory factor 1 (NHERF1) binding motif VTTLR (Tang et al., 2000). NHERF1 is a member of the NHERF family of scaffolding proteins that is important in maintaining and regulating cell function, e.g. in proximal tubule cells (Voltz et al., 2001). NHERF proteins form homo- and heterodimers and are suggested to participate in the formation of multiprotein complexes (Shenolikar et al., 2004; Voltz et al., 2001). The two family members NHERF1 and -2 are structurally related adaptor proteins characterized by the presence of two tandem PSD-95/Drosophila discs large/ZO-1 (PDZ) interaction domains. Additionally, NHERF proteins associate with the actin cytoskeleton via interactions with members of ezrin/radixin/moesin family (Tang et al., 2000). NHERF proteins are highly expressed in the kidney, small intestine, and other organs, where they associate with a number of transporters, ion channels, signaling proteins, transcription factors, GPCRs and tyrosine receptors (for a schematic representation of NHERF1 and its binding partners see Figure 9) (summarized in Weinman et al., 2006). NHERF proteins have been shown to associate with TRPC4 and -5, thereby modulating channel activity (Lee-Kwon et al., 2005; Obukhov and Nowycky, 2004; Tang et al., 2000). The expression profile and lysophospholipids dependency of TRPC5 channels have raised the question of a mechanically-gated TRPC5 channel activity. Indeed, TRPC5 can be indirectly activated by membrane stretch in a PIP_2-dependent mechanism that probably involves formation of second messengers (Gomis et al., 2008; Jemal

et al., 2014). Therefore, the properties of TRPC5 gating in heterologous and endogenous expression systems were carefully analyzed (Stroch et al., 2015).

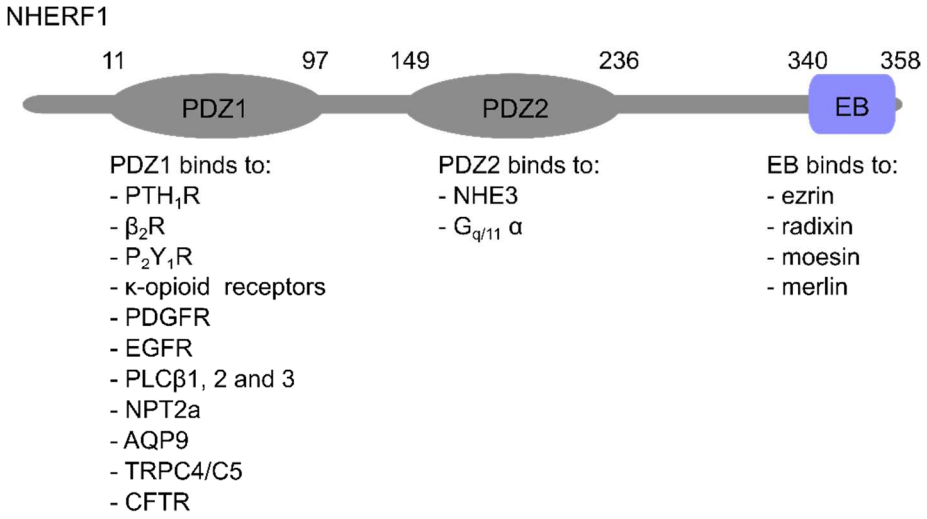

Figure 9: Schematic representation of human NHERF1 and its two tandem PDZ domains as well as the C-terminal ezrin-binding domain (EB). Additionally, several associated binding partners are listed below. Binding partners of the first PDZ domain (PDZ1) include G protein-coupled receptors such as the parathyroid receptor 1 (PTH_1R), the β2-adrenergic receptor (β_2R), purinergic receptor type 1 (P_2Y_1R), κ-opioid receptor as well as growth factor tyrosine kinase receptors such as the platelet-derived growth factor receptor (PDGFR) and the epidermal growth factor receptor (EGFR). Moreover, the PDZ1 domain was shown to bind to transporters such as the Na^+/phosphate transporter type 2a (NPT2a) and aquaporin 9 (AQP9), enzymes such as phospholipase C β1, -2, and -3 (PLCβ1, -2, -3) and ion channels like the cystic fibrosis transmembrane regulator (CFTR) or classical transient receptor potential channel 4 and 5 (TRPC4, -5). PDZ2 was shown to bind the Na^+/H^+ exchanger type 3 (NHE3) and the $G_{q/11}$ α subunit. The EB domain links NHERF1 to the actin cytoskeleton. The numbers above correspond to respective amino acid numbers. Sources: (Shenolikar et al., 2004; Voltz et al., 2001; Weinman et al., 2006)

In accordance with previous findings, using conventional electrophysiological whole-cell recordings of HEK293 cells, it was confirmed that heterologously expressed TRPC5 is inhibited by application of OAG (see Figure 10a) or accumulation of endogenous DAG using the DAG kinase inhibitor RHC-80267 (Storch et al., 2015). However, robust TRPC5 currents using OAG could be evoked when either PKC was inhibited by bisindolylmaleimide I (see Figure 10b) or TRPC5 was simultaneously co-expressed with a $G_{q/11}$PCR (see Figure 11a). Additionally, several PKC-phosphorylation sites that were shown to modify TRPC5 desensitization, including a threonine at position 972, were mutated (Zhu et al., 2005). Introduction of the non-phosphorable amino acid alanine at position 972 (T972A) also rendered TRPC5 perceptive to OAG while the pseudo-phosphorylated T972D mutant was not sensitive to OAG (see Figure

10c and 10d, respectively). Interestingly, this particular amino acid is present in the C-terminal VT^{972}TRL motif of TRPC5 known to be crucial for NHERF1 binding (Tang et al., 2000). We hypothesized that the observed susceptibility of TRPC5 to DAG was likely due to loss of endogenous NHERF1 binding to the C-terminus VTTRL of TRPC5.

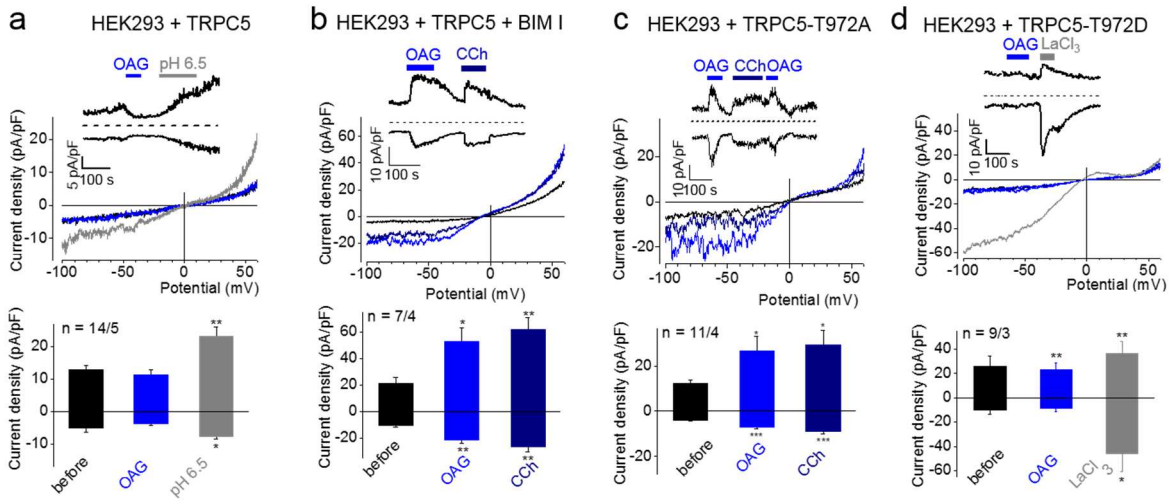

Figure 10: TRPC5 channels can be activated by 1-oleoyl-2-acetyl-sn-glycerol (OAG) if phosphokinase C (PKC) is inhibited or PKC phosphorylation sites within TRPC5 are modified. *Figure modified from Storch et al. (2015).* (a-d) Exemplary current density (CD) voltage curves, CD time courses and summaries of CDs at holding potentials of ±60 mV of whole-cell recordings of HEK293 cells expressing TRPC5 (a, b), TRPC5-T972A (c) or TRPC5-T972D (d). Stippled lines indicate zero currents. Applications of 100 µM OAG, of acid bath solution with pH 6.5, of 100 µM carbachol (CCh) and of 300 µM $LaCl_3$ are indicated. (b) TRPC5-expressing HEK293 cells were pre-incubated with the 1 µM of the PKC inhibitor bisindolylmaleimide I (BIM I) for 15 minutes. Numbers over bars indicate the number of measured cells and of independent transfections. Significant differences were calculated as compared to basal CDs before application of stimuli. (mean±sem. two-tailed, paired t-test; *p<0.05, **p<0.01, ***p<0.001).

In this scenario, inhibition of PKC would result in the dephosphorylation of T972 in the NHERF1 binding motif VT^{972}TRL. This results in loss of NHERF1 binding to the C-terminus of TRPC5 thereby making TRPC5 accessible to DAG. NHERF1 also binds with GPCRs using the same PDZ domain that is used to bind TRPC4 and TRPC5 (Tang et al., 2000). This PDZ domain is likely to have a higher affinity for $G_{q/11}$PCRs compared to TRPC5 channels. This would explain why simultaneous overexpression of GPCRs with TRPC5 channels resulted in OAG-sensitive TRPC5 channels. This hypothesis was tested by performing immunoprecipitation studies in CHO-K1 cells stably overexpressing human NHERF1. As expected, NHERF1 proteins co-immunoprecipitated with HA-tagged TRPC5 confirming the observations made by Tang et al. (2000). However, co-expression of the type-5 muscarinic acetylcholine receptor resulted in

loss of NHERF1 binding to TRPC5, confirming the hypothesis that NHERF1 has a higher affinity for GPCRs (see Figure 11b).

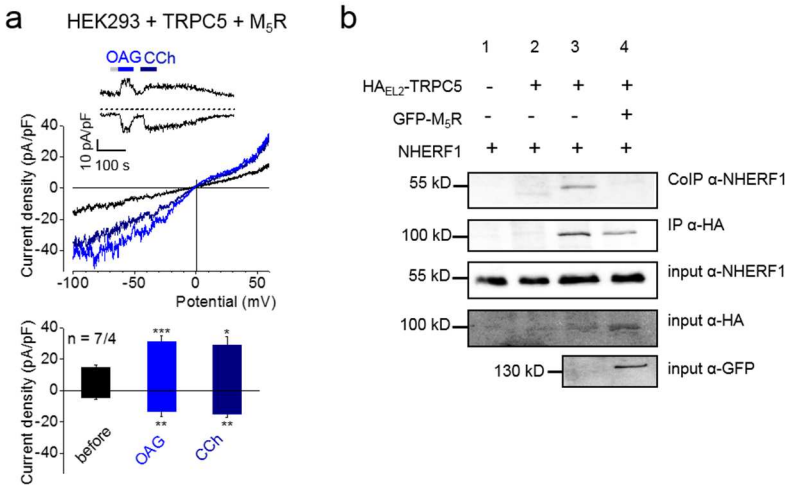

Figure 11: TRPC5 channels co-expressed with a $G_{q/11}$PCR ($G_{q/11}$ protein-coupled receptor) are 1-oleoyl-2-acetyl-sn-glycerol (OAG)-sensitive due to dissociation of NHERF1 from TRPC5. *Figure modified from Storch et al. (2015).* (a) Exemplary current density (CD) voltage curves, CD time courses and summaries of CDs at holding potentials of ±60 mV of whole-cell recordings of HEK293 cells co-expressing TRPC5 and muscarinic M_5 receptor (M_5R). Stippled lines indicate zero currents. Applications of 100 µM OAG and of 100 µM carbachol (CCh) are indicated. Numbers over bars indicate the number of measured cells and of independent transfections. Significant differences were calculated as compared to basal CDs before application of stimuli. (mean±sem. two-tailed, paired t-test; *p<0.05, **p<0.01, ***p<0.001). (b) Exemplary result of a co-immunoprecipitation where NHERF1 was co-immunoprecipitated with TRPC5 tagged with an HA-tag in the second extracellular loop (HA_{EL2}-TRPC5) in the absence (lane 3) or presence (lane 4) of N-terminally GFP-tagged M_5R in CKO-K1 cells. In lane 2, an irrelevant control antibody instead of anti HA antibody was used for immunoprecipitation.

To support the hypothesis that presence of NHERF is responsible for the lack of DAG sensitivity of TRPC5 channels, endogenous NHERF levels in HEK293 cells were reduced by transfection of specific anti-NHERF shRNAs. Again, reduction of either NHERF1 or -2 was sufficient to evoke OAG-mediated TRPC5 currents suggesting that the regulation by NHERF is not isoform-specific (see Figure 12a-c). Interestingly, a DAG sensitivity of TRPC5 was also observed when a mutated NHERF1 construct, in which a glutamate at position 68 within the first PDZ domain was altered into an alanine, was co-expressed (see Figure 12d). This NHERF1 E68A mutation was first identified in patients with dysfunctional renal phosphate reabsorption. In the kidney, NHERF1 normally binds to the main renal phosphate transporter NPT2a and to PTH_1R and regulates their expression and location at the apical plasma membrane of polarized renal proximal tubule cells. As a consequence of the amino acid

exchange at position 68, the NPT2a surface expression is reduced since the NHERF1-NPT2a interaction is disrupted and phosphate is wasted into the urine (Courbebaisse et al., 2012). In our cell systems, NHERF1 E68A mutants caused an OAG sensitivity of TRPC5 even in the presence of endogenous wild type NHERF1. This suggests that NHERF1 E68A is not impaired in its ability to bind to endogenous wild type NHERF1 but the NHERF1 heterodimers are unable to bind to TRPC5. Consequently, the NHERF1-free C-terminus of TRPC5 is now accessible to DAG.

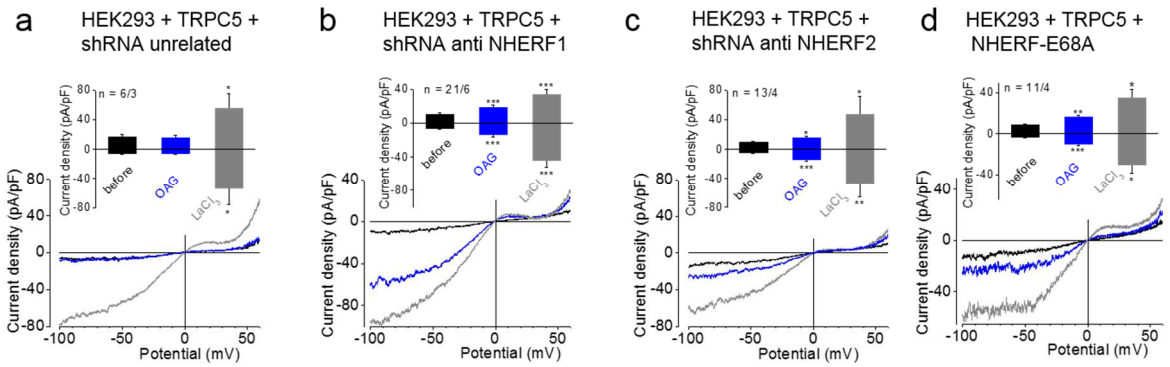

Figure 12: TRPC5 channels can be activated by 1-oleoyl-2-acetyl-sn-glycerol (OAG) if NHERF proteins do not bind to TRPC5. *Figure modified from Storch et al. (2015).* (a-d) Exemplary current density (CD) voltage curves and summaries of CDs at holding potentials of ±60 mV of whole-cell recordings of HEK293 cells expressing unrelated control shRNA (a), shRNA against NHERF1 (b), shRNA against NHERF2 (c) or the NHERF1 mutant NHERF1-E68A (d). Stippled lines indicate zero currents. Numbers over bars indicate the number of measured cells and of independent transfections. Significant differences were calculated as compared to basal CDs before application of stimuli. (mean±sem. two-tailed, paired t-test; *p<0.05, **p<0.01, ***p<0.001).

The importance of the C-terminal VTTRL motif was confirmed by creating a truncated TRPC5 construct that lacked the last five amino acids. However, functionality of the TRPC5 Δ971 mutant in whole-cell recordings was never observed likely because the truncated TRPC5 did not reach the plasma membrane (data not shown) (Storch et al., 2015). These results are in contrast to the observations made by Kaczmarek et al. (2012), who postulated that TRPC5 proteins can be cleaved by the protease calpain. Activation of calpain resulted in functional C-terminally truncated TRPC5 proteins that had higher activity compared to non-truncated TRPC5. The authors suggest that TRPC5 is likely cleaved at a threonine at position 857 within the calpain cleavage site. They confirmed that TRPC5 truncated at N854 still forms functional channels in the plasma membrane. However, it remains unclear how TRPC5 is activated upon cleavage of its C-terminus. The discrepancy observed in our own study (Storch et al., 2015) and that by Kaczmarek and coworkers (2012) could be explained due to use of different

truncation mutations. While only the last five amino acids were truncated in our own study, Kaczmarek et al. (2012) used a TRPC5 Δ855 mutant that might have overcome the obstacles that prevented the TRPC5 Δ971 mutant from reaching the plasma membrane.

Next to TRPC5, the close family member TRPC4 is also known to be regulated by NHERF proteins that bind to the C-terminus of TRPC4 using the same VTTRL motif that is present in TRPC5 (Tang et al., 2000). Similar to TRPC5, TRPC4 channels are normally not susceptible to DAG or its derivatives. Due to the high commonality between TRPC4 and -5 proteins, it can be hypothesized that TRPC4 might be similarly regulated by NHERF proteins. This hypothesis was confirmed by co-expression of TRPC4β with GPCRs in HEK293 cells. Indeed, co-expression of TRPC4β with the histamine receptor resulted in TRPC4-mediated currents upon simulation of cells with OAG (Storch et al., 2015). This result indicates that TRPC4 and -5 proteins are alike in their regulation by NHERF proteins and both channels can be activated by DAG or its derivatives when NHERF binding with their C-terminus is impeded.

To address the question of whether activation of TRPC4 or -5 by OAG is solely a phenomenon seen in heterologous cell systems, two cell lines that endogenously expressed either high levels of TRPC4 or -5 were used (see Figure 13). The human-derived renal proximal tubule cell line HKC8 expressed high levels of TRPC4 and NHERF1 and marginal levels of TRPC5 but no TRPC6 while the immortalized mouse hippocampal HT22 cell line expressed high levels of TRPC5 but no TRPC3, -6 or -7 (Storch et al., 2015). In electrophysiological whole-cell recordings of HKC8 cells, OAG was not sufficient to evoke a TRPC4-mediated response while the TRPC4 and -5 potentiator lanthanum evoked a significant increase in current (see Figure 13a). These results suggest that the highly expressed endogenous TRPC4 channels are not DAG sensitive. However, similar to our findings in HEK293 cells, either inhibition of PKC or the overexpression of NHERF1 E68A was sufficient to cause an OAG sensitivity of HKC8 cells (see Figure 13b and 13c), which confirms that TRPC4 activation via DAG is a physiologically meaningful phenomenon. Similar results were found for TRPC5 channels expressed in HT22 cells (Storch et al., 2015). While OAG alone was not sufficient to evoke TRPC5 activation, suppression of PKC activity caused a DAG sensitivity of HT22 cells (see Figure 13d and 13e respectively). The observation that the DAG sensitivity in the presence of the PKC inhibitor was indeed mediated by TRPC5 channels was confirmed by reducing endogenous TRPC5 levels using shRNA against TRPC5. Indeed, the DAG sensitivity of HT22 was abolished in the presence of TRPC5 shRNA confirming that endogenous TRPC5 is activated by DAG once PKC is suppressed (see Figure 13f).

TRPC5 and the long isoform of human TRPC4α channels are known to be inhibited by the presence of lysophospholipids which means that decreasing the levels of PIP_2 causes current potentiation (Kim et al., 2008; Trebak et al., 2009). It has been postulated that membrane-resident PIP_2 interacts with the C-terminus of TRPC4α and stabilizes the closed channel

conformation in the presence of NHERF1 (Otsuguro et al., 2008). We speculated that the consequence of PIP_2 depletion is the reconfiguration of the C-terminus of TRPC4 and -5. The newly adopted active conformation may now be susceptible to DAG, which means that the

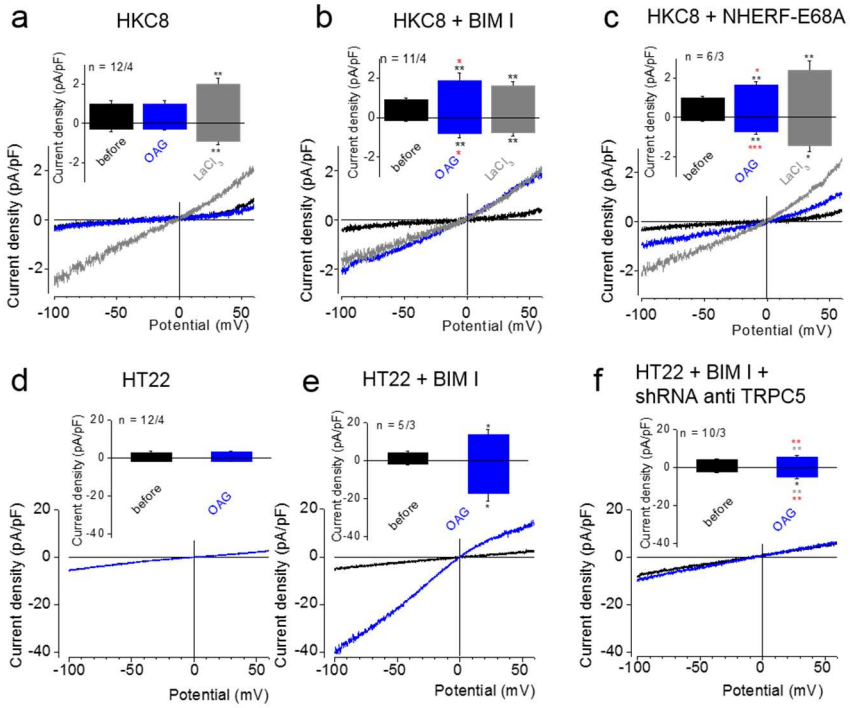

Figure 13: Endogenous TRPC4 and -5 can be activated by 1-oleoyl-2-acetyl-sn-glycerol (OAG) if PKC is suppressed or NHERF-E68A is co-expressed. *Figure modified from Storch et al. (2015).* (a-f) Exemplary current density (CD) voltage curves and summaries of CDs at holding potentials of ±60 mV of whole-cell recordings of the human-derived renal proximal tubule cell line HKC8 (a-c) and mouse hippocampal HT22 cells (d-f). (b, e) Cells were pre-incubated with the 1 µM of the PKC inhibitor bisindolylmaleimide I (BIM I) for 15 minutes. (c, f) Cells were transfected with mutant NHERF1-E68A (c) or shRNA against TRPC5 (f). Stippled lines indicate zero currents. Applications of 100 µM OAG and of 300 µM LaCl3 are indicated. Numbers over bars indicate the number of measured cells and of independent transfections. Significant differences were calculated as compared to basal CDs before application of stimuli. (mean±sem. two-tailed, paired t-test; *p<0.05, **p<0.01, ***p<0.001).

PLC product DAG would be the actual activator of the channels after PLC activation. PIP_2 depletion in whole-cell measurements with HEK293 cells overexpressing TRPC5 was sufficient to cause TRPC5 channel potentiation (see Figure 14a). In the study from Storch et al. (2015), it did not matter whether the PIP_2 depletion was introduced by blockage of PIP_2 production via phosphoinositide 3-kinase or phosphoinositide 4-kinase, by scavenging of existing PIP_2 using poly-L lysine or by rapamycin-induced conversion of PIP_2 to phosphoinositides (PI) using co-expressed phosphatases (for methodical details see Lindner et al., 2011). These findings demonstrate that activation of TRPC5 by PIP_2 depletion is not the result of PIP_2 degradation products that subsequently signal to TRPC5, but loss of PIP_2 *per se*

is sufficient to evoke channel activation. Interestingly, when OAG was applied after maximal PIP_2 depletion-evoked currents were reached, TRPC5 currents were further increased indicating that PIP_2 depletion provokes TRPC5 to adapt a conformation that is susceptible to DAG (see Figure 14b).

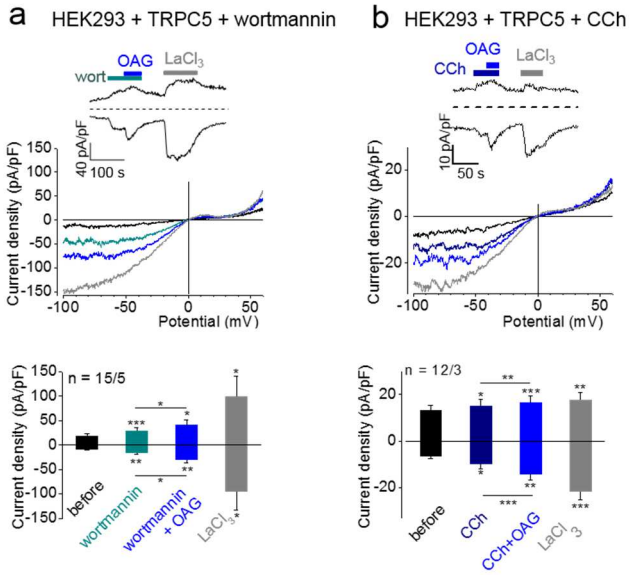

Figure 14: Phosphatidylinositol (3,4)-bisphosphate (PIP_2) depletion causes TRPC5 channel activation by 1-oleoyl-2-acetyl-sn-glycerol (OAG). *Figure modified from Storch et al. (2015).* (a, b) Exemplary current density (CD) voltage curves, CD time courses and summaries of CDs at holding potentials of ±60 mV of whole-cell recordings of HEK293 cells expressing TRPC5 (a, b). Applications of 100 µM OAG, 20 µM of the phosphoinositide-kinase inhibitor wortmannin (wort) (a), of 100 µM carbachol (CCh) (b) and of 300 µM $LaCl_3$ are indicated. Stippled lines indicate zero currents. Numbers over bars indicate the number of measured cells and of independent transfections. Significant differences were calculated as compared to basal CDs before application of stimuli. (mean±sem. two-tailed, paired t-test; *p<0.05, **p<0.01, ***p<0.001).

To investigate whether PIP_2 depletion indeed evokes a conformational change of the C-terminal region of TRPC5, dynamic FRET with HEK293 cells co-expressing the C-terminally CFP- and YFP-tagged TRPC5 construct was performed (Storch et al., 2015). Depletion of PIP_2 did result in decreased FRET signals, which indicates that the CFP- and YFP-tagged TRPC5 C-termini veer away from each other (data not shown). Additionally, dynamic FRET measurements using cerulean-tagged NHERF1 and eYFP-tagged TRPC5 constructs were performed (see Figure 15). Again, PIP_2 depletion caused decreasing FRET signals indicating that NHERF1 and TRPC5 move away from each other in the absence of PIP_2 (Figure 15a). Furthermore, NHERF1 separates from TRPC5 after simulation of cells with the endogenous muscarinic acetylcholine receptor agonist carbachol (Figure 15a). Thus, these findings confirm

our hypothesis that receptor activation results in PIP_2 cleavage and DAG formation that subsequently lead to NHERF dislocation from the C-terminus of TRPC5. TRPC5 now adapts to a new conformation that is sensitive to DAG. Interestingly, no alterations in FRET signals were observed upon PIP_2 depletion or stimulation with carbachol once the TRPC5 T972A mutant was expressed (see Figure 15b) while the pseudophosphorylated T972D mutant was still responsive to stimulation with both agents (Storch et al., 2015). This supports the electrophysiological findings that TRPC5 T972A is always susceptible to DAG because NHERF1 is not bound to the C-terminus of TRPC5. Since TRPC5 T972A is not bound to NHERF1, no change in FRET signals upon stimulation with wortmannin or carbachol was observed which would normally result in loss of NHERF1 binding with wild type TRPC5.

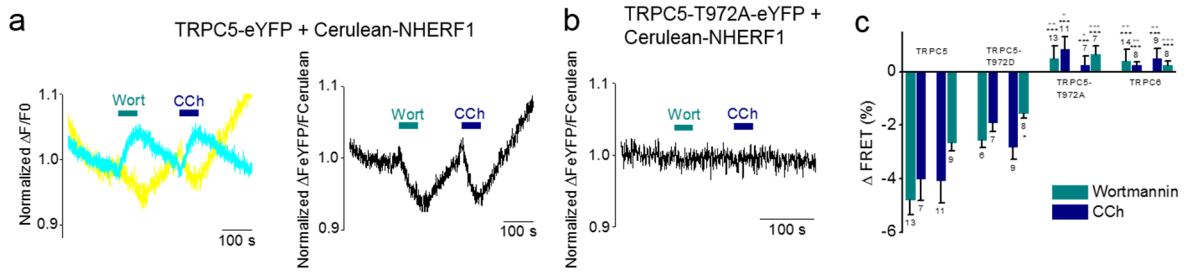

Figure 15: Phosphatidylinositol (3,4)-bisphosphate (PIP_2) depletion or $G_{q/11}$ protein-coupled receptor activation causes NHERF dissociation from the C-terminus of TRPC5. *Figure modified from Storch et al. (2015).* (a-c) Dynamic intermolecular FRET measurements with dual-emission photometry between N-terminally cerulean-tagged NHERF1 (Cerulean-NHERF1) and C-terminally eYFP-tagged TRPC5 (a) and C-terminally eYFP-tagged TRPC5-T972A (b). Applications of 20 µM wortmannin (Wort) and of 100 µM carbachol (CCh) are indicated. (a) Exemplary FRET measurement of TRPC5-eYFP and Cerulean-NHERF1 transfected HEK293 cells showing normalized fluorescence traces of cerulean (cyan) and eYFP (yellow) on excitation of 430 nm (left panel) and respective exemplary trace of the FRET signal (right panel). (b) Exemplary FRET signal of TRPC5-T972A-eYFP and Cerulean-NHERF1 transfected HEK293 cells. (c) Summary of changes of FRET signal amplitudes induced by wortmannin (cyan bars) or CCh (dark blue bars) in both orders of application. Numbers indicate the numbers of measured cells from at least 4 independent experiments. Significant differences as compared to wild-type TRPC5-eYFP expressing cells (mean±sem, two-tailed, unpaired t-test; **p<0.01, ***p<0.001, black asterisks). Significant differences as compared to TRPC5-T972D-eYFP expressing cells (mean±sem, two-tailed, unpaired t-test; **p<0.01, ***p<0.001, gray asterisk).

It is interesting to speculate on how PIP_2 depletion effects the C-terminal conformation of TRPC5. A direct binding of PIP_2 to the C-terminus of TRPC5 has never been demonstrated, although others reported that PIs, such as PIP_2 and phosphatidylinositol 3,4,5-trisphosphate (PIP_3), bind to the C-terminus of other TRPCs including TRPC1, -4α, -6 and -7 (Friedlova et al., 2010; Kwon et al., 2007; Otsuguro et al., 2008). In case of TRPC1, -6 and -7, PIP_3 binding

disrupts the binding of inhibitory calmodulin thereby activating the TRPC channels. The PIP_2 dependency of TRPC4 seems isoform-specific since only the longer TRPC4α isoform but not the shorter TRPC4β lacking 84 amino acids in the C-terminus was shown to be inhibited by PIP_2 (Otsuguro et al., 2008). Interestingly, Otsuguro and coworkers (2008) also reported that the PIP_2-dependent inhibition of TRPC4α was gone when the C-terminal TTRL motif was truncated. This is in accordance with our findings, which showed that the absence of NHERF (or the absence of PIP_2) leads to a conformational rearrangement of the C-terminus which subsequently confers OAG sensitivity to TRPC5. We postulate that the truncated TRPC4α establishes a new conformation that is incapable of binding to PIP_2 and is therefore susceptible to DAG. However, the DAG sensitivity of TRPC4 was not analyzed in greater detail. Therefore, subunit- or isoform-specific differences between TRPC4 and TRPC5 cannot be rigorously ruled out. In contrast to the above-mentioned TRPC channels, binding of PIs to the C-terminus of TRPC5 was not found (Kwon et al., 2007; Otsuguro et al., 2008). The binding of TRPC5 to PIP_2 might therefore be indirectly mediated by associated proteins. A possible PIP_2-binding partner could be the cytoskeletal protein spectrin.

Spectrins are large, cytoskeletal, and heterodimeric proteins composed of modular structure of α-and β-subunits that are crucial for the maintenance of cell stability, cell structure and cell shape (reviewed in Zhang et al., 2013). Furthermore, it is needed for diverse cellular functions including adhesion, spreading and cell cycle. A characteristic of spectrins are the 106 contiguous amino acid sequence motifs called spectrin repeats that are repeatedly present in all spectrin isoforms. There are two α- and five β-subunits of human spectrin (αI, αII, βI- βV). α- and β-subunits share approximately 30% similarity, and the subunits associate laterally to form anti-parallel heterodimers. These heterodimers then connect head-to-head to form heterotetrameric spectrin filaments that are linked by actin, thereby forming a pentagonal or hexagonal arrangement. The β-spectrins contain two binding sites for PIP_2: One located in the pleckstrin homology (PH) domain the other located in the N-terminal actin-binding site while α-spectrin contains no known PIP_2-binding sites (reviewed in Grzybek et al., 2006). Spectrins are known to associate with multiple proteins including TRPC4 (Odell et al., 2008), while TRPC5 and TRPC6 were shown to co-immunoprecipitate spectrin from rat brain (Goel et al., 2005).

Odell et al. (2008) demonstrated binding of TRPC4 depends on amino acids 730–754 in TRPC4 and on the last three spectrin repeats within αII spectrin. Comparison of TRPC4 and -5 shows that the binding site of spectrin is conserved in TRPC5 differing in only two amino acids while other TRPC proteins have less similarity in the putative spectrin-binding site (see Figure 16). It was shown that insertion of TRPC4 into the plasma membrane following activation of the epidermal growth factor receptor is accompanied by the dissociation of spectrin-TRPC4 interaction (Odell et al., 2008). Similar activation mechanisms can now be

postulated for TRPC5: In the non-agonist stimulated situation, the C-terminus of TRPC5 is occupied by NHERF and by spectrin, which in turn is bound to PIP_2. This TRPC5 conformation is not susceptible to endogenous DAG. However, upon activation of receptors and subsequent conversion of PIP_2 to DAG and IP_3, the TRPC5/spectrin/PIP_2/NHERF complex dissociates leading to a C-terminal rearrangement of TRPC5 and causing DAG sensitivity of the channel (see Figure 17).

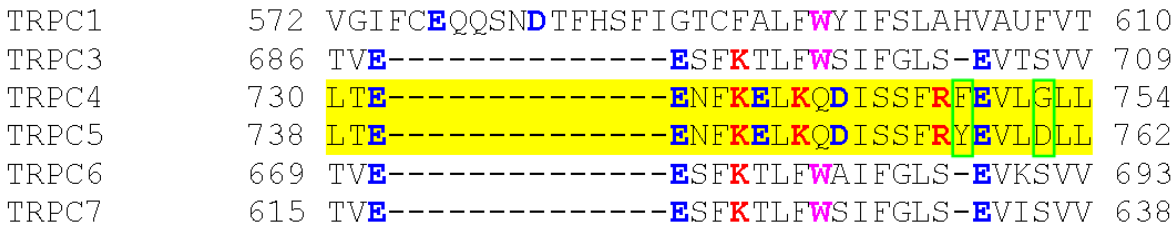

Figure 16: Sequence alignment of the putative spectrin-binding domain of human TRPC proteins. The putative spectrin-binding domain in TRPC4 and TRPC5 are highlighted in yellow. Negatively charged residues are indicated in blue while positively charged residues are shown in red. Highly conserved tryptophans are indicated in magenta. Green boxes highlight differences between TRPC4 and TRPC5.

The lipid dependency of TRPC5 channels has raised the question of whether TRPC5 channels can be mechanically activated as well. Gomis et al. (2008) proposed that hypoosmotic- and positive pressure-induced membrane stretch activates TRPC5 channels. In a follow-up study, the same group showed that activation of TRPC5 was likely subsequent to mechanically-induced and phospholipase C-dependent membrane translocation of TRPC5 to the plasma membrane (Jemal et al., 2014). These data argue against mechanically-gated TRPC5 channels and support our notion of mechanically activated $G_{q/11}$PCRs, which in turn enhance TRPC5 activity by regulating TRPC5 trafficking and PLC-dependent production of the TRPC5 activator DAG.

On the basis of our findings, we propose the following activation mechanism for TRPC4 and -5 channels (see Figure 17):

1. In the non-stimulated situation, the C-termini of TRPC4 and -5 are phosphorylated by PKC creating a binding site for NHERF. Additionally, the middle region of C-termini either binds to PIP_2 itself or binds a PIP_2-binding protein like spectrin. The resulting channel conformation is insensitive to DAG.
2. Agonist- or mechanically-induced activation of $G_{q/11}$PCRs results in the PLC-mediated conversion of PIP_2 to IP_3 and DAG.

3. PIP_2 depletion results in a rearrangement of the C-terminal region of TRPC4 and -5. This provokes NHERF1 to dislocate from TRPC4 and -5 making the channels accessible to DAG. It should be noted that in our investigation either NHERF1 depletion or PIP_2 depletion are sufficient to result in DAG-sensitivity of TRPC5. This suggests that the loss of NHERF1 at the C-terminus of TRPC5 can cause a TRPC5 re-conformation by itself.
4. The newly-adapted TRPC5 conformation is now susceptible to DAG that has been produced by PLC. TRPC5 is activated and channels sodium and calcium to the inside of the cell.

In summary, the findings from Storch et al. (2015) assert that receptor activation by mechanical stimuli or by the respective agonist results in PLC activation comprising PIP_2 cleavage and DAG formation. PIP_2 depletion leads to the dislocation of NHERF and reorganization of the TRPC4 and -5 channels arousing DAG sensitivity of TRPC5. Thus, TRPC4 and -5 channels are activated during receptor activation just like the other DAG-sensitive family members TRPC3, -6 and -7.

Non-stimulated:

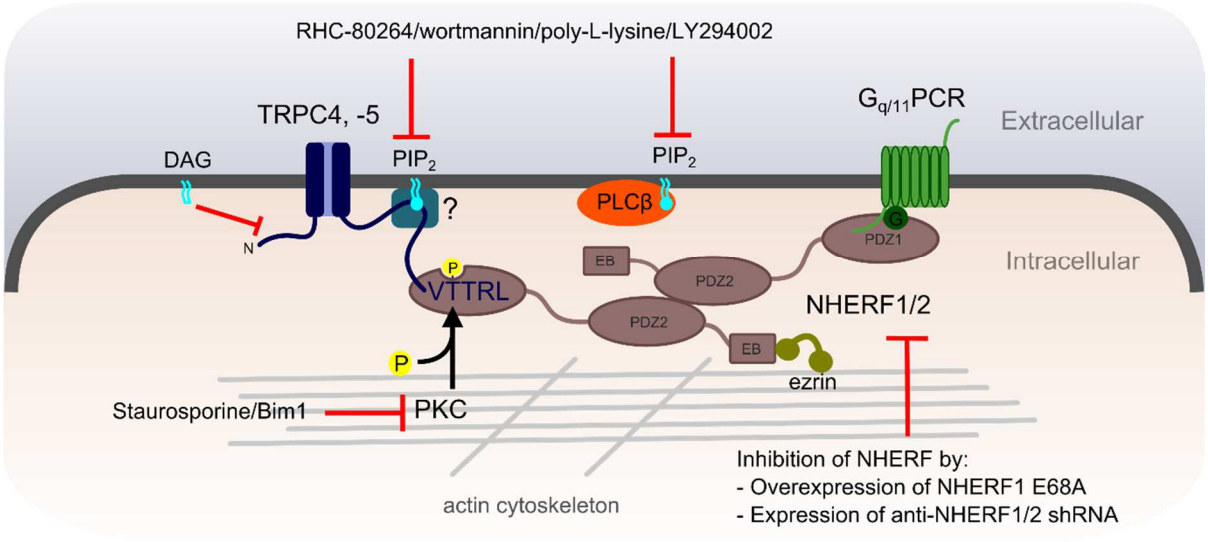

Stimulated:

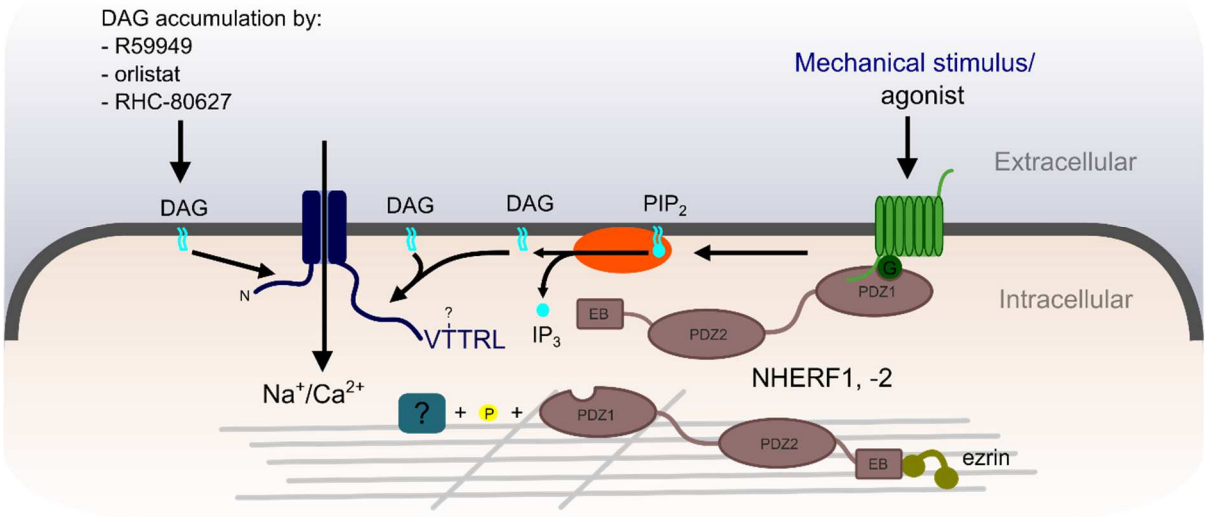

Figure 17: Proposed model of activation for TRPC4 and -5 channels. The channels are depicted in non-stimulated and non-diacylglycerol (DAG) sensitive situation (top) and in a stimulated, DAG-sensitive state (bottom). Additionally, possible intervention strategies causing DAG sensitivity of TRPC4 and -5 are listed. In the non-stimulated case, classical transient receptor channel TRPC4 and -5 are phosphorylated by phosphokinase C (PKC) and the C-terminus is either directly bound to phosphatidylinositol (3,4)-bisphosphate (PIP_2) or a PIP_2-binding protein (blue box) of unknown identity. This C-terminal conformation makes the VTTRL motif at the end of TRPC4 and -5 available for binding of the PDZ-containing adaptor proteins NHERF1 and -2. In this situation, TRPC4 and -5 are not susceptible to stimulation with DAG. However, if the $G_{q/11}$ protein-coupled receptors ($G_{q/11}$PCRs) are activated by mechanical stimuli or their respective agonists, phospholipase Cβ (PLCβ) converts PIP_2 to DAG and the second messenger inositol 1,4,5-trisphosphate (IP_3). Loss of PIP_2 in the vicinity of the TRPC channels results in a reconfiguration of the C-terminal region, triggering NHERF dislocation. The newly adapted TRPC4 and -5 conformation now makes the channels sensitive to stimulation with DAG.

Mechanosensitive elements in smooth muscle cells: Role of AT_{1B}

Arterial smooth muscle cells are intrinsically mechanosensitive cells that respond to increased internal pressure with vasoconstriction while vascular smooth muscle cells of larger vessels passively enlarge their diameter in order to maintain vascular tone (Bayliss, 1902). Previous studies have highlighted the importance of mechanically activated $G_{q/11}$PCRs in vascular smooth muscle cells in small resistance arteries and arterioles (Mederos y Schnitzler et al., 2008). Importantly, the activation of $G_{q/11}$PCRs occurred in an agonist-independent manner. In our study, the importance of various $G_{q/11}$PCRs in the signaling cascade leading to myogenic vasoconstriction was employed by comparing mRNA expression levels in resistance versus non-resistance arteries (Blodow et al., 2014). The expression of angiotensin AT_{1B}, vasopressin V_{1A}, endothelin ET_A, endothelin ET_B, adrenoceptors α_{1A}, α_{1B}, α_{1D}, and α_{2B} receptors in small resistance arteries was significantly enriched. Subsequent pharmacological blockage of the $G_{q/11}$PCRs showed that only AT_{1A}, AT_{1B}, ET_A and the α_1 receptors contributed to myogenic vasoconstriction. Interestingly, the selective suppression of the receptors by antagonists or reverse agonists showed a pressure dependency: Blockage of ET_A resulted in a suppressed myogenic tone at middle pressure ranges, blockage of AT_1 receptors resulted in impaired myogenic tone at middle-high internal pressures while inhibition of α_1 receptors led to suppression of myogenic tone at high pressures. This suggests that the receptors have individually distinct thresholds for mechanical activation and work in tandem to cover the whole physiologically relevant spectrum.

Of all the tested receptors, blockage of AT_1 receptors showed the most pronounced effect (Blodow et al., 2015). In contrast to humans, rodents possess two AT_1 receptor isoforms: AT_{1A} and AT_{1B}, both of which are very similar in structure and function (Tian et al., 1996) and cannot be rigorously differentiated by antibodies and blockers. The high expression of AT_{1B} compared to AT_{1A} was intriguing since it suggests that the AT_1 receptor isoforms have distinctly different functions. This notion is in accordance with studies using mice with a disrupted angiotensin signaling: AT_{1A}-deficient mice have reduced blood pressure but normal myogenic tone while AT_{1B}- and angiotensinogen-deficient mice have normal blood pressure but reduced myogenic tone (Chen et al., 1997; Tanimoto et al., 1994). See Table 2 for an overview of the mice with disrupted angiotensin systems, their blood pressure and myogenic tone. Interestingly, double AT_1-deficient mice have reduced blood pressure and show abnormal behavior to infusion of angiotensin II but respond normally to the vasoconstrictor epinephrine (Oliverio et al., 1998). Additionally, $AT_{1A/B}^{-/-}$ mice have diminished growth, vascular thickening within the kidney and atrophy of the inner renal medulla very much similar to angiotensinogen- and angiotensin-converting enzyme-deficient mice that are unable to synthesize angiotensin II. These data

support the notion of agonist-independent activation of AT_1 receptors and indicate distinctly different functions of the AT_1 receptor isoforms.

Mice	Blood pressure (mmHg)	Myogenic tone compared to wild type	References
$AT_{1A}^{-/-}$	Reduced: 89 ± 4 (systolic)	Reduced to 90%	(Blodow et al., 2014; Ito et al., 1995)
$AT_{1B}^{-/-}$	Unaffected: 114 ± 3	Reduced to 70 %	(Blodow et al., 2014; Oliverio et al., 1998)
$AT_{1A/1B}^{-/-}$	Reduced: 87 ± 3 (systolic)	Increased at low pressure ranges (10–80 mmHg), reduced to ~70% at high pressure ranges (90–120 mmHg)	(Oliverio et al., 1998; Storch et al., 2014)
$Agt^{-/-}$	Reduced: 67 +/- 4 (systolic)	Unaffected	(Blodow et al., 2014; Tanimoto et al., 1994)

Table 2: An overview of the properties of mice with a disrupted angiotensin system. Blood pressure values as well as reduction of myogenic tone of the gene-deficient mice compared to wild type mice and the relevant literature are listed. Abbreviations: AT1 = angiotensin II type1; Agt = angiotensinogen.

To investigate whether the pronounced role of AT_{1B} receptors in VSMCs was the result of higher receptor density, VSMCs were isolated and mechanically stimulated with hypotonic solution (Blodow et al., 2014). Interestingly, calcium recordings of freshly isolated VSMCs showed that VSMCs expressing only AT_{1B} were more sensitive to mechanical stimulation experiments in comparison to the VSMCs that solely expressed AT_{1A}. However, these results can be explained by much higher expression levels of AT_{1B} in AT_{1A}-deficient VSMCs as compared to AT_{1A} levels in AT_{1B}-deficient VSMCs and do not necessarily promote the idea of a more mechanosensitive AT_{1B} isoform. The question of a more mechanosensitive AT_{1B} receptor was addressed in experiments with cultured VSMC that exhibited similar AT_1 isoform levels. Calcium recordings revealed that VSMCs expressing only AT_{1B} proteins were significantly more sensitive to hypotonic stimulation in comparison to VSMCs expressing equal amounts of AT_{1A}, thereby supporting the hypothesis of a more mechanosensitive AT_{1B} isoform. However, loss of AT_{1B} accounted only for around 50% reduction in myogenic tone after blockage of AT_1R using losartan or 30% in AT_{1B}-deficient arteries, suggesting that other signaling pathways besides AT_1Rs might participate in myogenic tone. Surprisingly, a follow-up study by our own group showed that $AT_{1A/1B}$ double gene-deficient arteries exhibited an increased myogenic tone at low and a reduced myogenic tone at high intraluminal pressures

respectively (Storch et al., 2014). Double AT_1R-deficient mice have previously been shown to have reduced blood pressure but seemed unimpaired in their responsiveness to epinephrine (Oliverio et al., 1998). Additionally, mice without AT_1Rs show abnormalities in growth and body weight and kidney morphology as well as reduced survival rate, thereby highlighting the importance of AT_1Rs in viability and health. Since AT_1Rs are of pivotal importance for the regulation of blood flow, it seems likely that compensation mechanisms occur when AT_1Rs are missing. Indeed, Storch et al. (2014) found that the $G_{q/11}PCR$ $CysLT_1R$ was up-regulated in AT_1Rs-deficient arteries as an essential backup strategy to compensate for the loss of AT_1Rs. Up-regulation of $CysLT_1R$ explains the increased myogenic tone at low intraluminal pressure: $CysLT_1Rs$ possess a higher sensitivity for mechanical stimuli at low pressure ranges as compared to AT_1Rs resulting in hyperactivity of AT_1R-deficient arteries. However, at high intraluminal pressures, mechanical activation of $CysLT_1Rs$ cannot compensate for the loss of AT_1Rs, thereby explaining the reduced myogenic tone at higher pressure ranges. Interestingly, simultaneous loss of AT_1Rs and $CysLT_1Rs$ reduced myogenic tone to a total of 40% in comparison to wild type arteries. This implies that agonist-independent mechanical activation of $G_{q/11}PCRs$ AT_1Rs and $CysLT_1Rs$ determines roughly 60% of the myogenic tone. These results could be verified by using the selective $G_{q/11}$ protein blocker YM-254890 on wild type arteries. YM-254890 blocked myogenic tone to a similar extent as observed after simultaneous blockade of AT_1Rs and $CysLT_1Rs$, indicating that myogenic vasoconstriction is mainly mediated through the $G_{q/11}$ protein pathway.

Since mechanical activation of GPCRs does not account for 100% of myogenic tone, other intrinsic mechanosensitive proteins are likely to be involved. For example, $G_{i/o}PCRs$ or G_sPCRs could function as mechanosensors in VSMCs conveying force to cation channels. There are several studies that have reported mechanotransduction properties of both receptor types (Abdul-Majeed and Nauli, 2011; Makino et al., 2006; Zhang et al., 2009). Recent investigations have even revealed that the mechanotransducing TRPC4 and TRPC5 channels can be activated by the activation of $G_{\alpha i}$ subunits or by the G_s protein cascade involving cAMP (Hong et al., 2012; Jeon et al., 2013). Apart from GPCRs, PLA_2 isoforms could convey the mechanical stimulus to TRPC proteins. It has previously been shown that PLA_2 isoforms are indeed expressed in VSMCs and that mechanical activation of PLA_2 results in activation of TRPC6 (Inoue et al., 2009). PLA_2 liberates AA from the plasma membrane that is metabolized to 20-hydroxyeicosatetraenoic acid (20-HETE). The presence of 20-HETE was shown to potentiate TRPC6 activity (Inoue et al., 2009), but it is also known to be a potent myogenic vasoconstrictor by blocking potassium channels inside the cell which subsequently results in membrane depolarization (Roman and Harder, 1993).

On the basis of the findings from Blodow et al. (2014) and the relevant literature, we therefore propose the following mechanism for the regulation of myogenic tone in VSMCs (see Figure 18):

1. Increased intraluminal pressure results in mechanical activation of the mechanosensing GPCRs, including the highly mechanosensitive $G_{q/11}$PCR AT_{1B} and $CysLT_1$ receptor. Another mechanosensory element could be PLA_2 that generates AA. AA is converted to 20-HETE, a known potentiator of TRPC6 and blocker of potassium channel activity.
2. AT_{1B} and $CysLT_1$ receptors activate their associated $G_{q/11}$ proteins, which subsequently activate PLC.
3. PLC converts PIP_2 into inositol 1,4,5-trisphosphate (IP_3) and DAG.
4. Activation of the mechanotransducing TRPC channels by DAG results in depolarization of the membrane potential. Depolarization causes an increase in the open probability of L-type voltage-gated calcium channels resulting in calcium entry. Elevation of the free intracellular calcium concentration ends in vasoconstriction.

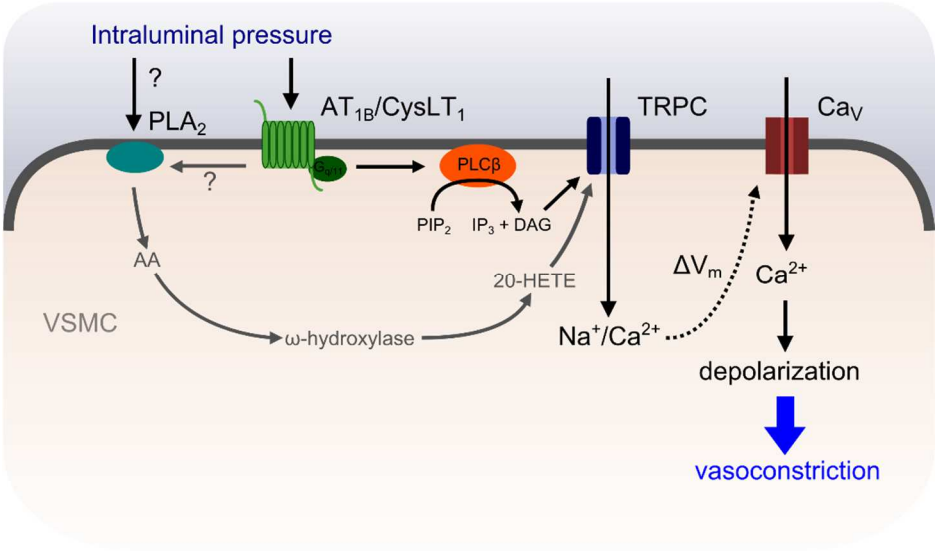

Figure 18: Mechanical activation of $G_{q/11}$ protein-coupled receptors ($G_{q/11}$PCRs) in vascular smooth muscle cells (VSMCs). The $G_{q/11}$PCRs angiotensin II type 1B (AT_{1B}) and cysteinyl leukotriene 1 receptors ($CysLT_1$Rs) are activated by increased intraluminal pressure. Activation of associated $G_{q/11}$ proteins activates TRPC channels resulting in an influx of cations. This results in a depolarized membrane potential (V_m) that subsequently opens voltage-gated L-type calcium channels (Ca_V). Calcium entry via Ca_V channels further depolarizes the cell that terminates in myogenic vasoconstriction. Activation of $G_{q/11}$PCRs accounts for roughly 60% of myogenic tone while the remaining 40% might be explained by mechanical activation of the mechanosensory element phospholipase A2 (PLA_2). PLA_2 potentiates TRPC currents via liberation of archidonic acid (AA), which is converted to 20-HETE by ω-hydroxylase. Additionally, 20-HETE can induce myogenic vasoconstriction by blocking potassium channels, which results in depolarized membrane potentials (pathway not shown).

In summary, the findings from Blodow et al. (2015) demonstrate that besides mechanosensitive cation channels of unknown identity, the ligand-independent activation of mechanosensitive $G_{q/11}$PCRs like CysLT_1R and AT_1Rs is responsible for up to 60% of myogenic tone. Special attention needs to be paid to the mechanosensory properties of the rodent AT_{1B}, which is more mechanosensitive than AT_{1A}. Humans do not possess two AT_1 receptor isoforms but seemingly combine the properties of AT_{1A} and AT_{1B} in one protein. A detailed understanding of the cellular mechanisms that are pertinent to myogenic vasoconstriction will help to identify new therapeutic targets in order to treat diseases with dysfunctional myogenic vasoconstriction such as systemic hypertension, diabetes, and stroke.

Mechanosensitive elements in podocytes: Role of P_2X channels

Podocytes are highly specialized visceral epithelial cells lining the Bowman's capsule in the kidneys that wrap around the capillaries of the glomerulus (see Figure 19, left). Podocytes contain a major body as well as major and secondary foot processes. The secondary processes are actin-rich and interdigitate with neighboring foot processes. These foot processes are bridged by special zipper-like dynamic protein-protein interactions called the slit membrane. Slit membrane proteins include cell-cell linker proteins such as nephrin and Neph1-3, regulatory proteins like the stomatin family member podocin or the ion channel TRPC6, and the actin-associated proteins CD2-associated protein (CD2AP) and synaptopodin (see Figure 19, right). Like other cell-cell contacts, the slit membrane is pivotal to the maintenance of cell polarity, cell survival and actin dynamics (for review see Huber and Benzing, 2005). However, the slit membrane is unique among other cell-cell contacts in serving as a filtration barrier that prevents loss of macromolecules to the urine. This observation was made after it became obvious that the loss of slit membrane components results in heavy proteinuria (summarized in Akchurin and Reidy, 2015; Machuca et al., 2009 and Zenker et al., 2009).

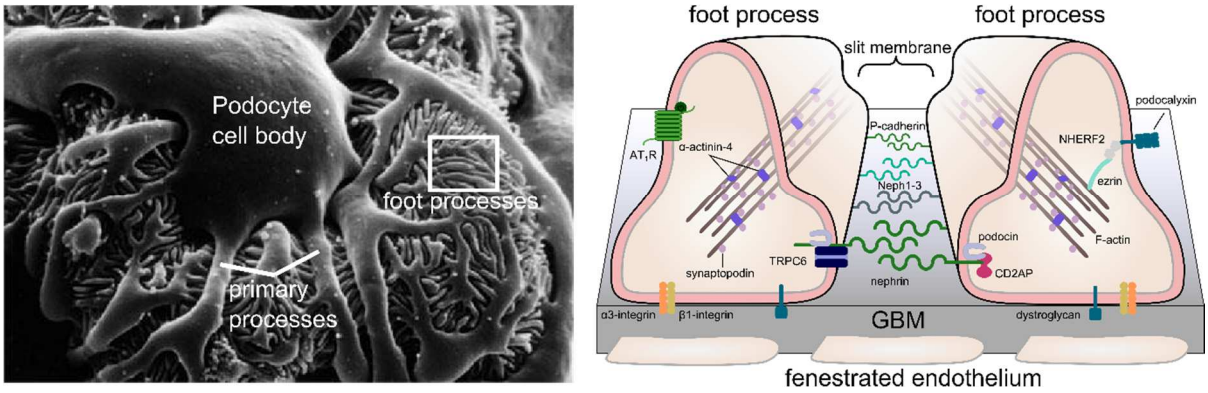

Figure 19: Podocyte structure and function. Left: *Image adapted from Smoyer and Mundel, 1998.* Scanning electron microscope micrograph of a glomerular podocyte as seen from the urinary space. The podocytes wrap the underlying capillaries completely with their major cell body from which thick primary processes branch. Primary processes further ramify into small foot processes that interdigitate with adjacent foot processes. Right: Schematic drawing of two adjacent podocyte foot processes sitting on top of the glomerular basal membrane (GBM). The foot processes are connected to each other by special protein-protein interactions called the slit membrane. Several proteins shown to be essential for proper podocyte function are depicted. Abbreviations: AT_1R = angiotensin II type 1 receptor, CD2AP = CD2-associated protein.

The slit membrane as well as the apical site of the podocytes are constantly exposed to mechanical stress generated by blood flow through the glomerular capillaries. Podocytes respond to high mechanical load, for instance, in diseases like hypertension, with retraction of

their foot processes that result in the loss of ultrafiltration barrier and therefore loss of proteins to the urine. This process is reversible and provides a protection mechanism for podocytes counteracting high-pressure situations. The mechanisms of sensing mechanical stimulation in podocytes is poorly understood, although several studies suggest that TRPC6 expressed at the slit membrane of podocytes could form a mechanosensitive ion channel complex (Huber et al., 2006). TRPC6 *per se* is not intrinsically mechanosensitive (Gottlieb et al., 2008; Mederos y Schnitzler et al., 2008), but podocytes express the MEC-2 homologue podocin. Podocin has been shown to regulate the activity of TRPC6 in a cholesterol-dependent manner (Huber et al., 2006). This has led to the hypothesis that a TRPC6/podocin channel complex could respond directly to deformation of the plasma membrane similar to the Deg/ENaC/MEC-2 channel complex that is known to transduce gentle touch in *C. elegans* (compare illustrations in Figure 20). In this scenario, podocin would alter the local lipid environment surrounding the TRPC6 channel, thereby facilitating the ability of TRPC6 to respond to mechanically-induced deformations in the plasma membrane.

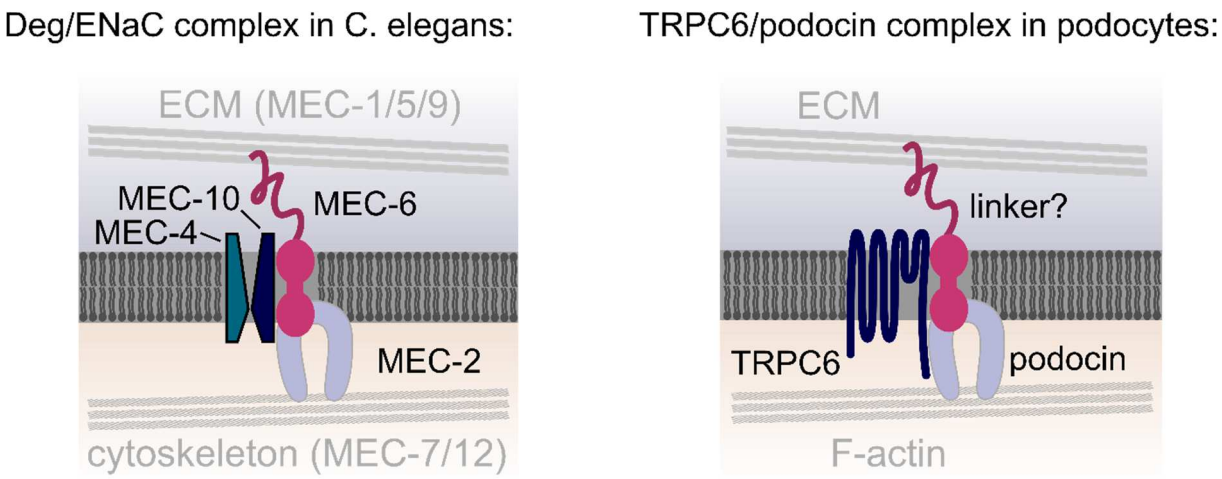

Figure 20: Schematic representation of the mechanosensitive ion channel complex Deg/ENaC in C. elegans and a putative ion channel complex containing TRPC6 in podocytes. In C. elegans, the mechanosensitive ion channel complex contains the ion channel-forming proteins MEC-4 and MEC-10, which are linked to the extracellular matrix (ECM) via MEC-6 and to the intracellular matrix via MEC-2. In podocytes, the classical transient receptor potential channel 6 (TRPC6) binds to the MEC-2 homologue podocin which is linked to F-actin fibers. Abbreviations: Deg/ENaC = degenerin/epithelial Na^+ channel.

To investigate the possibility of a TRPC6-containing mechanosensitive ion channel complex in podocytes, the mechanotransduction properties of murine podocytes were carefully analyzed with the use of conventional whole-cell recordings (Forst et al., 2015). Mouse podocytes from healthy three-week-old mice were isolated by using the sieve method and maintained the podocytes in culture for 10 days before experiments were performed. This

podocyte isolation protocol was successfully used previously by our own group to show native TRPM7 expression and PLCε-induced TRPC6 activation in podocytes (Chubanov et al., 2012; Kalwa et al., 2014). Additionally, our findings were confirmed by using differentiated conditionally immortalized murine podocytes. These podocytes are isolated from the Immortomouse and can be cultured at permissive conditions, that result in a proliferating phenotype and at non-permissive condition, that result in fully differentiated podocytes successfully expressing podocyte markers and constructing a slit membrane-like structure (Shankland et al., 2007). To ascertain that the primary podocytes and the conditionally immortalized cells were indeed podocytes, the expression of several podocyte-specific markers on mRNA level was confirmed. In addition, expression of podocin and nephrin was confirmed on the protein level. Morphologically, cultivated cells at Day 10 were morphologically large (up to 300 µm), flat, often binucleated and arborized cells with well-developed processes—a phenotype that resembles *in viv*o podocytes (Shankland et al., 2007). Dissociated cells usually presented less-pronounced processes, while the other characteristics did not alter. In whole-cell recordings, the large cell membrane capacity of roughly 71 pF (n = 362) for primary podocytes and 63 pF (n = 52) for conditionally immortalized podocytes was another useful criterion to distinguish podocytes from fibroblast (maximum of 50 pF), juxtaglomerular (3 pF) or endothelial cells (12 pF) (Friis et al., 1999; Walsh and Zhang, 2008; Zhang et al., 2008). Although several criteria were used to ascertain that our cells were indeed podocytes, it cannot rigorously be ruled out that cross-contaminations with other cell lines like fibroblast especially in multi-cell experiments were present. One way to circumvent this problem would be to use transgenic mice that express a reporter protein under the control of a podocyte-specific promoter. An example would be the double fluorescent Cre reporter mouse that carries a loxP-flanked Tomato cassette. Upon Cre-mediated excision of mTomato, the alternate reporter membrane-targeted GFP (mGFP) is expressed (Muzumdar et al., 2007). Placing the Cre recombinase placed under the control of the *NPHS2* promoter would result in green fluorescent podocytes while all the other cells would express the red fluorescent mTomato. In this way, the efficiency of the isolation could be assessed by using a fluorescent approach. Additionally, automated sorting of cells based on their fluorescence can be performed after isolation and culturing of the cells. Alternatively, instead of controlling mRNA expression of several podocyte-specific markers of a whole podocyte population, single-cell mRNA levels could be investigated by using single-cell polymerase chain reaction.

To mechanically stimulate the cells used in our study, cells were perfused with a 240 mOsmol•kg^{-1} hypotonic solution containing the same ions as the normal bath solution that was supplemented with mannitol to 300 mOsmol•kg^{-1}. Perfusion of cells with a hypotonic solution results in approximately 148.4 kPa osmotic pressure at room temperature using the Morse equation leading to water influx into the cell and, therefore, to membrane stretch.

However, hypotonic solution has several adverse effects, which include pH shifts and dilution of internal factors like calcium. These adverse effects were controlled by using a pipette solution containing 10 mM BAPTA resulting in 100 nM free calcium. Since the pipette solution is connected to the internal site of the cell in the whole-cell configuration, the inside of the cell is completely buffered with the pipette solution. Consequently, large pH shifts or change of calcium concentrations upon perfusion with hypotonic solution are not expected. Additionally, our findings using hypotonic solution were confirmed by the inflation of cells using the patch pipette.

Mechanical probing of our podocytes resulted in characteristic inward rectifying cation currents regardless of the mechanical stimulation used (Forst et al., 2015). These mechanically-evoked currents were not mediated by TRPC6 channels, since mechanically-evoked cation conductance persisted in podocytes isolated from TRPC6-deficient and TRPC1/C3/C6-deficient mice. The participation of any TRPC channel was ruled out by using the non-selective TRPC channel blocker SKF-96365. Control and TRPC1/C3/C6-deficient podocytes exhibited normal cation conductance upon mechanical activation that clearly ruled out the involvement of TRPC6 channel in mechanotransduction.

Even heterologous expression of TRPC5 (data not shown) or TRPC6 in HEK293 cells in combination with podocin and other slit membrane proteins mimicking the mechanosensitive ion channel complex found in podocytes failed to be activated by membrane stretch (Forst et al., 2015). These results do not support the hypothesis that any TRPC channel is either a mechanosensitive or a mechanostransducing element in podocytes. This is in contrast to observations made by the research group of Dryer (2013), who used conditionally immortalized murine podocytes and primary podocytes attached to glomerular capillaries in *ex vivo* glomerular explants that were mechanically probed with either a hypotonic solution or a second patch pipette that gently touched the cell (Anderson et al., 2013). Similar to our findings, the research group led by Dryer reported that their podocytes responded to mechanical stimulation with increased current amplitudes. However, the currents were outward rectifying as against our study in which only inward rectifying cation currents were observed. The stretch activation was blocked by reduction of TRPC6 proteins using siRNA, and in the presence of SKF-96365, while it persisted in the presence of PLC and PLA_2 inhibitors. Additionally, the present authors used the peptide GsMTx4 to block mechanosensitive channels receiving the force from the plasma membrane. The authors conclude from their results that TRPC6 senses the mechanical stimuli and is activated by force transmission transmitted to the channel through the plasma membrane. Additionally, knock-down of podocin markedly increased stretch-evoked activation of TRPC6 while activation of TRPC6 channels using the membrane-permeable DAG analogue OAG was nearly abolished. These results led the authors to conclude that podocin acts as a switch to determine the preferred mode of TRPC6 activation:

At the slit membrane, podocin interacts with TRPC6 and renders the channel mechanosensitive while the cell body contains no podocin, thereby leaving TRPC6 susceptible to DAG.

The results from Anderson et al. (2013) differ strongly from our own observations (Forst et al., 2015), but can be explained by several methodical differences between our respective studies: First, Anderson and coworkers (2013) used a hypotonic solution that was made by diluting the normal bath solution with 30% water. The resulting hypotonic solution contains fewer ions compared to the undiluted bath solution, which might already be sufficient to activate ion channels that are normally inhibited by the ion concentration present in the normal bath solution. Additionally, as a result of the altered ion concentrations, the equilibrium potentials between the iso- and hypotonic bath solutions are different, which will likely result in shifted reversal potentials upon stimulation with hypotonic solution (see Supplementary Table 3 for comparison). Indeed, the observed reversal potentials in the study by Anderson and coworkers (2013) shift from approximately $E_{rev\ (iso)}$ = -56.0 mV in isotonic solution to more positive potentials ($E_{rev\ (hypo)}$ = -33.4 mV) in hypotonic solutions (see Figure 21). If one calculates a hypothetical mixed potential of the monovalent cations cesium and sodium, under the presumption that both ions have a similar permeability, the monovalent cations' potential in the study from Anderson et al. (2013) would be $E_{rev\ Cs+Na\ (iso)}$ = -11,2 mV in isotonic bath solution and $E_{rev\ Cs+Na\ (hypo)}$ = -29,4 mV in hypotonic bath solution. The highly negative reversal potential observed in the isotonic bath solution in the study by Anderson et al. (2013) does not match the hypothetical mixed potential, thereby suggesting that the cell is permeable to other ions besides sodium and cesium. Since the observed reversal potential is more negative than sole cation conductance would suggest, it is likely that chloride conductance was measured as well. This would also explain why the reversal potential shifts to more positive potentials in the hypotonic solution. Additionally, activation of chloride-permeable channels upon stimulation with hypotonic solution is consistent with many previous studies reporting that hypotonic solution activates the chloride channel VRAC that is present in every cell (for review see Nilius et al., 2000). Indeed, the outwardly rectifying currents observed by Anderson et al. (2013) are strikingly similar to VRAC-mediated currents, which were also observed in our own podocytes (compare graphs in Figure 21). Due to the high VRAC activity in podocytes, chloride channel blockers were added to all our bath solutions in order to ensure that only cation conductance was measured. Indeed, the reversal potentials observed in our own study were always around 0 mV which is consistent with a hypothetical monovalent cations potential $E_{rev,\ Cs+Na}$ = -3.4 mV under the assumption that the cesium potential is -65 mV. Finally, in contrast to the study by Anderson et al. (2013) that reduced TRPC6 levels by using siRNA, our study used podocytes isolated from TRPC-deficient mice. Transfection of cells with siRNA has the general disadvantage of the possibility of adversely regulating other offsite targets. Consequently,

stretch-induced currents might be absent although they might not be mediated by TRPC6. Furthermore, our own findings do not promote the notion that TRPC channels are subsequently activated by mechanically activated $G_{q/11}$PCRs, since blockage of $G_{q/11}$-protein activation by inhibitor YM-254890 had no effect on stretch activation. Additionally, the non-selective P_2Y blocker suramin was used. The presence of suramin also had no effect on mechanically-induced currents, thereby confirming that $G_{q/11}$PCRs of the P_2Y family are not mechanotransducers. Rather, it was shown that mechanically induced cation currents were mediated by purinergic P_2X channels (Forst et al, 2015).

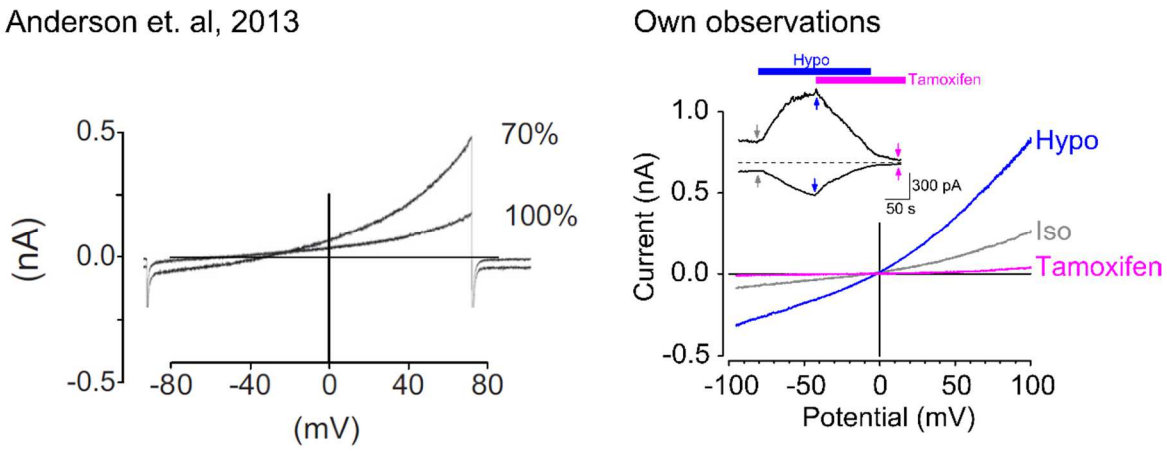

Figure 21: Comparison of hypotonically-induced currents in murine podocytes. Left: Current-voltage relationship of conditionally immortalized mouse podocytes patched in the whole-cell configuration stimulated with hypotonic solution that was diluted with water to 70% of the original bath solution (100%) in absence of chloride channel blockers. Hypotonic solution induces a current that is strikingly similar to VRAC-mediated currents. Reversal potentials are approximately E_{rev} = -56.0 mV before and E_{rev} = -33.4 mV after application of hypotonic solution. *Image modified from Anderson et al., 2013. For a better comparison of the currents, the grid lines x=0 and y=0 were added.* Right: Current-voltage relationship and mean currents at -100 mV and +100 mV over time (inlet) of primary isolated mouse podocytes measured in the whole cell configuration in the absence of chloride channel blockers. Forst et al. (2015) used an isotonic bath solution (iso) that was supplemented with mannitol to 300 mOsmol•kg^{-1}. Hypotonic solution contained no mannitol and had an osmolarity of 240 mOsmol•kg^{-1}. Currents seen under hypotonic solution (hypo) were clearly mediated by chloride channels since the chloride channel blocker tamoxifen could block the observed currents (tamoxifen). Reversal potentials for currents before (iso), during hypotonic solution (hypo) and in the presence of tamoxifen are always E_{rev} = 0.0 mV.

P_2X channels form a family of non-selective cation channels with seven family members (P_2X_1 to P_2X_7) that open in response to extracellular ATP. The N- and C-termini of purinergic channel face the inside of the cell and three channel subunits are needed to form a functional ion channel. P_2X channels are distinct from the P_2Y family which are purinergic GPCRs, and are

widely expressed in a variety of tissues. The activation of purinergic receptors results in increased intracellular calcium levels, thereby regulating diverse cellular functions (for review see North, 2002). Purinergic channels can be pharmacologically discriminated by their sensitivity to ATP and its derivatives, their desensitization kinetics in the presence of ATP, and several purinergic channels blockers such as suramin, TNP-ATP or the specific P_2X_4 channel blocker 5-BDBD. By using quantitative RT-PCR, it was confirmed that podocytes do express all purinergic channels (Forst et al., 2015). Remarkably high levels were found for P_2X_2 and P_2X_4. P_2X_2 and P_2X_4 are unique among the purinergic channels because of their slow desensitization kinetic in the presence of ATP (see Table 3 for a summary of several P_2X characteristics).

Channel	ATP EC_{50} in µM	Desensitization kinetic using 100 µM ATP	Suramin IC_{50} in µM	TNP-ATP IC_{50} in µM	5-BDBD IC_{50} in µM	Ivermectin EC_{50} in µM	Binding partners	Expression profile in podocytes
P_2X_1	1	Fast: <100 ms	1	0.006	na	na	P_2X_1, P_2X_2, P_2X_3, P_2X_5, P_2X_6	Low
P_2X_2	10	Slow: >5 s	10	10	na	na	P_2X_1, P_2X_2, P_2X_3, P_2X_5, P_2X_6	High
P_2X_3	1	Fast: <100 ms	3	0.001	na	na	P_2X_1, P_2X_2, P_2X_3, P_2X_4, P_2X_5, P_2X_6,	Moderate
P_2X_4	10	Slow: 5-10 s	>300	15	0.5	0.25	P_2X_4, P_2X_5, P_2X_6, P_2X_7(?)	High
P_2X_5	10	Slow, but current amplitude is very low (~50 pA)	4	na	na	na	P_2X_1, P_2X_2, P_2X_5, P_2X_6,	Moderate
P_2X_6	Not expressed at plasma membrane	na	na	na	na	na	P_2X_1, P_2X_2, P_2X_4, P_2X_5	Moderate
P_2X_7	100		~500	>30	na	na	P_2X_4 (?), P_2X_7	Moderate

Table 3: Overview of the several P_2X properties including response to ATP and desensitization kinetics and sensitivity to several inhibitors. Question mark indicates binding partners that were only found in heterologous expression systems. Abbreviations: na = not applicable, because values are not available. Sources: (Balazs et al., 2013; Forst, 2015; North, 2002; North and Surprenant, 2000; Priel and Silberberg, 2004)

The expression of purinergic channels on protein level was confirmed by the stimulation of podocytes with ATP. Perfusion of cells with 100 µM ATP maximally activated large inward rectifying currents with a slow desensitization kinetic lasting approximately 40 seconds, suggesting activation of the slowly inactivating P_2X_2 and P_2X_4 channels. The slow desensitization kinetic seen under ATP perfusion confirms that mainly P_2X_2 or P_2X_4 are expressed in these cells, since the other P_2X channels have a faster inactivation kinetic (P_2X_1, P_2X_3, P_2X_5) or do not desensitize in the presence of ATP (P_2X_7).

Interestingly, the currents observed under ATP stimulation were remarkably similar to the currents observed under membrane stretch, thereby insinuating that the same channels are activated under ATP stimulation and membrane stretch (Forst et al., 2015). With the use of several P_2X channel blockers, it could be shown that membrane stretch mainly activates P_2X_4 channels in podocytes. This conclusion was based on the following observations: First, blockage of stretch evoked currents was not reduced in the presence of 50 µM suramin. This concentration is, however, sufficient to block all purinergic channels except P_2X_4 and P_2X_7. Second, blockage of P_2X channels by using 75 µM TNP-ATP reduced mechanical currents. This concentration inhibits all P_2X channels except P_2X_7, suggesting that P_2X_4 is the main mediator of the mechanically induced currents. Third, specific blockage of P_2X_4 using 5-BDBD significantly reduced mechanically-induced currents while the specific P_2X_4 potentiator ivermectin resulted in increased mechanical response. Last, P_2X_4-deficient podocytes were clearly impaired in their response to membrane stretch. These results clearly support the importance of P_2X_4 channels as mechanotransducing elements in podocytes. However, it should be kept in mind that the mechanical response was never completely gone although 5-BDBD and TNP-ATP did reduce the currents to 35% and 25% respectively. This can be explained by the formation of heteromeric P_2X_4/P_2X_2 or P_2X_4/P_2X_7 channels that are not inhibited by either 5-BDBD or TNP-ATP.

The researcher group led by Dryer support the finding that podocytes respond to extracellular ATP (Roshanravan and Dryer, 2014). However, in contrast to our findings, Roshanravan and Dryer (2014) suggested that podocytes respond to extracellular ATP with activation of P_2Y receptors that in turn activate TRPC6 channels Similar to Dryer's previous study (2013), Roshanravan and Dryer (2014) used conditionally immortalized murine podocytes and primary podocytes still attached to the glomerulus that were probed with extracellular ATP. Perfusion with 10 µM ATP evoked a robust current that was inhibited by 100 µM suramin. Additionally, the present authors observed that ATP-induced currents were gone when TRPC6 levels were reduced by using siRNA and by treating podocytes with SKF-96365 or the TRPC1/3/6 channel blocker lanthanum chloride. Furthermore, the ATP effect was reduced when the G-protein signaling was disrupted by GDP-β-S or incubation of cells with the PLC/PLA_2 inhibitor D-609. These results led the authors to conclude that ATP activates the $G_{q/11}$ protein-coupled P_2Y

receptors that signal to TRPC6 in a G protein-dependent way. Surprisingly, ATP-evoked currents were also suppressed when podocin was absent. These observations are in striking contrast to the findings of our own study. An effect of suramin or the G protein blocker YM-254890 on mechanically induced currents was never observed. Additionally, the presence of GDP-β-S in pipette solution did not block G protein signaling although an altered inward rectification upon mechanical activation was seen (data not shown). Furthermore, no altered ATP-evoked currents were observed in podocytes with reduced podocin levels. Again, the discrepancies in our studies and the study by Roshanravan and Dryer (2014) can be explained by the lack of chloride channel blockers in their study. The presented current-voltage relationships in this study are consistent with leak currents or the activation of the outwardly rectifying chloride channels. Additionally, it was shown some time ago that extracellular ATP can induce chloride channel currents through activation of P_2Y receptors (Darby et al., 2003; Zhang and Jacob, 1994). Therefore, it is difficult to differentiate between ATP-induced currents in the absence of chloride channel blockers. Activation of chloride channels through P_2Y is an alternative hypothesis of why currents in the study by Roshanravan and Dryer (2014) were absent in the presence of the P_2Y channel blocker suramin.

Next, it was analyzed how P_2X_4 channels are activated on membrane stretch. No evidence of direct mechanical activation of P_2X_4 channels in heterologous expression systems was found either in the absence or in the presence of several slit membrane proteins such as podocin and CD2AP (Forst et al., 2015). This means that the mechanosensor in podocytes remains elusive.

Instead, the activation of purinergic channels was dependent on vesicle-mediated ATP release (Forst et al., 2015). This conclusion was based on the findings following the use of the ATP-converting enzyme apyrase, which suppressed mechanically-induced cation conductance and by a fluorescence approach that monitored ATP concentrations in the bath solution upon mechanical stimulation. In this manner, an ATP concentration of >400 nM was measured upon application of hypotonic solution. This concentration might seem very low in comparison to the high EC_{50} values of purinergic channels for ATP which are in the micromolar range. However, locally released ATP concentration might be higher than the 400 nM measured with a global fluorescent approach. Since the blockage of SNARE complexes via N-ethylmaleimide did abrogate the mechanically-induced cation current, we suggest that podocytes release ATP upon membrane stretch through the fusion of ATP-loaded vesicles with the plasma membrane. These findings are in line with previous studies showing that ATP can be released from cells upon mechanical stimulation, thereby activating purinergic channels (Darby et al., 2003; Homolya et al., 2000; Jensen et al., 2007). For example, it was shown that fluid flow mediated the activation of P_2X_4 in endothelial cells and oocytes (Kessler et al., 2011; Yamamoto et al., 2000).

Since P_2X_4 and exocytosis are clearly influenced by cholesterol (Li and Fountain, 2012), the importance of the plasma membrane fluidity on the stretch-evoked ATP release was investigated. Cholesterol strongly determines the characteristics of the lipid bilayer and removal of cholesterol results in strongly altered fluidity of the plasma membrane. Acute cholesterol depletion using methyl-β-cyclodextrin had an interesting effect on podocytes: Instead of the prominent inward currents, strong outward conductance was observed, clearly indicating the importance of cholesterol on the P_2X_4-mediated mechanotransduction response (Forst et al., 2015). Long-term removal of cholesterol using fluvastatin—an inhibitor of the hydroxymethylglutaryl-coenzyme A reductase, thereby effectively inhibiting the rate-limiting step in cholesterol biosynthesis—completely blocked the mechanically-induced currents, confirming the importance of cholesterol in the transduction of mechanical stimuli.

Since cholesterol binds to podocin in podocytes (Huber et al., 2006), the podocin-dependence of the mechanoresponse was investigated. By using podocin knock-down podocytes, it was shown that the stretch-induced cation currents were completely suppressed. However, these observations do not explain if an unidentified mechanosensor, other endogenous proteins or the mechanically induced vesicle fusion event were dependent on cholesterol.

The release mechanism was investigated in greater detail by altering the cytoskeleton of the podocytes (Forst et al., 2015). Disruption of actin fibers by cytochalasin D had no effect on the purinergic-mediated mechanotransduction. Additionally, the actin polymerizing agent jasplakinolide was used. Cell swelling-induced effects could be modulated by jasplakinolide in a concentration-dependent manner: High (e.g. 200 nM) concentration caused a complete collapse of the podocyte architecture after several minutes and resulted in higher basal and stretch-evoked currents, while low concentrations (e.g. 8 nM) strengthened the actin cytoskeleton and abolished the stretch-evoked currents. These results are surprising since the IC_{50} of jasplakinolide for actin binding is approximately 35 nM (Bubb et al., 2000). Therefore, 200 nM jasplakinolide should lead to actin polymerization and not the collapse of the actin architecture. However, similar observations of concentration-dependent disruption of the actin cytoskeleton by jasplakinolide were also observed by different researchers in neuronal cells and tobacco BY-2 cells (Bernstein and Bamburg, 2003; Ou et al., 2002). It can be concluded from our results that the mechanical response of podocytes is adversely regulated by the actin cytoskeleton: Strengthening of the actin cytoskeleton inhibits the mechanotransduction process, while disruption of the actin cytoskeleton reinforces the effects of membrane stretch.

Besides the actin cytoskeleton, the impact of microtubules on stretch activation was analyzed by using the microtubule disruptor thiocolchicine. Preincubation of podocytes with thiocolchicine had no effect on stretch-evoked currents, thereby suggesting that the ATP release was independent of the microtubules.

Podocytes clearly depend on their actin cytoskeleton in order to maintain proper filtration function (reviewed in Greka and Mundel, 2012). An increase in intracellular calcium was shown to activate calmodulin, which in turn activates the phosphatase calcineurin. Calcineurin dephosphorylates the actin-orchestrating protein synaptopodin as well as the transcription factor nuclear factor of activated T-cells (NFAT). Phosphorylated synaptopodin is bound by the regulatory protein 14-3-3 and was shown to regulate the two small GTPase of the Rho family RhoA and Cdc42. RhoA is positively regulated by synaptopodin and activation of RhoA promotes the formation of the contractile actin stress fibers in the cell body and rear by competitively blocking the Smurf1-mediated ubiquitination of RhoA, thereby preventing the targeting of RhoA for proteasomal degradation. On the other hand, Cdc42 is negatively regulated by synaptopodin by suppressing cell motility through the formation of lamellipodia. Dephosphorylation of synaptopodin by activated calcineurin results in the loss of 14-3-3 binding, that makes the protein accessible for cathepsin L mediated degradation. As a result, the stress fiber-inducing RhoA pathway is attenuated while the lamellipodia-inducing Cdc42 pathway is strengthened. Additionally, activated calcineurin dephosphorylates NFAT resulted in the translocation of NFAT to the nucleus where it was shown to induce the expression of several TRPC channels including TRPC3, TRPC4 and TRPC6. The podocytes now adapted a motile phenotype typically associated with retraction of foot processes and development of proteinuria.

While the rise of intracellular calcium was usually shown to be the result of angiotensin II- or bradykinin-induced activation of TRPC5 or TRPC6 ultimately reorganizing the actin cytoskeleton, Endlich et al. (2001) showed that exposing podocytes to fluid shear stress also resulted in calcium-dependent reorganization of actin fibers. Interestingly, shear stress promoted actin fiber organization in the so-called actin-rich centers (ARCs), which have a radial instead of a parallel orientation. Since a rise in intracellular calcium concentration upon mechanical stimulation was also observed in our study, we wondered whether the radial actin phenotype was mediated by P_2X_4 channels and if the blockage of P_2X_4 channels was beneficial for actin cytoskeleton organization (Forst et al., 2015). As expected, stretching of cells resulted in reorganization of the actin cytoskeleton into ARCs. However, this phenotype could partially be rescued by application of the P_2X_4 blocker 5-BDBD, which highlighted the importance of P_2X_4 activation in the pathophysiology of podocytes. To rule out the involvement of TRPC channels in mechanically induced actin reorganization, podocytes were stretched in the presence of SKF-96365. No difference was observed in stretch-evoked reorganization of the actin cytoskeleton into ARCs in the presence of SKF-96365, thereby refuting a short-term involvement of TRPC channels in the transduction of mechanical stretch.

In line with our own findings and relevant literature, we propose the following mechanism for mechanical activation of podocytes and the subsequent reorganization of the actin cytoskeleton (see Figure 22):

1. Podocytes perceive mechanical stimuli by a yet unidentified sensor that is independent of the cytoskeleton.
2. Podocytes release ATP by SNARE-mediated and cholesterol-dependent vesicle fusion.
3. Extracellular ATP subsequently activates the mechanotransducing P_2X_4 channel and other purinergic channels that result in increased intracellular calcium concentrations.
4. Rise in intracellular calcium activates calmodulin, which in turn activates the phosphatase calcineurin. Calcineurin dephosphorylates the actin-fibers regulating protein synaptopodin which in turns loses its binding partner 14-3-3. The loss of 14-3-3 binding to synaptopodin now makes synaptopodin accessible to cathepsin L-mediated proteolysis.
5. The degradated synaptopodin is unable to orchestrate the F-actin fibers via the small GTPase RhoA leading to the loss of parallel actin fibers. Additionally, synaptopodin-dependent inhibition of the small GTPase Cdc32 is absent, which results in the formation of lamellipodia. Usually, this podocyte phenotype is consistent with the loss of podocyte foot processes and proteinuria.

The significance of the cholesterol/podocin complex in this system is noteworthy. Both cholesterol and podocin depletion abolished the cation currents seen under membrane stretch. However, this study provides no explanation for whether the podocin/cholesterol complex is essential for the activity of the mechanosensor and if it modulates the SNARE-mediated vesicle fusion or influences the activity of purinergic channels or other plasma membrane-resident proteins. Since the stretch-evoked currents during acute cholesterol depletion using methyl-β-cyclodextrin are not absent but are largely modified, it seems more likely that cholesterol does not modify the activity of the mechanosensor but regulates the activity of the exocytose events, thereby regulating activation.

Altogether, a novel role of P_2X_4 as mechanotransduction elements in podocytes was shown in Forst et al., 2015. The mechanical stimulus is sensed by a yet unidentified structure but is mediated to the SNARE complex that initiates vesicle fusion of ATP-loaded vesicles which results in the activation of the mechanotransducing P_2X_4 channel and finally in calcium-dependent reorganization of the cytoskeleton. Since actin reorganization is normally accompanied by loss of podocyte function and, therefore, proteinuria, this signaling pathway might contribute to mechanically-induced podocyte injury and might offer novel strategies for nephroprotection.

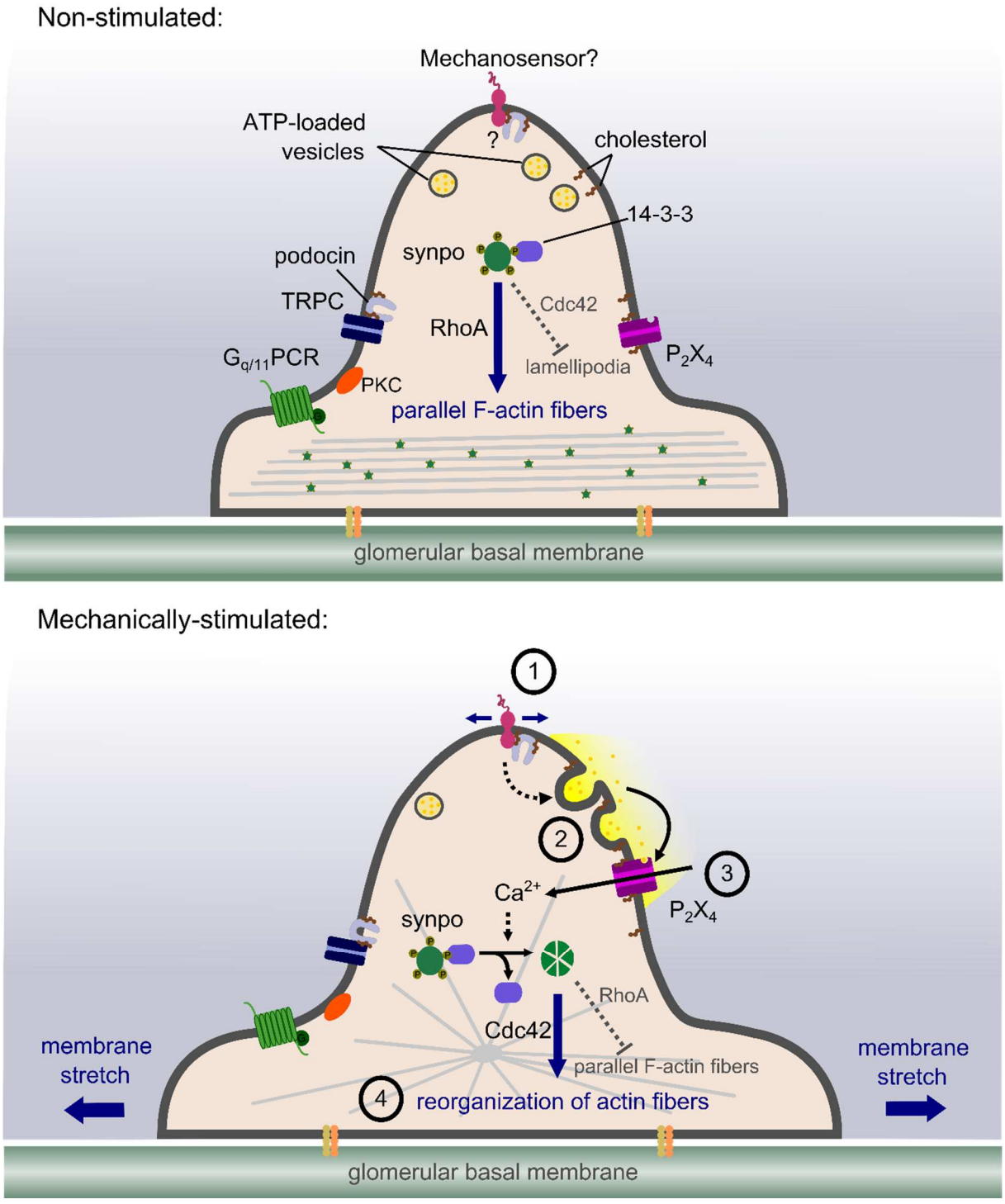

Figure 22: Proposed model of mechanically-induced P_2X_4 activation and the resulting reorganization of the actin cytoskeleton in podocytes. Top: Non-stimulated podocytes have parallel organized F-actin fibers that depend on the presence of phosphorylated synaptopodin (synpo). Synpo is an actin-binding protein that orchestrates the assembly of F-actin fibers in a RhoA-dependent manner. Additionally, synpo inhibits the small GTPase Cdc42, which is known to induce formation of lamellipodia. Above: Upon mechanical stretching of cells, a mechanosensor of unknown identity and localization is activated (1). $G_{q/11}$ protein-coupled receptors ($G_{q/11}$PCRs) and classical transient receptor potential

channels (TRPCs) do not appear to be involved in this process, although mechanical activation of $G_{q/11}$PCRs has been previously reported (Mederos y Schnitzler et al., 2008). Activation of the mechanosensor results in the fusion of ATP-loaded vesicles with the plasma membrane in a cholesterol- and SNARE-dependent way (2 Extracellular ATP subsequently activates P_2X_4 in podocytes thereby leading to an increase in intracellular calcium (3). Calcium activates calmodulin (CaM), which in turn activates the phosphatase calcineurin. Activated calcineurin dephosphorylates synpo that results in the loss of binding to the regulatory protein 14-3-3. This makes the dephosphorylated synpo accessible for degradation by the protease cathepsin L (CatL), leading to the reorganization of the cytoskeleton (4).

V Summary

The identification of mammalian mechanosensitive proteins is technically challenging and has led to false-positive results. Therefore, the aim of this thesis was the biophysical characterization of cation channels and an analysis of their role in mechanotransduction.

The analysis of heterologously expressed human classical transient receptor potential channels (TRPCs) revealed that TRPC1 subunits can only be inserted into the plasma membrane in TRPC3, -4, -5, -6 and -7-containing heterotetramers. Consequently, homotetrameric TRPC1 channels cannot function as mechanosensors. A more detailed analysis of TRPC1-containing heterotetramers revealed that all heterotetramers had effectively reduced calcium permeabilities. These findings were confirmed in murine gonadotropin-releasing hormone neuronal cells where the presence of endogenous TRPC1 reduced calcium permeation properties of the cells and, therefore, significantly impaired the migration of the cells. Altogether, a novel function of the TRPC1 proteins being negative regulator of calcium permeabilities and migration was revealed.

Additionally, the activation mechanism of the non-diacylglycerol (DAG)-sensitive family members TRPC4 and -5, which were activated upon receptor stimulation in a phospholipase C (PLC)-dependent manner, was elucidated. It was demonstrated, that TRPC4 and -5 channels were directly stimulated by DAG just like TRPC3, -6, and -7 channels. However, in contrast to TRPC3, -6 and -7 channels, this activation was dependent on the phosphokinase C (PKC)-induced phosphorylation of a C-terminal threonine in the Na^+/H^+ exchanger regulatory factor (NHERF) binding motif. Phosphorylation of the C-terminal threonine at the position 972 by PKC resulted in binding of the adaptor proteins NHERF1 and -2 to the C-terminal end of TRPC4 and -5, thereby rendering the channels insensitive to stimulation by DAG. Dislocation of the NHERF-proteins from the C-terminus of TRPC4 and -5 resulted in DAG-sensitivity of the channels. NHERF dislocation could be achieved by dephosphorylation of the threonine 972, phosphatidylinositol (3,4)-bisphosphate (PIP_2) depletion or activation of $G_{q/11}$PCRs. Receptor activation led to PLC-induced conversion of PIP_2 to inositol 1,4,5-trisphosphate and DAG, and likely evoked a conformational change in the C-terminus of TRPC4 and -5 that resulted in NHERF dislocation and direct DAG sensitivity of the channels. Mechanical activation of TRPC4 and -5 channels was not observed. On the basis of these findings, a general DAG-sensitivity for all TRPC can be proposed.

Previous studies have suggested that in myogenic resistance arteries the activation of TRPC channels is subsequent to mechanical activation of $G_{q/11}$PCRs Selective inhibition of the highly expressed endothelin A, adrenergic α_{1A}, α_{1B} and α_{1D}, and angiotensin II type 1 receptors (AT_1Rs) revealed that $G_{q/11}$PCRs regulated myogenic tone over a wide physiologically-relevant pressure range. A more detailed analysis of AT_1Rs confirmed that AT_1Rs are mechanically-

activated in an agonist-independent manner. Additionally, the higher-expressed murine AT_{1B} isoform was more mechanosensitive in comparison to the AT_{1A} isoform, which proved to be independent of the receptor density. This means that the higher mechanosensitivity of AT_{1B}Rs is an inherent property of AT_{1B}Rs in mice. In summary, it was demonstrated that mechanically-activated $G_{q/11}$PCRs, but not TRPC channels, contributed up to 50% of myogenic vasoconstriction without the involvement of mechanotransducing TRPC channels.

On the other hand, the mechanoresponsiveness of podocytes proved to be independent of $G_{q/11}$PCR or TRPC activation. In cultered murine podocytes, mechanical stimulation of the cells led to vesicle-mediated release of ATP to the extracellular space. ATP subsequently activated purinergic P_2X_4 channels in the plasma membrane. Therefore, P_2X_4 channels have to be rather considered as mechanotransducers and not mechanosensors. The mechanically induced P_2X_4 channel activation led to a reorganization of the actin cytoskeleton, which is regarded as a sign for podocyte damage. This damage could partially be prevented by pharmacological blockage of P_2X_4 channels. These findings reveal that P_2X_4 channels, but not TRPC channels, are mechanotransducing elements in podocytes that contribute to stretch-induced podocyte damage. This signaling pathway opens up novel strategies for nephroprotection in conditions such as hypertension.

To sum up, the results of this thesis do not support the notion that TRPC channels are inherently mechanosensitive. Instead, TRPC channels function as mechanotransducers in vascular smooth muscle cells, where the mechanical stimulus is perceived by $G_{q/11}$PCRs like the AT_1 receptors. In podocytes, P_2X_4 channels were identified as mechanotransducing elements. However, the mechanosensors in podocytes still remain to be identified.

VI Zusammenfassung

Die Identifizierung von mechanosensitiven Kationenkanälen in Säugetierzellen ist technisch anspruchsvoll und hat deshalb vielfach zu falsch positiven Ergebnissen geführt. Zielsetzung dieser Arbeit war daher die Charakterisierung von Säugetier-Kationenkanälen und deren Bedeutung für die Mechanotransduktion.

Die Analyse von heterolog exprimierten *classical transient receptor potential* (TRPC)-Kanälen zeigte, dass humane TRPC1 Kanaluntereinheiten erst in die Zellmembran eingebaut werden, wenn sie mit TRPC3-, -4-, -5-, -6-, oder -7-Kanaluntereinheiten Heterotetramere ausbilden. Somit können homomere TRPC1-Kanäle auch keine Mechanosensoren bilden. Eine biophysikalische Analyse von TRPC1-beinhaltenden heterotetrameren TRPC-Kanälen zeigte eine stets verminderte Kalziumpermeabilität dieser Kanäle. Auch in murinen Gonadotropin-Hormon sezernierenden Neuronen führte die endogene Präsenz von TRPC1 zu einer verminderten Kalziumdurchlässigkeit und damit zu einer signifikant reduzierten Migration dieser Zellen. Damit sind zwei neue Funktionen von TRPC1 charakterisiert worden.

Zudem wurde der Signalweg zur Aktivierung der Diacylglycerol (DAG)-insensitiven Mitglieder der TRPC-Kanalfamilie TRPC4- und -5 im Anschluss an eine Rezeptorstimulation untersucht. Es stellte sich heraus, dass TRPC4- und -5-Kanäle ebenso wie TRPC3-, -6- und -7-Kanäle direkt durch das PLC-Produkt DAG aktiviert werden können, jedoch im Gegensatz zu den TRPC3-, -6- und -7-Kanälen nur in Abhängigkeit von einer Proteinkinase C-vermittelten Phosphorylierung eines C-terminalen Threonins im *Na^+/H^+ exchanger regulatory factor* (NHERF) Bindemotiv. Die Phosphorylierung des Threonins an der Stelle 972 führte zur Bindung der Adaptorproteine NHERF1 und -2 an den C-Terminus von TRPC4 und -5, wodurch die DAG-Aktivierbarkeit der Kanäle verhindert wurde. Die Ablösung der NHERF-Proteine vom C-Terminus der Kanäle bewirkte stets eine DAG-Aktivierbarkeit. Diese Verlagerung der NHERF-Proteine konnte sowohl durch Dephosphorylierung des Threonins als auch durch Phosphatidylinositol-4,5-bisphosphat (PIP_2)-Depletion sowie durch Aktivierung von $G_{q/11}$-Protein-gekoppelten Rezeptoren herbeigeführt werden. Im Falle der Rezeptoraktivierung führte die PLC-vermittelte Umsetzung von PIP_2 zu Inositol-1,4,5-trisphosphat und DAG vermutlich zu einer Konformationsänderung des C-terminalen Endes von TRPC5, wodurch NHERF-Proteine abgelöst wurden, so dass TRPC4- und -5-Kanäle direkt durch DAG aktiviert werden konnten. Eine direkte mechanisch-induzierte Aktivierung von TRPC4- oder -5 konnte nicht beobachtet werden. Auf Grund dieser Ergebnisse kann man abschließend postulieren, dass alle Mitglieder der TRPC-Familie direkt DAG aktivierbar sind.

Frühere Untersuchungen haben gezeigt, dass in myogenen Widerstandsgefäßen TRPC-Kanäle über eine Signalkaskade durch mechanisch stimulierte $G_{q/11}$-Protein-gekoppelte Rezeptoren aktiviert werden. Durch selektive pharmakologische Blockade der hoch

exprimierten Endothelin A-, der adrenergen α_{1A}-, α_{1B}- und α_{1D}-, sowie der Angiotensin II Typ 1 (AT_1)-Rezeptoren konnte nachweisen werden, dass der myogene Gefäßtonus über den gesamten physiologischen Druckbereich von $G_{q/11}$-Protein-gekoppelten Rezeptoren reguliert wird. Eine genauere Untersuchung der AT_1-Rezeptoren zeigte, dass diese Agonisten-unabhängig direkt durch mechanische Stimulation aktiviert wurden. Zudem war die höher exprimierte murine AT_{1B}-Rezeptorisoform unabhängig von der Rezeptordichte mechanosensitiver als die AT_{1A}-Rezeptorisoform. Insgesamt waren $G_{q/11}$-gekoppelte-Rezeptoren und nicht TRPC-Kanäle als direkte Mechanosensoren für etwa 50% des myogenen Gefäßtonus verantwortlich.

In kultivierten Podozyten der Maus hingegen war die mechanische Reizvermittlung unabhängig von $G_{q/11}$-Protein-gekoppelten Rezeptoren sowie von TRPC-Kanälen. Hier führte die mechanische Stimulation zur Vesikel-vermittelten Freisetzung von ATP in den extrazellulären Raum. Das ATP wiederum aktivierte purinerge P_2X_4-Kanäle in der Podozyten-Zellmembran, was zu einem Kalziumeinstrom in die Zelle führte. Somit wurden P_2X_4-Kanäle als Mechanotransduktoren in Podozyten identifiziert. Die mechanische P_2X_4-Kanal-Aktivierung führte zu einer Reorganisation des Aktin-Zytoskeletts, was als Zeichen für eine Podozytenschädigung gilt. Diese Schädigung konnte durch eine pharmakologische Blockade des P_2X_4 Kanales zumindest teilweise verhindert werden. Zusammenfassend konnte ein neuer Signalweg beschrieben werden, bei dem P_2X_4- und nicht TRPC-Kanäle eine Schlüsselrolle für die mechanische Aktivierung von Podozyten spielen. P_2X_4-Kanäle könnten demnach als neue Zielstrukturen für Pharmaka zur Prävention von Podozytenschädigungen bei Krankheiten wie zum Beispiel der hypertensiven Nephropathie dienen.

Zusammengefasst zeigen die Ergebnisse dieser Arbeit, dass TRPC-Kanäle nicht inhärent mechanosensitiv sind, sondern als Mechanotransduktoren fungieren können. Im vaskulären System konnten $G_{q/11}$-gekoppelte-Rezeptoren wie die AT_1-Rezeptoren als direkte Mechanosensoren identifiziert werden. In Podozyten erwiesen sich P_2X_4 Kanäle als Mechanotransduktoren. Die Mechanosensoren in Podozyten sind jedoch noch unbekannt.

VII Supplements

Supplementary Table 1: Overview of putative mechanosensitive channels. The candidates and the form of the applied mechanical stimulation, the expression system, the physiological function and the proposed mechanical gating mechanism are depicted. The mechanism of mechanical activation is colorcoded in the following way: green color refers to candidates that have convincingly shown to be directly activated by mechanical force, blue color indicates experiments that likely point to a directly mechanogating property of the candidate, but confirming evidence is lacking, red color depicts candidates that have been demonstrated to be indirectly activated by mechanical force. Abbreviations: A7r5 = aorta 7 rat 7 smooth muscle cell; AA = arachidonic acid; AS = bulge-inducing amphiphatic substance; ASIC = acid sensing ion channel; COS – CV-1 originated with SV40; Deg/ENaC = Degenerin/Epithelial channel Na^+ channel; DRG = dorsal root ganglion; FSS = fluid shear stress; HeLa= Henrietta Lacks cervical cancer cell; hES = human embryonic stem cells; hiPS = human inducible pluripotent stem cells; HTC116 = human colon cancer cell; HTS = Hypotonicity; HUVEC = human umbilical vein endothelial cell; K_{2P} = K^+ two pore channel; LRRC8 = leucine-rich repeat–containing 8; LTMR = low threshold mechanoreceptors; MEC = mechanosensitive abnormalites; MscL = mechanosensitive channel large conductance; MscS = mechanosensitive channel small conductance; NompC = no mechanoreceptor potential channel; NS = not specified; OLVT = organum vasculosum laminae terminalis; P_2X = purinergic channels; SON = supraoptic nucleus; TMC = transmembrane-channel like protein; TRAAK = TWIK-related arachidonic acid-stimulated potassium channel; TREK = TWIK-Related potassium channel 1; TRP = transient receptor potential; TRPA = ankyrin TRP; TRPC = canonical TRP; TRPM = melastanin TRP; TRPML = mucolipin TRP; TRPN = NompC-like TRP; TRPV = vanilloid TRP; TRPY = yeast TRP; VRAC = volume regulated anion channel.

Candidate	Mechanical stimulation	Expression system	Proposed physiological relevance	Proposed mechanism of mechanical activation	Reference
Anion channels					
VRAC	HTS	Endogenously expressed in all animal cells.	Osmoregulation	Direct	For review (Nilius and Droogmans, 2003; Nilius et al., 2000)
LRRC8A	HTS	Knock-down of LRRC8A in various mammalian cell systems endogenously expressing VRAC. Heterologous expression of LRRC8A in HEK293 and HeLa	Osmoregulation	Direct?	(Qiu et al., 2014)
LRRC8A/LRRC8C/LRRC8E	HTS	Knock-down of LRRC8 isoforms in various cell systems endogenously expressing VRAC.	Osmoregulation	Direct?	(Voss et al., 2014)

		Heterologous expression of LRRC8 isoforms in HEK293 and HTC116			
Msc's					
MscL (bacterial)	HTS, AS	Endogenous expression in E. coli	Osmoregulation	Direct	(Martinac et al., 1990)
MscS (bacteria)	HTS, AS	Endogenous expression in E. coli	Osmoregulation	Direct	(Martinac et al., 1990)
Deg/ENaC					
MEC-4/MEC-10 (C. elegans)	Touch	Studies with MEC-deficient worms	Sensation of gentle touch	Direct, but requires several additional MEC subunits	(Chalfie and Sulston, 1981); (O'Hagan et al., 2005)
Deg/ENaC	FSS	Endogenous expression in human endothelial cells and rat arteries	Sensation of fluid flow in endothelial cells	Indirect?	(Wang et al., 2009)
BNC1α	Touch	Neurons isolated from BNC1$^{-/-}$ mice	Sensation of touch	Direct?	(Price et al., 2000)
ASIC	Painful touch	Analysis of dominant-negative ASIC3 mice	Sensation of noxious stimuli	Indirect	(Mogil et al., 2005)
Piezo					
Piezo1	Membrane indentation; Negative pipette pressure	Endogenous expression in neuro2A cells; Heterologous expression in HEK293	NS	Direct	(Coste et al., 2010)
Piezo1	AS: GsMTx4	Heterologous expression in HEK293 cells	Sensation of noxious stimuli	Direct?	(Bae et al., 2011)
Piezo1	FSS	Vascular analysis of Piezo1$^{-/-}$ embryos, heterologous expression in HEK293	Vascular development and cardiogenesis	Direct?	(Ranade et al., 2014)
dmPiezo (Drosophila)	Noxious touch; negative pipette pressure	Drosophila Piezo knock-down and reconstitution of droshophila Piezo in sensory neurons	Sensation of noxious stimuli	Direct	(Kim et al., 2012)
Piezo2	Membrane indentation, negative pipette pressure	Endogenous expression in DRG; heterologous expression in HEK293	NS	Direct?	(Coste et al., 2010)

Piezo2	Gentle touch	Skin cells deficient of Piezo2; Merkel cells deficient of Piezo2	Sensation of gentle touch, forms and textures	Direct?	(Woo et al., 2014)
Piezo2	Displacement of cell layer	Endogenous expression in whisker hair follicles	Sensation of gentle touch, forms and textures	Direct?	(Ikeda et al., 2014)
Piezo2	Membrane indentation	Endogenous expression in LTMRs derived from hES and hiPS and knock-down in LTMRs	Sensation of touch	Direct?	(Schrenk-Siemens et al., 2014)
TMC1	Deflection of hair cells	Endogenous expression in cochlear mouse hair cells; TMC1$^{-/-}$, TMC2$^{-/-}$ and M412K-TMC1$^{-/-}$ cochlear mouse hair cells	Hearing and balance	Direct?	(Pan et al., 2013)
TMC1 (Drosophila)	Touch, hypertonicity	Endogenous expression in ASH polymodal avoidance neurons	Salt sensing	None	(Chatzigeorgiou et al., 2013)
K_{2P}					
TREK-1	Positive and negative pipette pressure, AS, FSS HTS, Positive and negative pipette pressure	Heterologous expression in COS Heterologous exression in oocytes	Repolarization of cardiomyocytes?	Direct	(Patel et al., 1998)
TREK-1	Positive pipette pressure	Reconstitution in artificial liposomes	NS	Direct	(Berrier et al., 2013)
TREK-1	Positive and negative pipette pressure	Reconstitution in artificial liposomes	NS	Direct	(Brohawn et al., 2014)
TREK-1	Touching of skin, paw pressure	TREK-1$^{-/-}$ mice	Sensation of noxious stimuli	Direct	(Alloui et al., 2006)
TREK-1	Increased intraluminal pressure;	Mesenteric resistance arteries of TREK-1$^{-/-}$ mice;	Vasodilation	Indirect through GPCR-cascade	(Garry et al., 2007)

	local pressure-induced vasodilation	TREK-1$^{-/-}$ mice			
TREK-2	Positive and negative pipette pressure, ASs	Heterologous expression in COS-7	NS	Direct?	(Bang et al., 2000)
TRAAK	Positive and negative pipette pressure, ASs	Heterologous expression in COS-7	NS	Direct?	(Bang et al., 2000; Maingret et al., 1999a)
TRAAK	Positive and negative pipette pressure	Reconstitution in artificial liposomes	NS	Direct	(Brohawn et al., 2014)
TRP channels					
TRPY1 (yeast)	Hypertonicity, positive (?) pipette pressure	TRPY1-/- vacuoles of yeast *Saccharomyces cerevisiae*	Calcium release from vacuoles on osmotic shock	Direct?	(Zhou et al., 2003)
TRPV homologues					
OSM-9 (C. elegans)	Nose touch, Hypertonicity	OSM-9$^{-/-}$ worms	Sensation of touch, osmoregulation	Direct?	(Colbert et al., 1997)
Nanchung (Drosophila)	Sound; HTS	Inactive-deficient ciliated sensory neurons; Heterologous expression in CHO-K1	Hearing	Indirect	(Kim et al., 2003)
Inactive (Drosophila)	Sound; HTS	Inactive-deficient ciliated sensory neurons; Heterologous expression in CHO-K1	Hearing	Indirect	(Gong et al., 2004)
TRPV4	HTS	Heterologous expression in CHO	Osmoregulation	Direct?	(Liedtke et al., 2000)
TRPV4	Hypertonicity, Positive and negative pipette pressure	Heterologous expression in HEK293	Osmoregulation in kidney	Indirect	(Strotmann et al., 2000)
TRPV4	HTS, FSS	Heterologous expression in HEK293 cells and CKO-K1 cells at 37°C	Vasodilation	Direct?	(Gao et al., 2003)
TRPV4	Hypertonicity	Brain slices of TRPV4$^{-/-}$ mice	regulation of serum osmolality	Direct?	(Mizuno et al., 2003)

TRPV4	HTS	Heterologous expression in HEK293	NS	Indirect through activation of PLA_2	(Vriens et al., 2005)
TRPV4	Increased intraluminal pressure; HTS	Carotid arteries from $TRPV4^{-/-}$ mice; carotid artery endothelial cells	Vasodilation	Direct?	(Hartmannsgruber et al., 2007)
TRPV4	FSS	Knock-down of TRPV4 in epithelial cells	Kidney fluid flow sensing	Direct?	(Kottgen et al., 2008)
TRPV1	*In vivo* bladder contractions and *in vitro* stretch-evoked bladder contractions; HTS	$TRPV1^{-/-}$ mice; $TRPV1^{-/-}$ urothelial cells	Bladder contraction	Direct?	(Birder et al., 2002)
TRPV1	Hypertonicity	OVLT and SON neurons of $TRPV1^{-/-}$ mice	Body fluid homeostasis	Direct?	(Ciura and Bourque, 2006) (Sharif Naeini et al., 2006)
TRPV2	HTS	Aortic myocytes, heterologous expression in CHO-K1	Vasoconstriction	Direct?	(Muraki et al., 2003)
TRPV2	Membrane stretch	Endogenous TRPV2, TRPV2 knock-down using shRNA and heterologous expression of dominant negative TRPV2 in motor neurons	Axon elongation	Direct?	(Shibasaki et al., 2010)
TRPN homologues					
NompC (Drosophila)	Bristle touch and sound	Mutated Drosophila larvae	Touch and hearing	Direct?	(Walker et al., 2000)
NompC (Drosophila)	Sound	Ciliated sensory neurons	Hearing	Indirect	(Lehnert et al., 2013)
TRPN1 (Zebrafish)	Sound	Mutated zebrafish larvae	Hearing and balance	Direct?	(Sidi et al., 2003)
TRR-4 (C. elegans)	Bending of nose	Mutated worms	Proprioception	Direct?	(Li et al., 2006)
TRPA homologues					
Painless (Drosophila)	Noxious touch	$Painless^{-/-}$ flies	Sensation of noxious stimuli	Direct?	(Tracey et al., 2003)
TRPA1 (C. elegans)	Nose touch; Patch pipette pressure	$TRPA1^{-/-}$ worms; Heterologous expression in CHO	foraging	Direct?	(Kindt et al., 2007)

TRPA1	AS: GsMTx4, TNP, chlorpromazine	Heterologous expression in HEK293	NS	Direct?	(Hill and Schaefer, 2007)
TRPA1	Membrane stretch?	Heterologous expression in COS	NS	Indirect	(Sharif-Naeini et al., 2008)
TRPA1	Sound; Deflection of hair cells	TRPA1$^{-/-}$ mice; TRPA1$^{-/-}$ hair cells	Hearing and balance	Indirect	(Bautista et al., 2006)
TRPA1	Sound, paw pressure; Deflection of hair cells	TRPA1$^{-/-}$ mice; TRPA1$^{-/-}$ hair cells	Nociception	Direct?	(Kwan et al., 2006)
TRPPs					
TRPP1	Single molecule force spectroscopy	Recombinant TRPP1	NS	Direct?	(Qian et al., 2005)
TRPP1/TRPP2	FSS	Kidney epithelial cells lacking TRPP1; TRPP2 activity blocked by antibody.	Kidney fluid flow sensing	Direct activation of TRPP1?	(Nauli et al., 2003)
TRPP2/TRPV4	HTS	Co-expression of TRPP2 and TRPV4 in oocytes	Kidney fluid flow sensing	Direct?	(Kottgen et al., 2008)
TRPP1/TRPP2	Negative pipette pressure; Increased intraluminal pressure	Heterologous expression in several mammalian cells lines including COS-7, endogenous expression in VSMCs isolated from TRPP1-deficient mice; myogenic arteries	Myogenic vasoconstriction	Indirect	(Sharif-Naeini et al., 2009)
TRPML					
TRPML3	Sound	TRPML3 mutated mice	Hearing	Direct?	(Di Palma et al., 2002; Grimm et al., 2007)
TRPM					
TRPM3	HTS	Heterologous expression in HEK293	Renal calcium homeostasis	Direct?	(Grimm et al., 2003)

TRPM4	Increased intraluminal pressure	Endogenous expression in cerebral arteries, knock-down of TRPM4 in cerebal arteries	Myogenic vasoconstriction	Direct?	(Earley et al., 2004)
TRPM4	Negative pipette pressure	Heterologous expression in HEK293, Endogenous expression in cerebral myocytes	Myogenic vasoconstriction	Indirect through activation ryanodine receptors	(Morita et al., 2007)
TRPM4	Increased intraluminal pressure	vasculature of isolated hind limbs of TRPM4-/- mice	Blood pressure regulation	Indirect through catecholamine release from chromaffin cells	(Mathar et al., 2010)
TRPM7	FSS	Heterologous expression in A7r5 cells	Vessel wall injury	Indirectly through TRPM7 incorporation into the membrane	(Oancea et al., 2006)
TRPM7	HTS, FSS, negative pipette pressure	Heterologous expression in HEK293	Osmoregulation	Direct?	(Numata et al., 2007a)
TRPM7	HTS, negative pipette pressure	Endogenously expression in HeLa, knock-down of TRPM7 in HeLa	Osmoregulation	Direct?	(Numata et al., 2007b)
	HTS, Hypertonicity	Heterologous expression in HEK293, Endogenous expression in HEK293	NS	Indirect through molecular crowding of TRPM7 regulators	(Bessac and Fleig, 2007)
TRPC					
TRPC1	Negative pipette pressure	Heterologous expression in COS and CHO	NS	None	(Gottlieb et al., 2008)
TRPC1	Increased intraluminal pressure; HTS, inflation	cerebral arteries isolated from TRPC1$^{-/-}$ mice; Cerebral smooth muscle cells from TRPC1$^{-/-}$ mice		None	(Dietrich et al., 2007)
TRPC5	HTS, positive pipette pressure	Heterologous expression in HEK293	Osmoregulation in nervous system	Indirect	(Gomis et al., 2008)
TRPC5	HTS	Heterologous expression in HEK293	NS	Indirect through activation of $G_{q/11}$PCRs	(Jemal et al., 2014)
TRPC6	Negative pipette pressure	Heterologous expression in COS and CHO	NS	None	(Gottlieb et al., 2008)

TRPC6	HTS, negative pipette pressure	Heterologous expression in HEK293	NS	None	(Mederos y Schnitzler et al., 2008)
TRPC6	HTS	Heterologous expression in CHO-K1	NS	Direct?	(Wilson and Dryer, 2014)
Purinergic channels					
P_2X_4	FSS	Heterologous expression in ooocytes	NS	None, but HTS modulates ATP response	(Kessler et al., 2011)
P_2X_4	FSS	Endogenous expression in HUVEC, heterologous expression in HEK293	Sensation of fluid shear stress	Likely indirect through mechanically-mediated ATP release	(Yamamoto et al., 2000)

Supplementary Table 2: Protein sequence alignment of mouse and human TRPC1 isoforms. The following isoforms were used for sequence alignment: human TRPC1a (NP_001238774), mouse TRPC1α (NP_035773.1), extended mouse and human TRPC1α (NTX-TRPC1), as well as human TRPC1β (NP_003295.1) and TRPC1ε. Asterisks indicate identical amino acids in all TRPC1 proteins. Numbers at the end of each line indicate the respective amino acid number. The starting amino acids are highlighted in light magenta. Amino acids missing from other isoforms are highlighted in light blue. Transmembrane regions are indicated in yellow. A nucleotide sequence alignment of 13 homologs of TRPC1 mRNA can be found in the supplementary figure of (Ong et al., 2013).

```
mTRPC1α          ------------------------------------------------------------------------MGAPPP   6
NTX-mTRPC1α      LARSTLSSPDGRGPARPGRRRLGRGRWPRGRASAATNLGLSVEGECWFRGEATPFGANGPHADVAVGTTH----PFSSSGSGSGSAPMGAPPP  89
NTX-hTRPC1α      LARATLSSPDGRGPARPGRRRLGRGRWPRGRACAATNLGLSVEGECWFSGEATPFGANGPRAEAAVGTTHPFSSPGAWLGSGSGSGPVGAPPP  93
hTRPC1α          ------------------------------------------------------------------------------------------
hTRPC1ε          ------------------------------------------------------------------------------------------
hTRPC1β          ------------------------------------------------------------------------------------------

mTRPC1α          SPGLPPSWAAMMAALYPSTDLSGVSSSSLPSSPSSSSPNEVMALKDVREVKEENTLNEKLFLLACDKGDYYMVKKILEENSSGDLNINCVDVL  99
NTX-mTRPC1α      SPGLPPSWAAMMAALYPSTDLSGVSSSSLPSSPSSSSPNEVMALKDVREVKEENTLNEKLFLLACDKGDYYMVKKILEENSSGDLNINCVDVL 182
NTX-hTRPC1α      SPGLPPSWAAMMAALYPSTDLSGASSSSLPSSPSSSSPNEVMALKDVREVKEENTLNEKLFLLACDKGDYYMVKKILEENSSGDLNINCVDVL 186
hTRPC1α          ----------MMAALYPSTDLSGASSSSLPSSPSSSSPNEVMALKDVREVKEENTLNEKLFLLACDKGDYYMVKKILEENSSGDLNINCVDVL  83
hTRPC1β          ----------MMAALYPSTDLSGASSSSLPSSPSSSSPNEVMALKDVREVKEENTLNEKLFLLACDKGDYYMVKKILEENSSGDLNINCVDVL  83
hTRPC1ε          ----------MMAALYPSTDLSGASSSSLPSSPSSSSPNEVMALKDVREVKEENTLNEKLFLLACDKGDYYMVKKILEENSSGDLNINCVDVL  83
                           ************* ************************************************************

mTRPC1α          GRNAVTITIENESLDILQLLLDYGCQSADALLVAIDSEVVGAVDILLNHRPKRSSRPTIVKLMERIQNPEYSTTMDVAPVILAAHRNNYEILT 192
NTX-mTRPC1α      GRNAVTITIENESLDILQLLLDYGCQSADALLVAIDSEVVGAVDILLNHRPKRSSRPTIVKLMERIQNPEYSTTMDVAPVILAAHRNNYEILT 275
NTX-hTRPC1α      GRNAVTITIENENLDILQLLLDYGCQSADALLVAIDSEVVGAVDILLNHRPKRSSRPTIVKLMERIQNPEYSTTMDVAPVILAAHRNNYEILT 279
hTRPC1α          GRNAVTITIENENLDILQLLLDYGCQSADALLVAIDSEVVGAVDILLNHRPKRSSRPTIVKLMERIQNPEYSTTMDVAPVILAAHRNNYEILT 176
hTRPC1β          GRNAVTITIENENLDILQLLLDYGCQ----------------------------------KLMERIQNPEYSTTMDVAPVILAAHRNNYEILT 142
hTRPC1ε          GRNAVTITIENENLDILQLLLDYGCQSADALLVAIDSEVVGAVDILLNHRPKRSSRPTIVKLMERIQNPEYSTTMDVAPVILAAHRNNYEILT 176
                 ************ ************                                    **********************************

mTRPC1α          MLLKQDVSLPKPHAVGCECTLCSAKNKKDSLRHSRFRLDIYRCLASPALIMLTEEDPILRAFELSADLKELSLVEVEFRNDYEELARQCKMFA 285
NTX-mTRPC1α      MLLKQDVSLPKPHAVGCECTLCSAKNKKDSLRHSRFRLDIYRCLASPALIMLTEEDPILRAFELSADLKELSLVEVEFRNDYEELARQCKMFA 368
NTX-hTRPC1α      MLLKQDVSLPKPHAVGCECTLCSAKNKKDSLRHSRFRLDIYRCLASPALIMLTEEDPILRAFELSADLKELSLVEVEFRNDYEELARQCKMFA 372
hTRPC1α          MLLKQDVSLPKPHAVGCECTLCSAKNKKDSLRHSRFRLDIYRCLASPALIMLTEEDPILRAFELSADLKELSLVEVEFRNDYEELARQCKMFA 269
hTRPC1β          MLLKQDVSLPKPHAVGCECTLCSAKNKKDSLRHSRFRLDIYRCLASPALIMLTEEDPILRAFELSADLKELSLVEVEFRNDYEELARQCKMFA 235
hTRPC1ε          MLLKQDVSLPKPHAVGCECTLCSAKNKKDSLRHS-------RCLASPALIMLTEEDPILRAFELSADLKELSLVEVEFRNDYEELARQCKMFA 262
                 ********************************       **************************************************

mTRPC1α          KDLLAQARNSRELEVILNHTSSDEPLDKRGLLEERMNLSRLKLAIKYNQKEFVSQSNCQQFLNTVWFGQMSGYRRKPTCKKIMTVLTVGIFWP 378
```

```
NTX-mTRPC1α         KDLLAQARNSRELEVILNHTSSDEPLDKRGLLEERMNLSRLKLAIKYNQKEFVSQSNCQQFLNTVWFGQMSGYRRKPTCKKIMTVLTVGIFWP 461
NTX-hTRPC1α         KDLLAQARNSRELEVILNHTSSDEPLDKRGLLEERMNLSRLKLAIKYNQKEFVSQSNCQQFLNTVWFGQMSGYRRKPTCKKIMTVLTVGIFWP 465
hTRPC1α             KDLLAQARNSRELEVILNHTSSDEPLDKRGLLEERMNLSRLKLAIKYNQKEFVSQSNCQQFLNTVWFGQMSGYRRKPTCKKIMTVLTVGIFWP 362
hTRPC1β             KDLLAQARNSRELEVILNHTSSDEPLDKRGLLEERMNLSRLKLAIKYNQKEFVSQSNCQQFLNTVWFGQMSGYRRKPTCKKIMTVLTVGIFWP 328
hTRPC1ε             KDLLAQARNSRELEVILNHTSSDEPLDKRGLLEERMNLSRLKLAIKYNQKEFVSQSNCQQFLNTVWFGQMSGYRRKPTCKKIMTVLTVGIFWP 355
                    ************************************************************************************************

mTRPC1α             VLSLCYLIAPKSQFGRIIHTPFMKFIIHGASYFTFLLLLNLYSLVYNEDKKNTMGPALERIDYLLILWIIGMIWSDIKRLWYEGLEDFLEESR 471
NTX-mTRPC1α         VLSLCYLIAPKSQFGRIIHTPFMKFIIHGASYFTFLLLLNLYSLVYNEDKKNTMGPALERIDYLLILWIIGMIWSDIKRLWYEGLEDFLEESR 554
NTX-hTRPC1α         VLSLCYLIAPKSQFGRIIHTPFMKFIIHGASYFTFLLLLNLYSLVYNEDKKNTMGPALERIDYLLILWIIGMIWSDIKRLWYEGLEDFLEESR 558
hTRPC1α             VLSLCYLIAPKSQFGRIIHTPFMKFIIHGASYFTFLLLLNLYSLVYNEDKKNTMGPALERIDYLLILWIIGMIWSDIKRLWYEGLEDFLEESR 455
hTRPC1β             VLSLCYLIAPKSQFGRIIHTPFMKFIIHGASYFTFLLLLNLYSLVYNEDKKNTMGPALERIDYLLILWIIGMIWSDIKRLWYEGLEDFLEESR 421
hTRPC1ε             VLSLCYLIAPKSQFGRIIHTPFMKFIIHGASYFTFLLLLNLYSLVYNEDKKNTMGPALERIDYLLILWIIGMIWSDIKRLWYEGLEDFLEESR 448
                    ************************************************************************************************

mTRPC1α             NQLSFVMNSLYLATFALKVVAHNKFHDFADRKDWDAFHPTLVAEGLFAFANVLSYLRLFFMYTTSSILGPLQISMGQMLQDFGKFLGMFLLVL 564
NTX-mTRPC1α         NQLSFVMNSLYLATFALKVVAHNKFHDFADRKDWDAFHPTLVAEGLFAFANVLSYLRLFFMYTTSSILGPLQISMGQMLQDFGKFLGMFLLVL 647
NTX-hTRPC1α         NQLSFVMNSLYLATFALKVVAHNKFHDFADRKDWDAFHPTLVAEGLFAFANVLSYLRLFFMYTTSSILGPLQISMGQMLQDFGKFLGMFLLVL 651
hTRPC1α             NQLSFVMNSLYLATFALKVVAHNKFHDFADRKDWDAFHPTLVAEGLFAFANVLSYLRLFFMYTTSSILGPLQISMGQMLQDFGKFLGMFLLVL 548
hTRPC1β             NQLSFVMNSLYLATFALKVVAHNKFHDFADRKDWDAFHPTLVAEGLFAFANVLSYLRLFFMYTTSSILGPLQISMGQMLQDFGKFLGMFLLVL 514
hTRPC1ε             NQLSFVMNSLYLATFALKVVAHNKFHDFADRKDWDAFHPTLVAEGLFAFANVLSYLRLFFMYTTSSILGPLQISMGQMLQDFGKFLGMFLLVL 541
                    ************************************************************************************************

mTRPC1α             FSFTIGLTQLYDKGYTSKEQKDCVGIFCEQQSNDTFHSFIGTCFALFWYIFSLAHVAIFVTRFSYGEELQSFVGAVIVGTYNVVVVIVLTKLL 657
NTX-mTRPC1α         FSFTIGLTQLYDKGYTSKEQKDCVGIFCEQQSNDTFHSFIGTCFALFWYIFSLAHVAIFVTRFSYGEELQSFVGAVIVGTYNVVVVIVLTKLL 740
NTX-hTRPC1α         FSFTIGLTQLYDKGYTSKEQKDCVGIFCEQQSNDTFHSFIGTCFALFWYIFSLAHVAIFVTRFSYGEELQSFVGAVIVGTYNVVVVIVLTKLL 744
hTRPC1α             FSFTIGLTQLYDKGYTSKEQKDCVGIFCEQQSNDTFHSFIGTCFALFWYIFSLAHVAIFVTRFSYGEELQSFVGAVIVGTYNVVVVIVLTKLL 641
hTRPC1β             FSFTIGLTQLYDKGYTSKEQKDCVGIFCEQQSNDTFHSFIGTCFALFWYIFSLAHVAIFVTRFSYGEELQSFVGAVIVGTYNVVVVIVLTKLL 607
hTRPC1ε             FSFTIGLTQLYDKGYTSKEQKDCVGIFCEQQSNDTFHSFIGTCFALFWYIFSLAHVAIFVTRFSYGEELQSFVGAVIVGTYNVVVVIVLTKLL 634
                    ************************************************************************************************

mTRPC1α             VAMLHKSFQLIANHEDKEWKFARAKLWLSYFDDKCTLPPPFNIIPSPKTICYMISSLSKWICSHTSKGKVKRQNSLKEWRNLKQKRDENYQKV 750
NTX-mTRPC1α         VAMLHKSFQLIANHEDKEWKFARAKLWLSYFDDKCTLPPPFNIIPSPKTICYMISSLSKWICSHTSKGKVKRQNSLKEWRNLKQKRDENYQKV 833
NTX-hTRPC1α         VAMLHKSFQLIANHEDKEWKFARAKLWLSYFDDKCTLPPPFNIIPSPKTICYMISSLSKWICSHTSKGKVKRQNSLKEWRNLKQKRDENYQKV 837
hTRPC1α             VAMLHKSFQLIANHEDKEWKFARAKLWLSYFDDKCTLPPPFNIIPSPKTICYMISSLSKWICSHTSKGKVKRQNSLKEWRNLKQKRDENYQKV 734
hTRPC1β             VAMLHKSFQLIANHEDKEWKFARAKLWLSYFDDKCTLPPPFNIIPSPKTICYMISSLSKWICSHTSKGKVKRQNSLKEWRNLKQKRDENYQKV 700
hTRPC1ε             VAMLHKSFQLIANHEDKEWKFARAKLWLSYFDDKCTLPPPFNIIPSPKTICYMISSLSKWICSHTSKGKVKRQNSLKEWRNLKQKRDENYQKV 727
                    ************************************************************************************************
```

```
mTRPC1α            MCCLVHRYLTSMRQKMQSTDQATVENLNELRQDLSKFRNEIRDLLGFRTSKYAMFYPRN 809
NTX-mTRPC1α        MCCLVHRYLTSMRQKMQSTDQATVENLNELRQDLSKFRNEIRDLLGFRTSKYAMFYPRN 892
NTX-hTRPC1α        MCCLVHRYLTSMRQKMQSTDQATVENLNELRQDLSKFRNEIRDLLGFRTSKYAMFYPRN 896
hTRPC1α            MCCLVHRYLTSMRQKMQSTDQATVENLNELRQDLSKFRNEIRDLLGFRTSKYAMFYPRN 793
hTRPC1β            MCCLVHRYLTSMRQKMQSTDQATVENLNELRQDLSKFRNEIRDLLGFRTSKYAMFYPRN 759
hTRPC1ε            MCCLVHRYLTSMRQKMQSTDQATVENLNELRQDLSKFRNEIRDLLGFRTSKYAMFYPRN 786
                   ************************************************************
```

Supplementary Table 3: Comparison of ion concentrations and respective calculated equilibrium potentials in the solutions used in the study of Anderson et al. (2013) and Forst et al. (2015). Anderson et al. (2013) diluted the original isotonic bath solution with 30% water resulting in a hypotonic bath solution with reduced ion concentrations. As a consequence, the equilibrium potentials of the ions calculated using the Nernst equation at 22°C differ between iso- and hypotonic bath solution. In contrast, Forst et al. (2015) used an isotonic bath solution that was supplemented with non-membrane permeable sugar mannitol to prevent ion concentration differences between iso- and hypotonic bath solution resulting in constant equilibrium potentials.

Anderson et al. (2013)	**[Ion] in intracellular solution**	**[Ion] in isotonic extracellular solution**	**[Ion] in hypotonic extracellular solution**	**Calculated equilibrium potentials at 22°C in isotonic extracellular solution**	**Calculated equilibrium potentials at 22°C in hypotonic extracellular solution**
Cs^+	125.0 mM	5.4 mM	3.8 mM	$E_{Cs,\ iso}$: -80.7 mV	$E_{Cs,\ hypo}$: -89.8 mV
Cl^-	147.4 mM	167.8 mM	117.5 mM	$E_{Cl,\ iso}$: -3.3 mV	$E_{Cl,\ hypo}$: +5.8 mV
Na^+	10.0 mM	150.0 mM	105.0 mM	$E_{Na,\ iso}$: +69.5 mV	$E_{Na,\ hypo}$: +60.4 mV
Ca^{2+}	0 mM	5.4 mM	3.8 mM	$E_{Ca,\ iso}$: +∞ mV	$E_{Ca,\ hypo}$: +∞ mV

Forst et al. (2015)	**[Ion] in intracellular solution**	**[Ion] in iso- and hypotonic extracellular solution**	**Calculated equilibrium potentials at 22°C in iso- and hypotonic extracellular solution**
Cs^+	120.0 mM	0 mM	E_{Cs} : -∞ mV
Cl^-	137.0 mM	112.0 mM	E_{Cl} : +5.2 mV
Na^+	10.0 mM	110.0 mM	E_{Na} : +61.6 mV
Ca^{2+}	100.0 nM	0.1 mM	E_{Ca} : +88.7 mV

VIII Appendix

1. List of Figures

2. List of Tables

3. List of Supplements

IX References

Abdul-Majeed, S., and **Nauli, S.M.** (2011). Dopamine receptor type 5 in the primary cilia has dual chemo- and mechano-sensory roles. Hypertension *58*, 325-331.
Ainsley, J.A., Pettus, J.M., Bosenko, D., Gerstein, C.E., Zinkevich, N., Anderson, M.G., Adams, C.M., Welsh, M.J., and Johnson, W.A. (2003). Enhanced locomotion caused by loss of the Drosophila DEG/ENaC protein Pickpocket1. Curr Biol *13*, 1557-1563.
Akchurin, O., and **Reidy, K.J.** (2015). Genetic causes of proteinuria and nephrotic syndrome: Impact on podocyte pathobiology. Pediatr Nephrol *30*, 221-233.
Alfonso, S., Benito, O., Alicia, S., Angelica, Z., Patricia, G., Diana, K., and Vaca, L. (2008). Regulation of the cellular localization and function of human transient receptor potential channel 1 by other members of the TRPC family. Cell Calcium *43*, 375-387.
Alloui, A., Zimmermann, K., Mamet, J., Duprat, F., Noel, J., Chemin, J., Guy, N., Blondeau,N., Voilley, N., Rubat-Coudert, C.*, et al.* (2006). TREK-1, a K+ channel involved in polymodal pain perception. EMBO J *25*, 2368-2376.
Althaus, M., Bogdan, R., Clauss, W.G., and Fronius, M. (2007). Mechano-sensitivity of epithelial sodium channels (ENaCs): laminar shear stress increases ion channel open probability. FASEB J *21*, 2389-2399.
Anderson, M., Kim, E.Y., Hagmann, H., Benzing, T., and Dryer, S.E. (2013). Opposing effects of podocin on the gating of podocyte TRPC6 channels evoked by membrane stretch or diacylglycerol. Am J Physiol Cell Physiol *305*, C276-289.
Arnadottir, J., and **Chalfie, M.** (2010). Eukaryotic mechanosensitive channels. Annu Rev Biophys *39*, 111-137.
Awayda, M.S., Ismailov, II, Berdiev, B.K., and Benos, D.J. (1995). A cloned renal epithelial Na+ channel protein displays stretch activation in planar lipid bilayers. Am J Physiol *268*, C1450-1459.
Awayda, M.S., and **Subramanyam, M.** (1998). Regulation of the epithelial Na+ channel by membrane tension. J Gen Physiol *112*, 97-111.
Bae, C., Sachs, F., and Gottlieb, P.A. (2011). The mechanosensitive ion channel Piezo1 is inhibited by the peptide GsMTx4. Biochemistry *50*, 6295-6300.
Balazs, B., Danko, T., Kovacs, G., Koles, L., Hediger, M.A., and Zsembery, A. (2013). Investigation of the inhibitory effects of the benzodiazepine derivative, 5-BDBD on P2X4 purinergic receptors by two complementary methods. Cell Physiol Biochem *32*, 11-24.
Bandell, M., Story, G.M., Hwang, S.W., Viswanath, V., Eid, S.R., Petrus, M.J., Earley, T.J., and Patapoutian, A. (2004). Noxious cold ion channel TRPA1 is activated by pungent compounds and bradykinin. Neuron *41*, 849-857.
Bang, H., Kim, Y., and Kim, D. (2000). TREK-2, a new member of the mechanosensitive tandem-pore K+ channel family. J Biol Chem *275*, 17412-17419.
Bass, R.B., Strop, P., Barclay, M., and Rees, D.C. (2002). Crystal structure of Escherichia coli MscS, a voltage-modulated and mechanosensitive channel. Science *298*, 1582-1587.
Bautista, D.M., Jordt, S.E., Nikai, T., Tsuruda, P.R., Read, A.J., Poblete, J., Yamoah, E.N., Basbaum, A.I., and Julius, D. (2006). TRPA1 mediates the inflammatory actions of environmental irritants and proalgesic agents. Cell *124*, 1269-1282.
Bayliss, W.M. (1902). On the local reactions of the arterial wall to changes of internal pressure. J Physiol *28*, 220-231.
Beech, D.J. (2007a). Bipolar phospholipid sensing by TRPC5 calcium channel. Biochem Soc Trans *35*, 101-104.
Beech, D.J. (2007b). Canonical transient receptor potential 5. Handb Exp Pharmacol, 109-123.
Bernstein, B.W., and **Bamburg, J.R.** (2003). Actin-ATP hydrolysis is a major energy drain for neurons. J Neurosci *23*, 1-6.
Berrier, C., Pozza, A., de Lacroix de Lavalette, A., Chardonnet, S., Mesneau, A., Jaxel, C., le Maire, M., and Ghazi, A. (2013). The purified mechanosensitive channel TREK-1 is directly sensitive to membrane tension. J Biol Chem *288*, 27307-27314.

Bessac, B.F., and Fleig, A. (2007). TRPM7 channel is sensitive to osmotic gradients in human kidney cells. J Physiol *582*, 1073-1086.
Betanzos, M., Chiang, C.S., Guy, H.R., and Sukharev, S. (2002). A large iris-like expansion of a mechanosensitive channel protein induced by membrane tension. Nat Struct Biol *9*, 704-710.
Bevan, J.A., and **Laher, I.** (1991). Pressure and flow-dependent vascular tone. Faseb J *5*, 2267-2273.
Bianchi, L. (2007). Mechanotransduction: touch and feel at the molecular level as modeled in Caenorhabditis elegans. Mol Neurobiol *36*, 254-271.
Birder, L.A., Nakamura, Y., Kiss, S., Nealen, M.L., Barrick, S., Kanai, A.J., Wang, E., Ruiz, G., De Groat, W.C., Apodaca, G.*, et al.* (2002). Altered urinary bladder function in mice lacking the vanilloid receptor TRPV1. Nat Neurosci *5*, 856-860.
Blodow, S., Schneider, H., Storch, U., Wizemann, R., Forst, A.L., Gudermann, T., and Mederos y Schnitzler, M. (2014). Novel role of mechanosensitive AT1B receptors in myogenic vasoconstriction. Pflugers Arch *466*, 1343-1353.
Bounoutas, A., and Chalfie, M. (2007). Touch sensitivity in Caenorhabditis elegans. Pflugers Arch *454*, 691-702.
Bowman, C.L., Gottlieb, P.A., Suchyna, T.M., Murphy, Y.K., and Sachs, F. (2007). Mechanosensitive ion channels and the peptide inhibitor GsMTx-4: history, properties, mechanisms and pharmacology. Toxicon *49*, 249-270.
Brierley, S.M. (2010). Molecular basis of mechanosensitivity. Auton Neurosci *153*, 58-68.
Brierley, S.M., Castro, J., Harrington, A.M., Hughes, P.A., Page, A.J., Rychkov, G.Y., and Blackshaw, L.A. (2011). TRPA1 contributes to specific mechanically activated currents and sensory neuron mechanical hypersensitivity. J Physiol *589*, 3575-3593.
Brohawn, S.G., Su, Z., and MacKinnon, R. (2014). Mechanosensitivity is mediated directly by the lipid membrane in TRAAK and TREK1 K+ channels. Proc Natl Acad Sci U S A *111*, 3614-3619.
Brownlow, S.L., and **Sage, S.O.** (2005). Transient receptor potential protein subunit assembly and membrane distribution in human platelets. Thromb Haemost *94*, 839-845.
Bubb, M.R., Spector, I., Beyer, B.B., and Fosen, K.M. (2000). Effects of jasplakinolide on the kinetics of actin polymerization. An explanation for certain in vivo observations. J Biol Chem *275*, 5163-5170.
Candelario, J.C., Mirianas (2012). Mechanical Stress Stimulates Conformational Changes in 5-Hydroxytryptamine Receptor 1B in Bone Cells. Cellular and Molecular Bioengineering *5*, 277–286.
Cantor, R.S. (1997a). The lateral pressure profile in membranes: a physical mechanism of general anesthesia. Biochemistry *36*, 2339-2344.
Cantor, R.S. (1997b). Lateral Pressures in Cell Membranes: A Mechanism for Modulation of Protein Function. J Phys Chem B *101*, 1723-1725.
Cantor, R.S. (1999a). The influence of membrane lateral pressures on simple geometric models of protein conformational equilibria. Chem Phys Lipids *101*, 45-56.
Cantor, R.S. (1999b). Lipid composition and the lateral pressure profile in bilayers. Biophys J *76*, 2625-2639.
Carattino, M.D., Sheng, S., and Kleyman, T.R. (2004). Epithelial Na+ channels are activated by laminar shear stress. J Biol Chem *279*, 4120-4126.
Chachisvilis, M., Zhang, Y.L., and Frangos, J.A. (2006). G protein-coupled receptors sense fluid shear stress in endothelial cells. Proc Natl Acad Sci U S A *103*, 15463-15468.
Chalfie, M., and **Sulston, J.** (1981). Developmental genetics of the mechanosensory neurons of Caenorhabditis elegans. Dev Biol *82*, 358-370.
Chang, G., Spencer, R.H., Lee, A.T., Barclay, M.T., and Rees, D.C. (1998). Structure of the MscL homolog from Mycobacterium tuberculosis: a gated mechanosensitive ion channel. Science *282*, 2220-2226.
Chatzigeorgiou, M., Bang, S., Hwang, S.W., and Schafer, W.R. (2013). tmc-1 encodes a sodium-sensitive channel required for salt chemosensation in C. elegans. Nature *494*, 95-99.

Chen, X., Li, W., Yoshida, H., Tsuchida, S., Nishimura, H., Takemoto, F., Okubo, S., Fogo, A., Matsusaka, T., and Ichikawa, I. (1997). Targeting deletion of angiotensin type 1B receptor gene in the mouse. Am J Physiol *272*, F299-304.
Cheng, K.T., Ong, H.L., Liu, X., and Ambudkar, I.S. (2013). Contribution and regulation of TRPC channels in store-operated Ca2+ entry. Curr Top Membr *71*, 149-179.
Chubanov, V., Mederos y Schnitzler, M., Meissner, M., Schafer, S., Abstiens, K., Hofmann, T., and Gudermann, T. (2012). Natural and synthetic modulators of SK (K(ca)2) potassium channels inhibit magnesium-dependent activity of the kinase-coupled cation channel TRPM7. Br J Pharmacol *166*, 1357-1376.
Ciura, S., and **Bourque, C.W.** (2006). Transient receptor potential vanilloid 1 is required for intrinsic osmoreception in organum vasculosum lamina terminalis neurons and for normal thirst responses to systemic hyperosmolality. J Neurosci *26*, 9069-9075.
Clapham, D.E., Runnels, L.W., and Strubing, C. (2001). The TRP ion channel family. Nat Rev Neurosci *2*, 387-396.
Colbert, H.A., Smith, T.L., and Bargmann, C.I. (1997). OSM-9, a novel protein with structural similarity to channels, is required for olfaction, mechanosensation, and olfactory adaptation in Caenorhabditis elegans. J Neurosci *17*, 8259-8269.
Corey, D.P., Garcia-Anoveros, J., Holt, J.R., Kwan, K.Y., Lin, S.Y., Vollrath, M.A., Amalfitano, A., Cheung, E.L., Derfler, B.H., Duggan, A.*, et al.* (2004). TRPA1 is a candidate for the mechanosensitive transduction channel of vertebrate hair cells. Nature *432*, 723-730.
Coste, B., Houge, G., Murray, M.F., Stitziel, N., Bandell, M., Giovanni, M.A., Philippakis, A., Hoischen, A., Riemer, G., Steen, U.*, et al.* (2013). Gain-of-function mutations in the mechanically activated ion channel PIEZO2 cause a subtype of Distal Arthrogryposis. Proc Natl Acad Sci U S A *110*, 4667-4672.
Coste, B., Mathur, J., Schmidt, M., Earley, T.J., Ranade, S., Petrus, M.J., Dubin, A.E., and Patapoutian, A. (2010). Piezo1 and Piezo2 are essential components of distinct mechanically activated cation channels. Science *330*, 55-60.
Coste, B., Xiao, B., Santos, J.S., Syeda, R., Grandl, J., Spencer, K.S., Kim, S.E., Schmidt, M., Mathur, J., Dubin, A.E.*, et al.* (2012). Piezo proteins are pore-forming subunits of mechanically activated channels. Nature *483*, 176-181.
Courbebaisse, M., Leroy, C., Bakouh, N., Salaun, C., Beck, L., Grandchamp, B., Planelles, G., Hall, R.A., Friedlander, G., and Prie, D. (2012). A new human NHERF1 mutation decreases renal phosphate transporter NPT2a expression by a PTH-independent mechanism. PLoS One *7*, e34764.
Cummins, P.M., von Offenberg Sweeney, N., Killeen, M.T., Birney, Y.A., Redmond, E.M., and Cahill, P.A. (2007). Cyclic strain-mediated matrix metalloproteinase regulation within the vascular endothelium: a force to be reckoned with. Am J Physiol Heart Circ Physiol *292*, H28-42.
Darby, M., Kuzmiski, J.B., Panenka, W., Feighan, D., and MacVicar, B.A. (2003). ATP released from astrocytes during swelling activates chloride channels. J Neurophysiol *89*, 1870-1877.
Davis, M.J., and **Hill, M.A.** (1999). Signaling mechanisms underlying the vascular myogenic response. Physiol Rev *79*, 387-423.
Delmas, P., and **Coste, B.** (2013). Mechano-gated ion channels in sensory systems. Cell *155*, 278-284.
Di Palma, F., Belyantseva, I.A., Kim, H.J., Vogt, T.F., Kachar, B., and Noben-Trauth, K. (2002). Mutations in Mcoln3 associated with deafness and pigmentation defects in varitint-waddler (Va) mice. Proc Natl Acad Sci U S A *99*, 14994-14999.
Dietrich, A., Chubanov, V., Kalwa, H., Rost, B.R., and Gudermann, T. (2006). Cation channels of the transient receptor potential superfamily: their role in physiological and pathophysiological processes of smooth muscle cells. Pharmacol Ther *112*, 744-760.
Dietrich, A., Kalwa, H., Storch, U., Mederos y Schnitzler, M., Salanova, B., Pinkenburg, O., Dubrovska, G., Essin, K., Gollasch, M., Birnbaumer, L.*, et al.* (2007). Pressure-induced and store-operated cation influx in vascular smooth muscle cells is independent of TRPC1. Pflugers Arch *455*, 465-477.

Dietrich, A., Mederos y Schnitzler, M., Gollasch, M., Gross, V., Storch, U., Dubrovska, G., Obst, M., Yildirim, E., Salanova, B., Kalwa, H.*, et al.* (2005). Increased vascular smooth muscle contractility in TRPC6-/- mice. Mol Cell Biol *25*, 6980-6989.
Duc, C., Farman, N., Canessa, C.M., Bonvalet, J.P., and Rossier, B.C. (1994). Cell-specific expression of epithelial sodium channel alpha, beta, and gamma subunits in aldosterone-responsive epithelia from the rat: localization by in situ hybridization and immunocytochemistry. J Cell Biol *127*, 1907-1921.
Earley, S., Waldron, B.J., and Brayden, J.E. (2004). Critical role for transient receptor potential channel TRPM4 in myogenic constriction of cerebral arteries. Circ Res *95*, 922-929.
Eijkelkamp, N., Linley, J.E., Torres, J.M., Bee, L., Dickenson, A.H., Gringhuis, M., Minett, M.S., Hong, G.S., Lee, E., Oh, U.*, et al.* (2013). A role for Piezo2 in EPAC1-dependent mechanical allodynia. Nat Commun *4*, 1682.
Endlich, N., Kress, K.R., Reiser, J., Uttenweiler, D., Kriz, W., Mundel, P., and Endlich, K. (2001). Podocytes respond to mechanical stress in vitro. J Am Soc Nephrol *12*, 413-422.
Ernstrom, G.G., and Chalfie, M. (2002). Genetics of sensory mechanotransduction. Annu Rev Genet *36*, 411-453.
Fabian, A., Fortmann, T., Bulk, E., Bomben, V.C., Sontheimer, H., and Schwab, A. (2011). Chemotaxis of MDCK-F cells toward fibroblast growth factor-2 depends on transient receptor potential canonical channel 1. Pflugers Arch *461*, 295-306.
Fabian, A., Fortmann, T., Dieterich, P., Riethmuller, C., Schon, P., Mally, S., Nilius, B., and Schwab, A. (2008). TRPC1 channels regulate directionality of migrating cells. Pflugers Arch *457*, 475-484.
Flemming, P.K., Dedman, A.M., Xu, S.Z., Li, J., Zeng, F., Naylor, J., Benham, C.D., Bateson, A.N., Muraki, K., and Beech, D.J. (2006). Sensing of lysophospholipids by TRPC5 calcium channel. J Biol Chem *281*, 4977-4982.
Forst, A.L.;Olteanu., V.; Mollet, G.; Wlodkowski, T.; Schaefer, F.; Dietrich, A.; Reiser, J.; Gudermann, T.; Mederos y Schnitzler, M.; Storch, U. (2015). Purinergic P2X4 channels are crucial mechanotransducers in podocytes mediating disorganization of the cytoskeleton. J Am Soc Nephrol. 2015 Jul 9. pii: ASN.2014111144. [published ahead of print].
Friedlova, E., Grycova, L., Holakovska, B., Silhan, J., Janouskova, H., Sulc, M., Obsilova, V., Obsil, T., and Teisinger, J. (2010). The interactions of the C-terminal region of the TRPC6 channel with calmodulin. Neurochem Int *56*, 363-366.
Friis, U.G., Jensen, B.L., Aas, J.K., and Skott, O. (1999). Direct demonstration of exocytosis and endocytosis in single mouse juxtaglomerular cells. Circ Res *84*, 929-936.
Gao, X., Wu, L., and O'Neil, R.G. (2003). Temperature-modulated diversity of TRPV4 channel gating: activation by physical stresses and phorbol ester derivatives through protein kinase C-dependent and -independent pathways. J Biol Chem *278*, 27129-27137.
Garcia-Anoveros, J., Garcia, J.A., Liu, J.D., and Corey, D.P. (1998). The nematode degenerin UNC-105 forms ion channels that are activated by degeneration- or hypercontraction-causing mutations. Neuron *20*, 1231-1241.
Garry, A., Fromy, B., Blondeau, N., Henrion, D., Brau, F., Gounon, P., Guy, N., Heurteaux, C., Lazdunski, M., and Saumet, J.L. (2007). Altered acetylcholine, bradykinin and cutaneous pressure-induced vasodilation in mice lacking the TREK1 potassium channel: the endothelial link. EMBO Rep *8*, 354-359.
Geffeney, S.L., Cueva, J.G., Glauser, D.A., Doll, J.C., Lee, T.H., Montoya, M., Karania, S., Garakani, A.M., Pruitt, B.L., and Goodman, M.B. (2011). DEG/ENaC but not TRP channels are the major mechanoelectrical transduction channels in a C. elegans nociceptor. Neuron *71*, 845-857.
Geng, L., Okuhara, D., Yu, Z., Tian, X., Cai, Y., Shibazaki, S., and Somlo, S. (2006). Polycystin-2 traffics to cilia independently of polycystin-1 by using an N-terminal RVxP motif. J Cell Sci *119*, 1383-1395.
Gerka-Stuyt, J., Au, A., Peachey, N.S., and Alagramam, K.N. (2013). Transient receptor potential melastatin 1: a hair cell transduction channel candidate. PLoS One *8*, e77213.
Gillespie, P.G., and **Muller, U.** (2009). Mechanotransduction by hair cells: models, molecules, and mechanisms. Cell *139*, 33-44.

Gillespie, P.G., and **Walker, R.G.** (2001). Molecular basis of mechanosensory transduction. Nature *413*, 194-202.
Glazebrook, P.A., Schilling, W.P., and Kunze, D.L. (2005). TRPC channels as signal transducers. Pflugers Arch *451*, 125-130.
Goel, M., Sinkins, W., Keightley, A., Kinter, M., and Schilling, W.P. (2005). Proteomic analysis of TRPC5- and TRPC6-binding partners reveals interaction with the plasmalemmal Na(+)/K(+)-ATPase. Pflugers Arch *451*, 87-98.
Goel, M., Sinkins, W.G., and Schilling, W.P. (2002). Selective Association of TRPC Channel Subunits in Rat Brain Synaptosomes. J Biol Chem *277*, 48303-48310.
Gomis, A., Soriano, S., Belmonte, C., and Viana, F. (2008). Hypoosmotic- and pressure-induced membrane stretch activate TRPC5 channels. J Physiol *586*, 5633-5649.
Gong, Z., Son, W., Chung, Y.D., Kim, J., Shin, D.W., McClung, C.A., Lee, Y., Lee, H.W., Chang, D.J., Kaang, B.K.*, et al.* (2004). Two interdependent TRPV channel subunits, inactive and Nanchung, mediate hearing in Drosophila. J Neurosci *24*, 9059-9066.
Gonzalez-Perrett, S., Kim, K., Ibarra, C., Damiano, A.E., Zotta, E., Batelli, M., Harris, P.C., Reisin, I.L., Arnaout, M.A., and Cantiello, H.F. (2001). Polycystin-2, the protein mutated in autosomal dominant polycystic kidney disease (ADPKD), is a Ca2+-permeable nonselective cation channel. Proc Natl Acad Sci U S A *98*, 1182-1187.
Gottlieb, P., Folgering, J., Maroto, R., Raso, A., Wood, T.G., Kurosky, A., Bowman, C., Bichet, D., Patel, A., Sachs, F.*, et al.* (2008). Revisiting TRPC1 and TRPC6 mechanosensitivity. Pflugers Arch *455*, 1097-1103.
Greka, A., and **Mundel, P.** (2012). Calcium regulates podocyte actin dynamics. Semin Nephrol *32*, 319-326.
Greka, A., Navarro, B., Oancea, E., Duggan, A., and Clapham, D.E. (2003). TRPC5 is a regulator of hippocampal neurite length and growth cone morphology. Nat Neurosci *6*, 837-845.
Grimm, C., Cuajungco, M.P., van Aken, A.F., Schnee, M., Jors, S., Kros, C.J., Ricci, A.J., and Heller, S. (2007). A helix-breaking mutation in TRPML3 leads to constitutive activity underlying deafness in the varitint-waddler mouse. Proc Natl Acad Sci U S A *104*, 19583-19588.
Grimm, C., Kraft, R., Sauerbruch, S., Schultz, G., and Harteneck, C. (2003). Molecular and functional characterization of the melastatin-related cation channel TRPM3. J Biol Chem *278*, 21493-21501.
Grzybek, M., Chorzalska, A., Bok, E., Hryniewicz-Jankowska, A., Czogalla, A., Diakowski, W., and Sikorski, A.F. (2006). Spectrin-phospholipid interactions. Existence of multiple kinds of binding sites? Chem Phys Lipids *141*, 133-141.
Hamill, O.P., and McBride, D.W., Jr. (1997). Induced membrane hypo/hyper-mechanosensitivity: a limitation of patch-clamp recording. Annu Rev Physiol *59*, 621-631.
Hanaoka, K., Qian, F., Boletta, A., Bhunia, A.K., Piontek, K., Tsiokas, L., Sukhatme, V.P., Guggino, W.B., and Germino, G.G. (2000). Co-assembly of polycystin-1 and -2 produces unique cation-permeable currents. Nature *408*, 990-994.
Hartmannsgruber, V., Heyken, W.T., Kacik, M., Kaistha, A., Grgic, I., Harteneck, C., **Liedtke, W.**, Hoyer, J., and Kohler, R. (2007). Arterial response to shear stress critically depends on endothelial TRPV4 expression. PLoS One *2*, e827.
Haswell, E.S., Phillips, R., and Rees, D.C. (2011). Mechanosensitive channels: what can they do and how do they do it? Structure *19*, 1356-1369.
Hayakawa, K., Tatsumi, H., and Sokabe, M. (2008). Actin stress fibers transmit and focus force to activate mechanosensitive channels. J Cell Sci *121*, 496-503.
Herve, J.C. (2014). Reciprocal influences between cell cytoskeleton and membrane channels, receptors and transporters. Biochim Biophys Acta *1838*, 511-513.
Hill, K., and **Schaefer, M.** (2007). TRPA1 is differentially modulated by the amphipathic molecules trinitrophenol and chlorpromazine. J Biol Chem *282*, 7145-7153.
Hirono, M., Denis, C.S., Richardson, G.P., and Gillespie, P.G. (2004). Hair cells require phosphatidylinositol 4,5-bisphosphate for mechanical transduction and adaptation. Neuron *44*, 309-320.

Hoffman, B.D., Grashoff, C., and Schwartz, M.A. (2011). Dynamic molecular processes mediate cellular mechanotransduction. Nature *475*, 316-323.
Hofmann, T., Obukhov, A.G., Schaefer, M., Harteneck, C., Gudermann, T., and Schultz, G. (1999). Direct activation of human TRPC6 and TRPC3 channels by diacylglycerol. Nature *397*, 259-263.
Hofmann, T., Schaefer, M., Schultz, G., and Gudermann, T. (2002). Subunit composition of mammalian transient receptor potential channels in living cells. Proc Natl Acad Sci U S A *99*, 7461-7466.
Homolya, L., Steinberg, T.H., and Boucher, R.C. (2000). Cell to cell communication in response to mechanical stress via bilateral release of ATP and UTP in polarized epithelia. J Cell Biol *150*, 1349-1360.
Hong, C., Kim, J., Jeon, J.P., Wie, J., Kwak, M., Ha, K., Kim, H., Myeong, J., Kim, S.Y., Jeon, J.H.*, et al.* (2012). Gs cascade regulates canonical transient receptor potential 5 (TRPC5) through cAMP mediated intracellular Ca2+ release and ion channel trafficking. Biochem Biophys Res Commun *421*, 105-111.
Honore, E. (2007). The neuronal background K2P channels: focus on TREK1. Nat Rev Neurosci *8*, 251-261.
Honore, E., Maingret, F., Lazdunski, M., and Patel, A.J. (2002). An intracellular proton sensor commands lipid- and mechano-gating of the K(+) channel TREK-1. EMBO J *21*, 2968-2976.
Honore, E., Patel, A.J., Chemin, J., Suchyna, T., and Sachs, F. (2006). Desensitization of mechano-gated K2P channels. Proc Natl Acad Sci U S A *103*, 6859-6864.
Horner, V.L., and Wolfner, M.F. (2008). Mechanical stimulation by osmotic and hydrostatic pressure activates Drosophila oocytes in vitro in a calcium-dependent manner. Dev Biol *316*, 100-109.
Hua, S.Z., Gottlieb, P.A., Heo, J., and Sachs, F. (2010). A mechanosensitive ion channel regulating cell volume. Am J Physiol Cell Physiol *298*, C1424-1430.
Huang, C., Bruggeman, L.A., Hydo, L.M., and Miller, R.T. (2012). Shear stress induces cell apoptosis via a c-Src-phospholipase D-mTOR signaling pathway in cultured podocytes. Exp Cell Res *318*, 1075-1085.
Huang, H., Kamm, R.D., and Lee, R.T. (2004). Cell mechanics and mechanotransduction: pathways, probes, and physiology. Am J Physiol Cell Physiol *287*, C1-11.
Huber, T.B., and **Benzing, T.** (2005). The slit diaphragm: a signaling platform to regulate podocyte function. Curr Opin Nephrol Hypertens *14*, 211-216.
Huber, T.B., Schermer, B., and Benzing, T. (2007). Podocin organizes ion channel-lipid supercomplexes: implications for mechanosensation at the slit diaphragm. Nephron Exp Nephrol *106*, e27-31.
Huber, T.B., Schermer, B., Muller, R.U., Hohne, M., Bartram, M., Calixto, A., Hagmann, H., Reinhardt, C., Koos, F., Kunzelmann, K.*, et al.* (2006). Podocin and MEC-2 bind cholesterol to regulate the activity of associated ion channels. Proc Natl Acad Sci U S A *103*, 17079-17086.
Ikeda, R., Cha, M., Ling, J., Jia, Z., Coyle, D., and Gu, J.G. (2014). Merkel cells transduce and encode tactile stimuli to drive Abeta-afferent impulses. Cell *157*, 664-675.
Ikeda, R., and Gu, J.G. (2014). Piezo2 channel conductance and localization domains in Merkel cells of rat whisker hair follicles. Neurosci Lett.
Inoue, R., Jensen, L.J., Jian, Z., Shi, J., Hai, L., Lurie, A.I., Henriksen, F.H., Salomonsson, M., Morita, H., Kawarabayashi, Y.*, et al.* (2009). Synergistic activation of vascular TRPC6 channel by receptor and mechanical stimulation via phospholipase C/diacylglycerol and phospholipase A2/omega-hydroxylase/20-HETE pathways. Circ Res *104*, 1399-1409.
I**to, M.**, Oliverio, M.I., Mannon, P.J., Best, C.F., Maeda, N., Smithies, O., and Coffman, T.M. (1995). Regulation of blood pressure by the type 1A angiotensin II receptor gene. Proc Natl Acad Sci U S A *92*, 3521-3525.
Jarajapu, Y.P., and Knot, H.J. (2002). Role of phospholipase C in development of myogenic tone in rat posterior cerebral arteries. Am J Physiol Heart Circ Physiol *283*, H2234-2238.
Jemal, I., Soriano, S., Conte, A.L., Morenilla, C., and Gomis, A. (2014). G protein-coupled receptor signalling potentiates the osmo-mechanical activation of TRPC5 channels. Pflugers Arch *466*, 1635-1646.

Jensen, M.E., Odgaard, E., Christensen, M.H., Praetorius, H.A., and Leipziger, J. (2007). Flow-induced [Ca2+]i increase depends on nucleotide release and subsequent purinergic signaling in the intact nephron. J Am Soc Nephrol *18*, 2062-2070.
Jeon, J.P., Roh, S.E., Wie, J., Kim, J., Kim, H., Lee, K.P., Yang, D., Jeon, J.H., Cho, N.H., Kim, I.G.*, et al.* (2013). Activation of TRPC4beta by Galphai subunit increases Ca2+ selectivity and controls neurite morphogenesis in cultured hippocampal neuron. Cell Calcium *54*, 307-319.
Jiang, K. (2012). Firm Molecular Handshake Needed for Hearing, Balance, pp. Researchers describe for the first time the structure of a bond formed by two proteins critical for hearing and balance.
John Haynes, W., Zhou, X.L., Su, Z.W., Loukin, S.H., Saimi, Y., and Kung, C. (2008). Indole and other aromatic compounds activate the yeast TRPY1 channel. FEBS Lett *582*, 1514-1518.
Jordt, S.E., Bautista, D.M., Chuang, H.H., McKemy, D.D., Zygmunt, P.M., Hogestatt, E.D., Meng, I.D., and Julius, D. (2004). Mustard oils and cannabinoids excite sensory nerve fibres through the TRP channel ANKTM1. Nature *427*, 260-265.
Kaczmarek, J.S., Riccio, A., and Clapham, D.E. (2012). Calpain cleaves and activates the TRPC5 channel to participate in semaphorin 3A-induced neuronal growth cone collapse. Proc Natl Acad Sci U S A *109*, 7888-7892.
Kalwa, H., Storch, U., Demleitner, J., Fiedler, S., Mayer, T., Kannler, M., Fahlbusch, M., Barth, H., Smrcka, A., Hildebrandt, F.*, et al.* (2014). Phospholipase C epsilon-induced TRPC6 activation: A common but redundant mechanism in primary podocytes. J Cell Physiol.
Kato, H., Osajima, A., Uezono, Y., Okazaki, M., Tsuda, Y., Tanaka, H., Oishi, Y., Izumi, F., and Nakashima, Y. (1999). Involvement of PDGF in pressure-induced mesangial cell proliferation through PKC and tyrosine kinase pathways. Am J Physiol *277*, F105-112.
Katsumi, A., Orr, A.W., Tzima, E., and Schwartz, M.A. (2004). Integrins in mechanotransduction. J Biol Chem *279*, 12001-12004.
Kawashima, Y., Geleoc, G.S., Kurima, K., Labay, V., Lelli, A., Asai, Y., Makishima, T., Wu, D.K., Della Santina, C.C., Holt, J.R.*, et al.* (2011). Mechanotransduction in mouse inner ear hair cells requires transmembrane channel-like genes. J Clin Invest *121*, 4796-4809.
Ke, H.Z., Qi, H., Weidema, A.F., Zhang, Q., Panupinthu, N., Crawford, D.T., Grasser, W.A., Paralkar, V.M., Li, M., Audoly, L.P.*, et al.* (2003). Deletion of the P2X7 nucleotide receptor reveals its regulatory roles in bone formation and resorption. Mol Endocrinol *17*, 1356-1367.
Kellenberger, S., and Schild, L. (2002). Epithelial sodium channel/degenerin family of ion channels: a variety of functions for a shared structure. Physiol Rev *82*, 735-767.
Kessler, S., Clauss, W.G., and Fronius, M. (2011). Laminar shear stress modulates the activity of heterologously expressed P2X(4) receptors. Biochim Biophys Acta *1808*, 2488-2495.
Kim, B.J., Kim, M.T., Jeon, J.H., Kim, S.J., and So, I. (2008). Involvement of phosphatidylinositol 4,5-bisphosphate in the desensitization of canonical transient receptor potential 5. Biol Pharm Bull *31*, 1733-1738.
Kim, J., Chung, Y.D., Park, D.Y., Choi, S., Shin, D.W., Soh, H., Lee, H.W., Son, W., Yim, J., Park, C.S.*, et al.* (2003). A TRPV family ion channel required for hearing in Drosophila. Nature *424*, 81-84.
Kim, J., Kwak, M., Jeon, J.P., Myeong, J., Wie, J., Hong, C., Kim, S.Y., Jeon, J.H., Kim, H.J., and So, I. (2014). Isoform- and receptor-specific channel property of canonical transient receptor potential (TRPC)1/4 channels. Pflugers Arch *466*, 491-504.
Kim, S.E., Coste, B., Chadha, A., Cook, B., and Patapoutian, A. (2012). The role of Drosophila Piezo in mechanical nociception. Nature *483*, 209-212.
Kindt, K.S., Viswanath, V., Macpherson, L., Quast, K., Hu, H., Patapoutian, A., and Schafer, W.R. (2007). Caenorhabditis elegans TRPA-1 functions in mechanosensation. Nat Neurosci *10*, 568-577.
Kottgen, M., Buchholz, B., Garcia-Gonzalez, M.A., Kotsis, F., Fu, X., Doerken, M., Boehlke, C., Steffl, D., Tauber, R., Wegierski, T.*, et al.* (2008). TRPP2 and TRPV4 form a polymodal sensory channel complex. J Cell Biol *182*, 437-447.
Kung, C. (2005). A possible unifying principle for mechanosensation. Nature *436*, 647-654.

Kurima, K., Peters, L.M., Yang, Y., Riazuddin, S., Ahmed, Z.M., Naz, S., Arnaud, D., Drury, S., Mo, J., Makishima, T.*, et al.* (2002). Dominant and recessive deafness caused by mutations of a novel gene, TMC1, required for cochlear hair-cell function. Nat Genet *30*, 277-284.
Kuwahara, K., Wang, Y., McAnally, J., Richardson, J.A., Bassel-Duby, R., Hill, J.A., and Olson, E.N. (2006). TRPC6 fulfills a calcineurin signaling circuit during pathologic cardiac remodeling. J Clin Invest *116*, 3114-3126.
Kuznetsova, T.G., Starodubtseva, M.N., Yegorenkov, N.I., Chizhik, S.A., and Zhdanov, R.I. (2007). Atomic force microscopy probing of cell elasticity. Micron *38*, 824-833.
Kwan, K.Y., Allchorne, A.J., Vollrath, M.A., Christensen, A.P., Zhang, D.S., Woolf, C.J., and Corey, D.P. (2006). TRPA1 contributes to cold, mechanical, and chemical nociception but is not essential for hair-cell transduction. Neuron *50*, 277-289.
Kwon, Y., Hofmann, T., and Montell, C. (2007). Integration of phosphoinositide- and calmodulin-mediated regulation of TRPC6. Mol Cell *25*, 491-503.
Labay, V., Weichert, R.M., Makishima, T., and Griffith, A.J. (2010). Topology of transmembrane channel-like gene 1 protein. Biochemistry *49*, 8592-8598.
Leake, M.C., Wilson, D., Gautel, M., and Simmons, R.M. (2004). The elasticity of single titin molecules using a two-bead optical tweezers assay. Biophys J *87*, 1112-1135.
Lee-Kwon, W., Wade, J.B., Zhang, Z., Pallone, T.L., and Weinman, E.J. (2005). Expression of TRPC4 channel protein that interacts with NHERF-2 in rat descending vasa recta. Am J Physiol Cell Physiol *288*, C942-949.
Lee, K.P., Choi, S., Hong, J.H., Ahuja, M., Graham, S., Ma, R., So, I., Shin, D.M., Muallem, S., and Yuan, J.P. (2014). Molecular determinants mediating gating of Transient Receptor Potential Canonical (TRPC) channels by stromal interaction molecule 1 (STIM1). J Biol Chem *289*, 6372-6382.
Lehnert, B.P., Baker, A.E., Gaudry, Q., Chiang, A.S., and Wilson, R.I. (2013). Distinct roles of TRP channels in auditory transduction and amplification in Drosophila. Neuron *77*, 115-128.
Lehtonen, J.Y., and **Kinnunen, P.K.** (1995). Phospholipase A2 as a mechanosensor. Biophys J *68*, 1888-1894.
Lennertz, R.C., Kossyreva, E.A., Smith, A.K., and Stucky, C.L. (2012). TRPA1 mediates mechanical sensitization in nociceptors during inflammation. PLoS One *7*, e43597.
Lesage, F., Maingret, F., and Lazdunski, M. (2000). Cloning and expression of human TRAAK, a polyunsaturated fatty acids-activated and mechano-sensitive K(+) channel. FEBS Lett *471*, 137-140.
Li, J., and **Fountain, S.J.** (2012). Fluvastatin suppresses native and recombinant human P2X4 receptor function. Purinergic Signal *8*, 311-316.
Li, W., Feng, Z., Sternberg, P.W., and Xu, X.Z. (2006). A C. elegans stretch receptor neuron revealed by a mechanosensitive TRP channel homologue. Nature *440*, 684-687.
Liedtke, W., Choe, Y., Marti-Renom, M.A., Bell, A.M., Denis, C.S., Sali, A., Hudspeth, A.J., Friedman, J.M., and Heller, S. (2000). Vanilloid receptor-related osmotically activated channel (VR-OAC), a candidate vertebrate osmoreceptor. Cell *103*, 525-535.
Lindner, M., Leitner, M.G., Halaszovich, C.R., Hammond, G.R., and Oliver, D. (2011). Probing the regulation of TASK potassium channels by PI4,5P(2) with switchable phosphoinositide phosphatases. J Physiol *589*, 3149-3162.
Lumpkin, E.A., and Caterina, M.J. (2007). Mechanisms of sensory transduction in the skin. Nature *445*, 858-865.
Luo, Y., Vassilev, P.M., Li, X., Kawanabe, Y., and Zhou, J. (2003). Native polycystin 2 functions as a plasma membrane Ca2+-permeable cation channel in renal epithelia. Mol Cell Biol *23*, 2600-2607.
Ma, X., Nilius, B., Wong, J.W., Huang, Y., and Yao, X. (2011). Electrophysiological properties of heteromeric TRPV4-C1 channels. Biochim Biophys Acta *1808*, 2789-2797.
Machuca, E., Benoit, G., and Antignac, C. (2009). Genetics of nephrotic syndrome: connecting molecular genetics to podocyte physiology. Hum Mol Genet *18*, R185-194.
Maingret, F., Fosset, M., Lesage, F., Lazdunski, M., and Honore, E. (1999a). TRAAK is a mammalian neuronal mechano-gated K+ channel. J Biol Chem *274*, 1381-1387.

Maingret, F., Honore, E., Lazdunski, M., and Patel, A.J. (2002). Molecular basis of the voltage-dependent gating of TREK-1, a mechano-sensitive K(+) channel. Biochem Biophys Res Commun *292*, 339-346.
Maingret, F., Patel, A.J., Lesage, F., Lazdunski, M., and Honore, E. (1999b). Mechano- or acid stimulation, two interactive modes of activation of the TREK-1 potassium channel. J Biol Chem *274*, 26691-26696.
Makino, A., Prossnitz, E.R., Bunemann, M., Wang, J.M., Yao, W., and Schmid-Schonbein, G.W. (2006). G protein-coupled receptors serve as mechanosensors for fluid shear stress in neutrophils. Am J Physiol Cell Physiol *290*, C1633-1639.
Maksimovic, S., Nakatani, M., Baba, Y., Nelson, A.M., Marshall, K.L., Wellnitz, S.A., Firozi, P., Woo, S.H., Ranade, S., Patapoutian, A.*, et al.* (2014). Epidermal Merkel cells are mechanosensory cells that tune mammalian touch receptors. Nature *509*, 617-621.
Marcotti, W., Erven, A., Johnson, S.L., Steel, K.P., and Kros, C.J. (2006). Tmc1 is necessary for normal functional maturation and survival of inner and outer hair cells in the mouse cochlea. J Physiol *574*, 677-698.
Maroto, R., Raso, A., Wood, T.G., Kurosky, A., Martinac, B., and Hamill, O.P. (2005). TRPC1 forms the stretch-activated cation channel in vertebrate cells. Nat Cell Biol *7*, 179-185.
Martinac, B., Adler, J., and Kung, C. (1990). Mechanosensitive ion channels of E. coli activated by amphipaths. Nature *348*, 261-263.
Martinac, B., Buechner, M., Delcour, A.H., Adler, J., and Kung, C. (1987). Pressure-sensitive ion channel in Escherichia coli. Proc Natl Acad Sci U S A *84*, 2297-2301.
Mathar, I., Vennekens, R., Meissner, M., Kees, F., Van der Mieren, G., Camacho Londono, J.E., Uhl, S., Voets, T., Hummel, B., van den Bergh, A.*, et al.* (2010). Increased catecholamine secretion contributes to hypertension in TRPM4-deficient mice. J Clin Invest *120*, 3267-3279.
Matthews, B.D., Overby, D.R., Mannix, R., and Ingber, D.E. (2006). Cellular adaptation to mechanical stress: role of integrins, Rho, cytoskeletal tension and mechanosensitive ion channels. J Cell Sci *119*, 508-518.
Mederos y Schnitzler, M., Storch, U., and Gudermann, T. (2011). AT1 receptors as mechanosensors. Curr Opin Pharmacol *11*, 112-116.
Mederos y Schnitzler, M., Storch, U., Meibers, S., Nurwakagari, P., Breit, A., Essin, K., Gollasch, M., and Gudermann, T. (2008). Gq-coupled receptors as mechanosensors mediating myogenic vasoconstriction. EMBO J *27*, 3092-3103.
Miceli, I., Burt, D., Tarabra, E., Camussi, G., Perin, P.C., and Gruden, G. (2010). Stretch reduces nephrin expression via an angiotensin II-AT(1)-dependent mechanism in human podocytes: effect of rosiglitazone. Am J Physiol Renal Physiol *298*, F381-390.
Mizuno, A., Matsumoto, N., Imai, M., and Suzuki, M. (2003). Impaired osmotic sensation in mice lacking TRPV4. Am J Physiol Cell Physiol *285*, C96-101.
Mizuno, S. (2005). A novel method for assessing effects of hydrostatic fluid pressure on intracellular calcium: a study with bovine articular chondrocytes. Am J Physiol Cell Physiol *288*, C329-337.
Mogil, J.S., Breese, N.M., Witty, M.F., Ritchie, J., Rainville, M.L., Ase, A., Abbadi, N., Stucky, C.L., and Seguela, P. (2005). Transgenic expression of a dominant-negative ASIC3 subunit leads to increased sensitivity to mechanical and inflammatory stimuli. J Neurosci *25*, 9893-9901.
Montell, C. (2005). The TRP superfamily of cation channels. Sci STKE *2005*, re3.
Morita, H., Honda, A., Inoue, R., Ito, Y., Abe, K., Nelson, M.T., and Brayden, J.E. (2007). Membrane stretch-induced activation of a TRPM4-like nonselective cation channel in cerebral artery myocytes. J Pharmacol Sci *103*, 417-426.
Morris, C.E. (1992). Are stretch-sensitive channels in molluscan cells and elsewhere physiological mechanotransducers? Experientia *48*, 852-858.
Muraki, K., Iwata, Y., Katanosaka, Y., Ito, T., Ohya, S., Shigekawa, M., and Imaizumi, Y. (2003). TRPV2 is a component of osmotically sensitive cation channels in murine aortic myocytes. Circ Res *93*, 829-838.

Murata, N., Ito, S., Furuya, K., Takahara, N., Naruse, K., Aso, H., Kondo, M., Sokabe, M., and Hasegawa, Y. (2014). Ca influx and ATP release mediated by mechanical stretch in human lung fibroblasts. Biochem Biophys Res Commun.
Muzumdar, M.D., Tasic, B., Miyamichi, K., Li, L., and Luo, L. (2007). A global double-fluorescent Cre reporter mouse. Genesis *45*, 593-605.
Nauli, S.M., Alenghat, F.J., Luo, Y., Williams, E., Vassilev, P., Li, X., Elia, A.E., Lu, W., Brown, E.M., Quinn, S.J.*, et al.* (2003). Polycystins 1 and 2 mediate mechanosensation in the primary cilium of kidney cells. Nat Genet *33*, 129-137.
Nilius, B., and **Droogmans, G.** (2003). Amazing chloride channels: an overview. Acta Physiol Scand *177*, 119-147.
Nilius, B., Eggermont, J., and Droogmans, G. (2000). The endothelial volume-regulated anion channel, VRAC. Cell Physiol Biochem *10*, 313-320.
Nilius, B., Eggermont, J., Voets, T., and Droogmans, G. (1996). Volume-activated Cl-channels. Gen Pharmacol *27*, 1131-1140.
North, R.A. (2002). Molecular physiology of P2X receptors. Physiol Rev *82*, 1013-1067.
North, R.A., and Surprenant, A. (2000). Pharmacology of cloned P2X receptors. Annu Rev Pharmacol Toxicol *40*, 563-580.
Numata, T., Shimizu, T., and Okada, Y. (2007a). Direct mechano-stress sensitivity of TRPM7 channel. Cell Physiol Biochem *19*, 1-8.
Numata, T., Shimizu, T., and Okada, Y. (2007b). TRPM7 is a stretch- and swelling-activated cation channel involved in volume regulation in human epithelial cells. Am J Physiol Cell Physiol *292*, C460-467.
O'Hagan, R., Chalfie, M., and Goodman, M.B. (2005). The MEC-4 DEG/ENaC channel of Caenorhabditis elegans touch receptor neurons transduces mechanical signals. Nat Neurosci *8*, 43-50.
Oancea, E., Wolfe, J.T., and Clapham, D.E. (2006). Functional TRPM7 channels accumulate at the plasma membrane in response to fluid flow. Circ Res *98*, 245-253.
Obukhov, A.G., and Nowycky, M.C. (2004). TRPC5 activation kinetics are modulated by the scaffolding protein ezrin/radixin/moesin-binding phosphoprotein-50 (EBP50). J Cell Physiol *201*, 227-235.
Odell, A.F., Van Helden, D.F., and Scott, J.L. (2008). The spectrin cytoskeleton influences the surface expression and activation of human transient receptor potential channel 4 channels. J Biol Chem *283*, 4395-4407.
Oliverio, M.I., Kim, H.S., Ito, M., Le, T., Audoly, L., Best, C.F., Hiller, S., Kluckman, K., Maeda, N., Smithies, O.*, et al.* (1998). Reduced growth, abnormal kidney structure, and type 2 (AT2) angiotensin receptor-mediated blood pressure regulation in mice lacking both AT1A and AT1B receptors for angiotensin II. Proc Natl Acad Sci U S A *95*, 15496-15501.
Olsen, S.M., Stover, J.D., and Nagatomi, J. (2011). Examining the role of mechanosensitive ion channels in pressure mechanotransduction in rat bladder urothelial cells. Ann Biomed Eng *39*, 688-697.
Ong, E.C., Nesin, V., Long, C.L., Bai, C.X., Guz, J.L., Ivanov, I.P., Abramowitz, J., Birnbaumer, L., Humphrey, M.B., and Tsiokas, L. (2013). A TRPC1 protein-dependent pathway regulates osteoclast formation and function. J Biol Chem *288*, 22219-22232.
Orr, A.W., Helmke, B.P., Blackman, B.R., and Schwartz, M.A. (2006). Mechanisms of mechanotransduction. Dev Cell *10*, 11-20.
Otsuguro, K., Tang, J., Tang, Y., Xiao, R., Freichel, M., Tsvilovskyy, V., Ito, S., Flockerzi, V., Zhu, M.X., and Zholos, A.V. (2008). Isoform-specific inhibition of TRPC4 channel by phosphatidylinositol 4,5-bisphosphate. J Biol Chem *283*, 10026-10036.
Ou, G.S., Chen, Z.L., and Yuan, M. (2002). Jasplakinolide reversibly disrupts actin filaments in suspension-cultured tobacco BY-2 cells. Protoplasma *219*, 168-175.
Page, A.J., Brierley, S.M., Martin, C.M., Price, M.P., Symonds, E., Butler, R., Wemmie, J.A., and Blackshaw, L.A. (2005). Different contributions of ASIC channels 1a, 2, and 3 in gastrointestinal mechanosensory function. Gut *54*, 1408-1415.

Palmer, C.P., Zhou, X.L., Lin, J., Loukin, S.H., Kung, C., and Saimi, Y. (2001). A TRP homolog in Saccharomyces cerevisiae forms an intracellular Ca(2+)-permeable channel in the yeast vacuolar membrane. Proc Natl Acad Sci U S A *98*, 7801-7805.
Pan, B., Geleoc, G.S., Asai, Y., Horwitz, G.C., Kurima, K., Ishikawa, K., Kawashima, Y., Griffith, A.J., and Holt, J.R. (2013). TMC1 and TMC2 are components of the mechanotransduction channel in hair cells of the mammalian inner ear. Neuron *79*, 504-515.
Patel, A.J., and **Honore, E.** (2001). Properties and modulation of mammalian 2P domain K+ channels. Trends Neurosci *24*, 339-346.
Patel, A.J., Honore, E., Maingret, F., Lesage, F., Fink, M., Duprat, F., and Lazdunski, M. (1998). A mammalian two pore domain mechano-gated S-like K+ channel. EMBO J *17*, 4283-4290.
Patel, A.J., Lazdunski, M., and Honore, E. (2001). Lipid and mechano-gated 2P domain K(+) channels. Curr Opin Cell Biol *13*, 422-428.
Pazour, G.J., San Agustin, J.T., Follit, J.A., Rosenbaum, J.L., and Witman, G.B. (2002). Polycystin-2 localizes to kidney cilia and the ciliary level is elevated in orpk mice with polycystic kidney disease. Curr Biol *12*, R378-380.
Pelucchi, B., Aguiari, G., Pignatelli, A., Manzati, E., Witzgall, R., Del Senno, L., and Belluzzi, O. (2006). Nonspecific cation current associated with native polycystin-2 in HEK-293 cells. J Am Soc Nephrol *17*, 388-397.
Perozo, E., Cortes, D.M., Sompornpisut, P., Kloda, A., and Martinac, B. (2002a). Open channel structure of MscL and the gating mechanism of mechanosensitive channels. Nature *418*, 942-948.
Perozo, E., Kloda, A., Cortes, D.M., and Martinac, B. (2002b). Physical principles underlying the transduction of bilayer deformation forces during mechanosensitive channel gating. Nat Struct Biol *9*, 696-703.
Pittenger, M.F., Mackay, A.M., Beck, S.C., Jaiswal, R.K., Douglas, R., Mosca, J.D., Moorman, M.A., Simonetti, D.W., Craig, S., and Marshak, D.R. (1999). Multilineage potential of adult human mesenchymal stem cells. Science *284*, 143-147.
Potier, M., Gonzalez, J.C., Motiani, R.K., Abdullaev, I.F., Bisaillon, J.M., Singer, H.A., and Trebak, M. (2009). Evidence for STIM1- and Orai1-dependent store-operated calcium influx through ICRAC in vascular smooth muscle cells: role in proliferation and migration. Faseb J *23*, 2425-2437.
Price, M.P., Lewin, G.R., McIlwrath, S.L., Cheng, C., Xie, J., Heppenstall, P.A., Stucky, C.L., Mannsfeldt, A.G., Brennan, T.J., Drummond, H.A.*, et al.* (2000). The mammalian sodium channel BNC1 is required for normal touch sensation. Nature *407*, 1007-1011.
Price, M.P., McIlwrath, S.L., Xie, J., Cheng, C., Qiao, J., Tarr, D.E., Sluka, K.A., Brennan, T.J., Lewin, G.R., and Welsh, M.J. (2001). The DRASIC cation channel contributes to the detection of cutaneous touch and acid stimuli in mice. Neuron *32*, 1071-1083.
Priel, A., and Silberberg, S.D. (2004). Mechanism of ivermectin facilitation of human P2X4 receptor channels. J Gen Physiol *123*, 281-293.
Qian, F., Wei, W., Germino, G., and Oberhauser, A. (2005). The nanomechanics of polycystin-1 extracellular region. J Biol Chem *280*, 40723-40730.
Qiu, Z., Dubin, A.E., Mathur, J., Tu, B., Reddy, K., Miraglia, L.J., Reinhardt, J., Orth, A.P., and Patapoutian, A. (2014). SWELL1, a plasma membrane protein, is an essential component of volume-regulated anion channel. Cell *157*, 447-458.
Rakesh, K., Yoo, B., Kim, I.M., Salazar, N., Kim, K.S., and Rockman, H.A. (2010). beta-Arrestin-biased agonism of the angiotensin receptor induced by mechanical stress. Sci Signal *3*, ra46.
Ranade, S.S., Qiu, Z., Woo, S.H., Hur, S.S., Murthy, S.E., Cahalan, S.M., Xu, J., Mathur, J., Bandell, M., Coste, B.*, et al.* (2014). Piezo1, a mechanically activated ion channel, is required for vascular development in mice. Proc Natl Acad Sci U S A *111*, 10347-10352.
Resnick, A. (2010). Use of optical tweezers to probe epithelial mechanosensation. J Biomed Opt *15*, 015005.
Rho, J.Y., Ashman, R.B., and Turner, C.H. (1993). Young's modulus of trabecular and cortical bone material: ultrasonic and microtensile measurements. J Biomech *26*, 111-119.

Riccio, A., Li, Y., Moon, J., Kim, K.S., Smith, K.S., Rudolph, U., Gapon, S., Yao, G.L., Tsvetkov, E., Rodig, S.J.*, et al.* (2009). Essential role for TRPC5 in amygdala function and fear-related behavior. Cell *137*, 761-772.
Roman, R.J., and Harder, D.R. (1993). Cellular and ionic signal transduction mechanisms for the mechanical activation of renal arterial vascular smooth muscle. J Am Soc Nephrol *4*, 986-996.
Roshanravan, H., and **Dryer, S.E.** (2014). ATP acting through P2Y receptors causes activation of podocyte TRPC6 channels: role of podocin and reactive oxygen species. Am J Physiol Renal Physiol *306*, F1088-1097.
Roudaut, Y., Lonigro, A., Coste, B., Hao, J., Delmas, P., and Crest, M. (2012). Touch sense: Functional organization and molecular determinants of mechanosensitive receptors. Channels (Austin) *6*.
Runnels, L.W., Yue, L., and Clapham, D.E. (2002). The TRPM7 channel is inactivated by PIP(2) hydrolysis. Nat Cell Biol *4*, 329-336.
Sachs, F. (2010). Stretch-activated ion channels: what are they? Physiology (Bethesda) *25*, 50-56.
Sachs, N., Claessen, N., Aten, J., Kreft, M., Teske, G.J., Koeman, A., Zuurbier, C.J., Janssen, H., and Sonnenberg, A. (2012). Blood pressure influences end-stage renal disease of Cd151 knockout mice. J Clin Invest *122*, 348-358.
Sakmann, B., and **Neher, E.** (1984). Patch clamp techniques for studying ionic channels in excitable membranes. Annu Rev Physiol *46*, 455-472.
Sakura, H., and **Ashcroft, F.M.** (1997). Identification of four trp1 gene variants murine pancreatic beta-cells. Diabetologia *40*, 528-532.
Salameh, A., and Dhein, S. (2013). Effects of mechanical forces and stretch on intercellular gap junction coupling. Biochim Biophys Acta *1828*, 147-156.
Salido, G.M., Sage, S.O., and Rosado, J.A. (2009). TRPC channels and store-operated Ca(2+) entry. Biochim Biophys Acta *1793*, 223-230.
Satlin, L.M., Sheng, S., Woda, C.B., and Kleyman, T.R. (2001). Epithelial Na(+) channels are regulated by flow. Am J Physiol Renal Physiol *280*, F1010-1018.
Schaefer, M., Plant, T.D., Obukhov, A.G., Hofmann, T., Gudermann, T., and Schultz, G. (2000). Receptor-mediated regulation of the nonselective cation channels TRPC4 and TRPC5. J Biol Chem *275*, 17517-17526.
Schaldecker, T., Kim, S., Tarabanis, C., Tian, D., Hakroush, S., Castonguay, P., Ahn, W., Wallentin, H., Heid, H., Hopkins, C.R.*, et al.* (2013). Inhibition of the TRPC5 ion channel protects the kidney filter. J Clin Invest *123*, 5298-5309.
Schrenk-Siemens, K., Wende, H., Prato, V., Song, K., Rostock, C., Loewer, A., Utikal, J., Lewin, G.R., Lechner, S.G., and Siemens, J. (2014). PIEZO2 is required for mechanotransduction in human stem cell-derived touch receptors. Nat Neurosci.
Schubert, R., and **Brayden, J.E.** (2005). Stretch-activated Cation Channels and the Myogenic Response of Small Arteries.
Schwartz, M.A., and **DeSimone, D.W.** (2008). Cell adhesion receptors in mechanotransduction. Curr Opin Cell Biol *20*, 551-556.
Shankland, S.J., Pippin, J.W., Reiser, J., and Mundel, P. (2007). Podocytes in culture: past, present, and future. Kidney Int *72*, 26-36.
Sharif-Naeini, R., Dedman, A., Folgering, J.H., Duprat, F., Patel, A., Nilius, B., and Honore, E. (2008). TRP channels and mechanosensory transduction: insights into the arterial myogenic response. Pflugers Arch *456*, 529-540.
Sharif-Naeini, R., Folgering, J.H., Bichet, D., Duprat, F., Lauritzen, I., Arhatte, M., Jodar, M., Dedman, A., Chatelain, F.C., Schulte, U.*, et al.* (2009). Polycystin-1 and -2 dosage regulates pressure sensing. Cell *139*, 587-596.
Sharif Naeini, R., Witty, M.F., Seguela, P., and Bourque, C.W. (2006). An N-terminal variant of Trpv1 channel is required for osmosensory transduction. Nat Neurosci *9*, 93-98.
Shenolikar, S., Voltz, J.W., Cunningham, R., and Weinman, E.J. (2004). Regulation of ion transport by the NHERF family of PDZ proteins. Physiology (Bethesda) *19*, 362-369.

Shi, S., Ghosh, D.D., Okumura, S., Carattino, M.D., Kashlan, O.B., Sheng, S., and Kleyman, T.R. (2011). Base of the thumb domain modulates epithelial sodium channel gating. J Biol Chem *286*, 14753-14761.
Shibasaki, K., Murayama, N., Ono, K., Ishizaki, Y., and Tominaga, M. (2010). TRPV2 enhances axon outgrowth through its activation by membrane stretch in developing sensory and motor neurons. J Neurosci *30*, 4601-4612.
Sidi, S., Friedrich, R.W., and Nicolson, T. (2003). NompC TRP channel required for vertebrate sensory hair cell mechanotransduction. Science *301*, 96-99.
Smoyer, W.E., and **Mundel, P.** (1998). Regulation of podocyte structure during the development of nephrotic syndrome. J Mol Med (Berl) *76*, 172-183.
Spagnoli, C., Beyder, A., Besch, S., and Sachs, F. (2008). Atomic force microscopy analysis of cell volume regulation. Phys Rev E Stat Nonlin Soft Matter Phys *78*, 031916.
Spassova, M.A., Hewavitharana, T., Xu, W., Soboloff, J., and Gill, D.L. (2006). A common mechanism underlies stretch activation and receptor activation of TRPC6 channels. Proc Natl Acad Sci U S A *103*, 16586-16591.
Storch, U., Blodow, S., Gudermann, T., and Schnitzler, M.M. (2014). Cysteinyl Leukotriene 1 Receptors as Novel Mechanosensors Mediating Myogenic Tone Together With Angiotensin II Type 1 Receptors. Arterioscler Thromb Vasc Biol.
Storch, U., Forst, A.L., Pardatscher, F., Philipp, M., Gregoritza, M., Mederos y Schnitzler, M., and Gudermann, T., (2015). NHERF dissociation from TRPC4/5 proteins is required for channel gating by diacylglycerol. Submitted to Nature Cell Biology 29.07.2015
Storch, U., Forst, A.L., Philipp, M., Gudermann, T., and Mederos y Schnitzler, M. (2012a). Transient receptor potential channel 1 (TRPC1) reduces calcium permeability in heteromeric channel complexes. J Biol Chem *287*, 3530-3540.
Storch, U., Mederos y Schnitzler, M., and Gudermann, T. (2012b). G protein-mediated stretch reception. Am J Physiol Heart Circ Physiol *302*, H1241-1249.
Strotmann, R., Harteneck, C., Nunnenmacher, K., Schultz, G., and Plant, T.D. (2000). OTRPC4, a nonselective cation channel that confers sensitivity to extracellular osmolarity. Nat Cell Biol *2*, 695-702.
Su, Z., Anishkin, A., Kung, C., and Saimi, Y. (2011). The core domain as the force sensor of the yeast mechanosensitive TRP channel. J Gen Physiol *138*, 627-640.
Suchyna, T.M., Tape, S.E., Koeppe, R.E., 2nd, Andersen, O.S., Sachs, F., and Gottlieb, P.A. (2004). Bilayer-dependent inhibition of mechanosensitive channels by neuroactive peptide enantiomers. Nature *430*, 235-240.
Sukharev, S. (2002). Purification of the small mechanosensitive channel of Escherichia coli (MscS): the subunit structure, conduction, and gating characteristics in liposomes. Biophys J *83*, 290-298.
Sukharev, S.I., Blount, P., Martinac, B., and Kung, C. (1997). Mechanosensitive channels of Escherichia coli: the MscL gene, protein, and activities. Annu Rev Physiol *59*, 633-657.
Suzuki, M., Mizuno, A., Kodaira, K., and Imai, M. (2003). Impaired pressure sensation in mice lacking TRPV4. J Biol Chem *278*, 22664-22668.
Tang, Y., Tang, J., Chen, Z., Trost, C., Flockerzi, V., Li, M., Ramesh, V., and Zhu, M.X. (2000). Association of mammalian trp4 and phospholipase C isozymes with a PDZ domain-containing protein, NHERF. J Biol Chem *275*, 37559-37564.
Tanimoto, K., Sugiyama, F., Goto, Y., Ishida, J., Takimoto, E., Yagami, K., Fukamizu, A., and Murakami, K. (1994). Angiotensinogen-deficient mice with hypotension. J Biol Chem *269*, 31334-31337.
Tian, D., Jacobo, S.M., Billing, D., Rozkalne, A., Gage, S.D., Anagnostou, T., Pavenstadt, H., Hsu, H.H., Schlondorff, J., Ramos, A.*, et al.* (2010). Antagonistic regulation of actin dynamics and cell motility by TRPC5 and TRPC6 channels. Sci Signal *3*, ra77.
Tian, Y., Baukal, A.J., Sandberg, K., Bernstein, K.E., Balla, T., and Catt, K.J. (1996). Properties of AT1a and AT1b angiotensin receptors expressed in adrenocortical Y-1 cells. Am J Physiol *270*, E831-839.
Tracey, W.D., Jr., Wilson, R.I., Laurent, G., and Benzer, S. (2003). painless, a Drosophila gene essential for nociception. Cell *113*, 261-273.

Trebak, M., Lemonnier, L., DeHaven, W.I., Wedel, B.J., Bird, G.S., and Putney, J.W., Jr. (2009). Complex functions of phosphatidylinositol 4,5-bisphosphate in regulation of TRPC5 cation channels. Pflugers Arch *457*, 757-769.
Tsiokas, L., Arnould, T., Zhu, C., Kim, E., Walz, G., and Sukhatme, V.P. (1999). Specific association of the gene product of PKD2 with the TRPC1 channel. Proc Natl Acad Sci U S A *96*, 3934-3939.
Tsiokas, L., Kim, S., and Ong, E.C. (2007). Cell biology of polycystin-2. Cell Signal *19*, 444-453.
Vandenburgh, H.H., Shansky, J., Karlisch, P., and Solerssi, R.L. (1993). Mechanical stimulation of skeletal muscle generates lipid-related second messengers by phospholipase activation. J Cell Physiol *155*, 63-71.
Vassilev, P.M., Guo, L., Chen, X.Z., Segal, Y., Peng, J.B., Basora, N., Babakhanlou, H., Cruger, G., Kanazirska, M., Ye, C.*, et al.* (2001). Polycystin-2 is a novel cation channel implicated in defective intracellular Ca(2+) homeostasis in polycystic kidney disease. Biochem Biophys Res Commun *282*, 341-350.
Venkatachalam, K., Hofmann, T., and Montell, C. (2006). Lysosomal localization of TRPML3 depends on TRPML2 and the mucolipidosis-associated protein TRPML1. J Biol Chem *281*, 17517-17527.
Venkatachalam, K., and **Montell, C.** (2007). TRP channels. Annu Rev Biochem *76*, 387-417.
Venkatachalam, K., Zheng, F., and Gill, D.L. (2003). Regulation of canonical transient receptor potential (TRPC) channel function by diacylglycerol and protein kinase C. J Biol Chem *278*, 29031-29040.
Vennekens, R., and Nilius, B. (2007). Insights into TRPM4 function, regulation and physiological role. Handb Exp Pharmacol, 269-285.
Voltz, J.W., Weinman, E.J., and Shenolikar, S. (2001). Expanding the role of NHERF, a PDZ-domain containing protein adapter, to growth regulation. Oncogene *20*, 6309-6314.
Voss, F.K., Ullrich, F., Munch, J., Lazarow, K., Lutter, D., Mah, N., Andrade-Navarro, M.A., von Kries, J.P., Stauber, T., and Jentsch, T.J. (2014). Identification of LRRC8 heteromers as an essential component of the volume-regulated anion channel VRAC. Science *344*, 634-638.
Vreugde, S., Erven, A., Kros, C.J., Marcotti, W., Fuchs, H., Kurima, K., Wilcox, E.R., Friedman, T.B., Griffith, A.J., Balling, R.*, et al.* (2002). Beethoven, a mouse model for dominant, progressive hearing loss DFNA36. Nat Genet *30*, 257-258.
Vriens, J., Owsianik, G., Fisslthaler, B., Suzuki, M., Janssens, A., Voets, T., Morisseau, C., Hammock, B.D., Fleming, I., Busse, R.*, et al.* (2005). Modulation of the Ca2 permeable cation channel TRPV4 by cytochrome P450 epoxygenases in vascular endothelium. Circ Res *97*, 908-915.
Wada, Y., Ohsumi, Y., Tanifuji, M., Kasai, M., and Anraku, Y. (1987). Vacuolar ion channel of the yeast, Saccharomyces cerevisiae. J Biol Chem *262*, 17260-17263.
Walker, R.G., Willingham, A.T., and Zuker, C.S. (2000). A Drosophila mechanosensory transduction channel. Science *287*, 2229-2234.
Walsh, K.B., and Zhang, J. (2008). Neonatal rat cardiac fibroblasts express three types of voltage-gated K+ channels: regulation of a transient outward current by protein kinase C. Am J Physiol Heart Circ Physiol *294*, H1010-1017.
Wang, L., Chang, J.H., Paik, S.Y., Tang, Y., Eisner, W., and Spurney, R.F. (2011). Calcineurin (CN) activation promotes apoptosis of glomerular podocytes both in vitro and in vivo. Mol Endocrinol *25*, 1376-1386.
Wang, N., and **Ingber, D.E.** (1995). Probing transmembrane mechanical coupling and cytomechanics using magnetic twisting cytometry. Biochem Cell Biol *73*, 327-335.
Wang, S., Meng, F., Mohan, S., Champaneri, B., and Gu, Y. (2009). Functional ENaC channels expressed in endothelial cells: a new candidate for mediating shear force. Microcirculation *16*, 276-287.
Wang, Y., Botvinick, E.L., Zhao, Y., Berns, M.W., Usami, S., Tsien, R.Y., and Chien, S. (2005). Visualizing the mechanical activation of Src. Nature *434*, 1040-1045.

Weinman, E.J., Hall, R.A., Friedman, P.A., Liu-Chen, L.Y., and Shenolikar, S. (2006). The association of NHERF adaptor proteins with g protein-coupled receptors and receptor tyrosine kinases. Annu Rev Physiol *68*, 491-505.
Welsh, D.G., Morielli, A.D., Nelson, M.T., and Brayden, J.E. (2002). Transient receptor potential channels regulate myogenic tone of resistance arteries. Circ Res *90*, 248-250.
Wettschureck, N., and Offermanns, S. (2005). Mammalian G proteins and their cell type specific functions. Physiol Rev *85*, 1159-1204.
Wilson, C., and **Dryer, S.E.** (2014). A mutation in TRPC6 channels abolishes their activation by hypoosmotic stretch but does not affect activation by diacylglycerol or G protein signaling cascades. Am J Physiol Renal Physiol *306*, F1018-1025.
Woo, S.H., Ranade, S., Weyer, A.D., Dubin, A.E., Baba, Y., Qiu, Z., Petrus, M., Miyamoto, T., Reddy, K., Lumpkin, E.A*., et al.* (2014). Piezo2 is required for Merkel-cell mechanotransduction. Nature *509*, 622-626.
Xia, J., Lim, J.C., Lu, W., Beckel, J.M., Macarak, E.J., Laties, A.M., and Mitchell, C.H. (2012). Neurons respond directly to mechanical deformation with pannexin-mediated ATP release and autostimulation of P2X7 receptors. J Physiol *590*, 2285-2304.
Xiong, W., Grillet, N., Elledge, H.M., Wagner, T.F., Zhao, B., Johnson, K.R., Kazmierczak, P., and Muller, U. (2012). TMHS is an integral component of the mechanotransduction machinery of cochlear hair cells. Cell *151*, 1283-1295.
Yamamoto, K., Korenaga, R., Kamiya, A., and Ando, J. (2000). Fluid shear stress activates Ca(2+) influx into human endothelial cells via P2X4 purinoceptors. Circ Res *87*, 385-391.
Yasuda, N., Miura, S., Akazawa, H., Tanaka, T., Qin, Y., Kiya, Y., Imaizumi, S., Fujino, M., Ito, K., Zou, Y*., et al.* (2008). Conformational switch of angiotensin II type 1 receptor underlying mechanical stress-induced activation. EMBO Rep *9*, 179-186.
Yoshimura, K., Nomura, T., and Sokabe, M. (2004). Loss-of-function mutations at the rim of the funnel of mechanosensitive channel MscL. Biophys J *86*, 2113-2120.
Yoshimura, K., and Sokabe, M. (2010). Mechanosensitivity of ion channels based on protein-lipid interactions. J R Soc Interface *7 Suppl 3*, S307-320.
Yuan, J.P., Kim, M.S., Zeng, W., Shin, D.M., Huang, G., Worley, P.F., and Muallem, S. (2009). TRPC channels as STIM1-regulated SOCs. Channels (Austin) *3*, 221-225.
Zaninetti, R., Tacchi, S., Erriquez, J., Distasi, C., Maggi, R., Cariboni, A., Condorelli, F., Canonico, P.L., and Genazzani, A.A. (2008). Calcineurin primes immature gonadotropin-releasing hormone-secreting neuroendocrine cells for migration. Mol Endocrinol *22*, 729-736.
Zenker, M., Machuca, E., and Antignac, C. (2009). Genetics of nephrotic syndrome: new insights into molecules acting at the glomerular filtration barrier. J Mol Med (Berl) *87*, 849-857.
Zhang, J.J., and Jacob, T.J. (1994). ATP-activated chloride channel inhibited by an antibody to P glycoprotein. Am J Physiol *267*, C1095-1102.
Zhang, Q., Cao, C., Zhang, Z., Wier, W.G., Edwards, A., and Pallone, T.L. (2008). Membrane current oscillations in descending vasa recta pericytes. Am J Physiol Renal Physiol *294*, F656-666.
Zhang, R., Zhang, C., Zhao, Q., and Li, D. (2013). Spectrin: structure, function and disease. Sci China Life Sci *56*, 1076-1085.
Zhang, Y.L., Frangos, J.A., and Chachisvilis, M. (2009). Mechanical stimulus alters conformation of type 1 parathyroid hormone receptor in bone cells. Am J Physiol Cell Physiol *296*, C1391-1399.
Zheng, W., Christensen, L.P., and Tomanek, R.J. (2008). Differential effects of cyclic and static stretch on coronary microvascular endothelial cell receptors and vasculogenic/angiogenic responses. Am J Physiol Heart Circ Physiol *295*, H794-800.
Zholos, A. (2010). Pharmacology of transient receptor potential melastatin channels in the vasculature. Br J Pharmacol *159*, 1559-1571.
Zhou, X., Su, Z., Anishkin, A., Haynes, W.J., Friske, E.M., Loukin, S.H., Kung, C., and Saimi, Y. (2007). Yeast screens show aromatic residues at the end of the sixth helix anchor transient receptor potential channel gate. Proc Natl Acad Sci U S A *104*, 15555-15559.

Zhou, X.L., Batiza, A.F., Loukin, S.H., Palmer, C.P., Kung, C., and Saimi, Y. (2003). The transient receptor potential channel on the yeast vacuole is mechanosensitive. Proc Natl Acad Sci U S A *100*, 7105-7110.
Zhou, X.L., Loukin, S.H., Coria, R., Kung, C., and Saimi, Y. (2005). Heterologously expressed fungal transient receptor potential channels retain mechanosensitivity in vitro and osmotic response in vivo. Eur Biophys J *34*, 413-422.
Zhu, M.H., Chae, M., Kim, H.J., Lee, Y.M., Kim, M.J., Jin, N.G., Yang, D.K., So, I., and Kim, K.W. (2005). Desensitization of canonical transient receptor potential channel 5 by protein kinase C. Am J Physiol Cell Physiol *289*, C591-600.
Zhu, X., Jiang, M., Peyton, M., Boulay, G., Hurst, R., Stefani, E., and Birnbaumer, L. (1996). trp, a novel mammalian gene family essential for agonist-activated capacitative Ca2+ entry. Cell *85*, 661-671.
Zou, Y., Akazawa, H., Qin, Y., Sano, M., Takano, H., Minamino, T., Makita, N., Iwanaga, K., Zhu, W., Kudoh, S.*, et al.* (2004). Mechanical stress activates angiotensin II type 1 receptor without the involvement of angiotensin II. Nat Cell Biol *6*, 499-506.

X Acknowledgements

I would like to sincerely thank the following people for their support:

Head of the Walther-Straub Institute: **Prof. Dr. Thomas Gudermann**

My thesis supervisor: **Prof. Dr. Michael Mederos y Schnitzler**

My lab supervisor: **Dr. Ursula Storch**

My lab: **Serap, Julie, Franziska, Steffi, Michaela, Emily, Laura** and **Joanna**

The whole **Walther-Straub Institute of Pharmacology and Toxicology**

My husband **Tobias**

My **family**

THANK YOU!